The Geology and Tectonic Setting of the Shashe-Foley-Tonota area (Central Motloutse Complex), NE Botswana

By

MOLATLHEGI LARTY LOSTMAN MOSEKI

STUDENT NO. 208523856

Submitted in fulfillment of the academic requirements
For the degree of Master of Science
In the School of Agricultural, Earth and Environmental Sciences
University of KwaZulu-Natal, Durban

December 2013

PREFACE

The research work described in this dissertation was carried out in the School of Agriculture, Earth and Environmental Sciences, University of KwaZulu-Natal, Durban, from March 2008 to December 2010, and was continued at Lobatse (Botswana) during 2011 to 2013 under the supervision of Professor Stephen McCourt.

This study represents original work by the author and has not otherwise been submitted in any form for any degree or diploma to any tertiary institution. Where use has been made of the work of others it is duly acknowledged in the text

DECLARATION-PLAGIARISM

I, Molatlhegi Larty Lostman Moseki declare that

The research reported in this dissertation where otherwise indicated, is my original research

This dissertation has not been submitted for any degree or examination at any other university

This dissertation does not contain other persons' data, pictures, graphs or other information, unless specifically acknowledged as being sourced from other persons.

This dissertation does not contain other persons, writing, unless specifically acknowledged as being sourced from other researchers. Where other written sources have been quoted, then:

Their words have been re-written but the general information attributed to them has been referenced

Where their exact words have been used, then their writing has been placed in italics and inside quotation marks, and referenced.

This dissertation does not contain text, graphs or tables copied and pasted from the internet, unless specifically acknowledged, and the source being detailed in the dissertation and in the Reference sections

Signed…….

ABSTRACT

The well-developed NE-SW structural grain of the Shashe, Foley and Tonota (SFT) region is used to separate it from the NW-SE trending structures that characterise the Matsitama belt and adjacent area previously described as the Shashe belt. The study area is divided into 4 domains showing different geometrical and geological characteristics. Domain 2 (Shashe Dam shear zone) and Domain 3 lie to the NW and SE of the metasedimentary belt (Domain1). Domain 4 (the Gulushabe shear zone) is to the NE of the metasedimentary rocks. The rocks are characterised by NNE to ENE striking foliation present in both the the metasedimentary belt (supracrustal rocks) and the granitoid rocks. The metasedimentary rocks are deformed into large map scale NE to ENE trending folds structures (the Foley synform and the Gulushabe antiform) that deform bedding (So) and foliation (S_1). The deformation involved NW-SE or NNW-SSE horizontal compression and is explained by two main episodes of NE-ENE coaxial (F1/F2) folding followed by a younger phase (F_3) that produced NNE trending folds. The effect of F_3 folding is reflected in stereographic plots of poles to bedding and foliation in Domains 1and Domain 2 which indicate folds plunging to the NNE. The foliation and the shape of deformed pebbles in the pebbly-quartzite is a product of oblate strain (flattening) in response to NW or NNW horizontal compression. This pebble elongation is considered to reflect the end result of F_1 and F_2 folding produced by oblate strain. Likewise, the shape of the K-feldspar megacrysts in the megacrystic granite gneiss in Domain 2 can be attributed to flattening (pure shear) rather than simple shear. The kinematics of the deformation features recognized are not compatible with the accretion-linked models proposed by previous workers for the SW margin of the Zimbabwe craton.

Field based intrusive relationship studies indicate the granitoid gneisses were derived from igneous protoliths. Neoarchaean U-Pb zircon ages obtained confirm the order of granitoid emplacement obtained from field based studies. The ages obtained are 2724±48 Ma (Tonota biotite gneiss), 2698.9±9.2Ma (tonalite gneiss), 2647±24 Ma (megacrystic granite gneiss) and 2631.5±4 Ma (pink granite). Granitoid magmatism occurred between about 2724 Ma (biotite gneiss) and 2631 Ma (pink granite), a duration of ~ 94 Ma. The foliation (S_1) in the tonalitic gneiss (2699 Ma) and the megacrystic gneiss (2647 Ma) predate intrusion of the pink gneissic granite (2631 Ma). Since S_1 in the granitoid rocks is equated with S_2 in the metasedimentary sequence, deformation fabrics in both the metasedimentary sequence and granitoid rocks predate 2631 Ma. The U-Pb ages obtained in this study, together with previous U-Pb zircon ages for granitoids from adjacent parts of the Motloutse Complex, the Limpopo belt and the Mosetse Complex indicate a geotectonic link between the terranes during the interval 2.6-2.7 Ga

Domain 3 fabric is parallel to large scale ENE-WSW trending ductile dextral strike-slip shear zones (Regional D4 structures) that define the northern boundary to the Central Zone of the Limpopo belt but no kinematic indicators were found in the domain to confirm the shear sense. Structural evidence (this study) indicates thrust sense shearing characterises the SW vergent Gulushabe shear zone (Domain 4) which forms the boundary between the SFT area and the SE margin of the Tati greenstone belt. The Gulubashe shear zone dips N to NE thus deviating from the regional scale WNW/SSE trending system of thrust sense ductile shear zones which dips SW. The Gulushabe shear zone has the geometry of a back-thrust in an overall NE vergent system. The last deformation event is marked by widespread development of NE trending minor shear zones. The minor shear zones were not found in the pink granite gneiss implying that they are older than 2631 Ma. The development of these minor ductile shear zone is constrained between 2647 Ma and 2630 Ma. The structural history of the rocks and the kinematics of the deformation features recognised are given in table 3.1. Stable isotope analysis has shown that carbonate rocks (dolomites and calc-silicates) from the SFT region have high positive $\delta^{13}C$ values (4.8 to 14.2‰). Such elevated $\delta^{13}C$ values suggest a Palaeoproterozoic (2.4-2.1) age. However in the SFT area the regional foliation (S_2) present in the granitoid gneisses and metasedimentary rocks is older than 2631 Ma indicating that despite the high $\delta^{13}C$ values, the metacarbonate rocks are Neoarchaean in age. .

Contents

CHAPTER 1: INTRODUCTION

1.1 LOCATION AND ACCESS

The area of study lies in NE Botswana to the SW of Francistown (Fig. 1.1) and includes three main Villages; Shashe and Tonota in the N and Foley in the S and one settlement (Makomoto) midway between Foley and Tonota. The Makomoto settlement is not shown in the Foley QD sheet and should not be confused with the Makomoto cattlepost that lies NW of the Shashe Dam in the Shashe QD sheet. For convenience the study area will be referred to as SFT, the abbreviation derived from the names Shashe, Foley and Tonota Villages respectively. Geographically the study area is defined by longitudes 27°23'E and 27.63°'E and latitudes 21.30°S and 21. 69°S and covers an area of about 702 km^2, covering 26 km N-S and 26 km E-W.

The Shashe and Motloutse rivers control the drainage system of the study area with the Shashe River transecting the northern part of the area and the Motloutse River the southern part. Both rivers flow to the SE. The Gaborone-Francistown main road and railway line run NE/SW through the centre of the study area. Access into the area is gained via a number of unsurfaced or graveled roads that branch off from the main road to the surrounding cattle posts and farm land. Numerous such roads and tracks join the Villages, running both parallel and across the main Gaborone-Francistown tarred road. A four-wheel drive vehicle is required for some of these roads especially during rainy seasons and was additionally useful for traverses across sandy areas, at river crossings and along the Shashe River as the latter hosts a reasonable amount of rock exposure. In terms of Quarter Degree Sheets (QDS), the area lies in the central and southwestern parts of the region enclosed by Shashe, Foley, Francistown and Phikwe map sheets (Fig. 1.2).

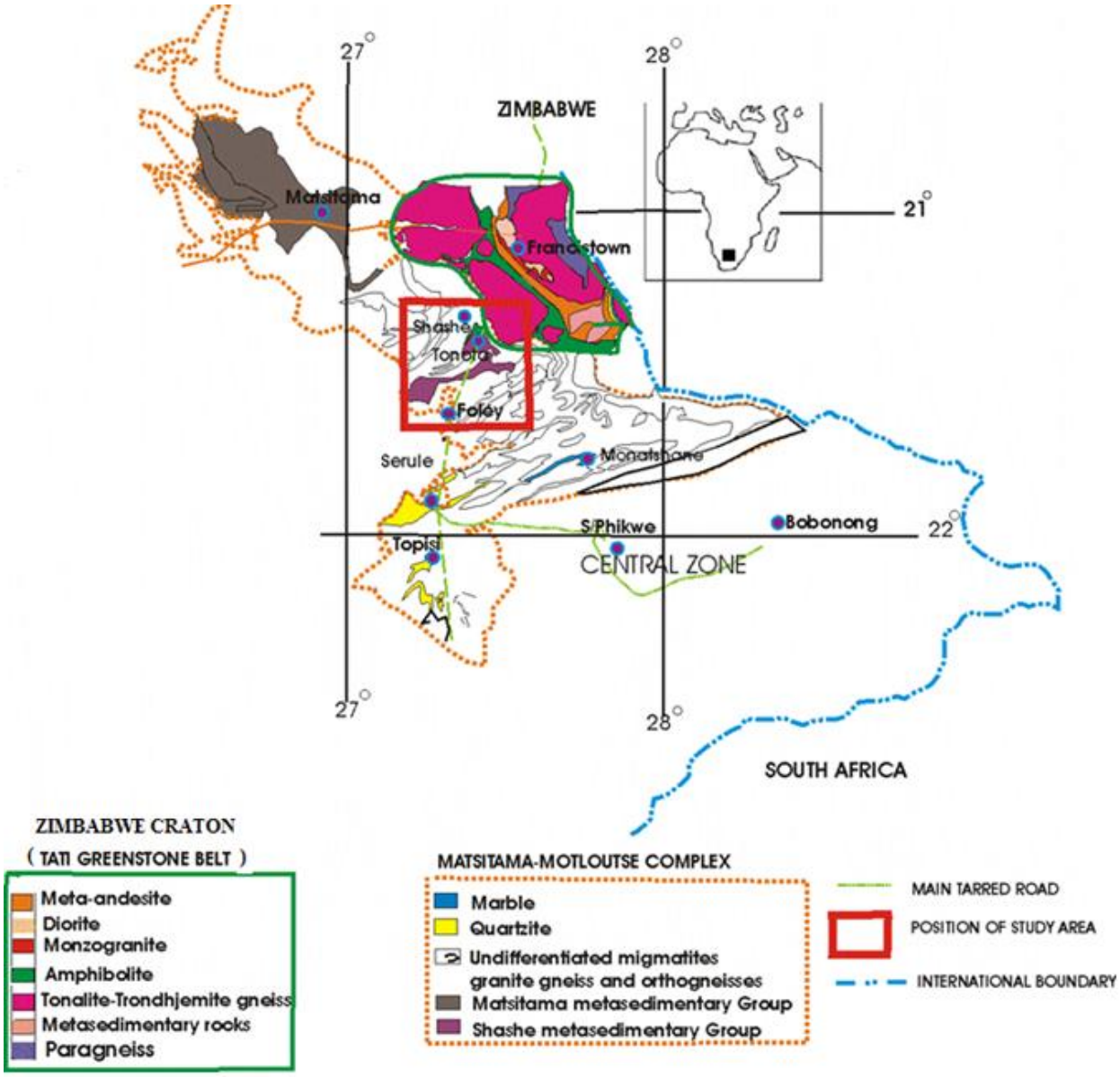

Figure 1.1: Location of the study area (red square). Geology after Key *et al*. (1994) and McCourt *et al*. (2004). Insert shows the location of Botswana in Africa.

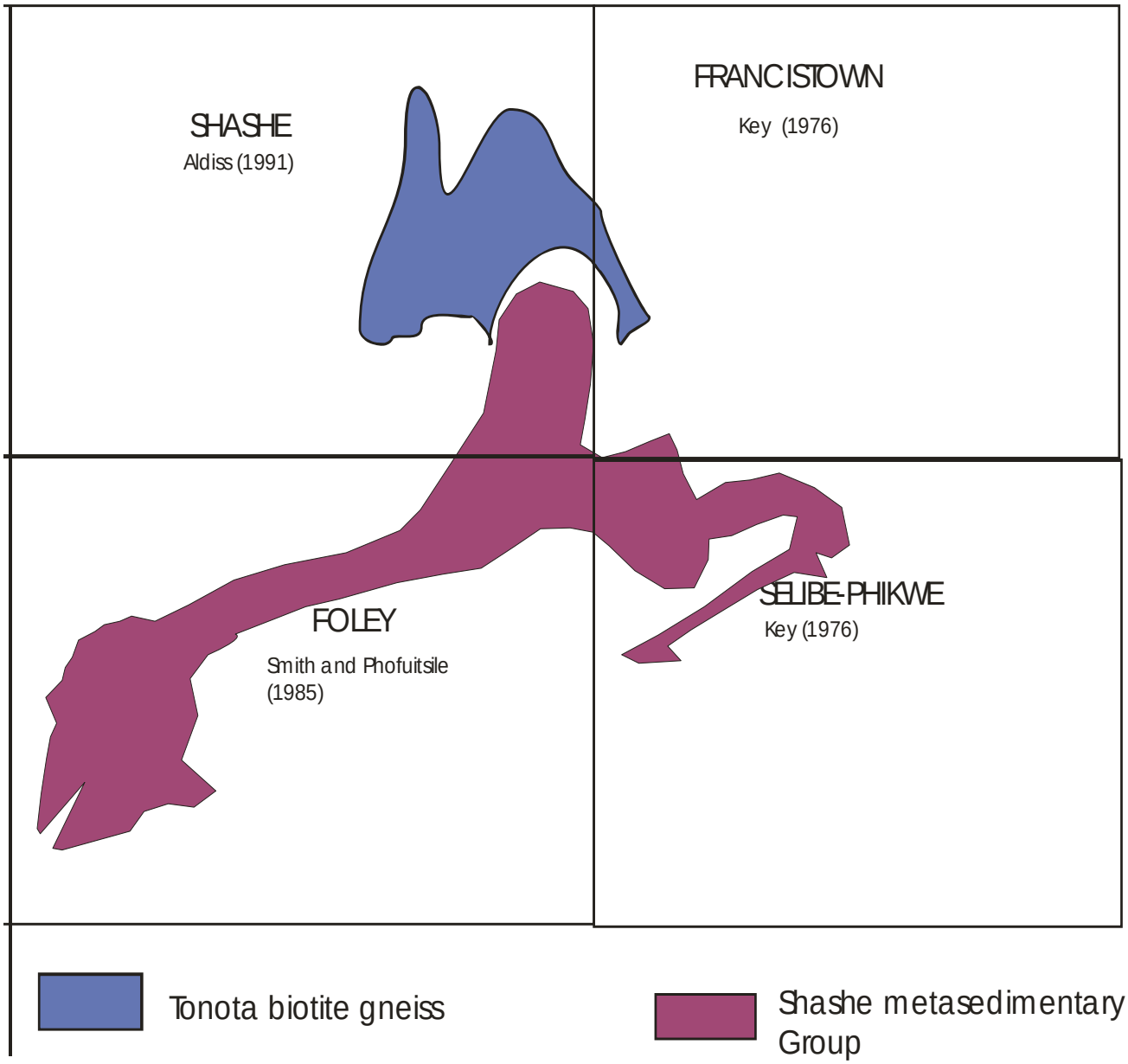

Figure 1.2: Sketch map showing position of the study area with respect to the Quarter Degree Sheets.

1.2 GEOLOGICAL SETTING OF THE STUDY AREA

The geology of NE Botswana (Fig. 1.3) comprises Archaean basement, overlain by Mesozoic (Karoo Supergroup) and Recent (Kalahari Group) cover rocks. The SFT area is underlain by rocks of the Archaean basement which regionally forms part of the Azanian Craton a fragment of Archaean continental crust comprising, from S to N, the Kaapvaal craton, the Limpopo belt and the Zimbabwe craton (McCourt *et al*. 2004). The geology of the study area can be linked to the Zimbabwe craton and the Central Zone of the Limpopo belt; the rocks of the Kaapvaal craton being obscured by younger cover. McCourt *et al.* (2004) describe the salient features of the Archaean basement in NE Botswana as follows. The Zimbabwe craton is a composite granite greenstone terrane comprising 26 individual greenstone belts and associated granitoids (*e.g.* Blenkinsop *et al.*, 1995; Jelsma and Dirks, 2002). The south-western part of the craton extends into Botswana where it has been mapped as the Tati-Vumba, Maitengwe and Matsitama granite greenstone terranes (Fig. 1.3). The full extent of the craton in Botswana is unknown, as the western boundary is obscured beneath Phanerozoic cover rocks and the southern boundary ill defined (see Bennett, 1970; Aldiss, 1991). The Limpopo belt (e.g. van Reenen *et al*., 2011) is an ENE trending granulite gneiss terrane situated between the Kaapvaal and Zimbabwe cratons. It is described in terms of three contrasting crustal domains referred to as the Southern Marginal Zone, the Central Zone and the Northern Marginal Zone (Cox *et al*., 1965). Within Botswana the Northern Marginal Zone is referred to as the Semolale Complex and the Central Zone is subdivided into the Phikwe and Mahalapye complexes (Aldiss, 1991; Carney *et al.*, 1994; Holzer *et al.*, 1999). The northern boundary of the Limpopo belt against the Zimbabwe craton is a matter of debate. Based on an interpretation of new gravity data, Ranganai *et al*. (2002) have interpreted the NW trending Shashe Mobile Belt (Bennett, 1970) as an extension of the Limpopo belt and recognised a continuous arc-shaped orogen (the Limpopo-Shashe belt) along the S and SW margin of the Zimbabwe craton (Fig. 1.3 and 1.4).

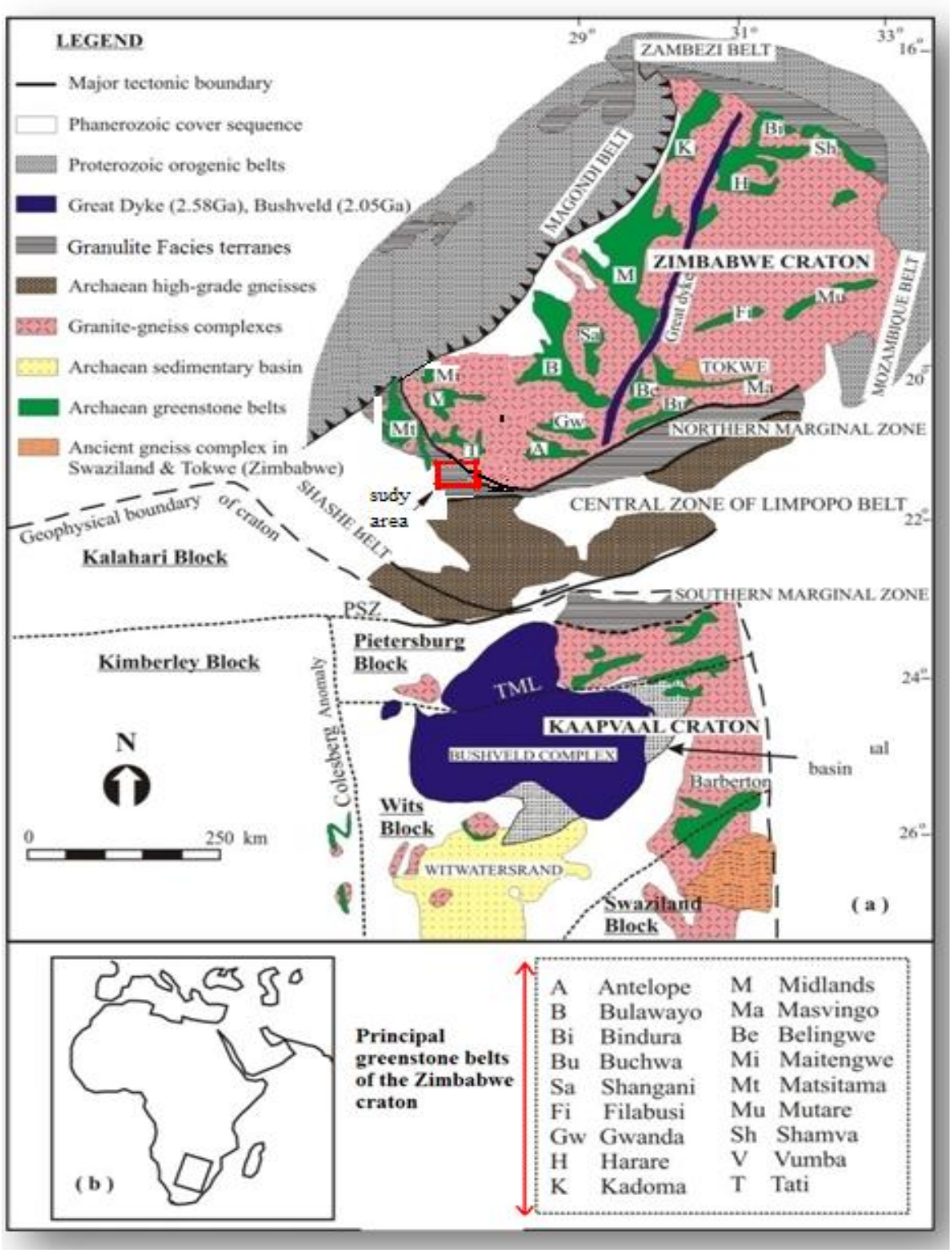

Figure 1.3: A map showing the regional geology of southern Africa (from Bagai, 2008). Red rectangle represent approximate position of study area and black rectangle in (b) outlines approximate area covered by (a)

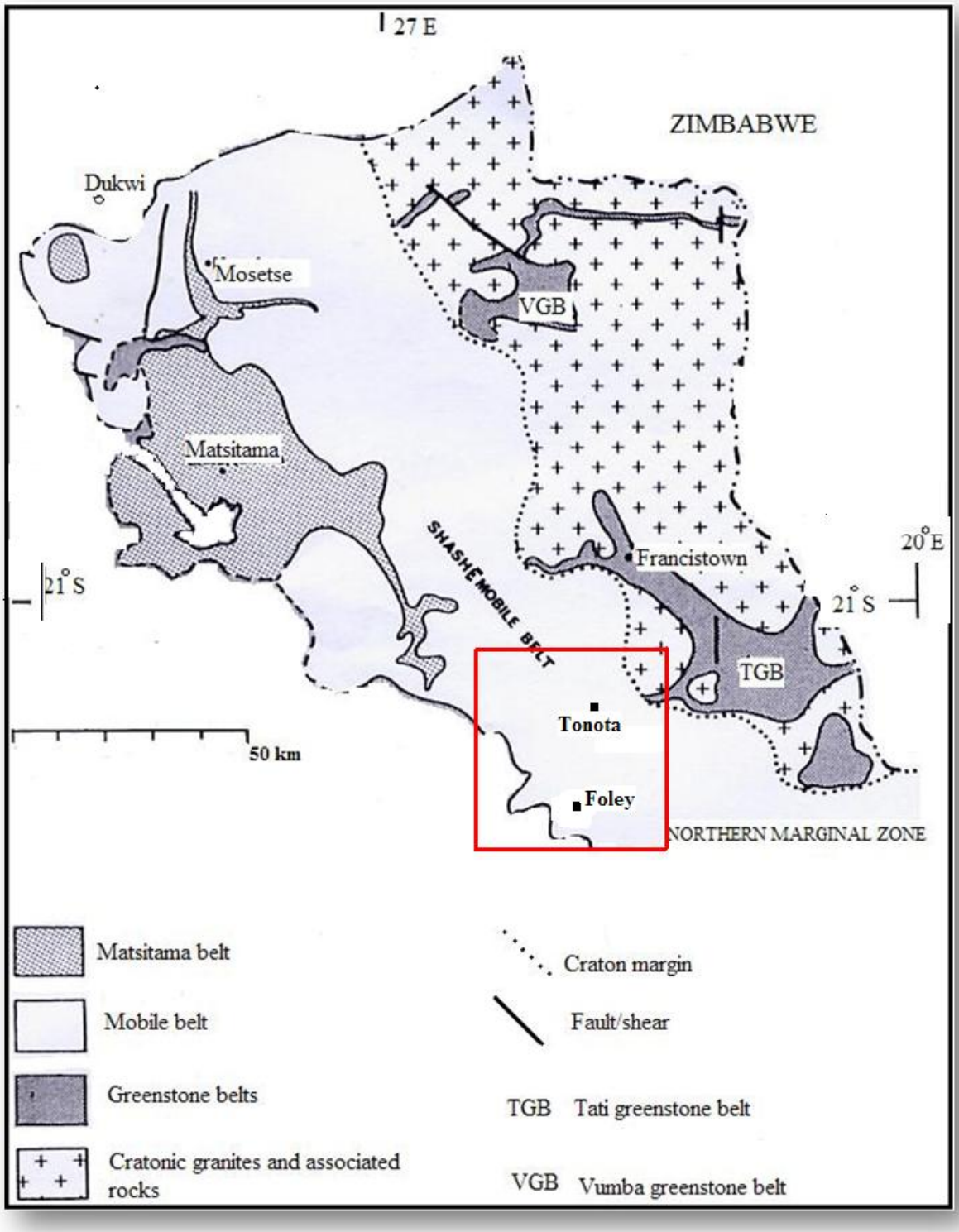

Figure 1.4: Bennett (1970) subdivision of the geology of NE Botswana showing the position of the Shashe belt relative to the SW margin of the Zimbabwe craton and the Mosetse-Matsitama areas.

In this model, the Shashe shear zone (Fig.1.5) is regarded as the boundary between the orogen and the Zimbabwe craton in NE Botswana. In Zimbabwe the northern boundary of the Limpopo belt against the Zimbabwe craton, is defined by the ductile North Limpopo Thrust Zone (Blenkinsop *et al.*, 1995; Rollinson and Blenkinsop, 1995) or Northern Marginal Thrust Zone shown in Fig. 1.5.

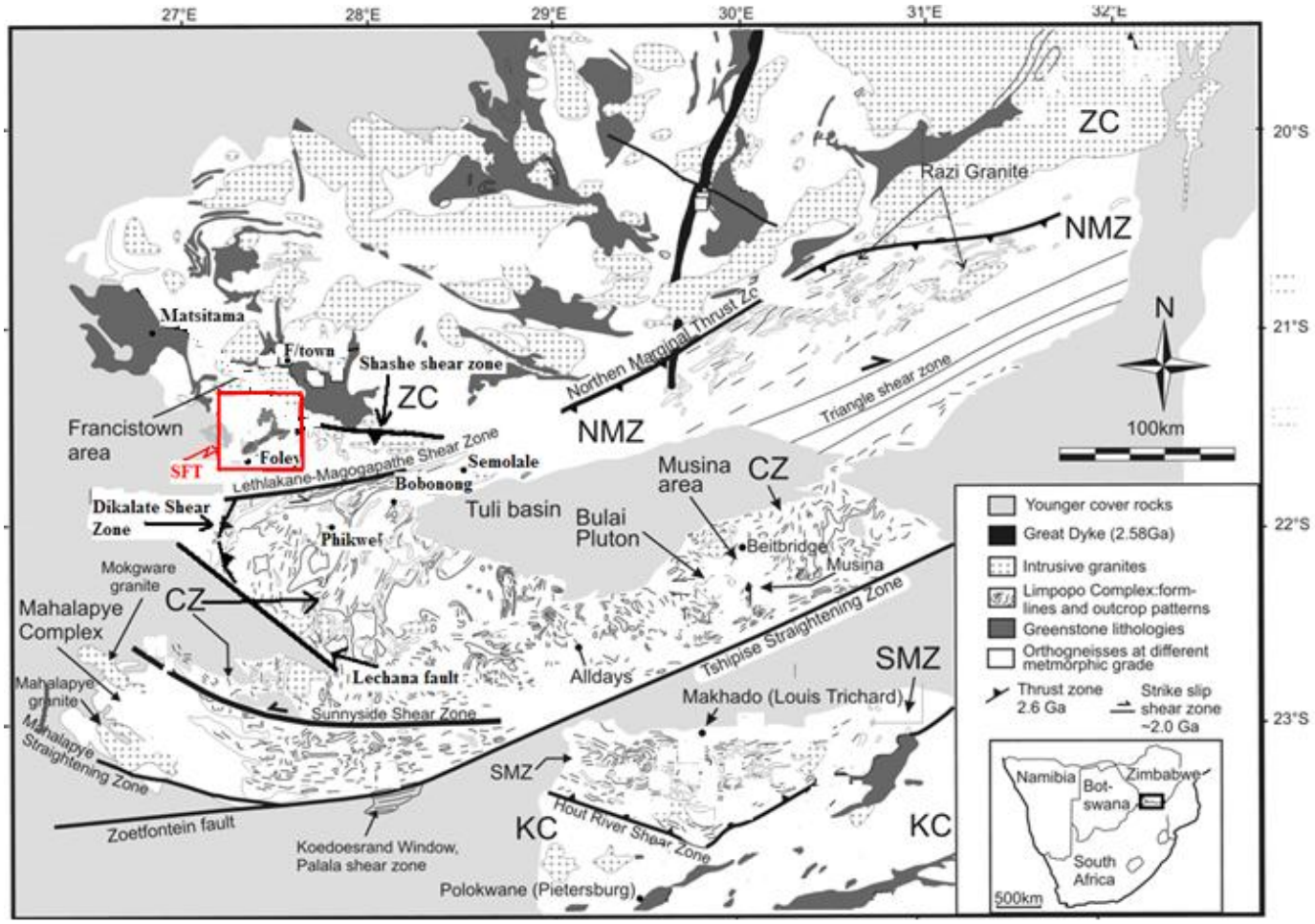

Figure 1.5: Geological map of the Limpopo belt (modified from Kramers *et al.* (2011), Dikalate shear zone from (Paya *et al*., 1997) and the Shashe shear zone from Aldiss (1991).

The 3-fold subdivision of the Limpopo belt has been expanded by the recognition in north-eastern Botswana, of a number of lithostratigraphic complexes (Fig. 1.6, Aldiss, 1991).

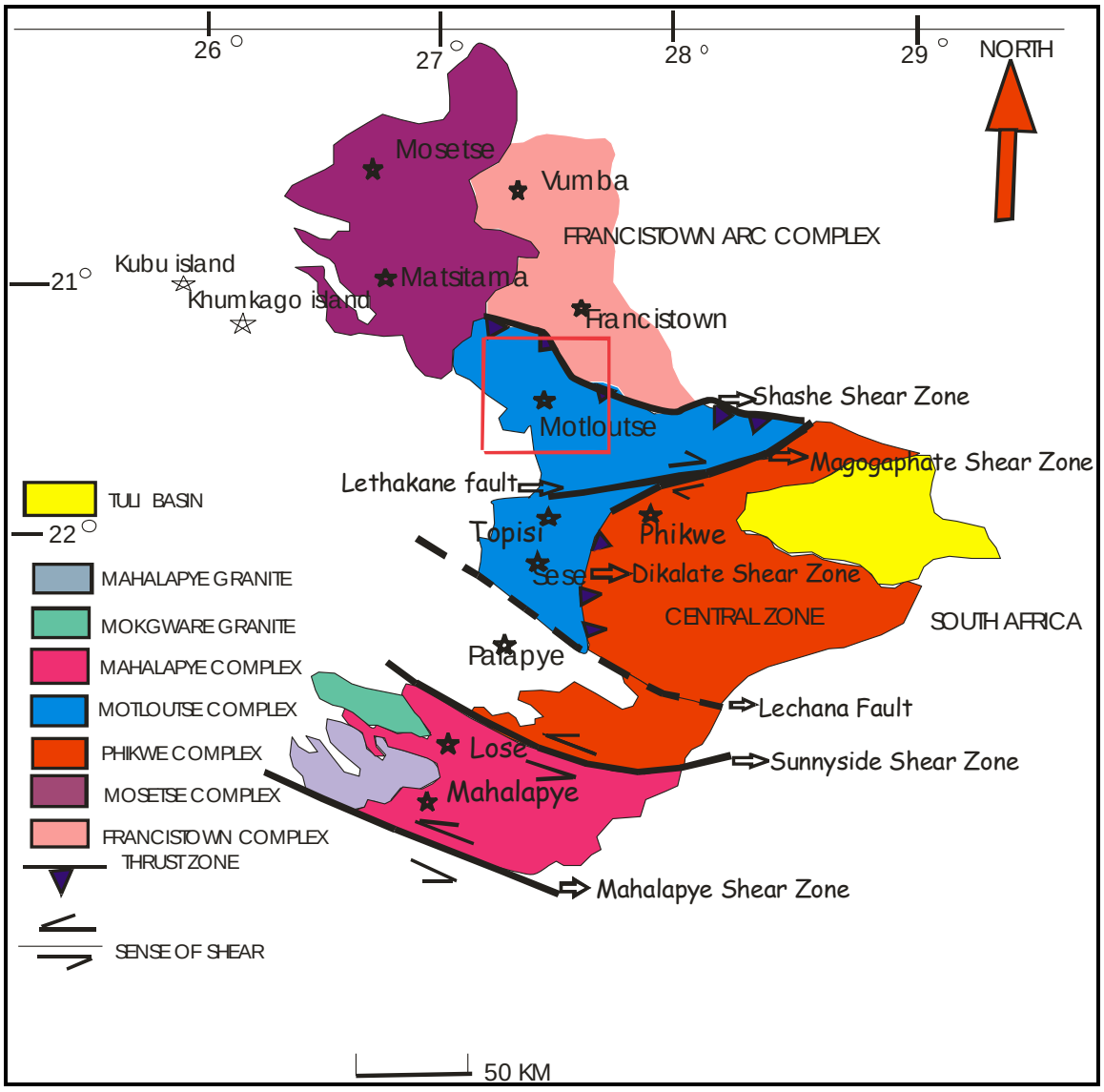

Figure 1.6: **Subdivision of the Archaean Archaean basement rocks in NE Botswana (slightly modified after Aldiss (1991) and McCourt *et al.* (2004). Red square is an outline of study area.**

1.3 RATIONALE FOR THE STUDY

NW-SE trending structures characterize the granite greenstone belts of the southwestern Zimbabwe craton (Aldiss, 1991, Bagai 2008) and adjacent areas previously described as the Shashe belt (Bennett, 1970, Section 1.7). These structural trends also characterize the Matsitama belt. The study area (SFT) is part of the Motloutse Complex and it is an anomalously oriented domain that trends NE-SW. The primary rationale of the current project is to provide an explanation for (or explain) these regionally anomalous structural trends; i.e. to place the kinematics of the SFT area (Motloutse Complex) into the regional framework. McCourt *et al*. (2004) linked the Motloutse Complex to the Matsitama belt (and therefore introduced the term "Matsitama-Motloutse Complex") based on similar rock types particularly the metasedimentary sequence but not on structural grain. It was assumed there was a kinematic link between NE vergent structures in the Matsitama belt and NE trending fabrics in the Motloutse Complex, but this was not explained.

Generally, the subdivision of Archaean crust in NE Botswana is unclear, largely due to complex structural history and debated field geological relationships. The origin, spatial and temporal relationships of this Archaean crust is not well understood. The Shashe area is underlain by Archaean granitoid gneisses and '*complexly'* folded metasedimentary sequences (Carney *et al*., 1994) which form part of the Shashe belt, which have been linked to the Limpopo belt (Ranganai *et al.,* 2002). The '*complexity'* of the folding in the metasedimentary rocks of the Shashe belt has never been investigated. Therefore knowledge about fold geometries is limited. The structural pattern of fold structures in the metasedimentary belt and granitoid gneisses need to be investigated. The depositional age of the protoliths to the metasedimentary rocks and the emplacement age of the protolith to the granitoid gneisses are poorly understood. Earlier work (e.g. Bennett, 1970; Mason, 1973 b; Key *et al.*, 1976; Smith and Phofuitsile, 1985; Aldiss (1989, 1991); Paya, 1996; McCourt *et al*., 2004; Bagai, 2008) in certain selected sectors include limited data on the structural and tectonic evolution of the SFT region. Little is known about the structure and chronology of events in this region, or of the tectonic setting. Structural data are scant and precise geochronology is inadequate. Published age data in the area are very scarce and the results indicate a complex geological history underlining the need for a

systematic well planned geochronological study. Knowledge of the timing of granitoid gneisses and deformation processes is fundamental for understanding the evolution of the SFT region. It is important to recognise and constrain periods of magmatism as well as the geometry and timing of shear zones in the SFT area. A lack of precise age data from this area, particularly U-Pb is a major impediment in constraining the evolution of the area and its regional correlation. The metasedimentary sequences and the gneisses in the area have been correlated on the basis of lithological and structural similarities (Aldiss, 1991) and the few available age data (McCourt *et al*., 2004). The granitoid gneisses have a complex history and the only way to resolve their initial crystallization age and to decipher their subsequent evolution is through high precision U-Pb geochronology and Hf-Lu isotope geochemistry. Field relations between the granitoid gneisses are conflicting since contradictory relationships are reported (Aldiss, 1991). A field based intrusive-relation study is necessary as a follow up on these.

Defining the position of and understanding the nature and geometry of the Botswana section of the Zimbabwe craton-Limpopo belt boundary has long been a question for debate (e.g. Bennett, 1970; Mason, 1973 a; Key *et al.,* 1976; Robertson and du Toit, 1981; Watkeys, 1983; Aldiss, 1991; Paya, 1996; Ranganai *et al.,* 2002, McCourt *et al*., 2004). In addressing this problem, theories and ideas ranged from a transitional boundary (Bennett, 1970; Mason, 1973 a; Key *et al.,* 1976; Robertson and du Toit, 1981 and Aldiss, 1991) to a shear zone boundary (e.g. Bennett, 1970; Key *et al.,* 1976; Robertson and du Toit, 1981; Watkeys, 1983; Aldiss, 1991; Paya, 1996; Ranganai *et al.,* 2002, Mc Court *et al.,* 2004). The Shashe shear zone is described as a NW-SE trending NE vergent dip-slip ductile shear zone that possesses a predominant E-W shear foliation with moderate to steep dips to the S. Rotated porphyroclasts and s-c fabrics along the shear zone indicate S over N movement. The Shashe shear zone considered the tectonic boundary between the Zimbabwe craton and the adjacent Limpopo belt (Paya, 1996; Ranganai *et al*., 2002) or between the Matsitama-Motloutse Complex and the Zimbabwe craton (McCourt *et al.,* 2004) shows northward thrusting of the Shashe section of the Limpopo-Shashe belt (Paya, 1996) or Matsitama-Motloutse Complex (McCourt *et al*., 2004) and has been interpreted as a westward extension of the North Limpopo Thrust

Zone in Zimbabwe (Paya, 1996; Holzer *et al.,* 1999; Ranganai *et al.,* 2002). The northward thrusting is taken to imply a northward transportation of the northeastern Botswana area (Paya, 1996) typical of the North Limpopo Thrust Zone. However, the documented direction of movement on these structures does not easily allow such a link. Displacement on the Shashe shear zone is to the NE whereas displacement in the North Limpopo Thrust Zone is towards NW. Further work is required to check if indeed the Shashe shear zone extends into the study area and establish the geometry and the movement direction defining the SFT section of this boundary. With the present state of knowledge, it is not clear whether the NW-SE trending Shashe shear zone is folded to produce NE-SW striking structural fabric in the SFT region or the NE shears cut across the NW-SE fabric or vice-versa. There is need to map out the field relationship between the NE-SW deformation fabrics (shear zone) and the Shashe shear zone and the timing and shear sense of the structures.

Magmatism and deformation associated with the SW margin of the Tati greenstone belt (Fig. 1.1) is linked to convergent tectonics along the margin of the Zimbabwe craton i.e. an Andean-type scenario (Kampunzu *et al*., 2003; McCourt *et al.,* 2004; Bagai, 2008). Based on geochemistry of the granitoids and related volcanics, the Tati greenstone belt was interpreted to have formed in a marginal arc due to subduction below the crust of the proto Zimbabwe craton. This arc was built on older crust (i.e. overriding plate) and the rocks of the Tati belt are not part of that older crust. Establishing whether SFT region is in the hanging wall of a NE vergent thrust and thus have been thrust over the margin of the Zimbabwe craton or in the footwall of the boundary with the Zimbabwe craton is of great importance in understanding the evolution of the area.

NE-SW directed compression related to southwesterly movements of the Zimbabwe craton (Table 1.4, Aldiss, 1991) would produce NW-SE striking planar fabrics but foliations and fold axes in the SFT region are trend NE-ENE. Aldiss (1991) proposed that during thrusting of the Motloutse Complex against the Zimbabwe craton, the crust forming the Motloutse Complex was highly ductile. This allowed rotation of structural elements e.g. folds into parallelism with the northeastwards movement direction during

NE-SW shearing (flow). It is also important to find evidence to confirm this interpretation and place the kinematics of the Motloutse Complex into the regional framework. To address some of these issues, the Geological Survey of Botswana approved the present study in the SFT region of NE Botswana.

1.4 GOALS

In an attempt to improve the understanding of the basement geology of NE Botswana, the following goals were set:

1. To study the structural geology of the rocks in the SFT region and based on observations draw conclusions about the structural history of the rocks and the kinematics of the deformation features recognised. Geochronology on zircon grains from selected rock types would be used to establish the minimum and maximum age of the deformation events recognised

2. To decide whether the structural and kinematic history of the rocks in the SFT region (Motloutse Complex) correlates best with that of the Central Zone of the Limpopo belt (Phikwe area) to the SE, the Tati granitoid-greenstone terrane (Francistown area) to the N or is different from both.

1.5 KEY QUESTIONS

The present study focused on establishing and clarifying field relationships between the main rock units, using these relationships to identify granitoids and granitoid gneiss that can serve as time markers and obtaining new precise U-Pb age data from these units to constrain the deformation history of the SFT region. To this end the following key questions were addressed and answers to these questions will contribute to the understanding of the crustal evolution of NE Botswana during the Neoarchaean.

- To establish the deformation history of the metasedimentary rocks of the study area

- To study the geometry, age and kinematics of the NE-SW trending zone of deformation fabrics that characterize the granitoid gneisses of the study area

- To establish the relative age relationships between the main types of granitoid rocks in the study area and between the granitoids and the metasedimentary rocks

- To identify suitable time markers in the study area and use U-Pb geochronology on zircon to establish the minimum and maximum ages of the deformation events

1.6 METHODOLOGY

This study was a field-based project involving lithological and structural mapping supported by laboratory work, specifically U-Pb zircon geochronology (Chapter 4) on granitoids and stable isotope geochemistry on carbonate rocks (Chapter 5). Thus a combination of geochronological data with structural and petrological information is used to unravel the evolution of the SFT region. The reliability of existing data was checked and augmented with newly acquired field and geochronological data. A combination of data from aerial photographs and 1: 50 000 ASTER imagery (ERSDAC, 2010) were used to delineate fold structures and photo-lineaments. Structural investigations entail observation and analysis of the major structural elements of the study area, delineation of shear zones, their morphology, evolution and significance. The geometry and the movement direction on shear zones were investigated. Planes have been measured as strike and dip (with strike being the maximum dip-90º) and written as XXXº/XXº. Lineations have been measured as plunge and plunge direction and written as XXº/XXXº. The orientation measurements recorded were taken using a Silva Compus and the Right Hand Rule was applied.

1.7 PREVIOUS WORK

In the sections that follow, relevant published literature and/or internal reports of the Botswana Geological Survey related to the basement geology of NE Botswana are summarized. Gerrard (1963) subdivided metasedimentary rocks in the Foley area (Fig. 1.1) into a Metaquartzite Formation and a Mixed Amphibolite and Metasedimentary Formation. The Mixed Amphibolite and Metasedimentary Formation is described as an association of amphibolite, quartzite, pelite and marble that are individually too thin to be mapped separately. Gerrard (1963) observed that the two formations are metamorphosed and interfolded. This hindered interpretations regarding their stratigraphic relationship. The Metaquartzite Formation was considered to be older than the Mixed Amphibolite and

Metasedimentary Formation but no substantial evidence in support of this interpretation is given. Gerrard (1963) noted that flaggy metaquartzite occurs towards the base of the sequence and that the proportion of quartz-mica schist increases towards the boundary with the Mixed Amphibolite and Metasedimentary Formation. The difference between the types of granitoid gneisses; grey biotite gneiss, porphyroblastic and augen gneiss, and pink granite gneiss was interpreted to be a result of "syn-kinematic feldspathisation and replacement". Gerrard (1963) reported that lithologically similar gneiss units lie stratigraphically above and below the metasedimentary formations.

Cox *et al*. (1965) recognised the widely accepted zoned nature of the Limpopo belt and divided it into a Central Zone characterized by N-S structural trends, flanked by Northern and Southern Marginal Zones (Figs 1.3, 1.5) characterized by ENE regional trends. This zoned subdivision of the Limpopo belt was extended into Botswana as far as the Foley area. Crockett (1968) mapped the Shashe area but only identified lithological units without undertaking detailed structural investigations. Crockett (1968) and Bennett (1970) identified a zone of high grade metamorphism encircling the southwestern part of Zimbabwe craton. The authors suggested a separate Shashe Mobile Belt which wraps around the SW margin of the Zimbabwe craton (Fig. 1.4), lying between the Matsitama and Vumba belts.

There are divergent views on the extent of the Limpopo belt in Botswana due largely to the interpretation of the Shashe belt. The Shashe belt was regarded as a continuation or offshoot of the Limpopo belt consisting of reworked basement (cratonic material) with infolded remnants of metasedimentary cover rocks (Crockett, 1968; Bennett, 1970). Mason (1973) suggested it was the retrogressed equivalent of the Northern Marginal Zone of the Limpopo belt in Zimbabwe. Key *et al*. (1976) rejected the existence of the Shashe belt and interpreted the terrane as a continuation of the Zimbabwe craton that was deformed and metamorphosed at high grade. In more recent literature (Ranganai *et al*., 2002), the Shashe belt is considered to be part of a continuous orogenic belt, the Limpopo-Shashe belt or part of a separate terrane termed the Matsitama-Motloutse Complex (McCourt *et al*., 2004).

Mason (1973) describes the Limpopo belt as an ENE trending granulite gneiss terrane characterized by repeated shear deformation, igneous intrusion and extrusion and viewed it as a zone of crustal weakness throughout geological time. The author observed that the Central Zone of the Limpopo belt is separated from the marginal zones by major shear zones. Mason (1973) divided rocks of the Motloutse area (Fig. 1.6) into "series" namely; arenaceous series, calcareous series, volcanic series, banded gneiss series and granitic series. The division was based on lithological differences with no implication for stratigraphical age. Determination of stratigraphical succession in the area was considered impracticable because of the high grade of metamorphism and polyphase deformation. Mason (1973) suggests that a series of impure arenaceous and calcareous metasedimentary rocks and volcanic rocks of basaltic compositions, were regionally metamorphosed to produce paragneisses, quartzite, marbles, calc-silicate rocks and amphibolite.

Coward *et al*. (1976) report that the Southern Marginal Zone of the Limpopo belt consists of high grade, intensely deformed and metamorphosed TTGs with minor greenstone sequences whereas the Northern Marginal Zone is dominated by enderbite and charnoenderbitic orthogneisses with minor greenstone sequences and granitoid rocks. The Southern Marginal Zone was interpreted to be a reworked counterpart of the northern Kaapvaal craton. Coward *et al*. (1976) interpreted the Northern Marginal Zone as a wide ductile shear zone with about 200 km dextral displacement. The ductile shear zone was extended westwards into the Foley area and therefore the geology of the Foley area was placed in the northern part of the Limpopo belt. However, Key and Hutton (1976) place the Foley area outside the Limpopo belt in the sense that regional scale shearing has died out west of 27° 30E. Coward *et al*. (1976) observed that the metasedimentary rocks within the Limpopo belt have been through the same deformation sequence as those on the craton and appear to be of similar age but different sedimentary facies. According to Coward *et al*. (1976) the tectonic phases affecting the Limpopo belt can be traced into the Zimbabwe craton and the margins of the Limpopo belt are difficult to define.

Key *et al*. (1976) described the Shashe gneiss as a unit composed of granitic augen gneiss and migmatitic gneiss. The migmatite zone was considered to mark the transition zone between the Zimbabwe craton and the Limpopo belt. Key (1976) suggested that the Shashe gneiss is older than the Tati greenstone belt but provide no evidence in support of this interpretation. Barton and Key (1981) and Barton (1983) suggest that the earliest geological events in the Foley area have probably been completely overprinted by the subsequent development of the Limpopo belt, which they linked to plate tectonics processes. Barton and Key (1981) based on gravity data, suggested the presence of a uniform, thick, low density crust in the Foley area and the possibility that that the supracrustal rocks in the Foley area unconformably overlies older basement (Rb-Sr ages of 3600 and 2900 Ma, Hickman, 1978) at depth.

Smith and Phofuitsile (1985) define the geological position of the Foley area as lying in an intermediate position between the Zimbabwe craton and the Limpopo belt. The authors report that in the Foley area, there is no distinction between the Central Zone and the Northern Marginal Zone as defined by Mason (1973) and Key (1976) further east. The Foley area comprises thick meta-arkoses and meta-psammites overlain by a shallow water, continental shelf type, sequence of quartzite and meta-pelites. According to Smith and Phofuitsile (1985), the tectono-metamorphic sequence affecting the supracrustal rocks in the Foley area is in many ways intermediate between the higher grade parts of the Northern Marginal and Central Zones of the Limpopo belt (as described by Key, 1976) and the Zimbabwe craton (Lintern, 1982). McCourt and Vearncombe (1987) contend that the Northern Marginal Zone and the Southern Marginal Zones of the Limpopo belt do not extend into Botswana such that in Botswana, the Limpopo belt is confined to the area between the Magogaphate and the Mahalapye Shear Zones (McCourt *et al.*, 2004, Fig. 1.6).

Published research on the Tati and Matsitama greenstone belts of the Zimbabwe craton and adjacent areas in NE Botswana include papers by Coward and James (1974); Coward *et al*. (1976); Key *et al.* (1976); Smith and Phofuitsile (1985) and Paya (1996). The papers document up to 5 deformational phases that include thrusting, isoclinal folding,

open folding and strike-slip shearing. The main findings are summarised in Tables 1.1, 1.2, 1.4, 1.5 and 1.6. Coward and James (1974) recognised an early NE vergent fold and thrust event (D1) which accounts for the stratigraphic inversion in the Tati and Matsitama greenstone supracrustal belts. The authors report that this event predated intrusion of foliated granitoids in the Tati greenstone belt and development of the regional pervasive foliation fabrics in both supracrustals and granitoid lithologies (D2). The second deformation (D2) structures and fabrics were re-orientated and locally overprinted during D3 and D4. Coward *et al*. (1976) linked the crustal shortening observed in the southwestern margin of Zimbabwe craton to collision, closing of basins, and thrusting of nappes over a region of high heat flow. Key (1976) recognised five (5) phases of deformation in the Tati greenstone belt in the Francistown area, and concluded that although the structural style differs, the same deformational phases also appear in the terrane to the S of the Tati greenstone in the Phikwe area. In support for this interpretation, Coward *et al*. (1976), Key (1976), Key *et al.,* 1976 and Smith and Phofuitsile (1985) suggest that the phases of deformation recognised in the Shashe area generally correspond to those described in adjacent areas, which are themselves basically similar. A comparison of the tectonic histories of the Zimbabwe craton, Limpopo belt and the zone between these terranes (Key, 1976) is given in Table 1.1. The information shown in Tables 1.1 to 1.6 (1.4 excluded) is copied directly from the literature cited.

Smith and Phofuitsile (1985) correlated deformation structures and metamorphism in the Foley area as shown in Table 1.2.

Table 1.1: Comparison of tectonic histories between Zimbabwe craton, the Limpopo belt and the transition zone between them. Slightly modified from Key (1976). F1-5 represents folding phases related to D1-D5

EVENT	Tectonic domain		
	Zimbabwe craton	**Transition zone**	**Limpopo belt**
F1	Upright isoclinal folding; weak cleavage	Isoclinal folding	Recumbent isoclinal folding
F2	Minor isoclinal folding, shearing, schistosity and sub-vertical lineation	Major isoclinal folding, shearing, schistosity and steeply plunging lineation	Upright isoclinal folding; major dextral shearing, cataclastic fabrics
F3	Minor folding	Refolding of F2 isoclines; dextral shearing	Refolding of F2 isoclines, dextral shearing; cataclastic fabrics.
F4	Not recognised	Semi brittle dextral shearing	Semi brittle dextral shearing
F5 (F4 of craton)	Monoclinal folding about 130°; crenulation cleavage.	Warping about 130°; crenulation cleavage.	Localized asymmetric folding about 120°
"Late events"	**Subsequent events restricted to orogenic waning processes i.e. minor open warping; semi-brittle shearing**		

Table 1.2: A synthesis of the structural and metamorphic histories in the Foley area, copied from Smith and Phofuitsile (1985). S1, 2 and L1, 2 represents foliation and lineation respectively

D1	Fold nappes/thrusts , NW-SE trend Development of (S1) and (L1)	Lower amphibolite facies, staurolite cores, S1mica alignment, and coarsening of foliation (S1) fabric. Continued staurolite, garnet and kyanite growth in pelite. Migmatisation in rocks with granitoid composition
D2	Isoclinal folding, NE-SW trend, curvilinear, change in facing, local mylonites	Some rotation of S1 into S2. Continued growth of staurolite, kyanite and garnet. Deformation of migmatites, mobilization of anatectic granite magma and syn-tectonic to post-tectonic intrusion. Influx of heat, growth of cordierite and sillimanite in meta-pelites. Local felspathisation of pelites. Intrusion of metadolerite dykes
D3	Overturned tight to open folds, NE-SW trend, some interference, Plunge NE to SW. Minor shearing	Development of crenulation cleavage locally Assemblage hornblende+andesite in metadolerites Recystallization of muscovite, biotite. Local growth of biotite and staurolite
D4	Local, close and open folds, N-S trend, plunge S.	Local kinks in micas, Growth of chlorite, epidote, actinolite, quartz often if fractures and veins.
Later	**Cataclasites, Faulting**	**Epidote, quartz, chlorite in fractures**

In addition to the general references sited above, there are a number of publications that focus on the tectonic framework of NE Botswana. According to Aldiss (1989) the Shashe area is located about 50 km NW of the Limpopo belt and lies in the most southwesterly exposed portion of the Archaean Zimbabwe craton. Within Botswana Aldiss (1989) restricted the Limpopo belt to the region of granulite facies metamorphism around Phikwe area (Fig. 1.6). No granulites were identified in the Shashe area. The terrane underlying the Shashe area was therefore not regarded as part of the Limpopo belt but was considered a zone of reworked Zimbabwe craton. Following McCourt and Vearncombe (1987)'s observation that subdividing complex orogenic belts into domains of unique character is an important approach in their description and interpretation, Aldiss (1991) divided the Archaean crust of NE Botswana into a number of lithostratigraphic complexes, each of which exhibit distinct characteristic features with respect to rock assemblages, relationships between metasedimentary belts and the granitoid gneisses that surround them as well as the type and nature of mineralization, metamorphism and structural style. The complexes defined by Aldiss (1991) are; the Francistown Granite Greenstone Complex, the Mosetse Complex, the Motloutse Complex, the Phikwe Complex and the Mahalapye Complex (Figs 1.6 &1.7). The Francistown Granite Greenstone Complex represents the southwesternmost exposed portion of the Zimbabwe craton in Botswana (Aldiss, 1991; Francistown Arc Complex of McCourt *et al.,* 2004; Bagai 2008). The Phikwe and the Mahalapye Complexes form part of the Central Zone of the Limpopo belt in Botswana (Aldiss, 1991). The Mahalapye Complex defines the southwestern edge of the Central Zone in Botswana. There is general consensus that it formed by reworking of the granulites of the Central Zone at ~ 2.0 Ga (e.g. McCourt *et al.,* 2004). The recognition of these complexes suggests a component of crustal accretion in the growth of the Zimbabwe craton and Limpopo belt during the Archaean. The main features of these complexes are summarised in Table 1.3.

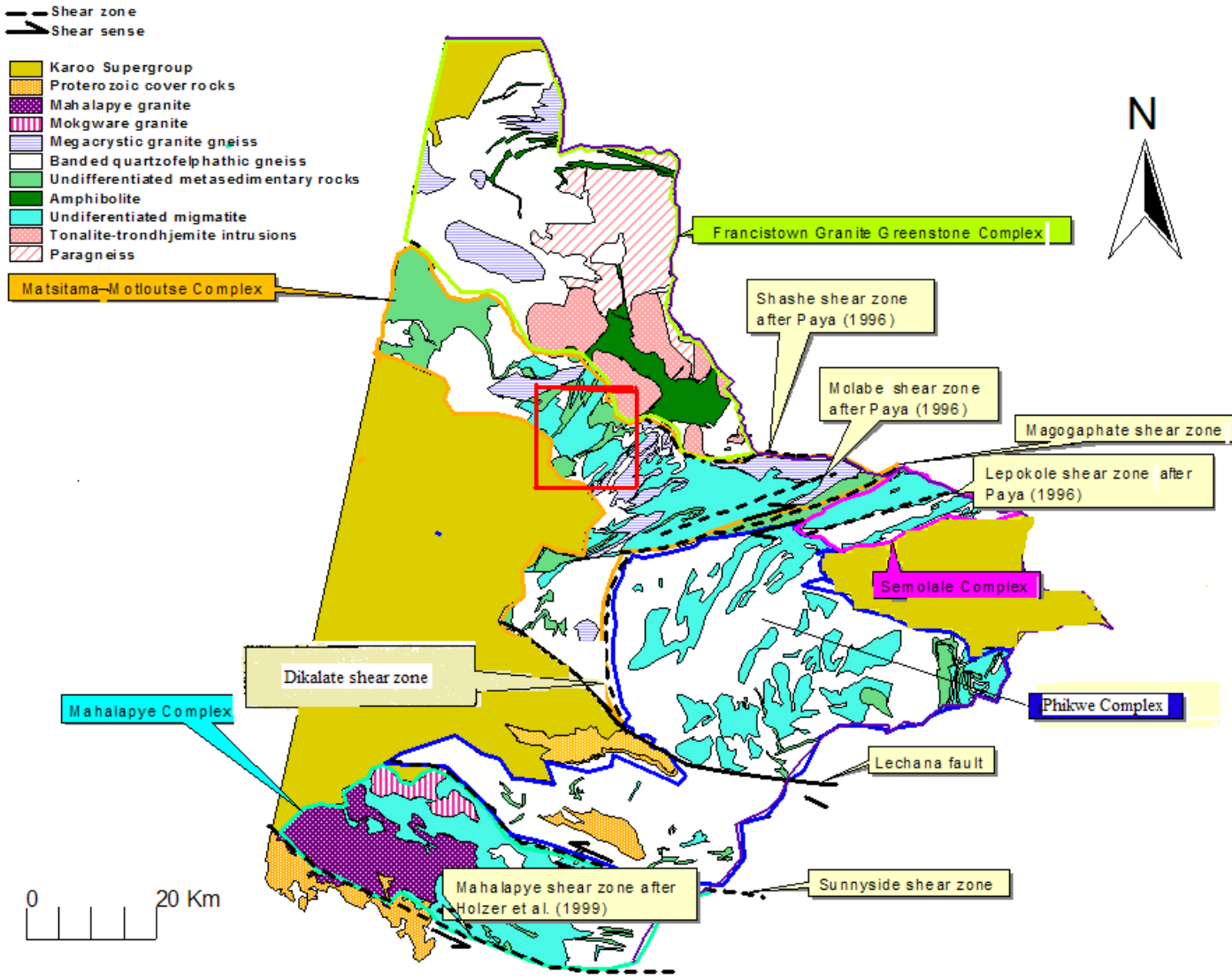

Figure 1.7: Subdivisions of the Archaean basement rocks in NE Botswana (Geology after Key (1976); Aldiss (1991); Carney *et al*., (1994); McCourt *et al*. (2004) and Bagai (2008). Red square represents study area. Shashe, Molabe, Lepokole shear zones after Paya (1996), Mahalapye shear zone after Holzer *et al* (1999).

Table 1.3: Summary of lithostratigraphic complexes in NE Botswana. Information compiled from: Bennett, 1968 a and b (1) ; Hickman, 1978 (2); Lintern,1982 (3); Aldiss, 1983 (4); Cahen *et al.*, 1984 (5) ; Aldiss, 1991 (6); Majaule, 1993 (7); Carney *et al.*, 1994 (8); *Key et al.*,1994 (9); Paya, 1996 (10); Majaule *et al.*, 1997 (11); Majaule and Davis, 1998 (12); McCourt and Armstrong, 1998 (13); Kroner *et al.*, 1999 (14); Holzer *et al*, 1999 (15); Majaule, 1999 (16); Bagai, 2000 (17); Chavagnac *et al.*, 2001 (18); Bagai *et al.*, 2002 (19); Kampunzu *et al.*, 2003 (20); McCourt *et al.*, 2004 (21); Zhai *et al.*, 2006 (22); Zeh *et al.*, 2007 (23) ;Bagai, 2008 (24); Millonig *et al.*, 2010 (25), Van Reenen *et al.*, 2011 (26)

Terrane	***Zimbabwe craton***				***Limpopo belt***		
Complex	*FGGC (6) (Francistown Arc Complex, 21)*	*Mosetse Complex (6)*	*Motloutse Complex (6)*	*Matsitama-Motoutse Complex (21)*	*Phikwe Complex (6)*	*Mahalapye Complex (6)*	*Semolale Complex (6) & (8)*
Granitoids	Foliated TTG gneisses, subordinate late kinematic granodiorite, monzonite &granite (17) & (20) Sanukitoids (High Mg granitoids); (22), (24).	Tonalitic to granodiorite TTG orthogneisses, leucocratic biotite bearing Jankie gneiss (6)	Grey orthogneiss, foliated tonalitic gneiss, megacrystic granite gneiss and granite, (7), (8) leucogneisses , Tonota biotite gneiss (6).	As in Motloutse and Mosetse Complexes, (7) & (20).	Paragneisses, banded quartzo-felspathic gneisses, anorthositic gneiss, minor ultramafic rocks and gneissic granite (4) & (9).	Mahalapye migmatite, syn-tectonic Mokgware granite & post-tectonic Mahalapye granite (6) (15) and (23)	Migmatites, coarse granites and granitic gneisses, including augen gneisses, minor charnokites (4) & (8)
Supracrustal rocks	Mafic and ultramafic metavolcanic rocks, overlain by intermediate to felsic rocks and minor metasedimentary rocks (6a) (8),(9),(19)	Matsitama metasedimentary Group: Quartzite, marble, metapelite & minor BIF, Matsitama belt (1a and b), (3), (7) and (11).	Shashe metasedimentary Group: quartzite-carbonate-pelite association; amphibolite *(6)*	Felsic metavolcanic rocks and metasedimentary rocks (21)	Abundant paragneisses and amphibolites; minor carbonates (4) and (9)	Xenolith of foliated amphibolite & paragneiss in migmatite (6) & (9)	Basic to ultrabasic amphibolite minor Fe-quartzite (8)
Metamorphism	Greenschist-amphibolite ,High grade at 2639 ± 7.9 Ma (24)	Greenschist and Amphibolite facies (8).	Amphibolite facies with anatexis (6), Upper Amphibolite (21)	Amphibolite facies (21)	Upper amphibolite and granulite, (6) & (21)	High grade; 2045-2035Ma (25).	Amphibolite to granulite; 2870 & 2600 Ma (2), (5), (6) & (8)

Table 1.3 continued

Terrane	*FGGC (Francistown Arc Complex)*	*Mosetse Complex*	*Motloutse Complex*	*Matsitama-Motoutse Complex*	*Phikwe Complex*	*Mahalapye Complex*	*Semolale Complex (NMZ)*
Geological setting	Continental margin arc, Andean type convergent margin (20), (21) & (24), subduction signature at 2.7Ga (21)	subduction zone magmatism; Back arc environment (11) Oceanic basin (6) shelf-type association (6)	Convergence tectonics NE subduction below the proto Zimbabwe craton at 2.66-2.50 Ga (21).	Accretionary assemblage, subduction occurring at 2.7 Ga and Age of accretion 2.65 Ga; continental margin-type supracrustal association; Andean type tectonics (21)	Central Zone could have been the shelf + accretionary prism on the leading edge at 2.7-2.65 Ga (lots of clastic sediments, some old detrital zircons in these)- (26).	SE subduction-2.06 Ga, back-arc spreading. Underplated & intruded by mantle derived mafic melts; 2.06 & 2.04 Ga, (25). Age; 2023 ± 7 Ma, (21)	**NMZ: magmatic arc-eastward continuation of the Francistown Arc Complex, (26)**
Type of contact between supracrustals and granitoids	Intrusive plutons enclose supracrustal belt; contacts tectonised, (6) & (8)	Supracrustal rocks either interlayered or intruded by enclosing gneisses, (6) & (8)	Thrusts or ductile shear zones, (6) & (8)	Thrusts or ductile shear zones (this work)	Deformed contacts; combination of all other types, (6) & (8)	None	**Deformed contacts; combination of all other types, (6) & (8)**
Strike of foliation	**NW to NNW, steep dips, (6) & (8).**	**N to NE, varying dips, (6) & (8). (excludes rocks of the Matsitama belt)**	**NNE to NE, steep dips ENE in SE, (6) & (8).**	**NW-SE (21)**	**ENE in Phikwe & N-S in the southern part (21), varying dips, (6) & (8).**	**WNW, moderate to steep dips to the NE, (6) & (8).**	**ENE, steep dips, (6) & (8).**

Table 1.3 continued

Terrane	***FGGC (Francistown Arc Complex)***	***Mosetse Complex***	***Motloutse Complex***	***Matsitama-Motoutse Complex***	***Phikwe***	***Mahalapye Complex***	***Semolale Complex (NMZ)***
Plunge of lineation	S and SW, steep, (6), (8) & (21).	SSW to SW, gentle (L very strong, (6) & (8) & (21)	SSW or NNE, gentle to moderate ((6) & (8).	SW, (21)	E to ESE in the N and steeply SE in the south. Gentle to steep, (6) & (8).	N, steep except in shear zones (9). WNW (15)	**ESE, gentle to moderate, (6) & (8)**
Age	2700-2600Ma				2870-2600 Ma		**2870-2600 Ma**
Mineralization	**Au (Ag), Ni-Cu, (Cr), (W); (6) & (8)**	**Cu, Cu-Zn-Pb (Ag); (6) & (8)**	**Cu (Au), Cu-Pb-Zn (Au), (6) & (8)**	**Cu, Cu-Zn-Pb (Ag), Cu (Au), (6) & (8)**	**Ni-Cu, (Cr), (6) & (8)**	**Cu (6) & (8)**	**None recognised (6) & (8)**

Aldiss (1991) working in the Shashe area reports that Matsitama-type metasedimentary rocks (i.e. similar to those in Matsitama belt (Fig. 1.1) and granitoid gneisses are inter-layered along southwest dipping thrust sense shear zones. The shear zones are characterized by foliated augen gneisses bearing an upright mineral elongation lineation. In keeping with this observation, Key *et al.* (1994) recognised early NE vergent folds and thrusts refolded along NE trending axial surfaces and associated with a southwest plunging mineral elongation lineation in the Topisi area (Fig. 1.6). Aldiss (1989) reports that in the Shashe and Tonota areas the metasedimentary rocks and adjacent granitic gneisses are both highly foliated, with mylonitised fabrics developed along and adjacent to the contacts.

The boundary with the Francistown Granite Greenstone Complex is shown by the change in regional strike of planar fabrics from NW-SE in the Francistown Granite Greenstone Complex to N to NNE in the Motloutse Complex (Aldiss, 1991, Table 1.3). According to Coward *et al.* (1976) and Key *et al.* (1976) the metasedimentary rocks in the southwestern part of the Zimbabwe craton were subjected to the same deformation as the enclosing gneisses. In support of this Aldiss (1991) proposed that the metasedimentary rocks from Matsitama belt were incorporated into migmatites of the Motloutse Complex during northeasterly thrusting. The detached portions of the supracrustals are nowhere seen to be thrust over the migmatites in the Motloutse Complex. Aldiss argues the detached portions of the supracrustal rocks are in thrust contact with the granitoid gneisses. Aldiss (1991) suggests that the granites were emplaced syn-tectonically, as intrusive sheets along thrusts contacts separating the metasedimentary rocks and the granitoid gneisses. Aldiss (1991) concluded that the Motloutse Complex formed due to convergence between the Zimbabwe craton and a structural segment to the southwest. The metasedimentary rocks in the postulated terrane to the southwest were thrust northeastwards over the margin of the Zimbabwe craton. This resulted in crustal thickening and high heat flow that promoted migmatisation, anatexis and ductile deformation. Sheets of anatectic granite were intruded syn-kinematically along thrust zones. The overthrust metasedimentary rocks were infolded with the underlying migmatites and gneiss. The protolith to the gneisses that surround metasedimentary belts in the Matsitama and Motloutse Complexes is unknown. The gneisses are a product of ductile deformation under high grade metamorphic conditions. Nevertheless, many of the gneisses have been interpreted as metamorphosed supracrustal lithologies dominated by felsic metavolcanics and metasedimentary rocks. Thus they have been considered to be of both sedimentary (Key *et al.*, 1976) and volcanic (Majaule and Davis, 1998; Aldiss, 1989) origin. Aldiss (1991) deformational episodes in the Motloutse Complex are summarized in Table 1.4.

Key *et al.* (1994) working in the Topisi area established that the Central Zone of the Limpopo belt has a western limit which coincides with the concave east arcuate trace of the extended Magogaphate shear zone. The area to the W and NW of the Magogaphate shear zone was named the Western Zone of the Limpopo belt, an area that coincides with

Aldiss (1991)'s Motloutse Complex. According to Key *et al.* (1994) the Western Zone of the Limpopo belt was characterized by repeated oblique and head-on collision between the Central Zone and the Zimbabwe craton and was interpreted as a "tectonically modified imbricate system". Key *et al*. (1994) recognised a sequence of events based on superposition of different generations of planar and linear structures. Large scale folds were interpreted as products of early ductile thrusting. The area is characterized by N-S trending folds some of which refolded to define interference patterns shown by different metasedimentary rocks e.g. at Sesweu hill. The metasedimentary rocks define N-S trending folds interpreted to be fold interference patterns due to F3 refolding of F2 structures.Key *et al*. (1994) note that the metasedimentary rocks are dominated by quartz and quartz-mica schist with subordinate amphibolite, marble and calc-slicates. These rocks are spatially associated with grey gneiss regarded as paragneiss, augen gneiss, ultramafic rocks and anorthosites. The relationship between the metasedimentary rocks and the granitoid gneisses is not clear but evidence suggests that they are sheared.

According to Key *et al*. (1994) the first deformation recognised in the Topisi area was a gneissification process defined by mineral layering in granitoid rocks. The formation of the gneissic fabric preceded deposition of the metasedimentary rocks based on the observation that the metasedimentary rocks do not have that gneissic fabric. Key *et al.* (1994) suggested the presence of an older basement to the metasedimentary rocks. The second deformation (D2) is represented by development of early NW-SE trending regional folds (implying north-eastward direction of thrust). These D2 folds are characterized by a strong down-dip lineation in quartzite that plunges to the southwest and SW-NE plunging lineation in the granitoid gneisses. This is succeeded by a D3 phase that produced N-S to NE-SW trending folds that plunges towards NE. The D3 phase generated interference folds e.g. at Sesweu Hill.

Table 1.4: Summary of regional deformation in the Motloutse Complex. Tabulated from Aldiss (1991).

Deformational Phase	
D1	**Inversion of Tati belt and parts of the Matsitama belt metasedimentary rocks by NE verging recumbent folding and thrusting (Litherland, 1975; Coward and James, 1974; Key *et al.*, 1976; Aldiss, 1991)** **Thrusting and nappe formation**
D2	**Considered the main fabric producing event (Litherland, 1975; Coward and James, 1974; Key *et al.*, 1976 and Aldiss, 1991; Paya 1996). Maximum compressive stress sub-horizontal and trending NE-SW (Key *et al.*, 1976). NE-SW compression in response to SW movement of the Zimbabwe craton relative to the Limpopo belt after thrust emplacement of the Matsitama-type metasedimentary rocks in the Motloutse Complex, formation of NE folds with NE-SW trending axial surface possibly with large-scale movement-parallel folds developed from northeasterly verging isoclines and syn-tectonic granites intruded along thrust zones (Aldiss, 1991). Tati greenstone belt shortened by 60% (Coward *et al.*, 1976).**
D3	**NW-SE compression leading to upright northeasterly trending folds, dextral strike-slip movements on southeasterly trending shear zones in the Tati belt and deformation at the boundary between Motloutse Complex and the Francistown Granite Greenstone Complex (Aldiss, 1991).**
D4	**NNW-SSE compression leading to development of dextral Magogaphate Shear zone and associated frontal thrust system caused by westerly motion in the Limpopo belt relative to Zimbabwe craton, rotation of D3 fold axis (Aldiss, 1991; Paya, 1996).**

The fourth deformational phase (D4) is characterized by ductile shearing while the fifth (D5) is associated with development of NW-SE open folds and crenulation structures (Key *et al.*, 1994). A summary of the deformational history of rocks in the Topisi area is given in Table 1.5.

Table 1.5: A summary of the relationship between deformation and metamorphism in the Topisi area (Key *et al*., 1994).

EVENT	GENERATED STRUCTURES	ACCOMPANYING METAMORPHISM	AREAL EXTENT
D1	Gneissosity in granitoid gneisses and possibly some hornblende gneisses.	Granulite to Upper Amphibolite Facies	Regionally uniform
D2	Gneissosity in anorthositic and amphibolitic intrusive rocks; migmatisation within granitoid gneisses; foliation in metasedimentary rocks; recumbent folds, intrafolial folds, thrusting (northeast directed), intersection and extensional lineation.	Granulite to upper Amphibolite Facies	Regionally uniform
D3	Upright folds with N-S to NE-SW axial traces and moderate plunges mostly northwards. Foliation, lineation, ductile shearing. Generation of interference folds notably at Sesweu Hill.	Amphilbolite Facies.	Regionally uniform
D4	Major ductile shearing. Local development of a new gneissosity and mineral lineation.	Greenschist or Amphibolite Facies	Extensive
D5	NW-SE trending open folds and crenulations. Local development of a new cleavage	Greenschist facies	Locally developed

Paya (1996) working in the Bobonong area (Figs 1.1 and 1.5) including the area to the N of Magogaphate Shear Zone (Motloutse Complex) recognised 5 deformational episodes, each of which was associated with a period of intrusion and related metamorphism. The established relationship between deformation, metamorphism and magmatism recognised by Paya (1996) is shown in Table 1.6.

Table 1.6: Relationship between deformation, metamorphism and igneous activity in the Bobonong area (from Paya, 1996). M1-M5 represents metamorphic events related to deformational sequences (D1-5).

	Deformation	***Metamorphism***		***Ultramafic and mafic intrusions***
D1	Recorded by intrafolial folds and ghost isoclinal fold limbs	M1	Granulite facies metamorphism of supracrustal gneisses and associated mafic and quartzofeldspathic gneisses (not observed in the Bobonong area). See Key, 1976; Barton and Key, 1981). Ultramafic remnant assemblage?	Banded gneiss protolith, Swejane granitic gneiss? Ultramafic intrusions? Basic tholeiitic dykes? Tobane gneiss?
D2	Regionally developed foliation. Trends NNE-SSW. Tight isoclinal fold. Overprints the D1 fabric	M2	Metamorphic banding concordant with D2 foliations. High grade metamorphism to produce most of the presently widespread metamorphic mineral assemblages. Migmatisation accompanied M2. Granulite facies were attained in some areas (recorded in the ultramafics and probably in the Lepokole granite enclaves).	Emplacement of granodioritic dykes in the Swejane granitic gneiss. Emplacement of pre-Lepokole intrusion granulitic batholith.
D3	Extension crenulation cleavage, associated with minor shear zones. Trends ESE-WNW. Open folds showing NNE-SSW trending fold axis	M3	Medium to high grade retrograde metamorphism. Alteration of M2 assemblages: clinopyroxene-biotite. Growth of biotite along crenulation cleavages. Migmatisation along minor shears of D3 extension crenulation	Emplacement of the Shashe and Lepokole granites. Emplacement of mafic and intermediate dykes in the Lepokole granite.

Table 1.6 continued. M1-M5 represents metamorphic events related to deformational sequences (D1-5)

Deformation		***Metamorphism***		***Granite, ultramafic and mafic intrusions***
D4	Development of major shear zones in the area (Magogaphate, Lepokole, Molabe and Shashe shear zones). Trends vary from ENE-WSW, to E-W. Development of the F4 folds which show NE-SW general fold axis trends.	M4	Medium to low grade retrograde metamorphism. Alteration of M2 and M3 mineral assemblages; Olivine and pyroxene-serpentinite; Hornblende-tremolite & actinolite; biotite-muscovite; plagioclase-epidote. Quartz and feldspar (microcline and plagioclase) straining.	An intrusion of late granite dykes in the Shashe and Lepokole granites. Pegmatitic and aplitic veins marking the culmination of granitoid magmatism in the Bobonong area.
D5	Late minor shears, exhibiting brittle deformation	M5	Low grade hydrothermal alteration: hornblende and biotite- chlorite; plagioclase-sericite	Emplacement of the Pre-Karoo (Proterozoic) dolerite dykes and sills. Emplacement of Karoo and post-Karoo dykes and sills.

Recent ideas on the Limpopo belt include Ranganai *et al.* (2002). Ranganai *et al*. (2002) adopt a different definition of the Limpopo belt. The latter include terranes that are not at granulite facies metamorphism and by so doing ignore the rationale of Aldiss (1991) for excluding the Shashe area from the Limpopo belt. Ranganai *et al.* (2002) based on an interpretation of new gravity data redefined the regional extent of the Limpopo belt and regarded the area between the Shashe shear zone in the N and the Lechana fault (Figs 1.6, 1.7 and 1.8) in the south as part of the Shashe belt. The Shashe belt was interpreted as an extension of the Limpopo belt and the same 3-fold division used for the Limpopo belt

was applied to the Shashe belt. In the model of Ranganai *et al*. (2002) the Limpopo-Shashe belt was defined as an arc shaped structure along the southern and south western margin of the Zimbabwe craton and the Shashe shear zone was interpreted as the boundary between this orogenic belt and the southwest margin of the Zimbabwe craton.

Based on similarity in ages of detrital zircon ages from quartzites, and also on a similar structural pattern characterized by NE verging folds, thrusts and ductile shear zones in the Matsitama and Topisi area (part of Motloutse complex), the southern part of the Mosetse Complex, including the Matsitama belt was combined with the Motloutse Complex into a single terrane that lies adjacent to the Francistown Arc Complex, and named the Matsitama-Motloutse Complex (Figs 1.7 and 1.8, McCourt *et al.,* 2004). In this interpretation, the northern boundary to the Matsitama –Motloutse complex was the Shashe shear zone a structure also recognised by Ranganai *et al*. (2002). However there is a difference in the two interpretations. Ranganai *et al*. (2002) interpret the Matsitama-Motloutse complex as the northern marginal zone to the Shashe section of the Limpopo-Shashe belt. McCourt *et al.* (2004) regard it as part of an accretionary complex distinct from the Limpopo belt. The only agreement being that the Shashe shear zone forms the northern boundary with the Zimbabwe craton. McCourt *et al.* (2004) based on geochronology and geochemistry of tonalitic rocks in Mosetse settlement (Majaule *et al.*, 1997) and Vumba belt (Bagai *et al.,* 2002) interpret the northern part of the Mosetse Complex as a continuation of the Francistown Arc Complex (Fig. 1.8).

By use of U-Pb zircon data from Khumkago Island, gneisses exposed southwest of Matsitama Village (Figs (1.8) that record Neoarchaean-tectono thermal activity (Majaule and Davis., 1998), McCourt *et al.* (2004) extended the Archaean crust of NE Botswana to the west as far as Khumkago Island (NW part of Fig. 1.8). McCourt *et al*. (2004) demonstrated that the metasedimentary sequences within the Matsitama-Motloutse Complex were deposited between 2661 and 2647 Ma with the provenance being the Francistown Granite Greenstone Complex and the regions behind it. This conclusion is at variance with a previous suggestion (Key, 1976) that the Shashe gneiss is older than the Tati greenstone belt. McCourt *et al*. (2004) suggested a NE- directed subduction below

the Zimbabwe protocontinent at 2.65 Ga, with the Matsitama-Motloutse Complex as part of the lower plate. The inferred subduction accretion tectonics involved the Matsitama-Motloutse Complex as the accreted terrane and the Francistown Arc Complex representing the overriding plate (McCourt *et al*., 2004).

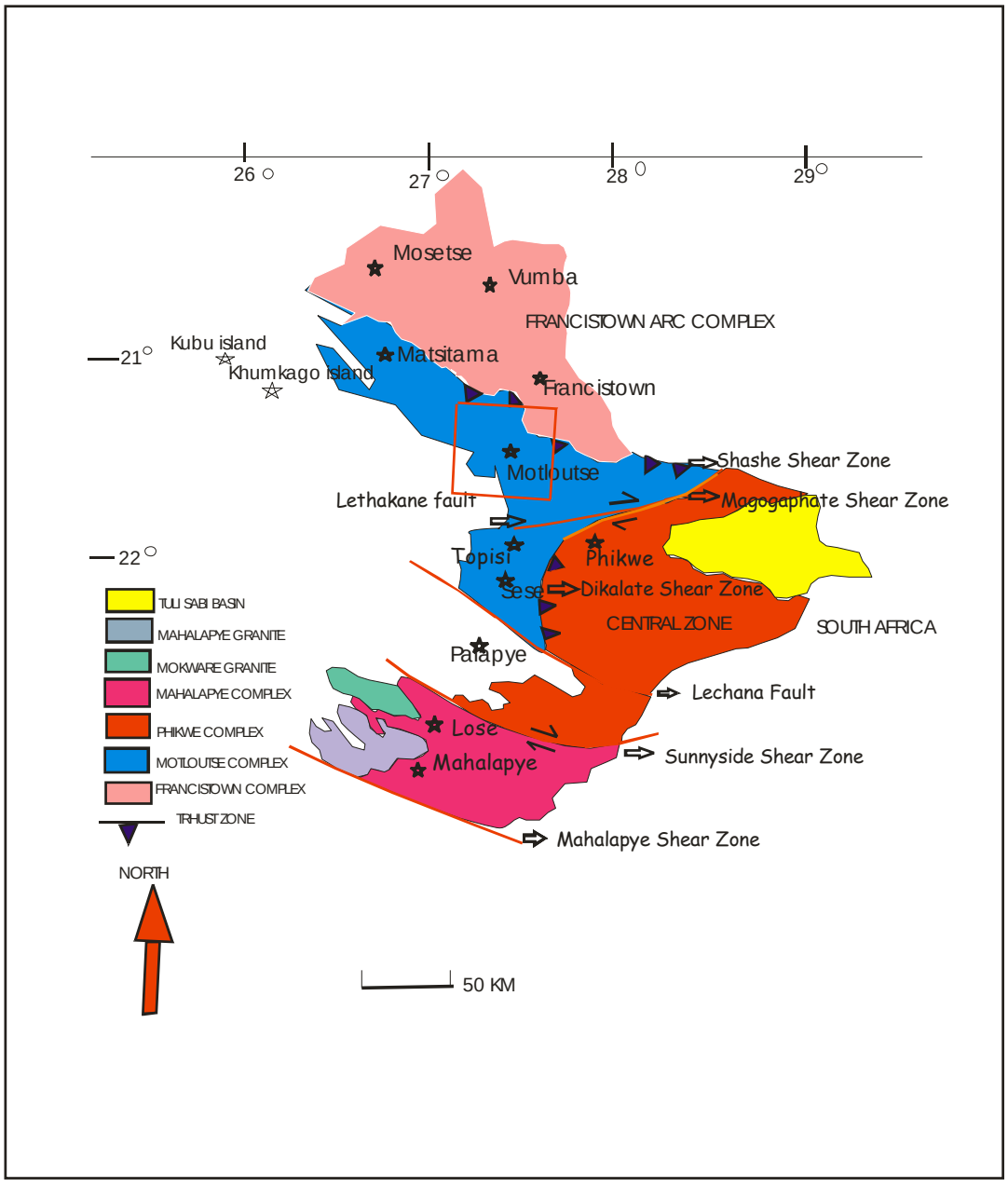

Figure 1.8: McCourt *et al.* (2004)'s subdivision of Archaean crust in NE Botswana (slightly modified). Geology from: Key (1976), Aldiss (1991) and Paya (1996). N.B the northern part

of Mosetse Complex is combined with the Francistown Arc Complex. Red rectangle indicates position of study area.

Accretionary tectonics involving the Matsitama-Motloutse Complex moving towards the southwestern margin of the Zimbabwe craton occurred between 2661Ma and 2647Ma. McCourt *et al.* (2004) further concluded that the Francistown, Phikwe and Matsitama-Motloutse Complexes were assembled and juxtaposed during the Neoarchaean in response to Andean-type convergent margin accretion tectonics along the southwestern margin of the Zimbabwe craton. The idea of the Matsitama-Motloutse Complex is at variance with Bagai (2008)'s view that the Francistown Granite Greenstone Complex is a large arc complex which also encompasses the Matsitama belt on the western side of the Vumba greenstone belt.

Published geotectonic interpretations of the Zimbabwe craton in Botswana focused on petrogenesis (geochemical), geochronological and tectonic setting with little emphasis on structure (e.g. Bagai *et al*., 2002; Kampunzu *et al.,* 2003). Majaule *et al*. (1997) suggested that the Matsitama belt formed in a back-arc environment by extensional tectonics during rifting at the margin of the Zimbabwe craton. The evolution of the Zimbabwe craton is linked to an Andean-type convergent margin (continental margin arc) and related thrusts and sedimentary belts related to northward directed subduction which occurred within the Limpopo-Shashe area between 3.8 and 2.65 Ga (Kampunzu *et al*., 2003; Bagai *et al*., 2002). In support of this, McCourt *et al*. (2004) suggested NE directed subduction below the Zimbabwe proto-continent at 2.65 Ga, with the Matsitama-Motloutse Complex as part of the lower plate The latter scenareos are not mutually exclusive. The arc behind which Majaule *et al*. (1997) put the Matsitama basin could have been the Francistown Arc. The difference lies in position of the Matsitama basin relative to this arc i.e. behind the arc as proposed by Majaule *et al*. (1997) or outboard of the arc as proposed by McCourt *et al*. (2004).

Jelsma and Dirks (2002) argue for a magmatic arc along the NW margin of the proto-Zimbabwe craton with associated SE directed subduction. The down-going slab would have been located to the NW of the Zimbabwe craton.

Bagai (2008) proposed that the downgoing slab was located in the Limpopo-Shashe belt and the overriding plate was the Tokwe continental crust (in Zimbabwe) and related blocks. TTG and sanukitoid suites display continental subduction zone signatures. Hf and Nd-isotopes from the Francistown Granite Greenstone Complex suggests a magmatic arc setting (Bagai, 2008). In addition, the production and emplacement of voluminous TTGs to sanukitoids and K-granites at ~2.7-2.6 Ga in the southern margin of the Zimbabwe craton is taken to indicate a shift from a flat subduction (for the production of TTGs) to a steep subduction (for the production of younger sanukitoids) and subsequent break off and detachment of the slab (Kampunzu *et al*., 2003; Bagai, 2008 and Fig. 1.9). The production of TTG rocks is related to partial melting of mafic igneous rock underplated in the lower crust (lower angle subduction), the sanukitoids (diorites and gabbros) are linked to partial melting of a sub-arc mantle wedge enriched in silica during ascent of the TTG rocks and the young K-granites resulted from partial melting of the TTG material. The detachment allowed hot mantle to rise up, melting earlier TTGs to produce the K-granites. Bagai (2008) observed an increase in the intensity of deformation fabric from the Tati greenstone belt, towards the boundary with the the Limpopo-Shashe belt and suggested a geotectonic link between terranes. According to Bagai (2008), the TTG gneisses in the SW complex (Fig. 1.9) were partially melted during a younger metamorphic event at 2639 ± 7.9 Ma. This period is within error with the age 2630 ± 4.7 Ma for the migmatisation of the Shashe gneiss (Bagai, 2008). The high grade metamorphic event is related to orogenesis in the Limpopo-Shashe belt linked to the final collision between the Zimbabwe craton and the Kaapvaal craton (Bagai, 2008). The collision event led to emplacement of syn-tectonic granite (granite augen gneiss) widespread within the Limpopo-Shashe belt.

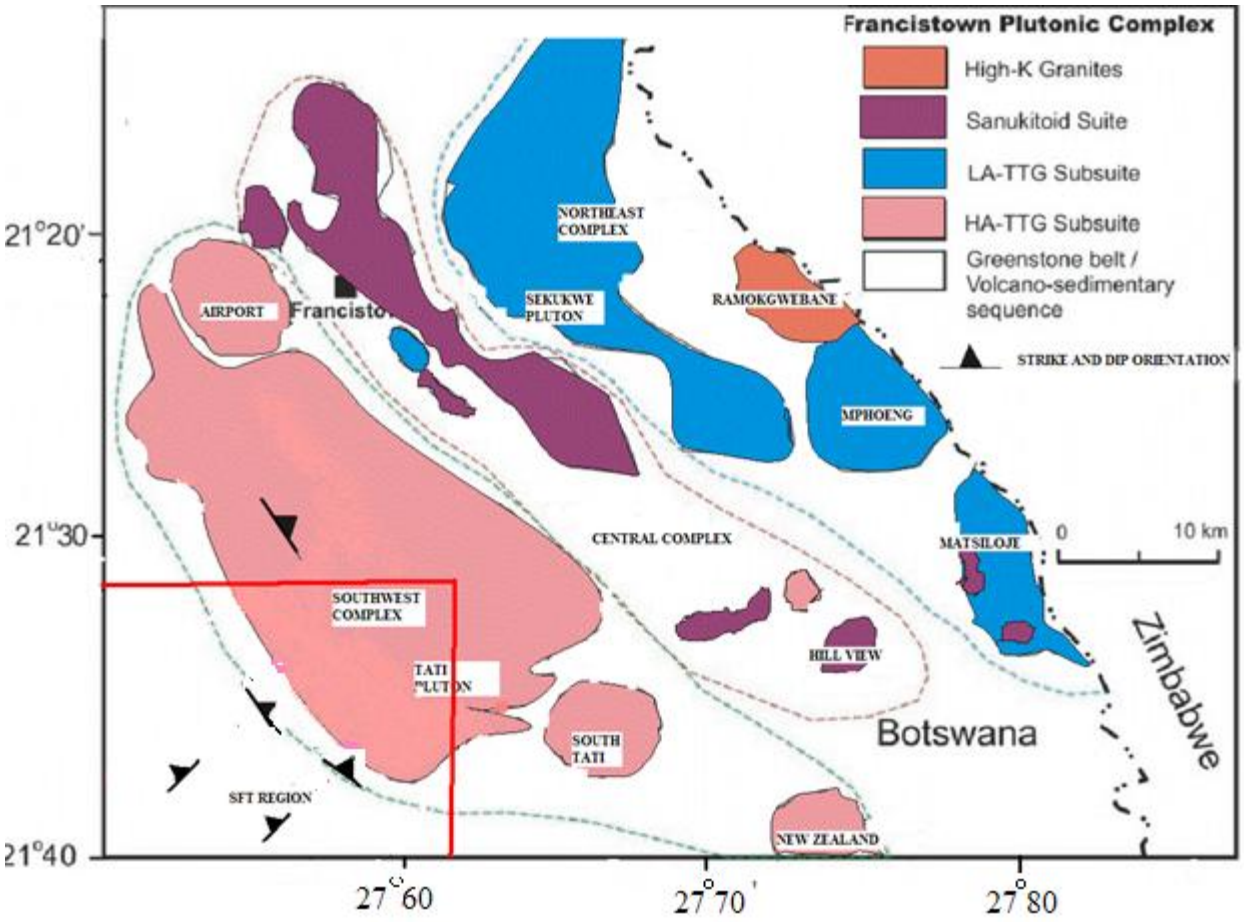

Figure 1.9: Simplified map outlining the three plutonic complexes of the Tati granitoid-greenstone terrane (Slightly modified from Kampunzu *et al*., 2003; Zhai *et al*., 2006 & Bagai. 2008). The northern part of the study area (SFT) is outlined red for reference (strike and dip measurements based on the current research). High aluminum tonalite-trondhjemite subsuite (HA-TTG) is equivalent to tonalite-trondhjemite gneiss of dissertation map and Fig. 1.1

1.7.1 BOUNDING SHEAR ZONES

Crustal scale ductile shear zones in the Limpopo belt (e.g. McCourt and Vearncombe, 1992) define the boundaries between the various zones within the belt and between the high grade of the Limpopo belt (e.g. the northern and southern boundaries of the Central Zone) and the adjacent cratons (e.g. the North Limpopo Thrust Zone and the Hout River Shear Zone). Investigations on geometries and kinematics of the shear zones and associated structural features help in better explaining the evolution of the boundaries (their temporal and regional significance, collision tectonics, metamorphic processes

involved and implications). According to Schaller *et al*. (1999), the Palala shear zone (Fig 1.5) records dextral strike-slip movements which occurred during the Palaeoproterozoic (1.97 < 1.92 Ga) whereas McCourt and Vearncombe (1987) interpret it as a sinistral strike-slip shear zone. The Palala shear zone trends ENE, dips N and lies along strike from the Tshipise shear zone which dips south so it is likely that the Palala shear zone represents a reactivation of part of the Tshipise shear zone at about 2.0 Ga (Kramers *et al.,* 2011). An important consideration is whether the Palala shear zone extends along strike to the WSW as the Zoetfontein Fault or swings to the north to become the Mahalapye shear zone (Figs 1.6 to 1.8). Alternatively the Mahalapye shear zone is a separate component of the system that links to the Palala shear zone. The Mahalapye straightening/shear zone defines the southern limit of the Mahalapye complex (Holzer *et al*., 1999).

The Central Zone of the Limpopo belt is structurally bounded by the Palala-Tshipise shear zone and Lethakane-Magogaphate-Triangle shear system against the Southern and Northern Marginal Zones respectively (Fig. 1.5). The south dipping Magogaphate shear zone is described as a dextral shear zone trending ENE to WSW (e.g. Aldiss, 1991) and separates the Phikwe Complex from the Motloutse Complex to the N (Aldiss, 1991; Key *et al*., 1994; McCourt *et al.,* 2004). The development of the Magogaphate shear zone is attributed to continued ductile deformation and migmatisation (Aldiss, 1991) during collision between the Zimbabwe and the Kaapvaal cratons. Kamber *et al*. (1995) obtained a Proterozoic age of ~ 2.0 Ga for the youngest deformation along the Triangle shear zone. According to Paya (1996) the northern boundary to the Central Zone comprise two dextral shear zones namely the Molabe and Lepokole shear zones, thought to have been active at the same time (Fig. 1.7). These shear zones dip SE. Paya (1996) refers to them as lateral ramps that accommodated emplacement of what he called the Magogaphate block and this model requires the Shashe shear zone to act as the frontal ramp. However the Molabe shear zone lies N of the Magogaphate shear zone and the Lepokole shear zone lies south. If the rocks deformed by the Molabe shear zone are part of the Motloutse Complex then the Molabe shear zone cannot define the northern boundary of the Central Zone. The Lepokole shear zone is a 5km wide ENE-WSW trending ductile strike-slip shear zone N of Bobonong Village. The Molabe shear zone is a strike-slip ductile shear

zone that possesses a predominant ENE-WSW general shear foliation trend with steep to moderate dips to the south (60°-80º). These are considered to be splays of the main Magogaphate-Triangle shear system. The steep dipping Palala-Zoetfontein and Lethakane-Magogaphate-Triangle shear zone systems were formed or reactivated under high grade metamorphic conditions at about 2.0 Ga (Holzer *et al*., 1999; Chavagnac *et al*., 2001).

The boundary between the Mahalapye and the Phikwe Complexes is the NW-SE trending Sunnyside Shear Zone (McCourt and Vearncombe, 1987). Paya (1996) has shown that the displacement on the Sunnyside Shear Zone was dip-slip rather than strike-slip thus it cannot be a western continuation of the Palala shear zone. Key *et al*. (1994) mapped a N-S trending sub-vertical shear zone along the western side of the Phikwe Complex, initially referred to as the Western Limpopo Shear Zone and later as the Dikalate Shear Zone (Paya *et al*., 1997). The Dikalate Shear Zone, (Figs 1.5 to 1.8) is described as a dip-slip ductile E to SE verging thrust zone in the western extremity of the exposed Limpopo belt (Paya *et al*., 1997). The thrust zone records N-S foliations with NW-SE trends occurring to the south of Topisi area. This shear zone is interpreted as an extension of the Lethakane-Magogaphate-Triangle shear system and taken to represent the western boundary to the Phikwe Complex. A change of structural trends from the E-W Magogaphate shear zone trend to a N-S trend along the Dikalate Shear Zone is interpreted as a transition from lateral to frontal ramps (McCourt and Vearncombe, 1987). McCourt and Vearncombe (1987) suggest westwards emplacement of the Central Zone based on kinematics of the shear zone along its margins i.e. dextral displacement on south dipping Triangle and Magogaphate shear zones and sinistral displacement on N dipping Palala shear zone (Fig. 1.5). In this interpretation, sense of displacement and dip direction (geometry/attitude) is compatible and define a single surface and a single structure. Contrary to this suggestion, Paya *et al.* (1997) observed that the geometry of asymmetrical porphyroclasts and S-C structures along the Dikalate Shear Zone indicate eastwards thrusting. Support for this interpretation comes from Holzer *et al*. (1999). According to Holzer *et al*. (1999), the Dikalate Shear Zone dips westwards, with a steeply westwards plunging lineation but the Magogaphate shear zone dips south and so

the shear zones do not define a single surface. The eastwards thrusting suggest W to E transportation of the Central Zone to the Limpopo belt (Paya *et al.*, 1997, Holzer *et al*., 1998). However, the Central Zone is in the footwall of the Dikalate shear zone in this model, so it is the area to the west (i.e. the hanging wall) that has been displaced W to E (S. McCourt pers.com. 2012).

1.7.2: GEOCHRONOLOGY OF ARCHAEAN CRUST IN NORTHEAST BOTSWANA

The earliest age data published on the basement rocks of NE Botswana are Rb-Sr dates by van Reenen and Dodson (1972), Hickman and Wakefield (1975) and Barton and Key (1981). The geochronological succession of granitoids classified as G1 to G5 (Key *et al*., 1976) based on their age relative to each other and on regional deformation events (presence or absence of foliation) has been questioned (Bagai, 2002). Bagai (2002)'s work has shown that the G1-G5 system is not supported by U-Pb ages of granites. More recent studies in NE Botswana have been based on crystallization of granitoids rocks (magmatic zircons) and detrital zircons on supracrustal rocks (Table 1.7). These studies include McCourt and Armstrong, (1998), Kröner *et al.* (1999), Chavagnac *et al*. (2001) and Zeh *et al*. (2009) on the Phikwe and Mahalapye Complexes, Majaule and Davis (1998) on the Mosetse area, Bagai (2002, 2008) on the Francistown Arc Complex and unpublished data by B.K Paya (pers. com. 2010). The ages calculated and the respective authors' interpretations are summarized in Table 1.7. In addition Holzer *et al*. (1999) published a series of PbSL ages on granitoid gneisses from the Phikwe and Motloutse complexes but the geological significance of these ages is unclear and they are not discussed further. More recently, McCourt *et al*. (2004) published detrital zircon ages obtained from quartzites from the Motloutse Complex. Additional unpublished U-Pb age data from granitoid rocks from the Phikwe and Motloutse areas were provided by [1]B.K Paya (pers com. 2010).

[1] Mr. Boikobo Paya, Permanent Secretary, Ministry of Minerals, Energy and Water Resources, Department of Geological Survey.

Table 1.7: Summary of age data from terranes in NE Botswana including information on: author, rock type, geochronological technique used and age obtained authors' interpretation. NB. "*emplacement age*" refers to emplacement age of granite or emplacement age of protolith to the host gneiss.

AUTHOR	SAMPLES	TECHNIQUE	AGE	INTERPRETATION
Millonig *et al*., 2010	Lose Quarry diorite gneiss (sample Ma1h)	U-Pb –Lu-Hf isotope analysis LA-SF-ICP-MS *(laser ablation-sector field-inductively coupled plasma-mass spectrometry*	2045 ± 8 Ma	metamorphic age
	Lose Quarry leucogranite (Ma1b)		2045 ± 8 Ma	metamorphic age
	Lose Quarry granodiorite (Ma 4a)		2037 ± 12 Ma	metamorphic age
	Mahalapye granite (Ma 2)			
	Metapelite (Ma 3c) **(Mahalapye Complex)**		2033 ± 9 Ma 2035 ± 9 Ma	metamorphic ages
			2035 ± 5 Ma	metamorphic age
[1]BK. Paya, unpublished data, 2010	Selibe-Phikwe granite gneiss	U-Pb zircon SHRIMP *(Sensitive High Resolution Ion Microprobe)*	2076 ± 55Ma	metamorphic age
	Nakwanapedi migmatite Lepokole granite		2633 ± 7.3 Ma	crystallization age
	Lepokole granite dyke		2617 ± 15 Ma	emplacement age
			2622 ± 3Ma	minimum age of deformation in Lepokole granite
	Swejane granite (**Phikwe Complex**)		2621 ± 3.6 Ma	emplacement age
			2609 ± 8 Ma	emplacement age
	Shashe megacrystic granite gneiss, (**Motloutse Complex**)	U-Pb zircon SHRIMP	2692 ± 10 Ma	emplacement age
			2705 ± 11Ma	emplacement age
Zeh *et al*., 2009	Granites from Selibe-Phikwe area (**Phikwe Complex**)	U-Pb-*Lu-Hf isotope analysis LA-SF-ICP-MS *(laser ablation-sector field-inductively coupled plasma-mass spectrometry*	2658 ± 9 Ma (SP2)	emplacement age
			2612 ± 12 Ma (SP3)	emplacement age
			2610 ± 7 Ma (SP4)	emplacement age
			2000 Ma (SP 4)	metamorphic age

Table 1.7 continued

***NB.** Lu-Hf data indicate presence of xenocryst zircons, evidence for crustal recycling (remelting of older crust) and depleted mantle source in Mahalapye and Phikwe Complexes, (Zeh *et al*., 2009).

	Granites (**Motloutse Complex**)	U-Pb-Lu-Hf isotope obtained by LA-SF-ICP-MS	2645 ± 22 Ma(SP1) 2056 ± 12 Ma(SP1)	emplacement age metamorphic overprint
	Mokgware diorite (**Mahalapye Complex**)	U-Pb-Lu-Hf isotope obtained-LA-SF-ICP-MS	2040 ± 18 Ma	intrusion age
	Shashe gneiss (**Motloutse Complex**)	U-Pb-Lu-Hf isotope obtained by LA-SF-ICP-MS	2645 ± 22 Ma 2056 ± 12 Ma	emplacement age metamorphic- overprint
	Hill view tonalite Sekukwe TTG Aiport granite Sekukwe TTG Tati TTG Selkirk sanukitoid (**Francistown Arc Complex, Tati greenstone belt**)	U-Pb-Zircon (SHRIMP)	2649 ± 9 Ma 2662 ± 6 Ma 2648 ±12 Ma 2700 ± 8 Ma 2734 ± 39 Ma 2707 ± 7 Ma	emplacement age emplacement age emplacement age emplacement age emplacement age emplacement age
	Granites from Selibe-Phikwe area **(Phikwe Complex)**		2658 ± 9 Ma 2612 ± 12 Ma 2610 ± 7 Ma	emplacement age emplacement age emplacement age
Bagai, 2008	Leucosome in Shashe gneiss (migmatite outcrop)	U-Pb zircon (SHRIMP)	2629 ± 3.2 Ma	partial melting
	Shashe gneiss-Augen granitic gneiss exposed in Shashe River bed **(Motloutse Complex)**		2630 ± 4.4 Ma	partial melting
Bagai, 2008 continued	Paragneiss Andesite Dacite Tonalite-trondhjemite Tonalite-trondhjemite Tonalite-trondhjemite Tonalite-trondhjemite Tonalite-trondhjemite Leucosome from TT Leucosome from TT Melanosome from TT Tonalite-trondhjemite **(Tati greenstone belt)** Tonalite-trondhjemite		2755 ± 100 Ma 2737 ± 3.2 Ma 2735 ± 30 Ma 2911 ± 5 Ma 2876 ± 160 Ma 2647 ± 30 Ma 2732.7 ± 4.4 Ma 2673 ± 4.5 Ma 2703.5 ± 4.1 Ma 2639 ± 7.9 Ma 2670 ± 10 Ma 2684 ± 22 Ma 2672.9 ± 2.8 Ma	metamorphic age magmatic age magmatic age inherited age (xenocryst) magmatic age (xenocryst) metamorphic age magmatic age metamorphic age magmatic age metamorphic age magmatic age magmatic age magmatic age

	Tonalite-trondhjemite Diorite Trondhjemite Monzogranite Dacite **(Tati greenstone belt)**		2739 ± 7.2 Ma 2651.1 ± 3.4 Ma 2715.9 ± 2.5 Ma 2715.2 ± 2.7 Ma 2716.1 ± 3.7 Ma 2695.9 ± 5.9 Ma	magmatic age metamorphic age magmatic age magmatic age magmatic age magmatic age
Zeh *et al*., 2007	Mokgware granite Lose Quarry diorite gneiss Leucosome (Lose Quarry) (**Mahalapye Complex**)	U-Pb-Lu-Hf isotope obtained by LA-SF-ICP-MS	2026 ± 10 Ma 2019 ± 8 Ma 2061± 6 Ma 2711 ± 11 Ma	emplacement age emplacement age emplacement age of protolith age of magmatic zircon xenocyst
McCourt *et al*., 2004	Quartzite units from Motloutse Complex (Sesweu and Dilolwane Hills, Topisi area (**Motloutse Complex)**	U-Pb zircon (SHRIMP)	2661 ± 8 Ma	maximum age of deposition of quartzite
Bagai *et al*, 2002	NW of Francistown Arc Complex (comprising Vumba and Mosetse area) Quartz diorite dyke Monzogranite Mafic xenolith Granodiorite Granodiorite Tonalite Tonalite (**Vumba greenstone belt**)	U-Pb-zircon SHRIMP data	2710 ± 19 Ma 2647 ± 4 Ma 2696 ± 3.5 Ma 2647 ± 4 Ma 2733 ± 5 Ma 2686 ± 6 Ma 2673 ± 6 Ma 2690 ± 4 Ma 2669 ± 6 Ma	emplacement age of TTG rock emplacement age of K-granite magmatic age magmatic age inherited age magmatic age metamorphic age magmatic age metamorphic age

Table 1.7: Continued

AUTHOR	SAMPLES	METHOD	AGE	INTERPRETATION
Chavagnac *et al*., 2001	Leucosome in Mahalapye migmatite	Sm-Nd on garnet	2023 ± 7 Ma	metamorphic age
	Leucosome in Lose Quarry migmatite		1982 ± 38 Ma	metamorphic age
	Leucosome in Mahalapye granite (**Mahalapye Complex**)	U-Pb monazite	2002 ± 10 Ma 1996 ± 38 Ma	metamorphic age metamorphic age
Holzer *et al*., 1999	Swejane granite	U-Pb zircon	2517 ± 33 Ma	minimum age for emplacement of granite
	Swejane granite	U-Pb apatite	1997 ± 7 Ma	emplacement age of granite
	Swejane granite	PbSL	2001 ± 6 Ma	time of ductile deformation in the northern part of Phikwe Complex
	Garnitiferous amphibolite, Selebi ore body (Phikwe Complex)	PbSL garnet	2076 ± 55Ma	time of garnet growth, maximum age for deformation
Holzer *et al*., 1999	Shashe granite	PbSL	2497 ± 19 Ma	minimum age for emplacement of granite
	Dikalate granite		2592 Ma	emplacement age
	Maope granite (Motloutse Complex)		2623 ± 24 Ma	emplacement age
	Lose Quary migmatite (Mahalapye Complex)	U-Pb apatite	1998 ± 4 Ma	metamorphic age
	Mahalapye granite		2002 ± 10 Ma	metamorphic age
Kroner *et al*., 1999	Zanzibar TTG gneiss in South Africa	U-Pb zircon SHRIMP	2614 ± 13 Ma to 2653 ± 5Ma	emplacement age
	Alldays gneiss		2659 ± 10 Ma	emplacement age
			2650 ± 21 Ma	emplacement age
			2637 ± 3 Ma	

Table 1.7 continued.

AUTHOR	SAMPLES	METHOD	AGE	INTERPRETATION
Majaule and Davis, 1998	Tonalitic gneiss Granodiorite gneiss Monzodiorite gneiss **Mosetse Complex**)	U-Pb zircon (SHRIMP)	2710 ± 9 Ma 2648 ± 2.5Ma 2648 ± 2 Ma 2646 ± 3 Ma	emplacement age emplacement age emplacement age emplacement age
McCourt and Armstrong, 1998	Syn to post kinematic granites (**Phikwe Complex)**	U-Pb zircon (SHRIMP)	2652 ± 15 Ma 2595 ± 13 Ma	emplacement ages of granite; minimum age of deformation in the host gneisses
	Tonalitic and trondhjemitic gneisses (**Phikwe Complex)**	U-Pb zircon (SHRIMP)	2.74-2.60 Ga	emplacement age
	Mahalapye granite, Syn to post kinematic granites (**Mahalapye Complex**)	SHRIMP	2023 ± 13 Ma	age of crystallization, minimum age for migmatization and deformation
	Lose Quarry granodiorite (**Mahalapye Complex)**	U-Pb zircon (SHRIMP)	2053 ± 21 Ma	age of crystallization
Barton and Key, 1983	Zanzibar gneiss (**Phikwe Complex**)	Rb-Sr whole isochron isotope dating	3227 ± 140 Ma	emplacement age
Hickman and Wakefield, 1975	Selibe-Phikwe granite	Rb-Sr isotope	2900 ± 40 Ma	emplacement age
	Anorthositic and granitoid gneisses	Rb-Sr wr isochron	2660 ± 40 Ma	emplacement age
	Granitoid gneisses (**Selibe-Phikwe area**)	Rb-Sr thin slices, errorchron	2100 Ma	metamorphic age
Van Reenen and Dodson, 1972	Migmatite Granitoid gneisses Granitoids, Magogaphate area (**Phikwe Complex**)	Rb-Sr biotite Rb-Sr biotite Rb-Sr biotite	2010 ± 50 Ma 2000 ± 50 Ma 1970 ± 50 Ma	metamorphic age metamorphic age metamorphic age
	Migmatite Migmatite (**Mahalapye Complex)**	Rb-Sr-biotite-feldspar Rb-Sr-wr-feldspar	2010 ± 50 Ma 1970 ± 50 Ma	metamorphic age metamorphic age

CHAPTER 2: LITHOLOGICAL UNITS

2.1 INTRODUCTION

The Archaean crust of the SFT area consists of two contrasting metamorphic sequences deformed together (see dissertation map in the dissertation, folded at the back of cover). The first sequence comprises medium to high grade metasedimentary rocks ([2]metaquartzite-marble-amphibolite). The metasedimentary rocks have been subdivided into two main units comprising quartzite/quartz-mica schist association and a mixed metasedimentary association (Table 2.1). The rock units are metamorphosed and interfolded with each other such that their original relationship is difficult to establish. Only resistant quartzite, marble and calc-silicates are well exposed. In many instances during this mapping, reliance was much more on float lithologies to establish the distribution of units.

Table 2.1: Subdivision of SFT Archaean crust into metasedimentary rocks and granitoid gneisses showing metamorphic facies and lithological units

Lithological unit	Metasedimentary belt (medium to high grade, Smith and phofuitsile, 1985)		Granitoid gneisses Upper Amphibolite facies (McCourt *et al.*, 2004)
description	quartzite/quartz-mica schist association	mixed metasedimentary association	Tonota biotite gneiss, banded tonalitic gneiss, megacrystic granite gneiss, megacrystic tonalite gneiss and pink gneissic granite
Rock types	Quartzite with minor quartz-mica schist	Marble, calc-silicate rocks, biotite schist and amphibolite	

The second constitutes the predominant rock assemblage and consists of granitoid gneiss. The gneisses have been subjected to intensive metamorphism resulting in partial melting. In support of the latter, Aldiss (1989) reports amphibolite facies metamorphism with

[2] 'Metaquartzite' is a term commonly used by Geological Survey geologists in southern Africa but quartzite is a metamorphic rock after quartz arenite. Calling the metamorphic rock (recrystallized) rock 'metaquartzite' is misleading as it implies the protolith was quartzite. In view of this, it is preferred in the present study to identify the rock as "quartzite".

anatexis (partial melting) in the gneiss terrane. The granitoid gneisses show evidence for partial melting and formation of migmatite in the banded tonalitic gneiss and the granitic gneiss. The broad distribution of the different rock types could be inferred from aerial photographic interpretation and ASTER imagery. Field relations between the metasedimentary belt and the granitoid gneisses are difficult to establish. The contacts are poorly exposed and characterized by flat lying outcrops. There is a lack of clear intrusive relations and no evidence for unconformable relationship between the metasedimentary rocks and the granitoid gneisses. The granitoids are nowhere seen to intrude the metasedimentary rocks and likewise no metasedimentary rocks were found as enclaves within the gneissic unit. However, both units are deformed and the deformation fabrics are compatible suggesting the current boundaries are tectonic. The geometry of the boundary is given by fabrics in the granitoid gneiss to the W and E of the metasedimentary belt. Structural interpretation of fold geometry and fabric relationships was hampered by the lack of good outcrop and in particular by the nature of most outcrops; typically flat rock pavements providing no opportunity to view structural elements in the vertical section.

2.2 METASEDIMENTARY ROCKS

2.2.1 QUARTZITE/QUARTZ-MICA SCHIST UNIT

In outcrop the quartzite/quartz-mica schist unit comprises massive through foliated to finely laminated rocks. The foliation (S_1) and lamination are defined by alignment of quartz and biotite grains in a predominantly NE-SW orientation and as a result the unit generally shows NE-SW trends with moderate to steep dips towards NW (Fig. 2.1). The laminated quartzite form thin layers that often grades into quartz-mica schist. Both lithologies are commonly iron-rich, though non-ferrugineous units also occur. Quartz-mica schist forms micaceous partings within the quartzite

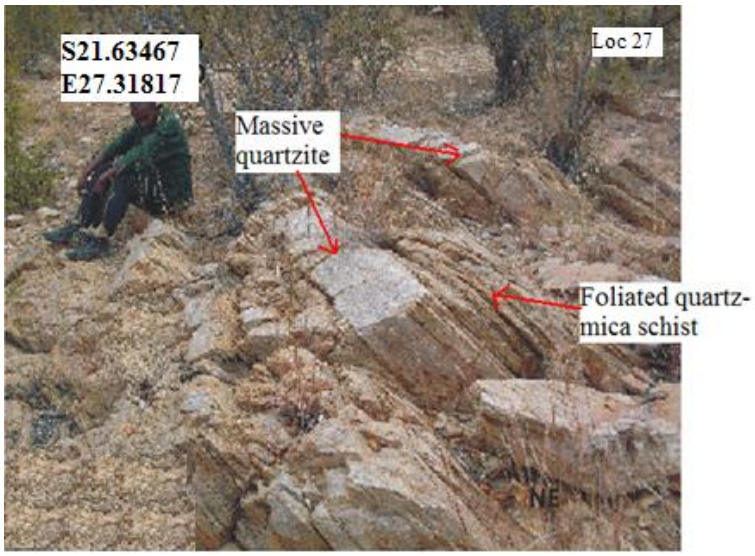

Figure 2.1: Quartz-mica schist forms micaceous parting within the massive quartzite. NB. There has been flattening perpendicular to foliation (S_1) plane and elongation parallel to the foliation plane; bedding orientation; 240º/62º. Photograph captured facing NW.

Texturally the quartzite ranges from very fine grained to medium grained. The massive quartzite units are typically milky white in colour although pale/dark grey and brown varieties are also found. The darker grey varieties contain concentrations of opaque minerals (Fig. 2.2).

Figure 2.2: Outcrop of massive pale grey quartzite from the quartzite/quartz-mica schist unit in the Gulushabe area.

2.2.2 MIXED METASEDIMENTARY UNIT

An undifferentiated association of marbles and calc-silicate rocks interfolded with quartzite, amphibolites and granitoid gneiss were mapped in the Gulushabe area (dissertation map). The marbles are dull grey, brown, white-weathering, massive medium grained rocks (Fig. 2.3 A-C) and are associated with thin layers of calc-silicate rock. The calc-silicate protrudes on weathered surfaces usually parallel lamination. The marbles have internal laminations in thicker layers and alternations of marble and calc-slicate minerals both of which probably represent original bedding (Fig. 2.3 C). The marbles are composed of recrystallized carbonate minerals, most commonly calcite and dolomite (Tables 4.2 and 4.3).

A W of Gulushabe settlement

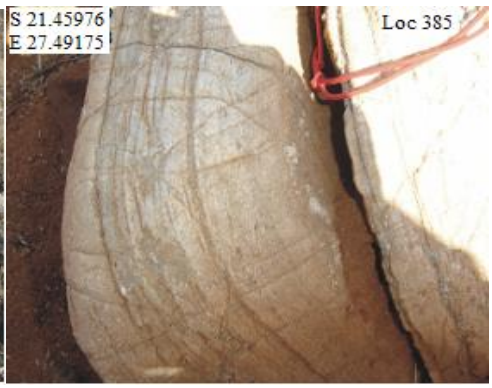

B. N of Gulushabe settlement

C. ESE of Gulushabe settlement

Figure 2.3 A-C: Typical marble outcrops from the Gulushabe area, A: massive dull grey marble unit from the western part of the Gulushabe structure.Strike and dip of foliation is B: Pale coloured marble unit north of Gulushabe area, near Shashe River. Bedding strikes; 310º/40° and C: Interdigitated marble and calc-silicate rock. bedding strikes; 256°/66º, eastern part of Gulushabe fold structure.

Contacts between the marbles and the amphibolites are sharp and concordant with the mineral layering. The stratigraphic relationship between the marbles, the quartzite and the amphibolite has not been established due to folding and thrusting deformation events that affected rocks in the area. Graphite schist occurs associated with the marble-calc-silicate rocks on top of a hill to the SE of Shashe Dam in Shashe Village. The graphite schist is very fine grained and weathers with a white tint (Fig. 2.4).

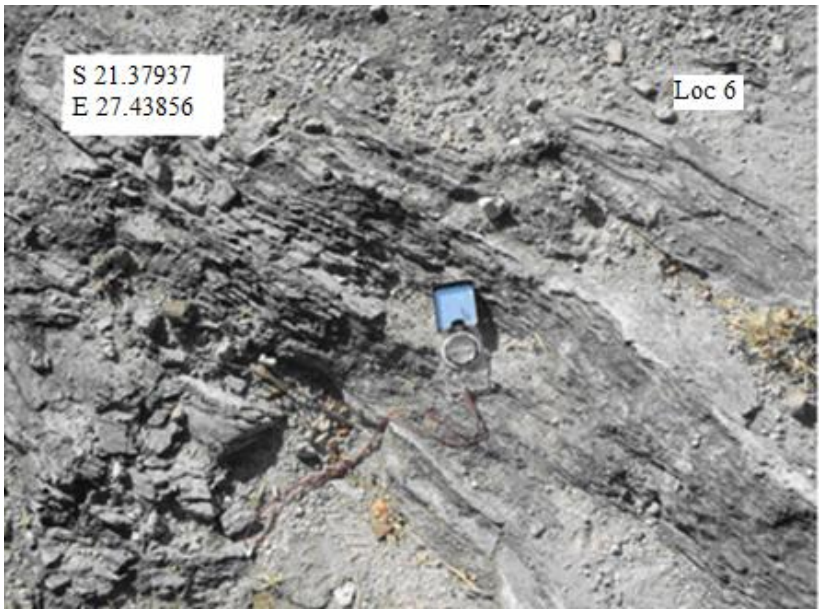

Figure 2.4: Graphite schist associated with marbles SE of Shashe Dam. Strike and dip of foliation (S_1) is 210°/55º.

The marbles vary from massive to layered types, the layering is the result of minor variations in composition of the marble. Nodules of marble occur in calc-silicate rocks. The nodules are rimmed by thin layers of calc-silicate (Fig. 2.5). The nodules are elongated parallel to the foliation (S_1) which is defined by alignment of quartz, muscovite, carbonate minerals and hornblende.

Figure 2.5: Nodules of marble enveloped by calc-silicate. Locality 222, SE of Shashe Dam. Strike and dip of foliation is 230º/82°. In plan view, the nodules have a preferred orientation thereby helping define foliation (S_1).

Marble and calc-slicate rocks form a low ridge E of the Shashe Village with amphibolite and graphite schist in the adjacent low lying areas. Prominent amphibolite bands are interrelated with marbles and calc-silicates in the vicinity of Gulushabe settlement. The outcrops are often covered by a thin layer of calcrete. In hand specimen, the mineralogy of these rocks comprises hornblende, plagioclase and quartz. The amphibolites are layered, fine to medium grained equi-granular rocks and are speckled white with plagioclase (Fig. 2.6). Contacts between the marbles and amphibolite have not been observed.

Biotite schist is of limited distribution and only occurs in the fold hinge and on the south-eastern limb of the Gulushabe fold structure. The biotite schist is up to 2m thick and best exposed in a stream section adjacent to a marble horizon. On the southeastern limb, the biotite schist is associated with marbles, amphibolites, and quartzite. Foliation (S_2) in schist in the hinge and on limb dips steeply WNW and carries deformed veins of quartz.

Elsewhere in the study area the metasedimentary rocks exposed include features of both the quartz-rich unit and the carbonate-bearing unit. For example close to the Shashe River soouthеast of Tonota amphibolite and marble occurs in association with tonalitic gneiss (Fig. 2.7). The contact between the rock units are sharp, concordant with the mineral layering and are emphasized by textural and colour dissimilarity.

Figure 2.6: Amphibolite unit displaying white spots of plagioclase feldspar, SE part of the Gulushabe fold structure. Strike and dip of foliation (S_1) is 220º/62°.

Figure 2.7: Interlayered amphibolite, marble and tonalitic gneiss, north of eastern closure of the Gulushabe fold structure, NE of Gulushabe settlement, strike and dip of foliation (S_1) is 242º/82°.

Close to the Seswe cattlepost NW of Foley Village, pebble-bearing quartzite (Fig. 2.8 A) is intercalated with amphibolite (Fig. 2.8 B) and granitoid gneiss (Fig. 2.8 C and D). The pebble-bearing quartzite in particular carries a strong foliation (S_1) and pebbles are flattened perpendicular to the foliation plane and elongated parallel to the foliation (Fig. 2.8 A).

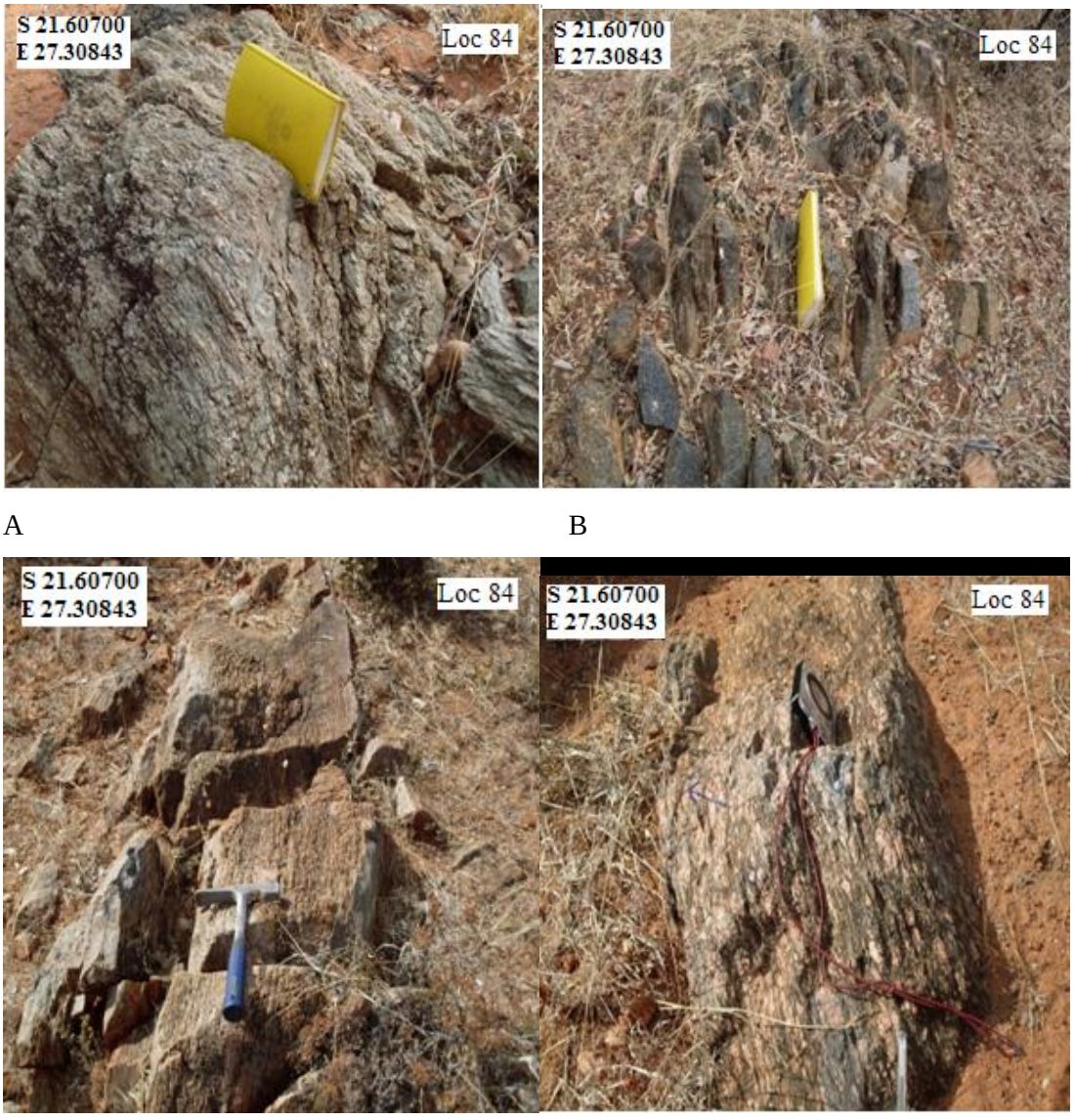

Figure 2.8 A-D: Examples interlayered rock units at Seswe area, NW of Foley Village A. deformed pebble-bearing quartzite, 240/81°, B: amphibolite, strike/dip of foliation (S_1); 242/80°, C: granite gneiss, strike/dip of foliation (S_1); 243º/82° and D: deformed megacrystic granite gneiss, strike/dip of foliation (S_1); 243º/79°, Compression perpendicular to foliation plane has resulted in elongation parallel to the foliation-an overall flattening (oblate strain).

An association of amphibolite, quartz-muscovite schist, biotite schist, quartzite and subordinate marble occurs SW of the Foley Village. The biotite schist forms thin layers between amphibolite (Fig. 2.9).The biotite schist is highly weathered and the area it underlies is easily identified from its residual dark soil.

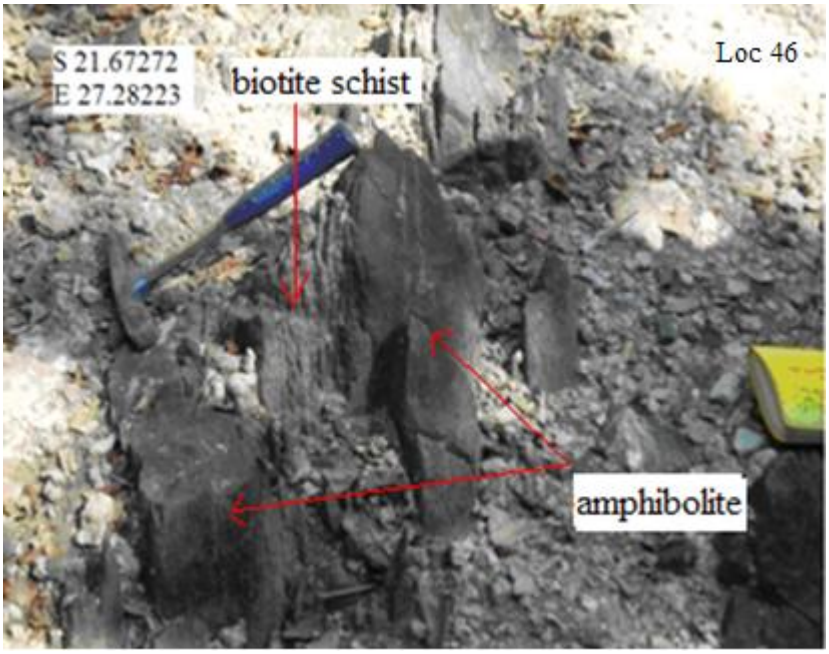

Figure 2.9: Amphibolite interbedded with biotite-mica schist southern part of Foley structure. Strike and dip of foliation (S_1) is 220º/86º.

2.3 GRANITOID GNEISSES

In the following account the general features of the granitoid gneisses are described and then the more significant lithologies are dealt with in more detail. Migmatitic gneisses are medium to coarse grained and textures are very variable. The migmatite is interlayered with banded gneiss and granitic gneisses and contacts are both gradational and sharp the latter due to shearing. Aldiss (1991) mentions occurrences of enclaves of calc-silicate gneiss, marble and quartzite in migmatite of the Shashe area but similar occurrences were not seen in the study area. Based on composition and texture the granitoid gneisses have been classified into 5 main types. The different variants of the granitoid are classified as Tonota biotite gneiss, megacrystic granite gneiss, megacrystic tonalite gneiss, banded tonalitic gneiss, pink gneissic granite and tonalite-trondhjemite gneiss. The Tonota biotite gneiss is considered to have been derived from a sedimentary protolith (Key 1976) but in

this work it is treated as an orthogneiss gneiss based the limited age range of the zircon grains and their physical character (section 4.3.4). Evidence for an intrusive relationship between the megacrystic granite gneiss, pink gneissic granite and tonalitic gneiss is given in sections (2.3. 2 and 2.3.5). The pink gneissic granite is not shown separately on the map because it occurs as non-mappable bands closely associated with the megacrystic granite gneiss. Although the foliation (S_1) in the banded tonalitic gneiss, megacrystic gneiss and pink gneissic granite is typically concordant there are local cross-cutting relationships that probably represent original intrusive contacts.

2.3.1 TONOTA BIOTITE GNEISS

The Tonota biotite gneiss is a sequence of biotite gneiss with small lenses and interlayers of amphibolite (Fig. 2.10 A and B) exposed in the vicinity of Tonota Village. The biotite gneiss is leucocratic, not banded, homogeneous, fine to medium grained, strongly foliated and includes grey to pink varieties. Compositionally the gneiss is a quartzo-felspathic rock containing a variable amount of biotite. Very sparse K feldspar megacrysts are present in the gneiss. The Tonota biotite gneiss contains veins of felsic material (comparable to white granitoid veins of Aldiss, 1989) in apparent concordance with the S_1 foliation (Fig. 2.10 C). The rock is typically weathered.

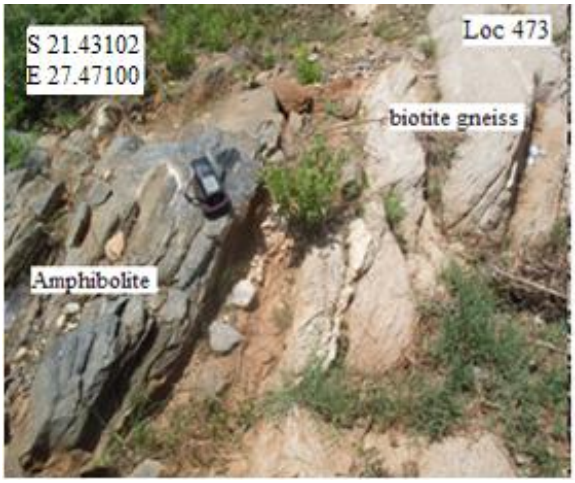

A: strike/dip of foliation (S_1): 270º/58º

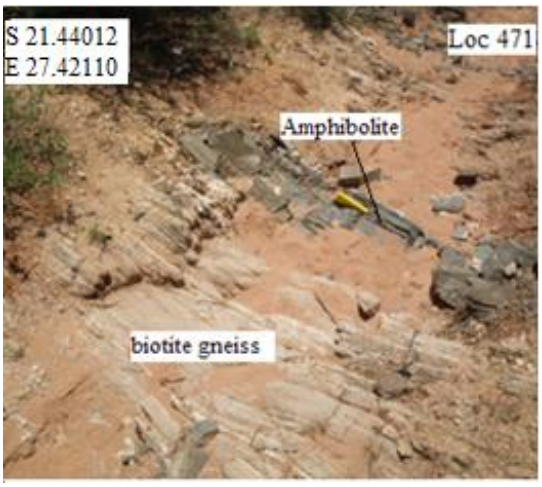

B: strike/dip of foliation (S_1): 220º/78°

C:strike/dip of foliation (S_1); 330º/58°

Figure 2.10 A-C : Outcrops of the Tonota biotite gneiss interlayered with thin layers of amphibolite south of Tonota (A and B). Note thin veins of quartz concordant to the foliation (S_1) in the biotite gneiss in C.

The distribution of the gneissic and amphibolite components of the Tonota biotite gneiss is heterogeneous. Three areas of heterogeneity are recognised based on the proportion of amphibolite and biotite gneiss as well on textural basis. The northern zone is amphibolite-rich and contains subordinate narrow interlayers of biotite gneiss. The amphibolite also encloses deformed fragments of biotite gneiss. The biotite gneiss is exposed in the form of koppies and boulders (Fig. 2.11).

A B

Figure 2.11 A-B: Examples of outcrops of the Tonota biotite gneiss, nothern part of Tonota, E of Francistown main Road, strike/dip of foliation (S_1): 278°/68°.

Biotite gneiss dominates the outcrop pattern in the area to the immediate south of Tonota, with amphibolite occurring as thin coherent layers while further south along the Tholotsane River, there are occurrences of weathered medium to coarse grained biotite gneiss interlayered with minor amphibolite. In all the outcrops visited the amphibolite and the biotite gneiss form concordant layers of contrasting composition and contacts between them are sharp, emphasized by colour dissimilarity. Fabrics present in the amphibolite and the biotite gneiss are the same. Although the Tonota biotite gneiss is typically characterised by thin layers of felsic material, there are also minor exposures of homogeneous foliated granitoid gneiss without the felsic layers (Fig. 2.12).

Figure 2.12: Homogeneous foliated Tonota biotite gneiss devoid of thin felsic layers. Photograph from southeastern part of Tonota Village near Shashe River. Strike/dip of foliatio340/86°.

The amphibolite and theTonota biotite gneiss lie in concordance with the Shashe metasedimentary rocks and the stratigraphic relationship between the two is unclear as contacts relationships have not been observed. The contact between the Tonota biotite gneiss and the megacrystic granite gneiss NNE of Thombane Hill (locality 44 on dissertation map) appears to be tectonic, given by kinematic indicators in the megacrystic granite gneiss which suggest top to ESE sense of thrusting. The area underlain by Tonota biotite gneiss is poorly exposed and largely inaccessible since it falls within the centre of the Tonota Village, with numerous homes.

Three main types of amphibolites associated with the Tonota biotite gneiss are identified. These are: 1. dark massive amphibolites that include thin veins of leucogranitic material (Fig. 2.13). Such veins are mostly concordant, but discordant veins also occur 2. Foliated speckled plagioclase amphibolite which is grey in colour (2.14 A). Some of the amphibolite is coarse grained in texture and could represent metamorphosed gabbroic or coarse grained dolerite sheets emplaced in the gneiss sequence prior to deformation (Fig. 2.14 B).

Figure 2.13: Dark massive amphibolite (type 1) with concordant thin white veins of leucocratic material, SE of Tonota, strike and dip, 270º/70°.

A: Type 2: strike/dip of foliation (S_1), 210º/56º N of Tonota Village to the W of main tarred road.

B: Type 2, NNE of Tonota Village, 270/84º East of main tarred road.

Figure 2.14 A-B: Speckled (spotted white) plagioclase amphibolite (Type 2) of the Tonota biotite gneiss unit exposed SE of Shashe Village.

Distinct from types 1 and 2 is a fine grained rock of blotchy appearance due to light coloured vein material and having pillow-like structures (type 3, Fig. 2.15) suggesting the protolith to the amphibolite could have been a lava, but no uneqivocal metavolcanic rocks have been found in the area.

Figure 2.15: Amphibolite with pillow-like structures (type 3) suggesting a volcanic protolith, NNE of Tonota to the E of Francistown main road, 260º/42°.

2.3.2 MEGACRYSTIC GRANITE GNEISS

This rock unit crop out extensively throughout the map area. It forms low lying whalebacks roughly concordant with the regional foliation (S_1). The megacrystic granite gneiss flanks the metasedimentary belt to the NW and SE but the contacts are not exposed thus making it difficult to define the field/age relationship between the two rock units. The megacrystic granite gneiss is interdigitated with banded tonalitic gneiss in the northwestern part of the metasedimentary belt. The megacrystic granite gneiss displays variable strain such that its appearance varies between gneissic granite, with very little evidence of strain through to granitic gneiss, in which deformed K-feldspar megacrysts define an obvious and often well developed augen texture (Fig. 2.16 A) to mylonitic granite gneiss that is locally ultramylonitic with less than 20% megacrysts and an intense

foliation (S_1). In zones of high strain, the foliation defined by biotite and K-feldspar megacrysts is intense (2.16 B). The unit is a medium to coarse grained rock with varying content of K-feldspar megacrysts. The gneiss shows a high degree of compositional segregation with light-coloured feldspar megacrysts alternating with biotite-rich zones. Foliation (S_1) planes defined by an alignment of dark mica grains are asymmetrically distributed around the megacrysts. The megacrysts are interpreted to be porphyroclasts (i.e. where the K-feldspar megacrysts have become oval or augen shape) after original phenocrysts.

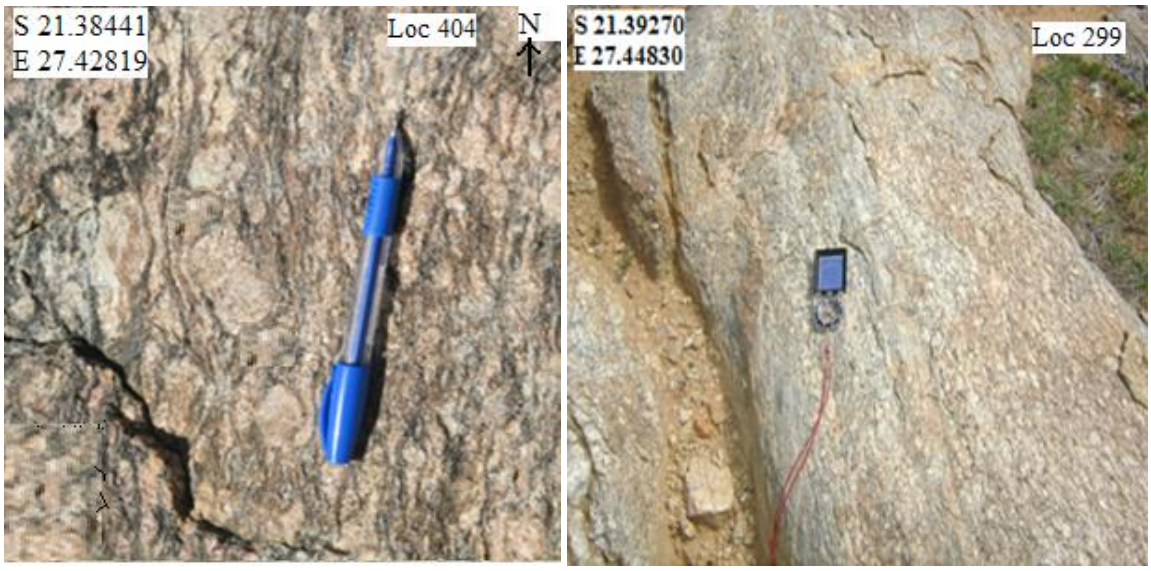

A: Augen gneiss near Shashe Dam, gneiss, N of strike and dip of foliation, 200º/68º

B: Intensely foliated megacrystic granite Tonota Village, strike and dip of foliation, 198º/88º.

Figure 2.16 A and B: A: Plan view of megacrystic granite displaying augen texture. B: an intense foliation (S_1) in megacrystic granite gneiss, note reduction in grain size in zones of higher strain.

The megacrystic granite gneiss intrudes the banded tonalitic gneiss and both units are intruded by coarse unfoliated felsic melt. Enclaves of tonalitic gneiss occur within megacrystic granite gneiss (Fig. 2.17). The observation indicates that the tonalitic gneiss is older than megacrystic granite gneiss. The megacrystic granite gneiss and the pink gneissic granite share similar foliation (S_1) trends implying that the pink granite either intruded syn-tectonically or the foliation forming event continued after emplacement of

the pink granite (section 2.4). Curved cuspate contacts were observed between the megacrystic granite gneiss and the pink gneissic granite. The cuspate shape of the contact in Fig. 2.18 could be a response to competency contrast due to deformation or possibly indicate intrusive relationship.

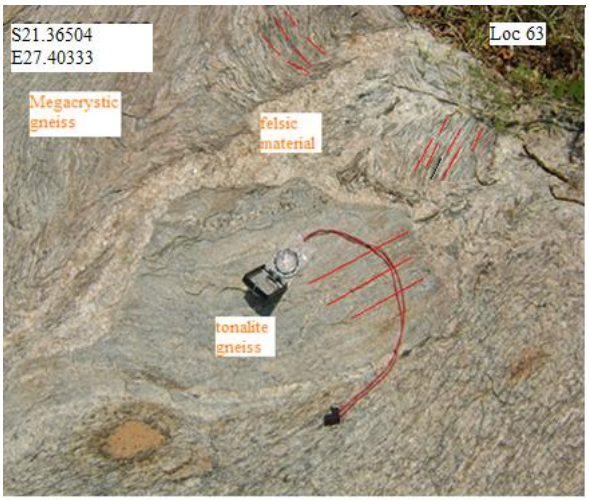

Fig. 2.17: Enclave of tonalitic gneiss in megacrystic granite gneiss S of Shashe Dam. Note the foliation (S_1) in the megacrystic granite gneiss on (top left of photograph) is at a high angle to that in the enclave and the two rock types are separated by coarse unfoliated felsic material, NW of Tonota to the south of Shashe dam, strike and dip of foliation in megacrystic granite to the bottom right of photograpgh, 210 º/54º.

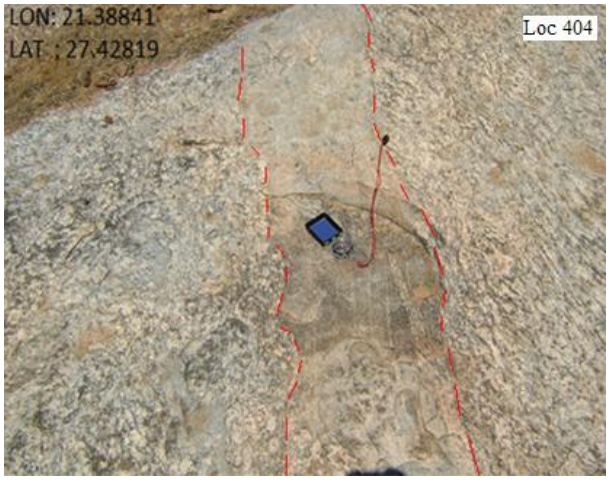

Fig. 2.18: Dyke of pink gneissic granite in the megacrystic granite gneiss concordant to foliation (S_1) in megacrystic granite gneiss, south of Shashe Dam, strike and dip of foliation,

200º/68º. Note: foliation in the pink gneissic granite and the megacrystic granite gneiss is near concordant.

2.3.3 MEGACRYSTIC TONALITE GNEISS

The unit is distinguished from megacrystic granite on the basis of grain composition and texture, in differing trends of structural fabric and spatial distribution in the SFT area. The megacrystic tonalite gneiss texturally resembles megacrystic granite gneiss and comprises K-feldspar megacrysts set in a medium to coarse grained dark grey matrix of quartz, plagioclase feldspar, biotite and minor k-feldspar (Fig. 2.19). It is a homogenous, coarse grained foliated rock with about 5-30% by volume of K-feldspar megacrysts. The unit has more plagioclase feldspar than K-feldspar in the matrix as compared to megacrystic granite gneiss. However, horizons of megacrystic granite gneiss occur intercalated with megacrystic tonalite gneiss and likewise, sheets of megacrystic tonalite gneiss occur within main outcrops of megacrystic granite gneiss. Whereas megacrystic granite gneiss is widely distributed across the study area and dominated by NE-SW trending foliation (S_1) fabric, megacrystic tonalite gneiss is restricted to a narrow zone in the north-eastern part of the study area named the Gulushabe shear zone and is dominated by E-W to WNW trending structural fabric. As in the megacrystic granite gneiss, in areas of higher strain the megacrysts are flattened perpendicular to foliation.

Figure 2.19 A: Veined megacrystic tonalite gneiss flattened perpendicular to foliation (S_1). Locality to the S of Shashe River, N of Gulushabe shear zone, 280°/54°. Note discordant, dyke-like unit of felsic material adjacent to pencil.

2.3.4: BANDED TONALITIC GNEISS

The banded tonalitic gneiss occurs throughout the area but particularly in the NW part where it occurs intercalated with megacrystic granite gneiss along a zone of high strain (shear zone). It is best exposed at Thombane Hill, west of Makomoto settlement. The unit generally appears medium to dark grey in colour, medium to fine grained in texture, banded (Fig. 2.20) and felsic granitoid veins are boundinaged (Fig. 2.21). Mineralogy is dominated by biotite, plagioclase and quartz. The tonalitic gneiss is intruded by the megacrystic granite gneiss (as previously mentioned in section 2.3.2) and a felsic granitoid that is typically concordant with the foliation (S_1).

Amphibolite bands are found enclosed by the tonalitic gneiss often occurring as boudinaged layers. The boudin neck is cut by a younger felsic dyke (Fig. 2.22A). The amphibolite bands are gneissic with the foliation (S_1) in the amphibolite parallel to that in the tonalitic gneiss. Although both units are gneissic and highly strained, there is local evidence to suggest the tonalitic gneiss is intrusive into the amphibolite. This evidence

includes protrusions of felsic gneiss into amphibolite and detached enclaves of amphibolite in tonalitic gneiss (Figs 2.22 B and 2.23).

A: SW of Tonota, strike and dip of 220º/56°

B: SW of Tonota, strike and dip of foliation, foliation (S_1), 220/66°

Figure 2.20 A-B. Banded tonalitic gneiss outcrops southwest of Tonota. The banding is emphasised by concordant layers of white felsic granitoid.

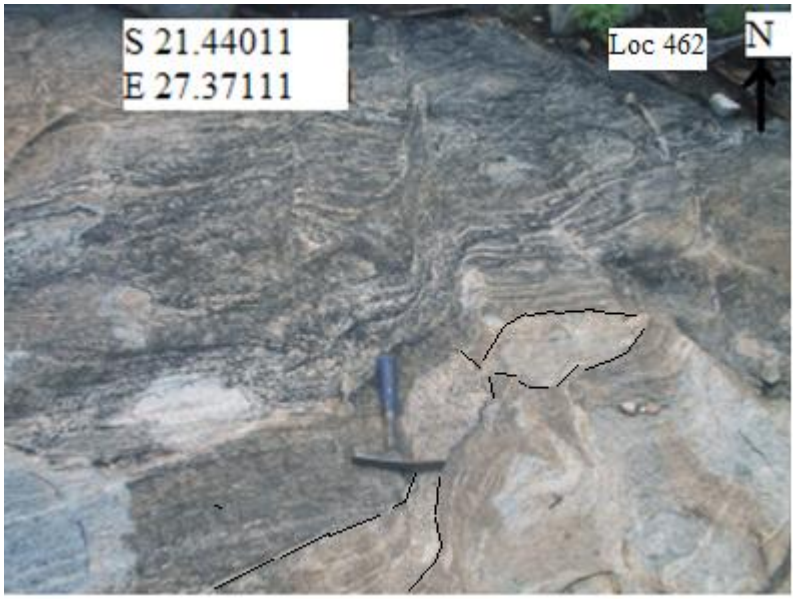

Figure 2.21: Boundinaged felsic granitoid unit in banded tonalitic gneiss, SW of Tonota, W of Francistown Road, Foliation (S_1) at this locality generally strike NE-SW; strike and dip of foliation, 220°/56º.

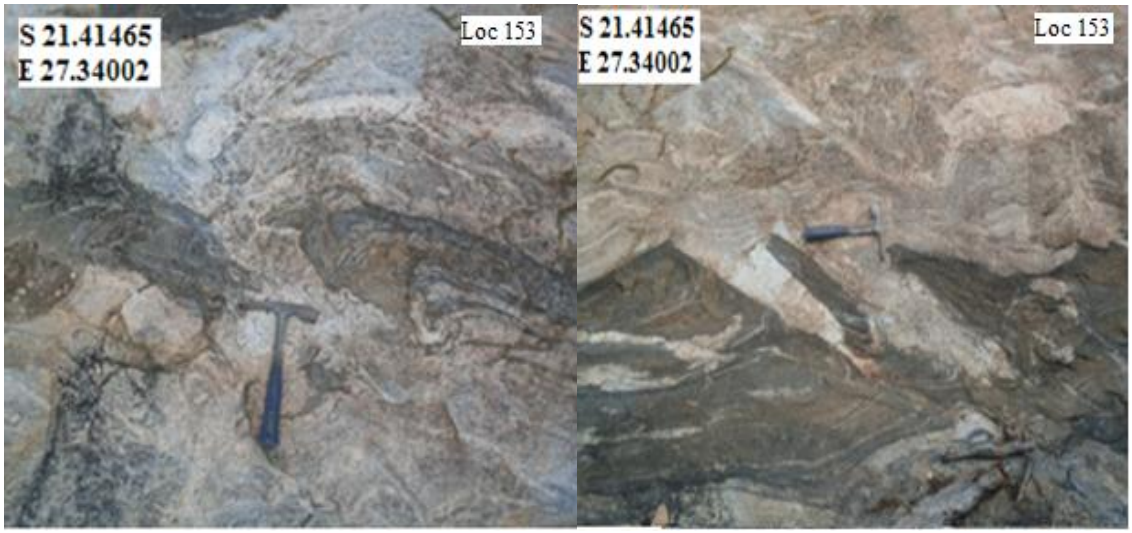

A B

Figure 2.22 A: Boudinaged amphibolite with cross-cutting coarse felsic unit SW of Shashe Village, predominant foliation (S_1) at this locality is orientated NNE-SSW; strike and dip, 212º/58°. B: Tonalitic gneiss discordant to foliation in amphibolite unit. Note the obvious cross-cutting relationship between the felsic material in the amphibolite enclave to the left of the hammer in B indicating intrusive relationship (amphibolite is older).

Fig. 2.23: Interlayered migmatitic banded tonalitic gneiss and foliated amphibolite west of Gulushabe structure, 232º/60°. Red circle encloses an enclave of amphibolite in tonalitic gneiss.

The banded tonalitic gneiss shows sheared contacts with the amphibolite and display pinch and swell structures (Fig. 2.24).

Figure 2.24: Sheared contact between banded tonalitic gneiss and amphibolite, indicated by a red dotted line. Note thinning of the amphibolite horizon and pinch and swell structure to the left of hammer, 232º/60°.

The tonalitic gneiss is intruded by felsic bands, some of which are folded and lie parallel to the foliation (S_1) while others are discordant (Fig. 2.25).

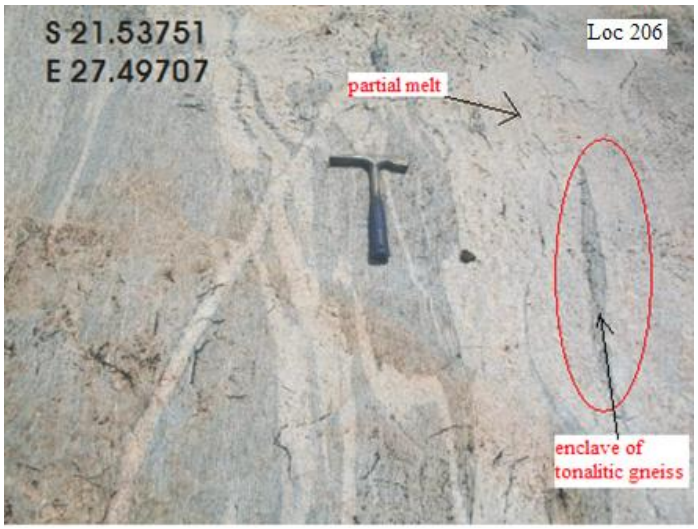

Figure 2.25: Felsic bands lying both concordant and discordant to the foliation (S_1) in tonalitic gneiss. NB: Enclave of tonalitic gneiss on the right of photograph is enclosed by a white felsic material (product of partial melting). Tonalitic gneiss is older, southern part of Gulushabe structure. Strike and dip of foliation is (S_1), 230°/40°.

2.3.5 PINK GNEISSIC GRANITE

The pink gneissic granite is medium to coarse grained and homogeneous. It is exposed as dykes crosscutting the steeply dipping foliation (S_1) in both the megacrystic granite gneiss unit (Fig. 2.26) and tonalitic gneiss (Fig. 2.27). This field relationship demonstrates that the pink gneissic granite is younger than both the megacrystic granite gneiss and the tonalitic gneiss. In addition based on evidence in Fig. 2.27, the tonalitic gneiss was migmatised and deformed prior to intrusion of the pink granite

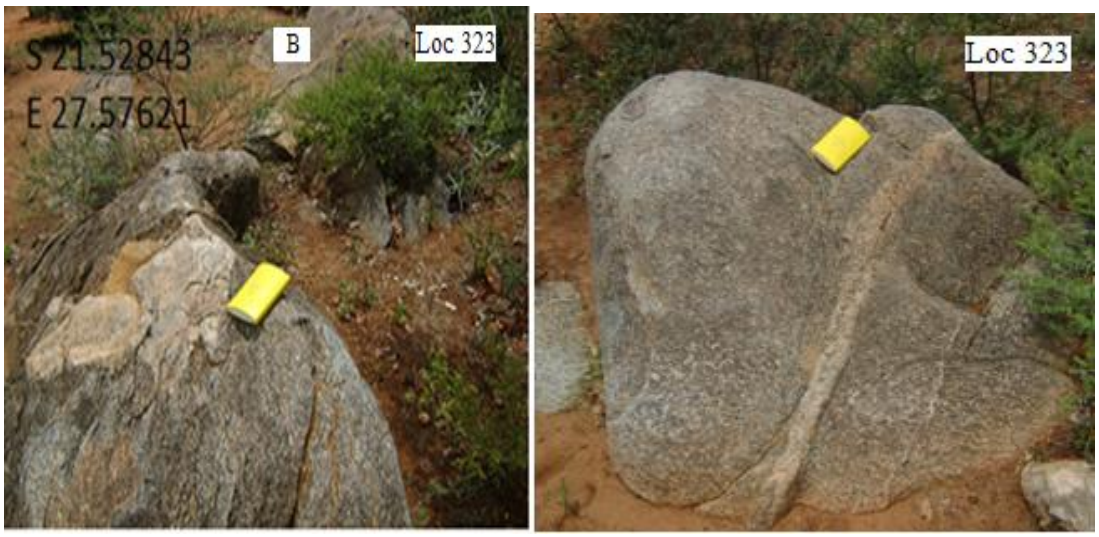

A B

Figure 2.26: A. dyke of pink gneissic granite unit cutting across megacryrstic granite gneiss unit, E of Gulushabe structure. Strike and dip of foliation (S_1) is 220°/66°. B: Steeply dipping dyke of pink gneissic granite in megacrystic granite gneiss. Photograph B was captured at locality B in Fig. 2.27 A.

Figure 2.27: Pink gneissic granite cutting deformation fabrics in banded tonalitic gneiss exposed SW of Tonota. Strike and dip of foliation (S_1) is 232°/60°.

2.3.6 TONALITE-TRONDHJEMITE GNEISS

The tonalite-trondhjemite gneiss exposed in the NE part of the SFT area is an extension of the Tati Pluton (or SW Complex, Fig. 1.9, Bagai 2008). The Tati pluton comprises foliated to banded gneisse that flank the Tati greenstone belt. Only a small part exposed to the N of the Gulushabe fold structure was mapped during this study. The tonalite-trondhjemite gneiss displays a penetrative deformational fabric that has been linked to convergent tectonics along the SW margin of the Francistown Arc Complex (e.g. McCourt *et al*., 2004; Kampunzu *et al*., 2003). The deformation fabric in the tonalite-trondhjemite gneiss trends NW-SE, parallel to the trend of the Tati greenstone belt. The intensity of the tectonic fabric increases towards the boundary with the Gulushabe shear zone. The common mineral assemblage of the tonalite-trondhjemite gneiss is biotite, plagioclase, alkali feldspar and quartz. The proportions of alkali feldspar to plagioclase are variable resulting in granitic to tonalitic compositions. This gneiss has not been investigated in detail during the current study. The reader is referred to Bagai (2008) and references therein for detailed geochemical, petrological and geochronological descriptions of the tonalite-trodhjemite gneiss.

2.4 DISCUSSION

The metasedimentary rocks in the SFT area comprise quartzite/quartz- mica schist with amphibolite, marble, calc-silicate rocks and and minor graphite schist. In some places, the metasedimentary rocks are intercalated with the granitoid gneisses (Figs 2.7 and 2.8). Foliation (S_1) generally strikes NE to ENE and dip predominantly NW and WNW. The metasedimentary rocks in the adjacent Phikwe Complex (Limpopo Central Zone) to the east are characterized by abundant paragneisses and amphibolites with minor carbonates (Key *et al*., 1994; Aldiss, 1983. They are generally orientated ENE with varied dip directions (Carney *et al*., 1994; Aldiss,1991).The metasedimentary rocks occur interlayered with the paragneisses and the contacts are deformed (Carney eta., 1994; Aldiss, 1991). Those in the Tati greenstone belt are enclosed by intrusive plutons and the contacts are tectonised. They are dominated by mafic and ultramafic metavolcanic rocks overlain by intermediate to felsic rocks (Bagai *et al*., 2002; Key *et al*., 1994). They general show NW to NNW strikes with steep dips (Aldiss, 1991). Based on lithology the metasedimentary rocks in the SFT may be correlated with those of the Phikwe Complex.

Within the study area, the megacrystic granite gneiss is nowhere seen to cut across the foliation (S_1) in the banded tonalitic gneiss thus the relative age of the deformation fabrics in these two units is unknown. The lack of this evidence could suggest that the protolith to the megacrystic granite gneiss (presumably porphyritic granite) intruded into tonalitic gneiss and then was deformed implying two tectonometamorphic events separated in time by intrusion of the protolith to the megacrystic granite gneiss. These could also imply that porphyritic granite intruded into tonalitic (the protolith to the tonalitic gneiss) and then they were deformed and metamorphosed together but the age relationship was preserved. This would indicate one tectonometamorphic event with the age of the "porphyritic granite" being the maximum age of that event.

The field relationship in Figure 2.17 has been interpreted as indicating that the tonalitic gneiss is older than the megacrystic gneiss. However the discordance between the foliation in these gneisses could be due to rotation of the blocks of tonalitic gneiss during intrusion of the coarse unfoliated felsic material. In support of the preferred interpretation of Figure 2.17, Aldiss (1989) reports that locally the megacrystic granite gneiss intrudes the migmatitic gneisses which in the study area are typically tonalitic in composition. Although field relations shows that the pink gneissic granite intrudes the tonalitic gneiss and megacrystic gneiss, the character and orientation of deformation fabrics in the pink gneissic granite is the same as that in the tonalitic and the megacystic gneisses, generally trending NE-SW (Fig. 2.18). Deformation in the SFT area predates intrusion of the pink granite but the pink granite has been deformed i.e. it is now gneissic in character and has the regional deformation fabric (S_2). This suggests that the pink granite was emplaced syntectectonically (i.e. intruded during deformation). However, the presence of pink granite dykes cutting the foliation (S_1) in the older megacrystic granite and tonalitic gneisses (Fig. 2.26 and 2.27) suggest that the intrusion of pink granite was progressive and continued even after deformation. The following magmatic sequence is therefore proposed; emplacement of the precursor to the tonalitic banded gneiss followed by emplacement of porphyritic (megacrystic) granite and finally intrusion of pink gneissic granite. As will be reported later, U-Pb zircon ages obtained from the tonalitic gneiss, the megacrystic granite gneiss and the pink granite gneiss are in keeping with this sequence.

CHAPTER 3: STRUCTURE

3.1 INTRODUCTION

In this section the structural geology of the study area is documented based on observations and measurements of structural elements, both planar and linear, which are developed at the outcrop-scale. Field photographs are used to illustrate the main structural elements. Localities where the photographs were captured are indicated on the photographs. Orientation measurements are reported in terms of strike/dip for bedding, foliation and axial planes of folds, plunge angle/direction for fold axes and plunge angle/trend for lineations.

The use of minor structures to indicate the geometry of major structures is a well-established practice based on the supposition that minor structures identified at single outcrops are a reliable indication of the structural history across the study area. The deformation that is responsible for the formation of a foliation will normally also produces folds. Foliation is however also produced in ductile shear zones (Ramsay and Huber, 1987). When these structures are produced during the same deformation event by the same stress field, they bear a simple geometrical relationship to each other i.e. same orientation of structures. These criteria have been applied in linking different sets of minor folds and related axial planar foliation to specific phases of deformation recognized. The presence of small scale folds at outcrop and map scale is often useful during the analysis of folding. A similar geometry of small scale folds on both limbs of a large scale structure (both s-shaped or z—shaped) would imply an origin by simple shear while different but geometrically compatible fold shapes on both limbs would imply parasitic folding (development by flexure). The parasitic folds should have different shapes on the limbs of a specific larger scale fold (s or z shaped) but unfortunately the occurrence of small scale folds in the study area was limited and insufficient to confirm this relation.This chapter comprises a photographic illustration of deformation structures established from field investigations of small scale structures and concludes with a discussion of these structures in terms of regional analysis and implications. Discussions and conclusions on the structure, evolution and geological history of the study area are covered in Chapter 6.

The geological map of the SFT area (in envelope on back cover of the dissertation) shows the distribution of the main planar and linear structural elements. From a preliminary inspection of the variation in strikes of foliation and distribution of rock types on dissertation map, it was decided to subdivide the region into 4 domains showing different geometrical and geological characteristics. Domain 1 is dominated by ENE trending linear belt of metasedimentary (supracrustal) rocks extending from west of Foley Village to Gulushabe settlement. Based on recognition of large scale fold structures (Figs 3.1, 3.2 and dissertation map), it is divided into 2 main fold structures namely the Foley structure in the WSW and Gulushabe structure in the ENE. In the Foley structure foliation strikes ENE to NE (070°-050º) and dips NNW and NW. Two episodes of folding (F_1 and F_2 coaxial folding) are recognized in the metasedimentary belt.

The metasedimentary rocks are flanked to the NW, SE and NE by granitoid gneisses divisible into 3 domains. The NE to ENE trending (010°-054°) granitoid gneisses to the NW of the metasedimentary belt represents Domain 2. Domain 3 is represented by the ENE trends (strike values~040°-073°) of fabric to the SE of the metasedimentary belt. Domain 4 is represented by a narrow zone of E-W to WNW striking foliation (270°-334°) to the NE of the metasedimentary rocks. The foliation in the granitoid rocks in the northern part of Domain 3 seems to be traced around the folds deforming the metasedimentary rocks. The granitoids form part of the fold structures deforming the metasedimentary rocks but they show no evidence for refolding. Contacts between units are concordant with the mineral layering. Gneissic foliation is the common continuous deformation foliations observed in the granitoid gneisses. The granitoid gneisses have a single foliation that is pervasive across the study area and this is regarded as (S_1), the oldest deformation fabric. S_1 in the granitoid gneisses is equivalent to S_2 in the metasedimentary rocks. The foliation is defined by medium–coarse grained minerals that form compositional banding with a preferred planar orientation of platy, tabular mineral grains and by parallel alignment of lenticular mineral aggregates. The compositional banding occurs at all scales from thick (metres to km scales) continuous bands that can be mapped across the entire field area to discontinuous laminae (mm to cm scales) that pinch out within individual outcrops.

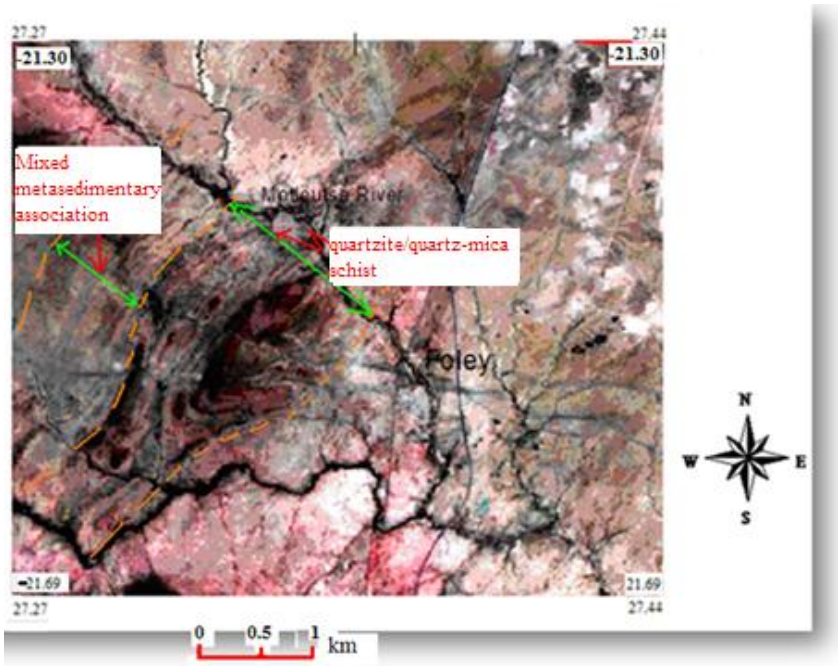

Figure 3.1: The SSW closing Foley structure on ASTER imagery. The dark unit with fold structures near the centre of the image comprises quartzite/quartz-mica schist association and is bound by the mixed metasedimentary association to the west as illustrated.

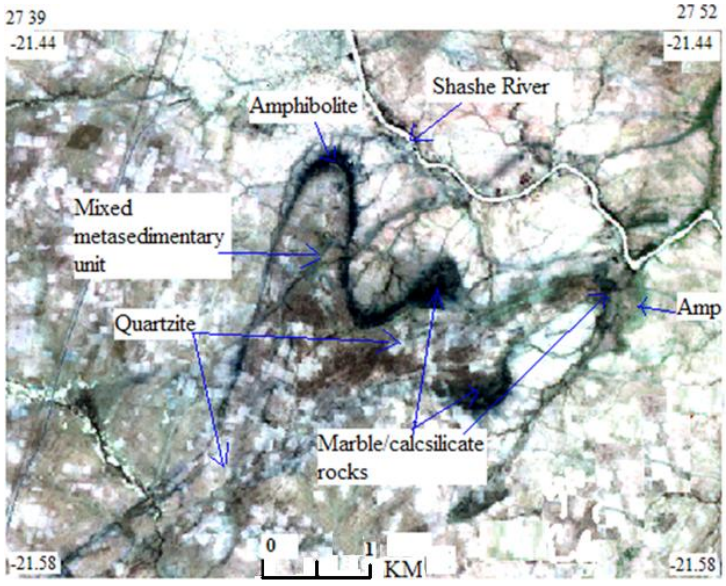

Figure 3.2 ASTER image showing the NNE and ENE closing Gulushabe structure. The dark units represent carbonate rocks, the green unit is amphibolite and the pale brown areas occupying the middle of the structure are underlain by quartzite.

Generally there is a poor development of reliable minor fold structures and associated lineations in the SFT area, especially in Domains 2 and 3. The association of lineations

with other structures can help in understanding the structural geometry of an area and in interpreting the conditions in which the structures formed (Ramsay and Huber, 1987; Twiss and Moore, 1992). Because lineations are generally smaller scale structures than folds and because small-scale structures commonly reflect the geometry of large-scale structures, it is often easier to map the orientation of folds structures by mapping the orientation of lineation that can be geometrically related to the fold hinges. Considering a situation where layering/bedding is buckled by pure shear under plane strain conditions, lineations that develop will be:

1. Fold axis, orientated parallel to the Y-axis of strain ellipsoid

2. Elongation lineation. The elongation lineation develops parallel to the X (long axis) of the strain ellipsoid, and pre-existing structures are rotated towards this axis and elongate by varying amounts depending on the amount of rotation. Under plane strain conditions the Y axis of the strain ellipsoid does not change length. There is shortening in the Z direction with equal extension in the X direction and this result in the development of an S: L fabric. The S fabric represents the axial planar cleavage and the L fabric (lineation) develops normal to the fold axis in the plane of the S fabric

3. Intersection lineation is formed by the intersection of the folded bedding or layering with the S fabric. An intersection lineation defined by a folded surface and by the axial foliation to the folds must lie parallel to the surfaces that defines them (i.e. in the plane of the layering) and plunges parallel to the fold axis if the folding is close to cylindrical

4. Slickenlines develop on the interface between layers at right angle to the fold axis when a layer is buckled by flexural slip. Slickenlines are found on bedding surfaces especially associated with flexural slip folds.

In the SFT area linear structures may be divided into mineral elongation lineation, slickenlines, lineations defined by long axis of deformed pebbles in quartzite units and lineations defined by fold axis in both the supracrustal rocks and the granitoid gneisses.

The lineations are treated geometrically and statistically using stereographic projection technique. A plot of linear and planar data in stereographic projections yields information about the geometry and orientation of each fold structure and orientation of deformation fabrics in each domain. The stereographic projections were generated using "GEORIENT 32V9" software on an Equal area, Lower Hemisphere nets and the contours are at 1% projection circle.

3.2 DEFORMATION FABRICS IN THE METASEDIMENTARY ROCKS (DOMAIN 1)

3.2.1 THE FOLEY STRUCTURE

In the Foley West area (dissertation map), folded metasedimentary outcrops form an elongated shape. The metasedimentary rocks consist of quartzite and associated quartz-mica schist, marble and a mixed metasedimentary unit that comprises an association of marbles and calc-silicate rocks interfolded with quartzite and amphibolites. These rocks are bound by K-feldspar megacrystic granite to the NW and SE. Deformation in the quartzite-quartz-mica schist unit in the Foley structure is characterized by a NE to ENE striking bedding (S_0) and bedding parallel foliation (S_1) that dips predominantly to the NW and NNW. Foliation (S_1) can be traced around tight to open fold closures (F_2) and is defined by an alternation of quartz and micas. The geometries of both small scale and map scale structures are compatible with folding along NE trending axial surfaces. Small-scale and map-scale folds show SE vergence indicating SE directed rotation and displacement. Trend lines on the geological map define fold structures closing to the SSW. Exposures of quartzite are characterized by elongation lineation or slickenlines on bedding surfaces that plunge parallel to dip.

3.2.2.1 FOLIATION AND LINEATION

Lineations are best developed in the quartzite unit but show a poor development in the mixed metasedimentary unit. In units of quartzite with pebble beds or pebble-bearing quartz-mica schist (e.g. localities 11, 12, 23 and 40 on the accompanying large scale geological map), deformed pebbles define a shape fabric. The pebbles have 2 axes of extension and 1 axis of shortening: pebbles are extended parallel to the fabric in cross

section, extended parallel to the fabric in plan and shortened perpendicular to the fabric in both cross-section and plan (Fig. 3.3 - 3.6). The geometry of this fabric is always the same; the maximum elongation direction (X-strain axis) plunges down dip typically NNW with subordinate elongation parallel to the ENE strike of the S_1 foliation. This NNW plunging pebble elongation suggests the Z axis was close to horizontal. This pebble elongation is considered to reflect the end result of F_1 and F_2 folding produced by oblate strain. According to (Ramsay and Huber, 1987) if subjected to flattening, a sphere is deformed into a pancake-shaped (oblate) ellipsoid. If subjected to constriction, it becomes a cigar-shaped (prolate) ellipsoid and if subjected to simple shear, it becomes an ellipsoid with axes inclined relative to the shear plane and no deformation parallel to the Y axis under plane strain conditions.

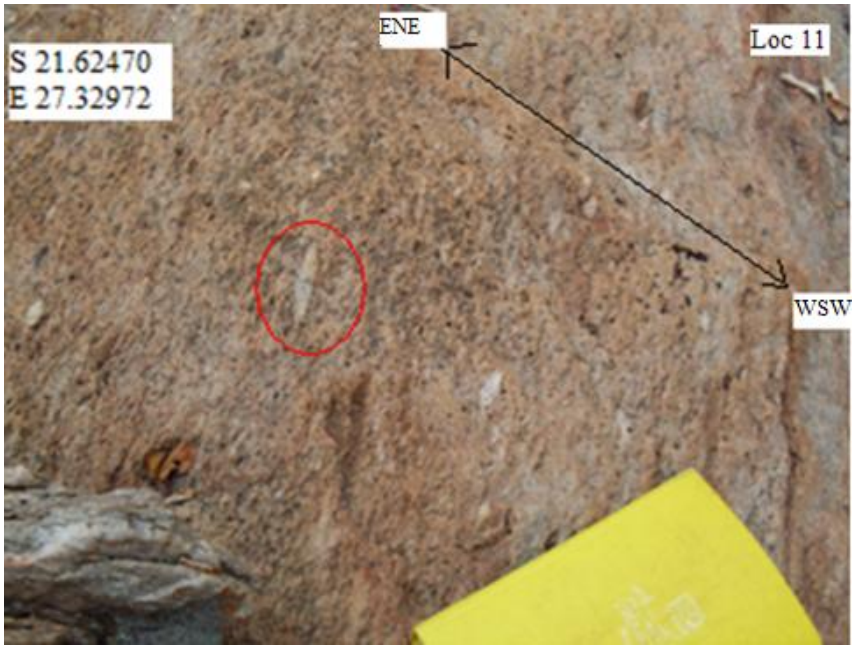

Figure 3.3: Section view of steeply NNW dipping quartzite outcrop. The maximum elongation defined by the long axis of pebbles plunges 80º/340°. Strike and dip of foliation is 250°/88°.

Figure 3.4: Dip profile of deformation fabrics in pebble-bearing quartz-mica schist within the Foley structure. Well-developed foliation dips NW and lineation defined by long axes of deformed pebbles plunge parallel to dip (60°/310°). Strike and dip of foliation is 226°/60°.

Figure 3.5: ENE-WSW striking foliation dipping NNW in pebble-bearing quartz-mica schist in the Foley structure. Elongation lineation plunges down dip towards NNW. Most of the flattened pebbles are obvious on the strike section. Plunge and trend of maximum elongation is 66°/340°. Strike and dip of foliation is 250°/88°.

Figure 3.6: Outcrop of deformed quartz pebble bed in mica schist unit. Photograph was captured looking down plunge of elongation lineation defined by pebbles. Dip of foliation and plunge of lineation is to the NNW. Plunge of lineation, 62°/329°. Strike and dip of foliation is 239°/62°. X and Y axes of strain are identified on deformed pebbles. Sketch to the right shows X, Y and Z axis of strain ellipsoid in relation to the shape of the deformed pebble.

3.2.1.2 FOLD STRUCTURES

Small scale folds related to the ENE trending large scale folds obvious from the geological map are linked to NNW-SSE compression. The small scale folds generally plunge to the NE to ENE and axial surfaces strike ENE-WSW and dip to the NNW. The folds deform bedding (So) and foliation (S_1) in the quartzite unit (Fig. 3.7 to 3.10) and are therefore F_2. At locality 33, a sub horizontal lineation is developed parallel to ENE-WSW trending fold axis (Fig. 3.7). The trend of the fold axis is parallel to the strike of the main regional ENE-WSW foliation fabric.

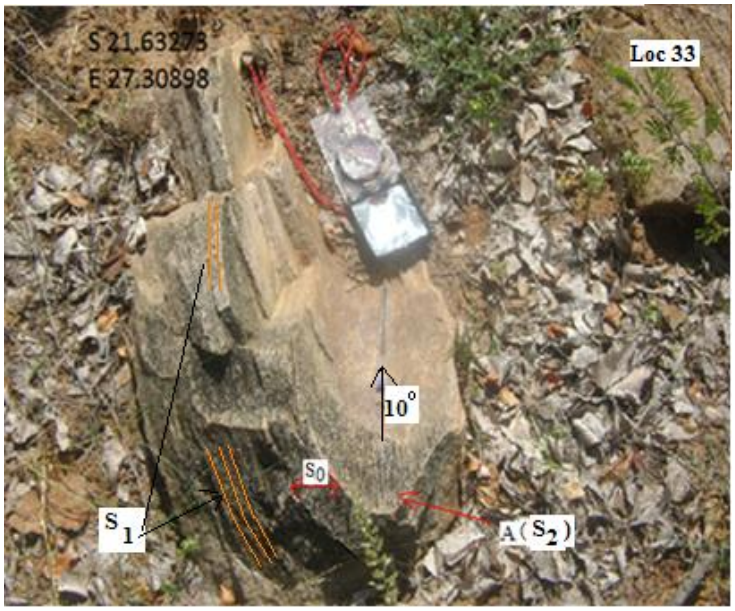

Figure 3.7: Small-scale fold (F_2) deforming bedding (S_0) and bedding parallel foliation (S_1). Folds plunge NE (10°/050°) parallel to pen. Note evidence for axial foliation at A. strike and dip of foliation (S_1), 250°/65°.Strike and dip of axial surface is 230º/65.º

A folded quartzite unit (Fig. 3.8) displays an axial planar foliation fabric denoted S_2 occurring at high angle to bedding (S_0) in fold closures. The primary surface (bedding, S_0) and the secondary surface (foliation, S_1) defines the fold and the fold is F_2.

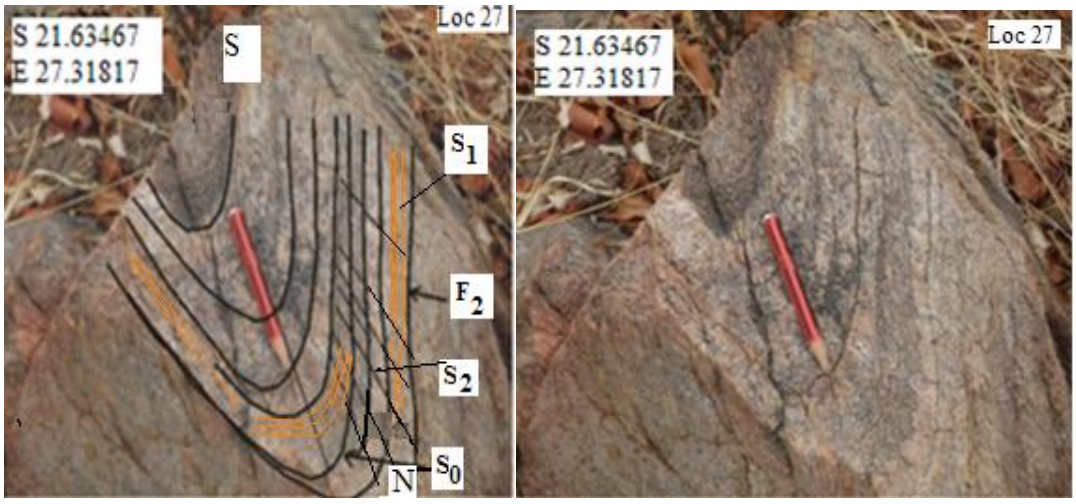

Figure 3.8: Profile view of an ENE plunging F_2 minor fold in the quartzite unit. Bedding (S_0) and foliation (S_1) define an F_2 fold. Strike and dip of fold axial plane is 240°/62°. Plunge of fold 32°/055°. F_2 axial planar foliation is designated S_2. Photograph from SW closure of Foley structure.

Figure 3.9: Minor F_2 fold in quartz-dominated schist plunging towards ENE, 60°/070°. Strike and dip of axial surface, 250º/68º, Foley structure.

Evidence for structural overprinting/refolding is the occurrence of crinkle lineation (asymmetric folds) deforming foliation in quartz-mica schist units (Figs 3.10 and 3.11). These folds typically deform bedding and a bedding parallel foliation (S_1) and are therefore F_2. Locally however there are a set of tight to open folds deforming flattened pebbles and foliation (Fig. 3.11). These folds plunge NNE and are interpreted as F_3.

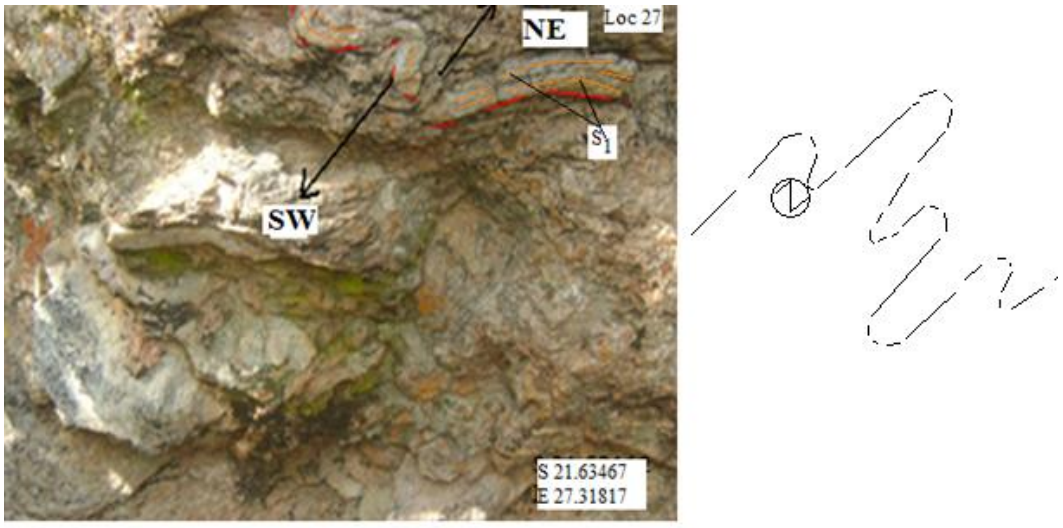

Figure 3.10: An elongation fabric on bedding in quartzite plunging ENE parallel to the axis of minor (F_2) fold. The minor fold is Z shaped suggesting the outcrop is from the limb left hand limb of the antiform as indicated on the sketch beside the photograph. Note the very obvious linear element going into the page and some asymmetrical folds (F_2) deforming older foliation carrying the linear element. Plunge of minor fold, 32°/055°.Strike and dip of axial surface, 240º/50º.

Figure 3.11: A unit of pebble-bearing quartz-mica schist that has been folded so that the foliation (S_1) and the flattened pebbles are deformed by small-scale folds (F_3) that plunges at 32°/010°, strike and dip of axial plane of minor fold is 220°/86°. Note slightly larger folds in more quartz rich bands to left of compass clinometer. Photograph captured from the N side of Foley structure.

3.2.1.3 GEOMETRICAL ANALYSIS OF STRUCTURAL ELEMENTS

The attitude of 49 foliation (S_1) and bedding planes measured from the Foley synformal structure are plotted in Fig. 3.12. The stereographic projection shows two concentrations of poles that plot on a great circle signifying folding. There is an obvious orientation of poles in the SE quadrant, signifying that the bedding and foliations steeply dip towards NNW. The poles in this quadrant represent data from the fold limbs. In addition there is a set of poles which plot in the SW quadrant. These represent bedding (S_0) and foliation (S_1) surfaces dipping to the NE and were measured around the fold closure. Bedding is dipping ENE around the SSW closure of the Foley structure and therefore this closure structure is a synform. The data from the Foley structure indicate a fold axis plunging towards NNE. The plunge and trend of the fold axis was calculated to be 50°/006° by fitting a great circle to the poles to bedding (bedding (S_0) and foliation (S_1) and data. This trend is not compatible with the plunge of minor folds measured in the field except at locality 12 (Fig 3.11), and is thus interpreted as F_3. The axial surface has a strike of 244º and a dip of 55º. The structural data indicate that the Foley structure is comprised of steeply NNW dipping rocks which have been folded into an ENE trending belt. The

elongation lineation of the Foley structure plunges down dip and is orientated at a high angle to the fold axis (Fig 3.12).

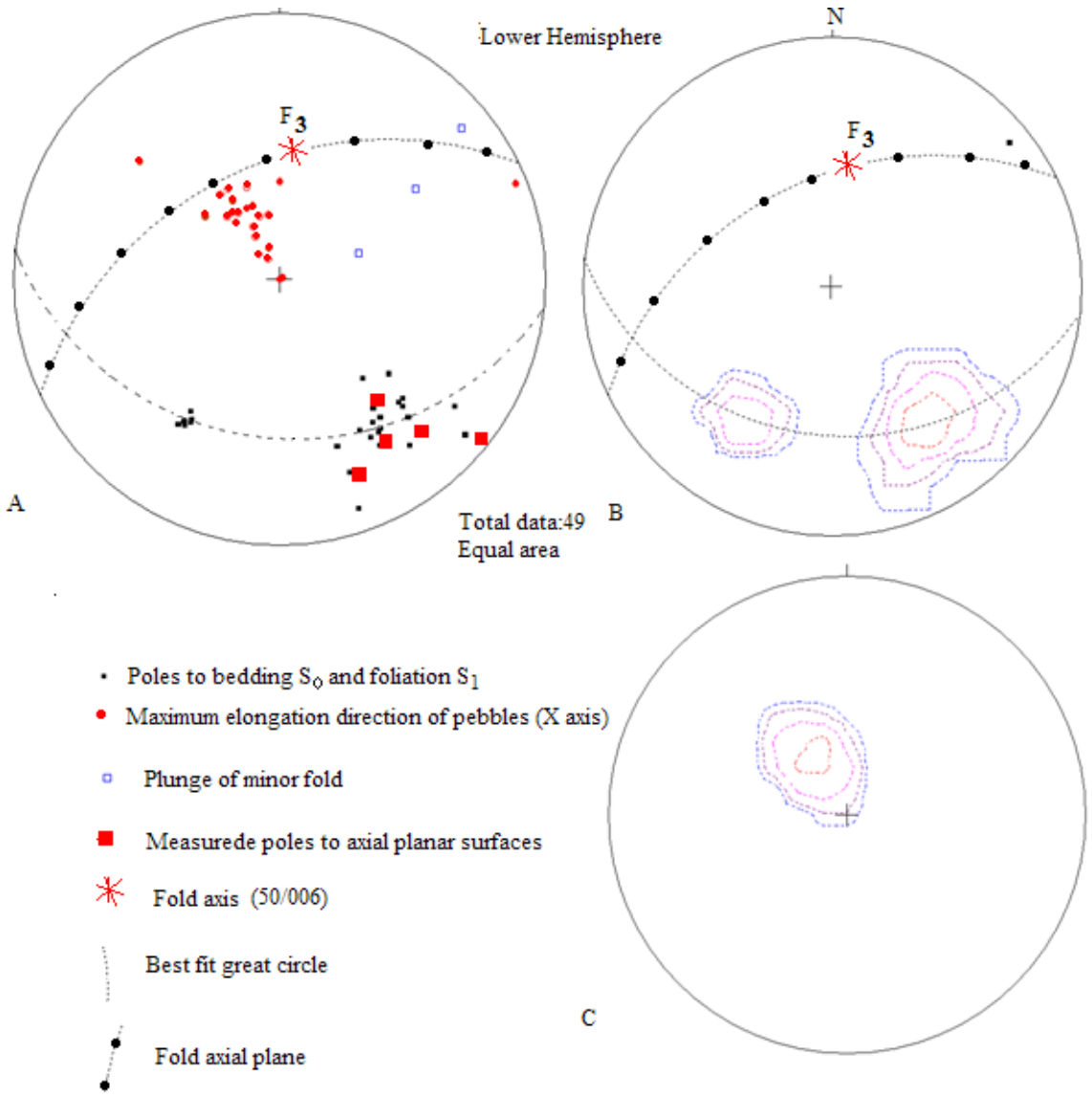

Figure 3.12: A-B: Structural orientation data from the Foley synformal structure
A) Equal area, Lower hemisphere projections of poles to bedding (S_o)/foliations (S_1), plunge of long axis of pebbles and plunge of measured minor folds (excluding Locality 12).
B) Contoured diagram of poles to bedding/foliation in A. C. Contoured plot of steeply NNW plunging elongation lineation defined by deformed quartz pebbles in the Foley structure (Domain 1).

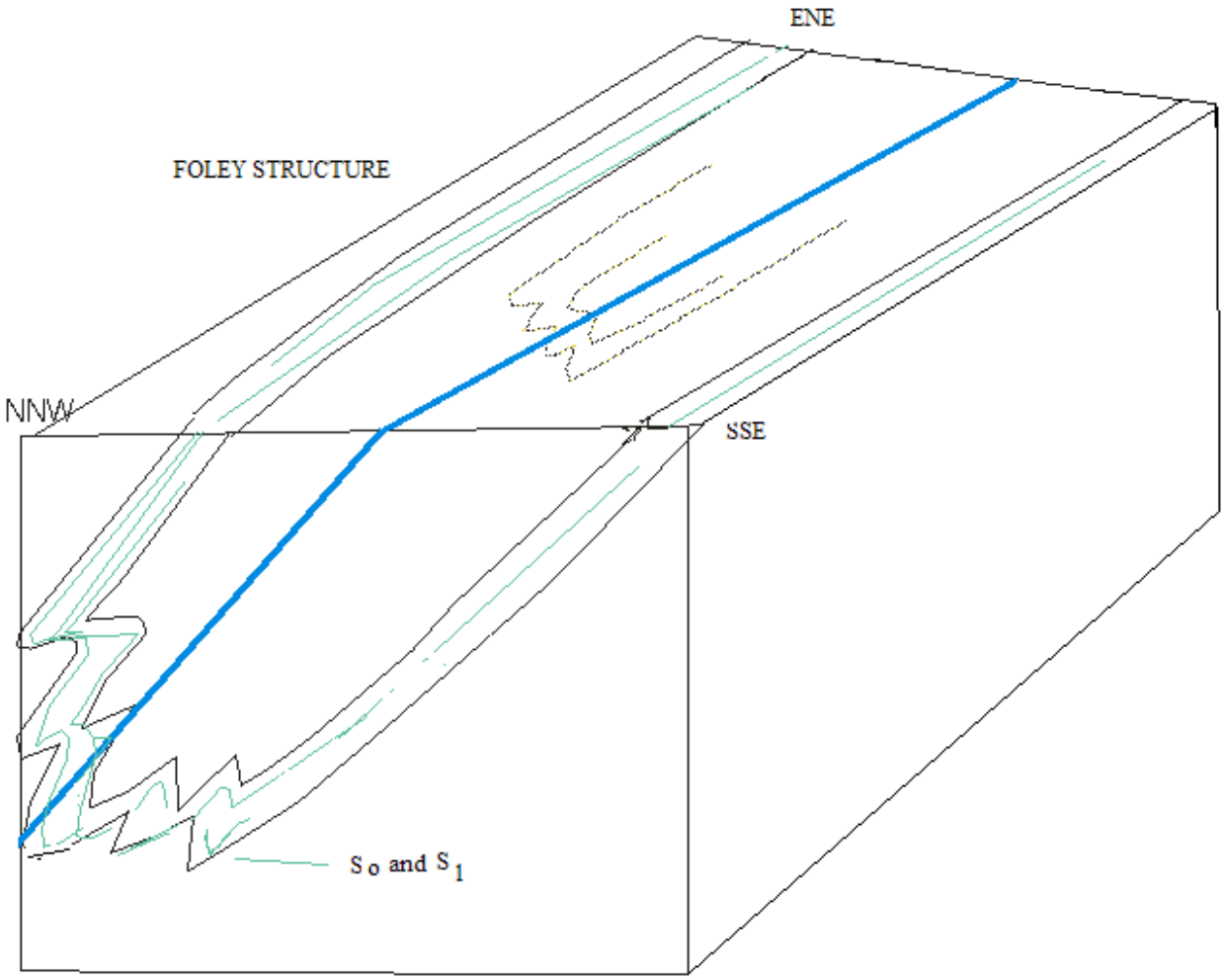

Figure 3.13: Cross section across the Foley synformal structure. F_2 axial plane strike and dip, 244°/55°. NB. Strike and dip values used were derived from plot on Figure 3.12.

3.2.2 THE GULUSHABE STRUCTURE

The Gulushabe structure is made up of a folded metasedimentary sequence that forms an ENE-WSW structure. Quartzite, marble, amphibolite and a mixed metasedimentary unit characterize the sequence. Foliations (S_1) dipping consistently NNW were recorded in the southeastern limb of the fold structure. Beds in the NW limb have been reoriented by folds trending NNE-SSW (F_3) thus dip and strike varies (Fig.3.14). Based on the regional trend on the dissertation map, the general shape of the Gulushabe structure is attributed to

coaxial folds trending ENE (such that F_1 and F_2 fold axes plunge to the NE and a younger NNE trending F_3 deformation.

The map shape of the main Gulushabe fold is an example of a Type 3 interference pattern also referred to as fish Hook fold (Fig. 3.14, Ramsay, 1962). With this type of pattern, the axial trace of the first fold (F_1) is curved, and the axial trace of the second fold (F_2) cuts the trace of F_1 (Fig. 3.14). The different types of interference patterns depend on two angles: the angle between the first generation axial surface and the second generation slip direction and the angle between the first generation fold axis and the second generation axial surface (e.g. Ramsay, 1967, Ramsay and Huber, 1987, Twiss and Moore, 1992). The trend of F_1 and F_2 axial trace on Figure 3.14 complies with ENE closing minor folds but not with the N closing folds on the NW limb of the main structure. As in the Foley structure, the rocks are flattened parallel to the S_1 foliation plane and elongated within the foliation. The tonalitic gneiss in the SE part of the Gulushabe structure (see dissertation map) truncates the F_1 axial trace implying that its intrusion was post-F_1.

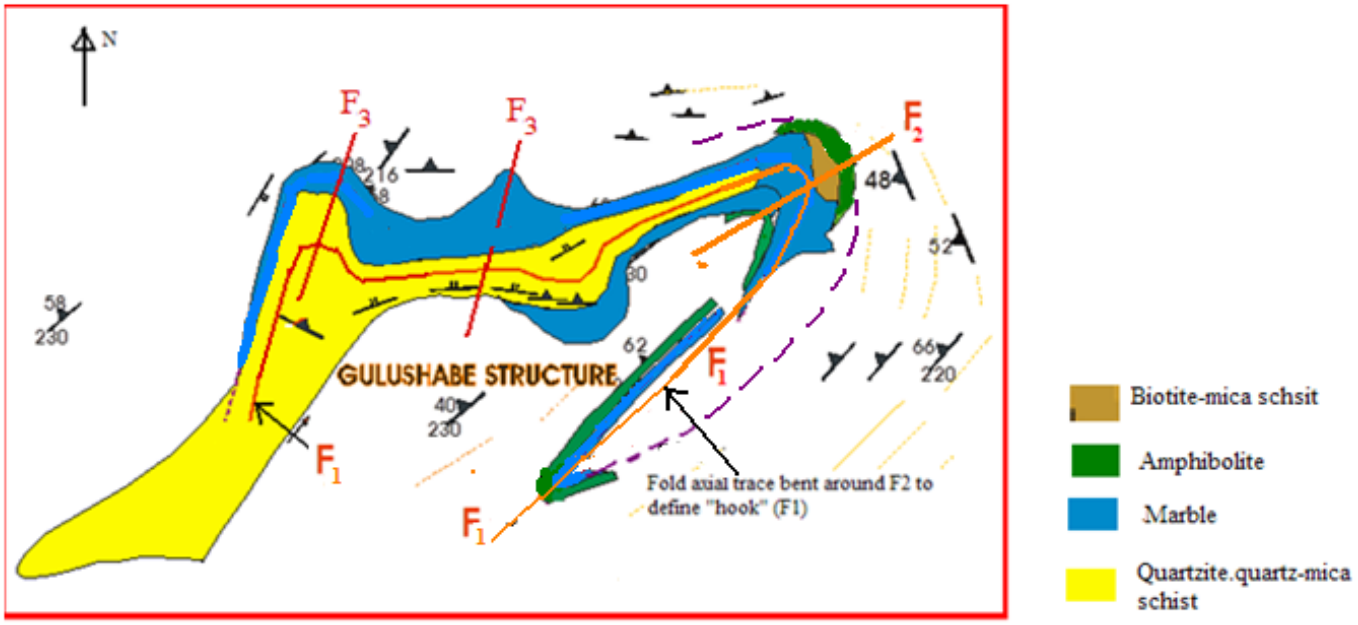

Figure 3.14: A Type 3 interference fold (plan view) due to refolding of F_1 axial surface trace by F_2. The N closing folds along the NW limb of the map pattern are interpreted as F_3 structures.

3.2.2.1 FOLIATION AND LINEATION

Generally, the elongation lineation in the Foley structure plunges steeply NW to NNW but in the Gulushabe structure the elongation lineation in pebbly quartzite unit developed on bedding planes in competent quartzite units plunge steeply N and NE (Figs 3.16 to 3.19) with an exception to Locality 188 (Figure 3.15) around the core of the Gulushabe structure where the elongation plunges NNW.

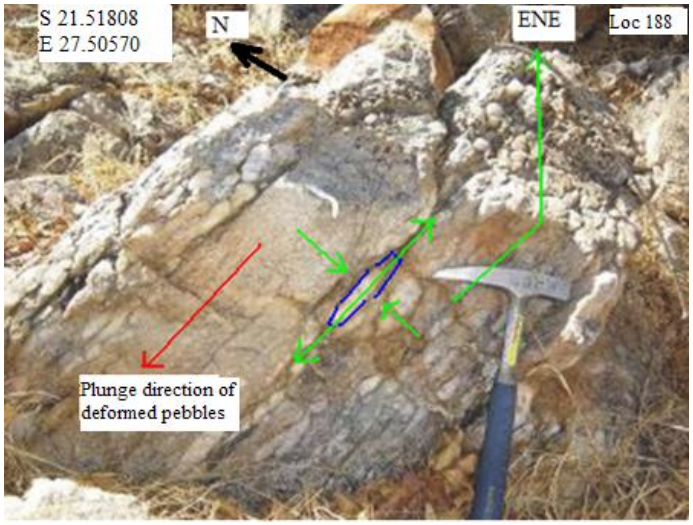

Figure 3.15: An alternation of pebbly quartzite and a non-pebbly bed defining bedding in the Gulushabe structure. Elongation lineation is defined by deformed pebbles, angle and direction of plunge; 66°/335°. Strike/dip of foliation (S_1), 243°/66°.

Figure 3.16: subvertical plunging lineation on WNW-ESE striking foliation (S_1). Strike and dip of foliation is; 300°/80°. Lineation plunges 75°/030°.

Figure 3.17: Elongation lineation defined by streaked quartz grains on bedding surface of the quartzite outcrop. Bedding (S_0) orientation, 300°/90°. Lineation plunges and trends 85°/030°, parallel to dip.

Figure 3.18: NNE trending elongation lineation on a quartzite unit defined by recrystallized quartz. The lineation plunges towards NNE (50°/005°). Strike and dip of foliation (S_1) is 270º/52º.

Figure 3.19: Elongation lineation on the bedding surface of quartzite plunging parallel to dip (60°/360°). Strike/dip of bedding (S_0), 268°/60°. Photograph from SE of Gulushabe settlement.

The biotite schist in the ENE closure of the Gulushabe structure (Locality 287) shows axial planar foliation. Felsic bands in the schist show evidence of flattening perpendicular to the foliation and elongation parallel to dip (Fig. 3.20). The foliation dips NNW and based on the position of the locality 287 in the fold closure, it is interpreted as S_2.

Figure 3.20: Well developed S_2 foliation (S_1) in biotite schist dipping steeply to the NW with deformed felsic material; strike and dip of foliation, 242°/68° in the closure of the Gulushabe structure.

3.2.2.2 FOLD STRUCTURES

The geometries of both small scale and map scale structures are compatible with folding along ENE-WSW trending axial surfaces. Small-scale folds in the Gulushabe structure (Fig 3.21 and 3.22) have steeply dipping axial surfaces (248º/88º) and fold axes plunging ENE (65º/050º). Both bedding (S_0) and foliation (S_1) are deformed.

A B

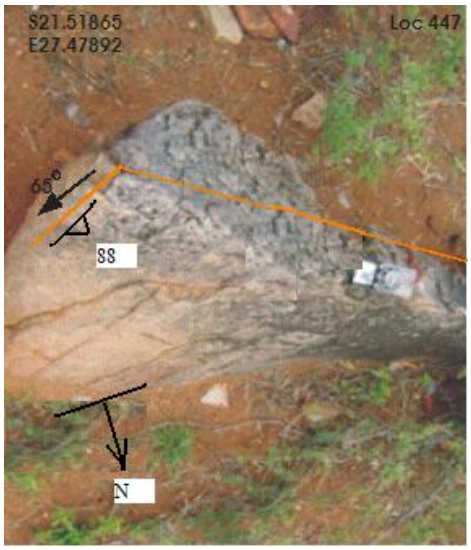

C

Figure 3.21 A, B and C: F_2 minor fold structure in the quartzite from the Gulushabe structure. Photograph B and C are the same structure captured from different views. Figure A was captured facing NE, B captured facing SW and C captured facing SE. Axial surface is orientated ENE-WSW; 248°/88°. Plunge of fold axis 65°/068°.

Figure 3.22: A-B: Example of NE-SW trending small scale fold structures in quartz-mica schist. **Plunge of fold 60°/248°**

3.2.2.3 GEOMETRICAL ANALYSIS OF STRUCTURAL ELEMENTS

The attitude of 24 foliation (S_1) and bedding planes that were measured in the Gulushabe structure are plotted on Figure 3.23. The projection shows a concentration of poles in the SE quadrant and a spread of poles in the SW quadrant. Those in the SE quadrant represent NNW dipping bedding (S_0) and foliation (S_1) in the southeastern limb of the Gulushabe fold. Poles to bedding (S_0) /foliation (S_1) in the SW quadrant were measured from the fold closure.The poles plot along a great circle and gave a value for the fold axis plunge and plunge direction of 49º/014º. The axial surface has a strike and dip of 254º/53º. Bedding and foliations around the closure of Gulushabe structure (Locality 287 on dissertation map) strike 345 and dip 60 ENE indicating a fold closure is antiformal and plunging ENE. Of note is the similarity between the steep NE plunges of elongation lineation in the Gulushabe structure and those in the Gulushabe shear zone (Domain 4). A NW-SE cross section across the antiformal structure is sketched in Figure 3.24. The elongation lineations of the Gulushabe antiformal structure are steeper than the F_3 axis, suggesting that the X axis of the strain ellipsoid is at an angle to the F_3 fold axis indicated in Figure 3.23.

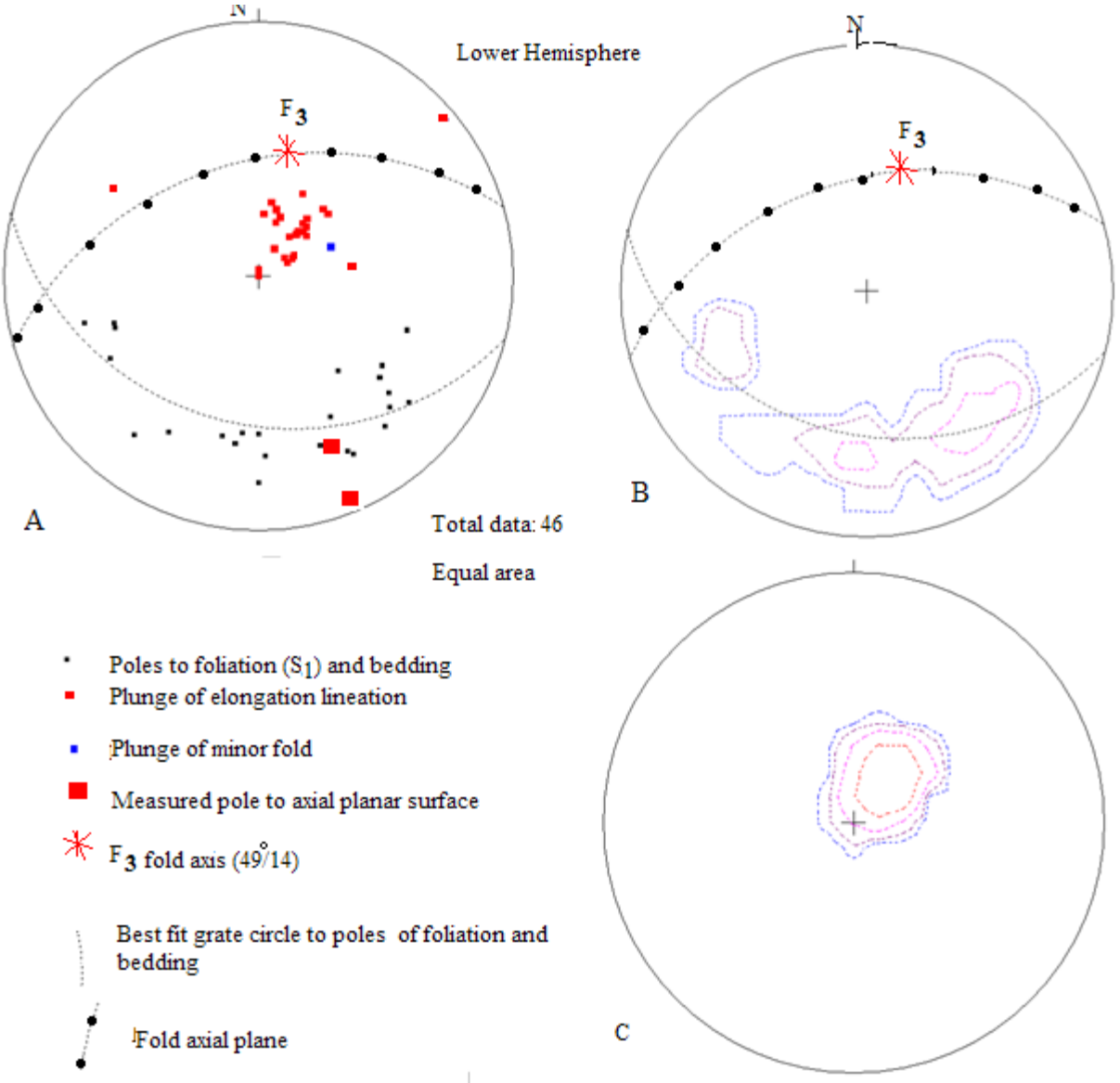

Figure 3.23 A: Stereographic projection of poles to bedding (S_0) /foliation(S_1) with lianeations, plunge of elongation lineations and plunge of minor folds from the Gulushabe structure. B: contoured plot of poles to bedding (S_o)/foliation (S_1). C. Contoured plot of elongation lineations.

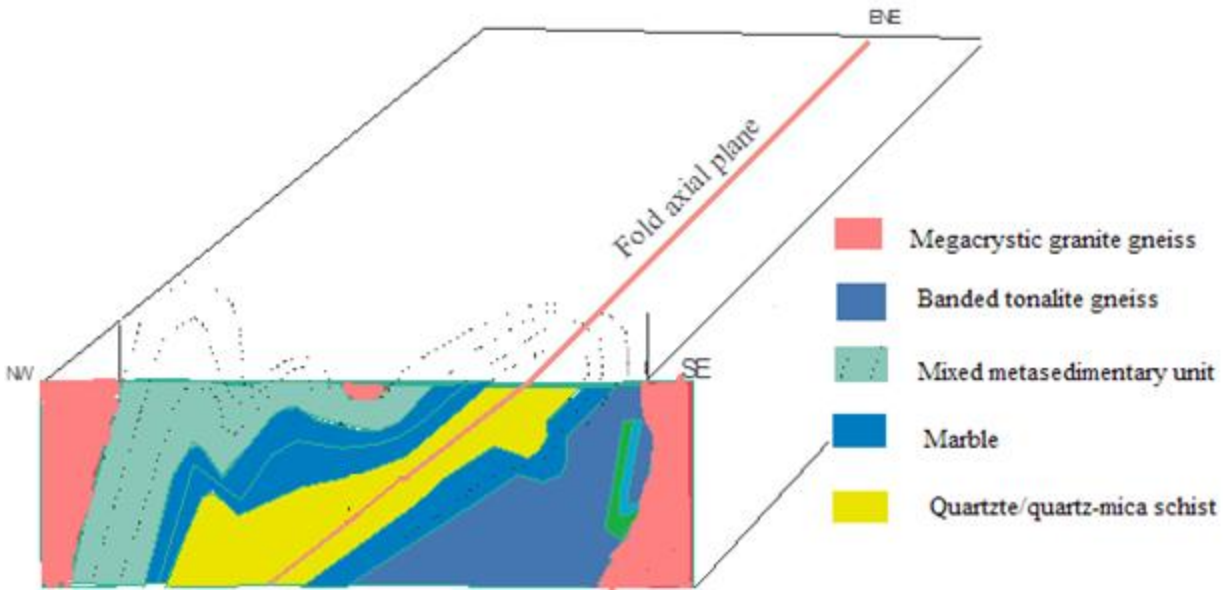

Figure 3.24. NW-SE cross section across the Gulushabe structure. Fold axial plane has a strike and dip of 242°/68°

3.2.3 DISCUSSION

On the dissertation map the trend of the metasedimentary belt and the large scale folds indicated by the outcrop pattern is generally ENE or NE. The map scale folds (the Foley and Gulushabe structures) and minor folds deforming bedding (S_0) and foliation (S_1) plunge to the ENE and are related to NNW or NW or compression.

The outcrop pattern of the Foley fold structure closes to the SSW indicating a synform plunging ENE. Elongation lineation on the fold limbs defined by the long axes of deformed pebbles plunges NNW (Fig 3.23). It is worth noting that stereographic projections of bedding (S_0) and foliation (S_1) and indicate a fold plunging NNE (006º) with an axial surface striking ENE-WSW (244°). This fold axis is not compatible with the overall ENE trace of the Foley structure and the plunge of minor folds in Figure 3.21.

The overall map shape of the Gulushabe fold suggests that it is an antiform that closes to the ENE. The map pattern of the Gulushabe structure shows that it plunges ENE. Minor folds deforming bedding plunge ENE. Lineation developed in the quartzite unit plunges N to NE subparallel to bedding and probably represents slickenlines. The stereographic projection of poles to bedding (S_0) and foliation (S_1) in the Gulushabe structure indicates

a fold plunging at 49° to the NNE (014º). As in the Foley structure, the NNE plunge of this fold axis (Fig.3.23) does not correspond with the map scale folds trending ENE. This NNE plunging axis is interpreted to represent a younger (F_3) deformation. A younger set of folds (F_3) plunging NNE such as the one in Fig. 3.11 from the Foley structure, deform the foliation. Both the foliation (S_2) and the pebbles at this outcrop are deformed indicating the crinkle lineation is post F_2.The orientation of these folds is related to map scale NNE trending folds around the N closure of the Gulushabe structure, near Shashe and N of Tonota Village. These NNE trending folds reflect a third generation of folding deformation in both the Foley and Gulushabe areas. The production of these folds is attributed to WNW-ESE horizontal compression. The NNE plunge of the fold axis of the Foley structure as plotted in Figs3.12 reflects this deformation, hence the contradiction in orientation between the map scale folds and the projected folds in Domain 1.

Based on field analysis of metasedimentary rocks, the first evidence for deformation in the metasedimentary rocks is represented by ENE-WSW orientated foliation (S_1) that is axial planar to folding of bedding (S_0). F_2 folds plunge NE to ENE parallel to F_1 folds, implying that folding was coaxial. The coaxial deformation in the metasedimentary belt is attributed to NW-SE compression causing flattening perpendicular to layering. The Foley and Gulushabe structures are products of the F_1/F_2 coaxial folding deformation (NW-SE compression) modified by F_3 deformation (WNW-ESE compression). The map pattern shows that the Foley synformal and Gulushabe antiformal structures do not lie along strike and are therefore not easily connected. Based on the stereographic projections (Figs.312 and 3.23) the deformation fabrics in the supracrustal rocks indicate folding with fold axis trending NNE-SSW which is compatible with local (F_3) minor folds seen in the field but not with the NE to ENE (F_1+F_2) trending minor folds (Figs 3.7,3.8,3.9 and 3.10).

3.3 DEFORMATION OF THE GRANITOID ROCKS

3.3.1 DOMAIN 2

3.3.1.1 DEFORMATION FABRICS

Domain 2 is dominated by megacrystic granite gneiss interpreted to have been formed by the deformation of porphyritic granite. Although the geometry of the foliation (S_1) is consistent across Domain 2, the intensity of the foliation differs, with the fabric in the gneisses exposed SW of Shashe Dam much more intense than the rest of Domain 2. The foliation (S_1) is defined by the preferred orientation of deformed K-feldspar megacrysts and mineral alignment (Fig. 3.25, 3.26 and 3.27). The foliation (S_1) strikes dominantly NNE (020º) and dips moderately to steeply (44°-70°) WNW. Compositional banding is also present (Fig. 3.28 B). In the megacrystic gneiss, the shape of the K-feldspar megacrysts indicates flattening perpendicular to the foliation and elongation parallel to both dip and strike of the foliation (S_1) surface (Figs 3.25, 3.26 and 3.28 A), with maximum elongation parallel to the dip of the foliation (3.28A).

The orientation of the intersection lineation on the dyke contact (as indicated in Figure 3.29 has the same orientation as the elongation defined by deformed K-feldspar megacrysts in Figure 3.28 A, implying that they are geometrically related or were developed by the same deformation event. There is an elongation lineation that lies oblique on the foliation (S_1) surface and plunges moderately to gently N to NNE (Figs. 3.32 and 3.33) and locally SW (Fig. 3.31).

The maximum elongation direction of the megacrysts is consistently parallel to the dip of the foliation but no zones of intense elongation with associated shear sense indicators related to zones of simple shear (ductile shear zones) were obvious possibly due to the lack of good outcrop in the vertical section. Evidence against simple shear includes lack of well developed elongation lineation and kinematic indicators such as asymmetrical tails to porphyroclasts in megacrystic granite gneiss and asymmetrical folds of the foliation. The evidence (asymmetrical folds) to support simple shear is restricted to a few

of outcrops along the boundary between the granitoids of Domain 2 and the Tonota biotite gneiss (Locality 44 on dissertation map).

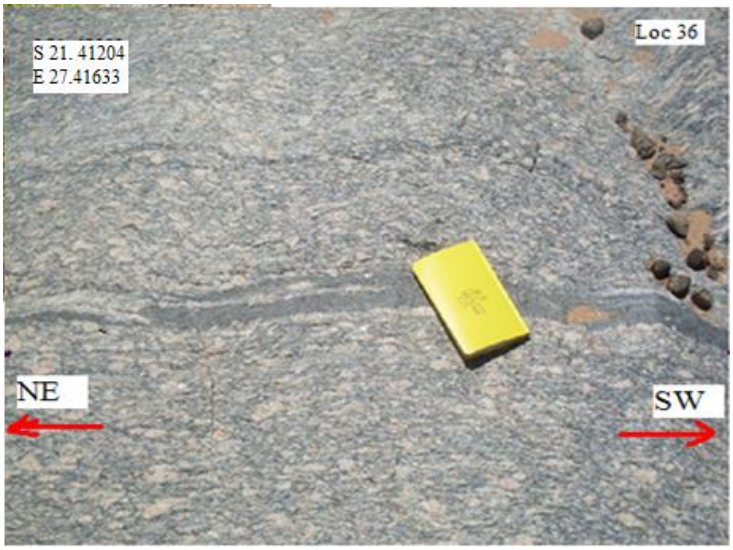

Figure 3.25: Plan view of shape fabric foliation (S_1) in megacrystic granite gneiss NW of Tonota Village. Strike and dip of foliation is 220°/76. Shapes of megacrysts indicate shortening NW-SE.

Figure 3.26: Well developed foliation (S_1) in oblique view in megacrystic granite gneiss such that both strike and dip directions are obvious. Strike and dip of foliation is 190°/70°. Handle of hammer at top left corner of photograph is pointing NE and placed parallel to strike of foliation.

Figure 3.27: Steeply WNW dipping foliation (S_1) in the megacrystic granite gneiss (190º/70º) to the SSW of Tonota Village. Note asymmetric tails to feldspar megacrysts indicating dextral rotation and therefore down dip displacement. NB: Plan view of photograph in Figure 3.26.

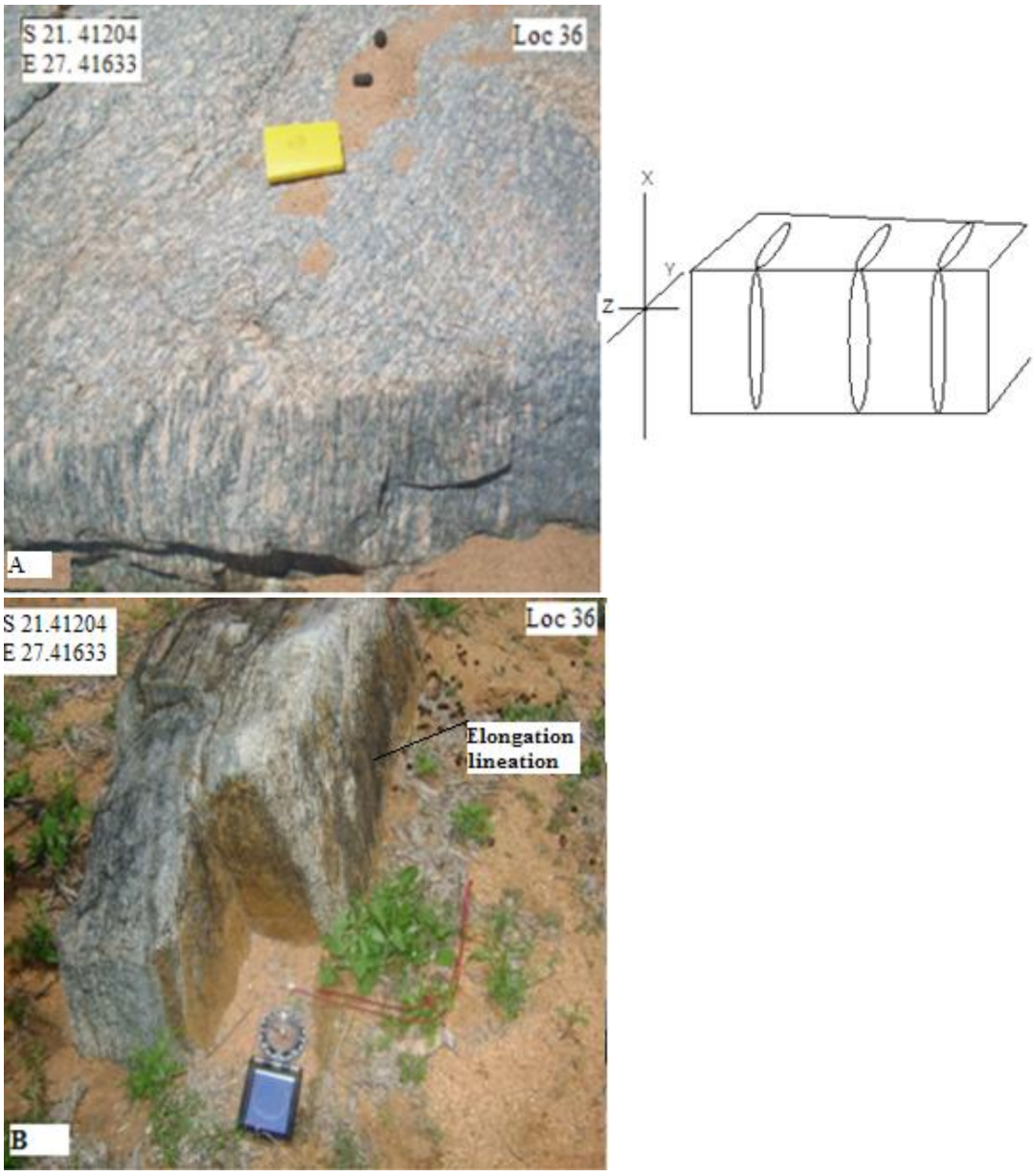

Figure 3.28: A: Well developed planar deformation fabric (foliation, S_1) in megacrystic granite gneiss. Strike and dip of foliation is220º/88º. Shape of K-feldspar megacrysts indicate flattening perpendicular to the foliation and elongation parallel to the foliation surface with maximum elongation direction parallel to dip. B. Compositionally banded granite gneiss inclusion within main outcrop of megacrystic granite gneiss outcrop displaying evidence for flattening perpendicular to foliation and elongation parallel to the foliation. Elongation lineation plunges plunges 76°/310° in B.

Sketch beside photograph shows the shape fabric of the steeply plunging lineation in relation to the axes of the strain ellipsoid.

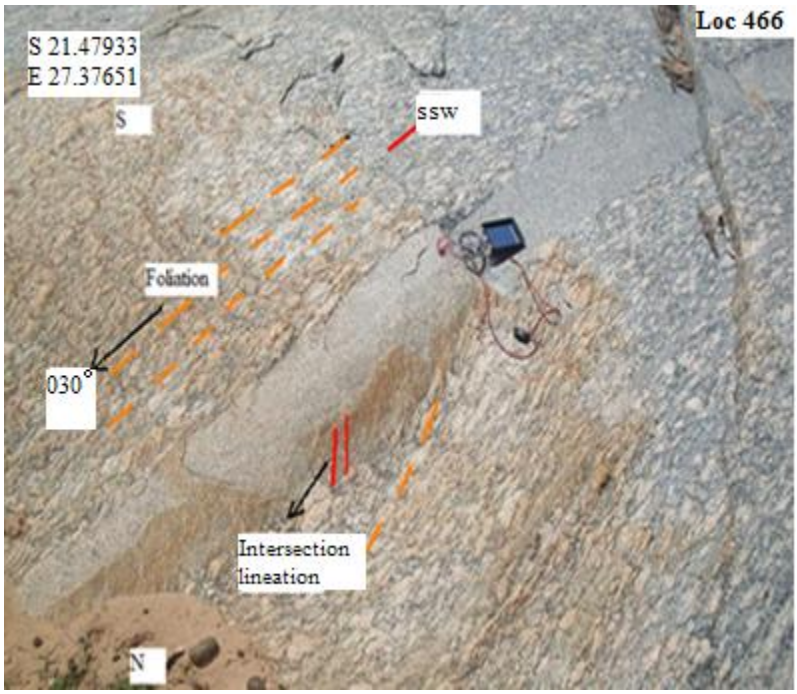

Figure 3.29: Well developed intersection lineation of foliation (S_1) with dyke contact in megacrystic granite gneiss. The lineation plunges 90°/300°. Foliation strikes NNE-SSW (210) and dips vertically (90°). Note fine grained felsic dyke slightly discordant to foliation. SSW of Tonota.

The extension direction during boudinage is down dip i.e. parallel to the WNW plunging elongation lineation defined by both deformed K-feldspar megacryst and elongation lineation on dyke surfaces (Fig. 3.29). Felsic bands are elongated parallel to the foliation (S_1) and flattened perpendicular to the foliation such that they appear "augen" shaped.

Figure 3.30: Well developed foliation (S_1) in banded tonalitic gneiss with boudinage developed in more competent felsic unit. Photograph captured W of Tonota. Strike and dip of foliation is 212°/52°.

Figure 3.31: Mineral elongation lineation in megacrystic granite gneiss plunging obliquely to the SW; 45º/220°. Photograph from N of Shashe Village. Strike and dip of foliation (S_1) is 210°/60°.

Figure 3.32: Elongation lineation gently plunging obliquely to the N (28º/360º) in a banded tonalite unit layer occurring within the main outcrop of megacrystic granite gneiss. Photograph captured W of Makomoto Village. Strike and dip of foliation (S_1) ~ 224°/70°.

Figure 3.33: Elongation lineation in megacrystic granite gneiss plunging gently to the NNE: 25º/020°. Photograph from N of Shashe Village. Strike and dip of foliation is 200º/78º.

3.3.1.2 FOLD STRUCTURES

Minor fold structures with axes trending NNE-SSW and axial surfaces dipping to the WNW have been recognized in the gneisses S and SE of the Shashe Dam; At locality 44 (along the boundary between Domain 1 and the metasedimentary belt SW of Tonota, Figure 3.34), Locality 299 (N of Tonota Village, Figure 3.35) and Locality 9 (SW of Shashe Village, Figure 3.36) and Locality 16 (N of Shashe Village, Fig 3.37). These tight to isoclinal folds deform the WNW dipping foliation (S_1) in the megacrystic granite gneiss (Figs 3.34-3.38) and indicate up dip rotation to the ESE (Locality 44), down dip rotation to the ESE (Locality 299) and down dip rotation to the WNW (locality 9). The kinematics at these localities are ambiguous showing conflicting senses of rotation. As the folds deform S_1 they are F_2. The folds have NNE to SSW trending axial surfaces and the trend of the fold axis is parallel to the NNE strike of the main regional foliation fabric.

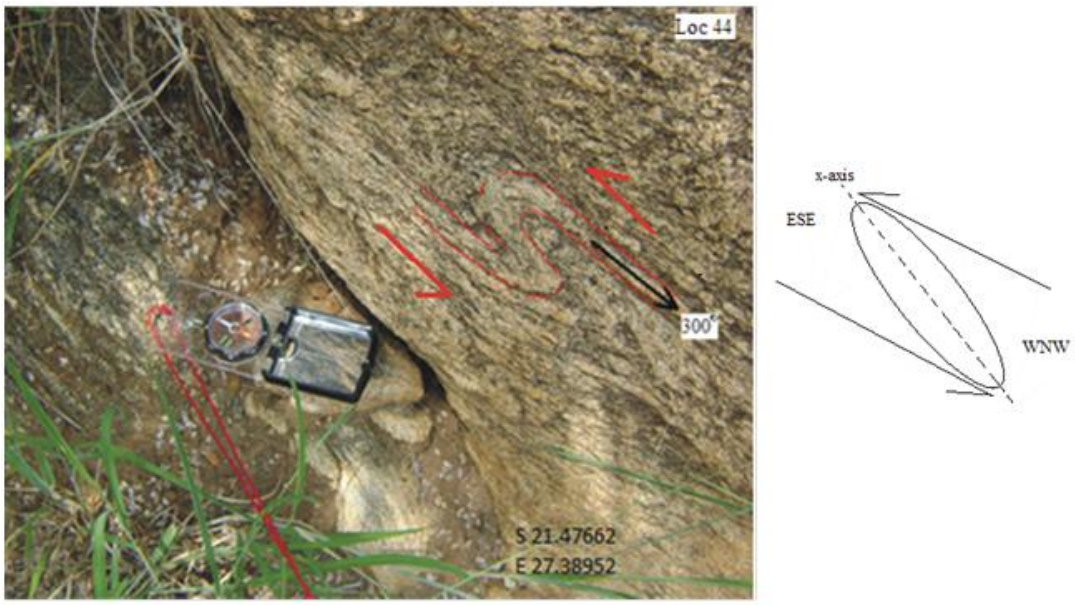

Figure 3.34: Minor fold plunging at 005 to 010º, with axial surface dipping WNW. Deformed foliation (S_1) dips at 58° WNW (191°/58º). Strike and dip of axial surface is 191°/58º. The minor fold is asymmetric indicating rotation to the ESE. Photograph from SW of Tonota Village. Sketches to the right of photograph show photographic interpretations of movement directions.

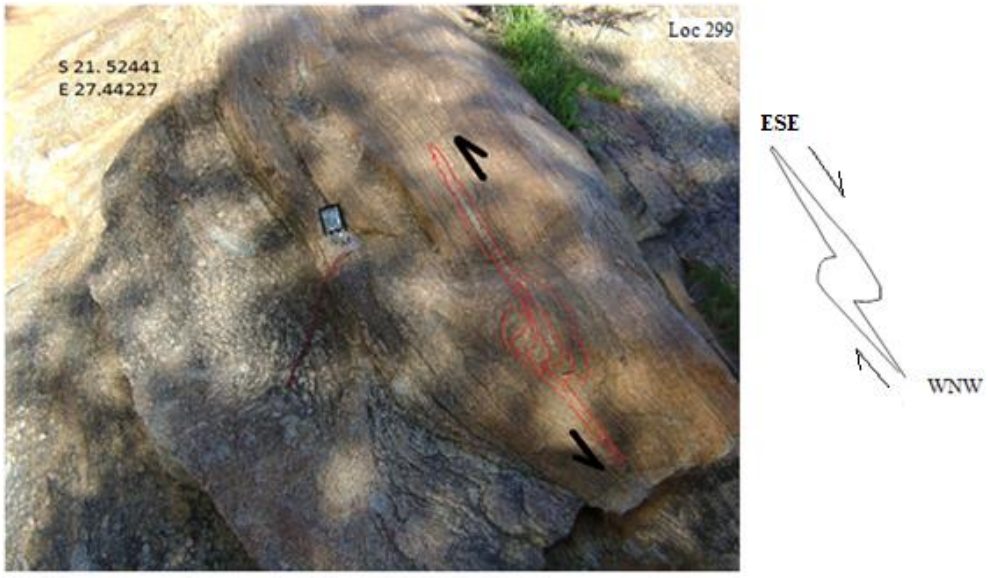

Figure 3.35: Outcrop of foliated granite gneiss interlayered with megacrystic granite gneiss at locality 299, photograph from N of Tonota Village. Foliation (S_1) that is deformed dip WNW (198/60º) and kinematic indicators as highlighted suggest shear sense displacement to the ENE (down dip displacement). Sketch beside to the right shows interpretation sense of movement directions based on the photograph.

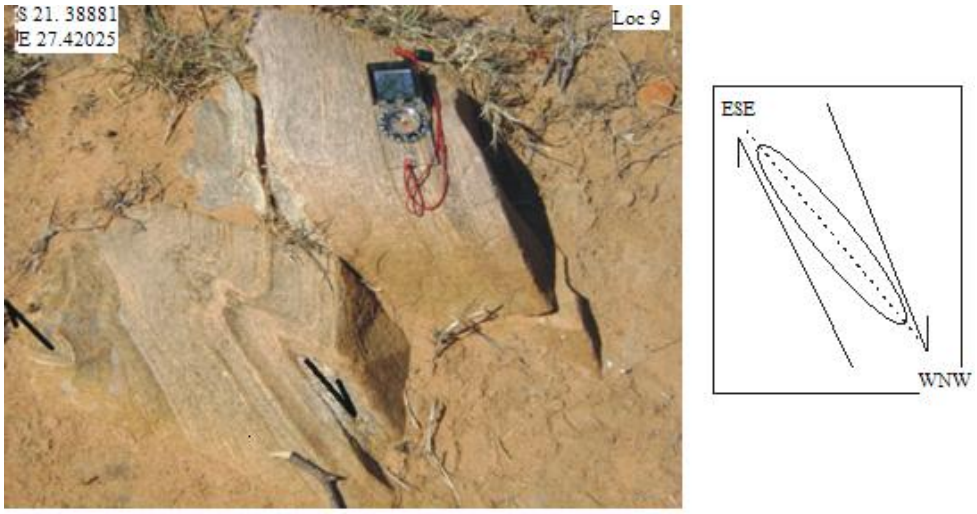

Figure 3.36: Outcrop of high strain tonalitic granite gneiss with well-developed NNE-SSW trending, WNW dipping foliation (S_1), strike and dip, (190º/70º) that is deformed by reclined folds with N-S axial plane plane and a minor fold suggesting dextral shearing orientated NNE-SSW. Minor fold at the dark arrow to the left of photo plunges, 00º/020º. Strike and dip of axial plane is 200º/70º. A down dip sense of displacement is indicated. Photograph from SW of Shashe Village. Sketch beside photograph is an interpretation of movement direction.

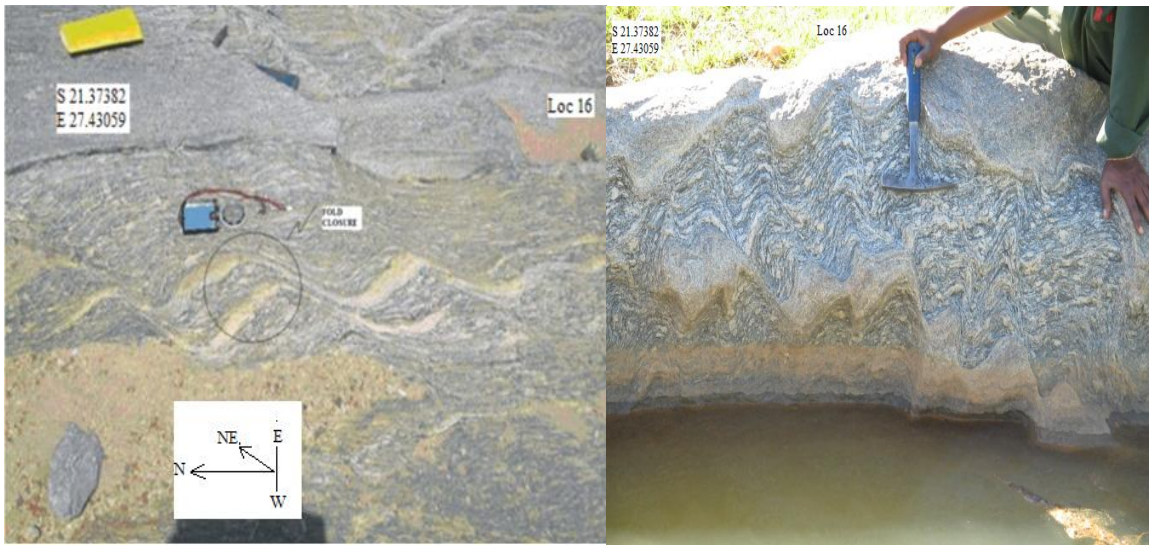

A **B**

Figure 3.37: A: NNE-SSW trending small-scale open drag folds in megacrystic granite gneiss. Strike and dip of foliation (S_1) is 180°/60°. B. Section view of fairly symmetrical folds with close to upright axial surfaces at the same locality. Whereas folds in A show a top to NW movement, those in B are slightly rotated to the SW. Minor fold in A plunges subhorizontally (03º) towards 030º. Strike and dip of axial surface in A is 210º/90º. Note: Figure A is a plan view of minor folds in Figure B and figure 3.38.

Figure 3.38: A. Section view of NNE-SSW trending asymmetrical folds with closely spaced (cm-scale) axial planes deforming foliation (S_1) in megacrystic granite gneiss. Folds trend NNE and verge to the WNW. Pen lies parallel to fold axis. Strike and dip of fold axial planes 210°/56º. The red lines are axial planes of the asymmetric folds. Plunge of minor fold 00º/030º

3.3.1.3 GEOMETRICAL ANALYSIS OF STRUCTURAL ELEMENTS

The attitudes of 35 foliation (S_1) planes were measured in Domain 2. The stereogram in Figure 3.39 shows a general concentration of poles to foliation (S_1) in the ESE quadrant of the projection signifying that the foliations (S_1) are steeply dipping towards WNW and the centre of the contoured pattern corresponds to an average foliation surface. The pole to the best fit great circle gives a value for the plunge of the fold axis of 28º/017º. The strike and dip of the axial plane was calculated to be 215º/60º. The sets of data in the NE and SW quadrants (red dots) represent N and NNE (Fig 3.32 and 3.33), SW (Fig 3.31) and sub- vertical to vertically plunging elongation lineation (3.28 A, 3.29). Measured minor folds indicated in Figure 3.39 plunge NNE or almost due N.

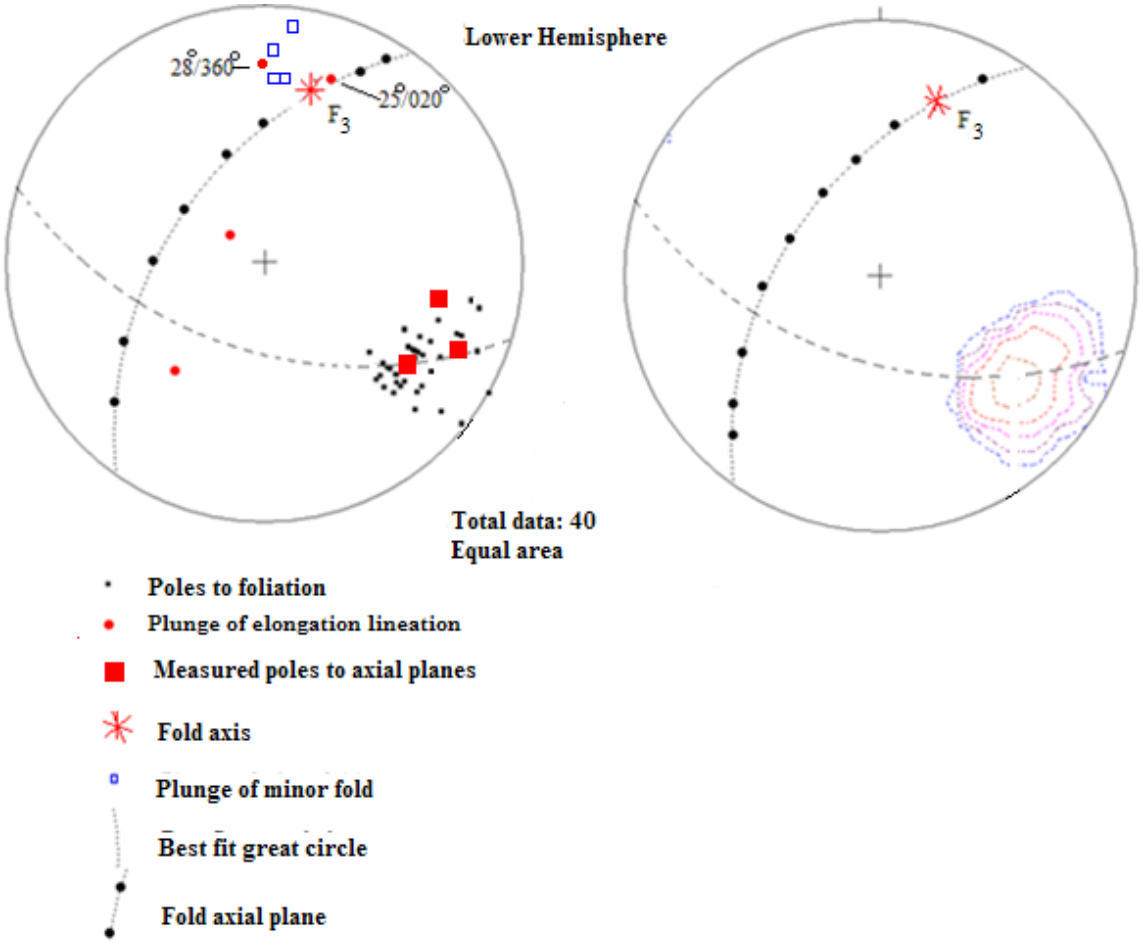

Figure 3.39: A: Equal area, lower hemisphere projection of poles to foliation (S_1), plunge of elongation lineation and plunge of minor folds from Domain 2. B: Contoured diagram of poles to foliation (S_1) in A.

3.3.2 DOMAIN 3

3.3.2.1 DEFORMATION FABRICS

Foliation (S_1) in granitoid gneisses in Domain 3 trends ENE-WSW and dips steeply to the NNW. Lineation in this domain is not well developed but where found, elongation lineation plunges gently WSW (Fig. 3.40) and ENE (Fig. 3.42 and 3.43). At locality 405 (to the west of position of Fig. 3.40) close to Foley settlement, outcrops of megacrystic granite gneiss are characterized by a strongly developed elongation lineation but weak foliation (S_1) to produce a L>S tectonite. Due to the strongly developed linear extension direction in these outcrops, loose blocks have an almost prolate shape (Fig. 3.41). On surfaces perpendicular to the elongation direction (X) the K-feldspar megacrysts show minimal shape change and only weakly developed shape preferred orientation (shape fabric foliation (S_1), Fig. 3.42). No minor folds were found in this domain.

Figure 3.40: A shallow plunging elongation lineation on megacrystic granite gneiss plunging WSW, and defined by quartz on a surface that is folded. Foliation (S_1) strikes 252°/62°, Lineation plunges 30°/260. E of Foley. Drawing to the right shows orientation of lineation with respect to the axis of strain ellipsoid.

Figure 3.41: L>S fabric development in megacrystic granite gneiss at Foley settlement. Note elongation aspect of loose block and weak shape fabric foliation (S_1) on broken surface.

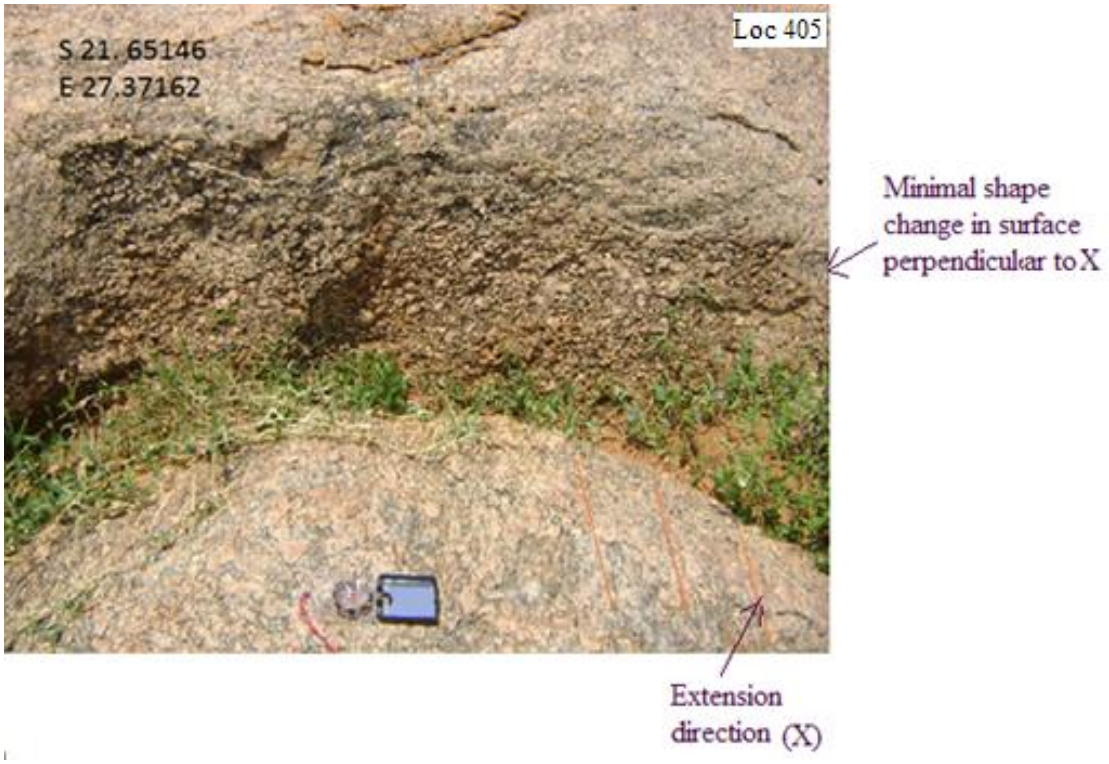

Figure 3.42: L-tectonite with K-feldspar showing minimal shape change in surface perpendicular to extension direction. Elongation lineation plunges ENE; 24º/070°.

3.3.2.2 GEOMETRICAL ANALYSIS OF STRUCTURAL ELEMENTS

The attitude of 16 foliation (S_1) planes and 2 elongation lineation measured in Domain 3 from the area SE of the metasedimentary belt is plotted in Figure 3.43. The diagram shows 2 distinct maxima with one situated in the SSE quadrant indicating foliation (S_1) dipping to the NNW. The 5 poles to foliation in the NE quadrant reflect readings from the northern part of Domain 3 (Localities 327 and 328) where foliation strikes ~155 and dips WSW. The cause of this change is unknown but may reflect folding of the foliation (S_1) in the megacrystic gneiss around the Gulushabe structure or deformation associated with the Gulushabe shear zone. The fold axis indicated on the plot plunges 42º towards 280º, a direction not recognised in the field. The strike and dip of the associated axial surface is 223º/47º (Fig. 3.43). The L-tectonite developed between Foley village and Mankha Hill (see dissertation map) trends at about 070-250 and plunges to the ENE and SSW.

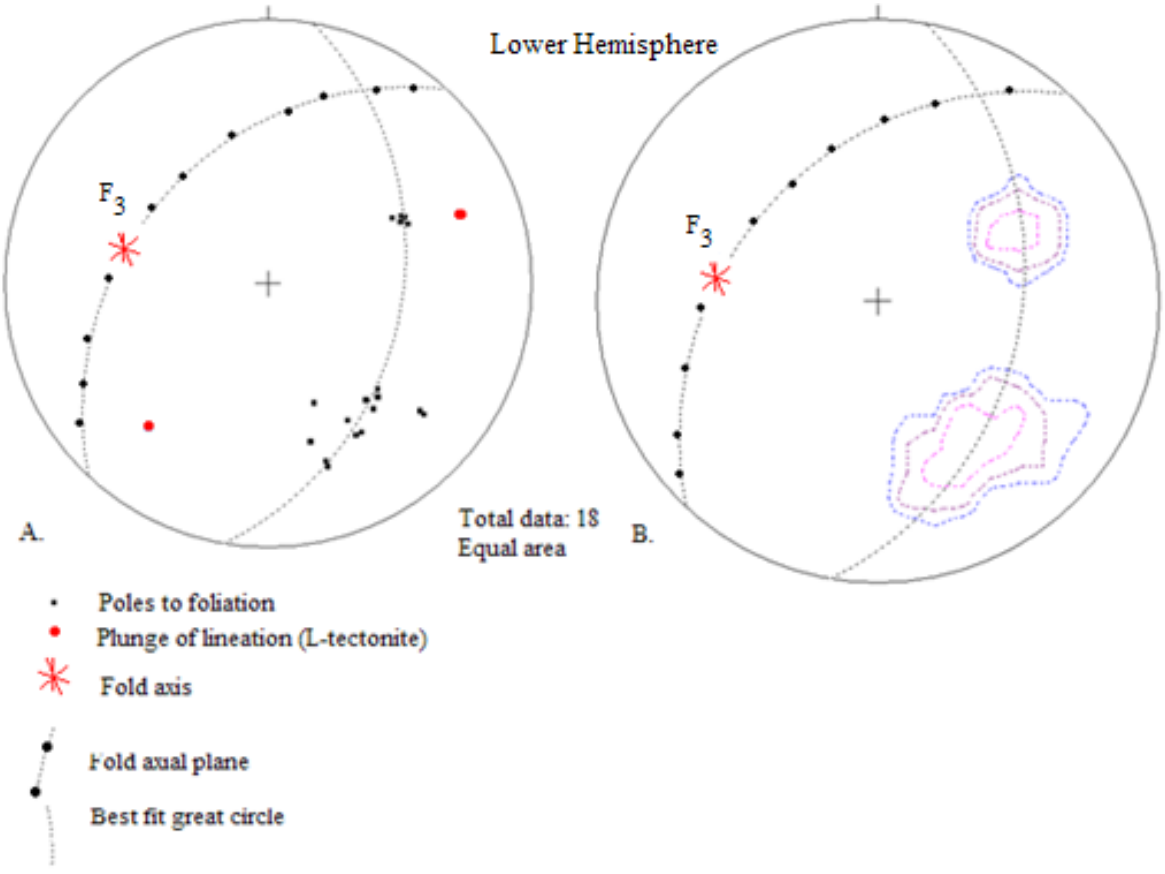

Figure 3.43 A: Equal area, lower hemisphere projections of poles to foliation (S_1) and measured plunge of lineation (L-tectonite) from Domain 3. B: contoured plot of A.

3.3.3 DOMAIN 4

3.3.3.1 DEFORMATION FABRICS

Domain 4 is characterized by an E-W to WNW trending pervasive foliation (S_1) best developed in gneissic outcrops (grey biotite gneiss, grey megacrystic granite gneiss, megacrystic granite gneiss and banded gneiss) occurring in an area dominated by megacrystic tonalitic gneiss. These rocks occur in a narrow intensely deformed zone in the northeastern part of the study area. The foliation (S_1) dips steeply N to NE (Fig. 3.44 to 3.48). In this domain, grey megacrystic tonalitic gneiss is deformed leading to formation of augen gneiss and mylonitic gneiss. The high strain rocks are present in discontinuous layers. Sheared amphibolites, carbonates and tonalitic gneiss (Fig. 3.45) are associated with the mylonitic gneiss to the NE of Tonota (locality 413). Elongation lineation defined by streaks of deformed K-feldspar and quartz plunges N and NNE (3.47 and 3.48).

A B

Fig. 3.44 A and B: Grey slightly megacrystic granite gneiss with well-developed foliation (S_1) in Domain 4. B occurs interlayered with A. Strike and dip of foliation, 312°/75°.

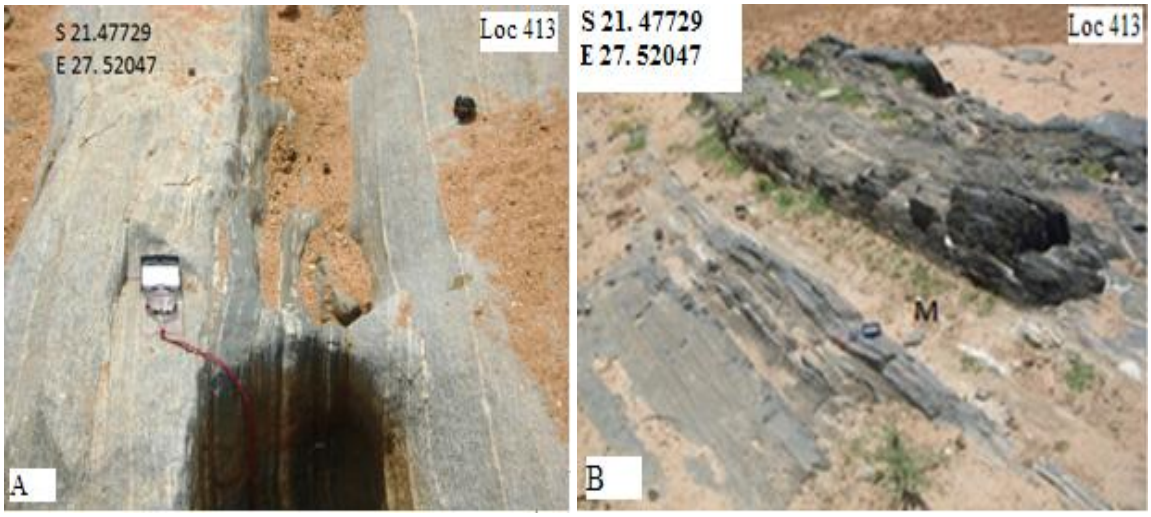

Figure 3.45: Grey biotite gneiss with vertical WNW-ESE trending foliation (strike and dip of foliation (S_1), 312º/90º). B. Zone marked 'M' in is underlain by marble and is bounded by amphibolite.

Figure 3.46: Sub vertical foliation (S_1) ° in foliated grey granite gneiss unit. Strike and dip of foliation is 323º/88º. Shape of feldspar crystals at left side of outcrop suggests ENE-WSW shortening.

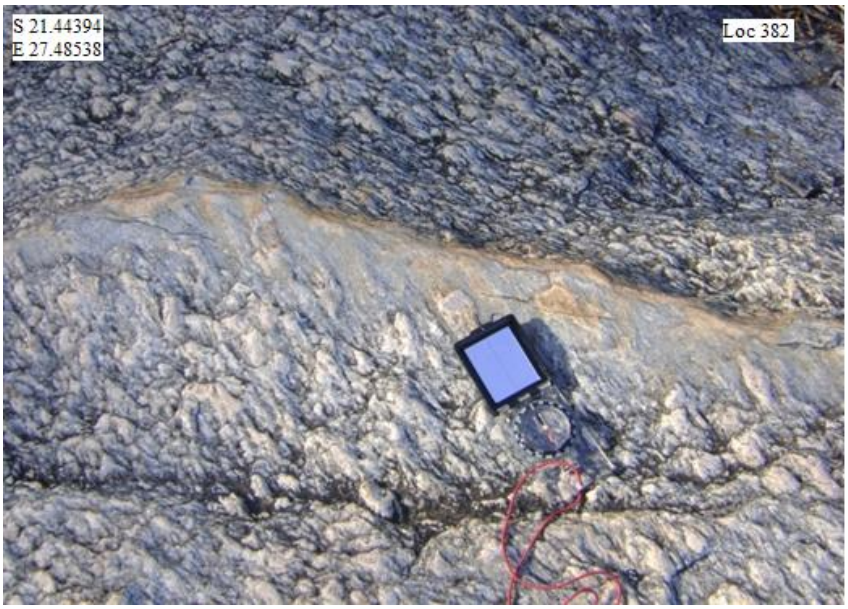

Figure 3.47: K-feldspar megacrysts defining an elongation lineation orientated parallel to the long edge of the compass clinometer and plunging 50º/360º. Foliation (S_1) is well developed and strikes NNW-SSE (340º) and dips steeply ENE (86º). Locality 382, N of Gulushabe structure.

A down dip elongation lineation plunging steeply to the NNE is common and is strongly developed in localised areas (Fig. 3.48).

Figure 3.48: Good example of an upright elongation lineation plunging NNE, 80º/005º. NB. pen is placed parallel to the plunge of elongation lineation. Photograph captured facing south. Locality 161, N of Tonota. Strike/dip of foliation 323°/86°.

Based on the deformation fabric present, Domain 4 is interpreted as a dip-slip ductile shear zone which will be referred to as the Gulushabe shear zone.

3.3.3.2 FOLD STRUCTURES

Two generations of minor folds with orthogonal axial surfaces were recognised. These are designated Set 1 and 2. The two generation of folds are represented by:

Set 1. Folds plunging sub-horizontally to the NW with an axial planes dipping moderately to the NE (Fig. 3.49). These may be interpreted as having formed by top to SW movement during NE-SW horizontal compression.

Set 2. Folds plunging at 60º to the NE with a steep axial plane trending NE-SW (Fig 3.50). These may be interpreted as having formed by NW-SE horizontal compression.

The minor folds are present in the form of S, Z and M folds (Fig. 3.49 and 3.50).

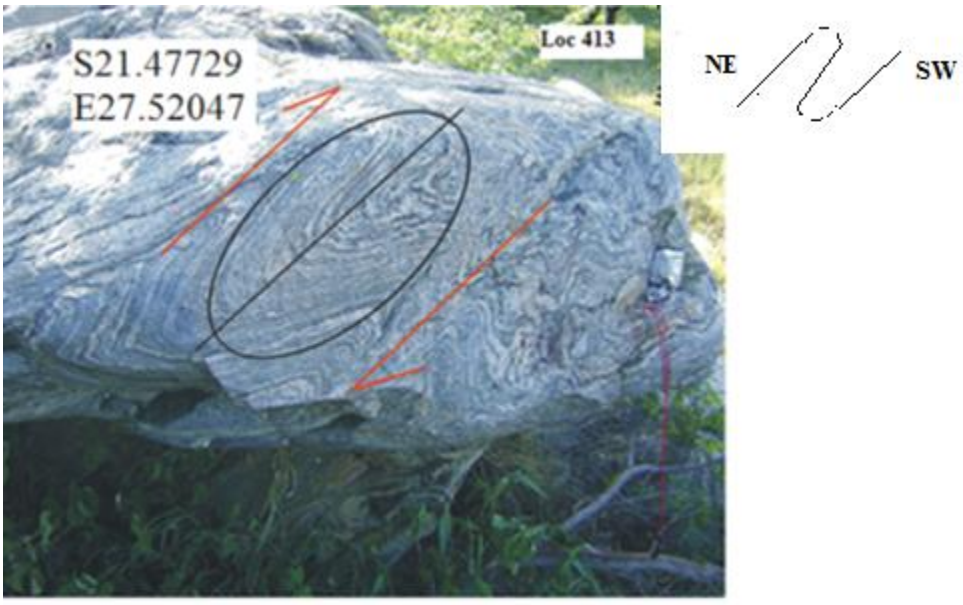

Figure 3.49: Subhorizontally NW plunging (Set 1) folds deforming foliation (S_1) in grey megacrystic tonalitic gneiss. The photograph is a NE-SW section. Folds verge to the SW. Axial plane dips moderately to the NE. strike and dip of axial plane; 312°/40°. Plunge of fold axis 03°/310°.The folds formed by top-to-SW movementduring NE-SW horizontal compression. Locality N of the Gulushabe structure.

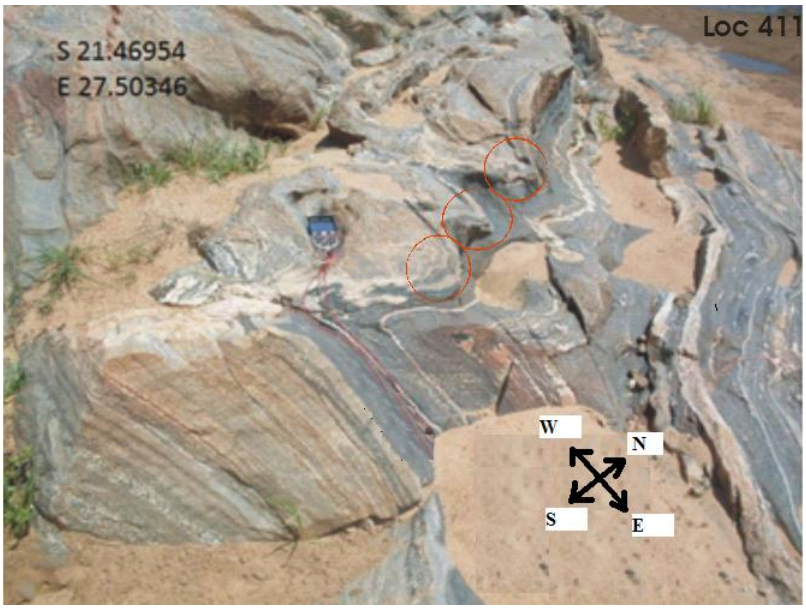

Figure 3.50: Steeply plunging minor folds (Set 2, circled in red) developed in banded gneiss with the direction of plunge parallel to the dip direction of the banding. The folds plunge at 60º to the NE (60º/052º) and have axial planes dipping steeply NW 220º/88º. Folds interpreted as having formed by NW-SE horizontal compression.

3.3.3.3 GEOMETRICAL ANALYSIS OF STRUCTURAL ELEMENTS

A stereoplot of poles to shear foliation (S_1) and lineation data from Domain 4 is given in Figure 3.51. Poles to foliation (S_1) define a best fit great circle indicating a fold plunging at 60° towards 027º. The strike and dip of axial plane is 312º/60º. Of note is the similarity between the contoured plot of lineation in Domain 4 (Fig 3.51 C) and that of the Gulushabe structure (Fig.3.23). The fold axis in Figures 3.49 and 3.50 are plotted on Figure 3.51 A.

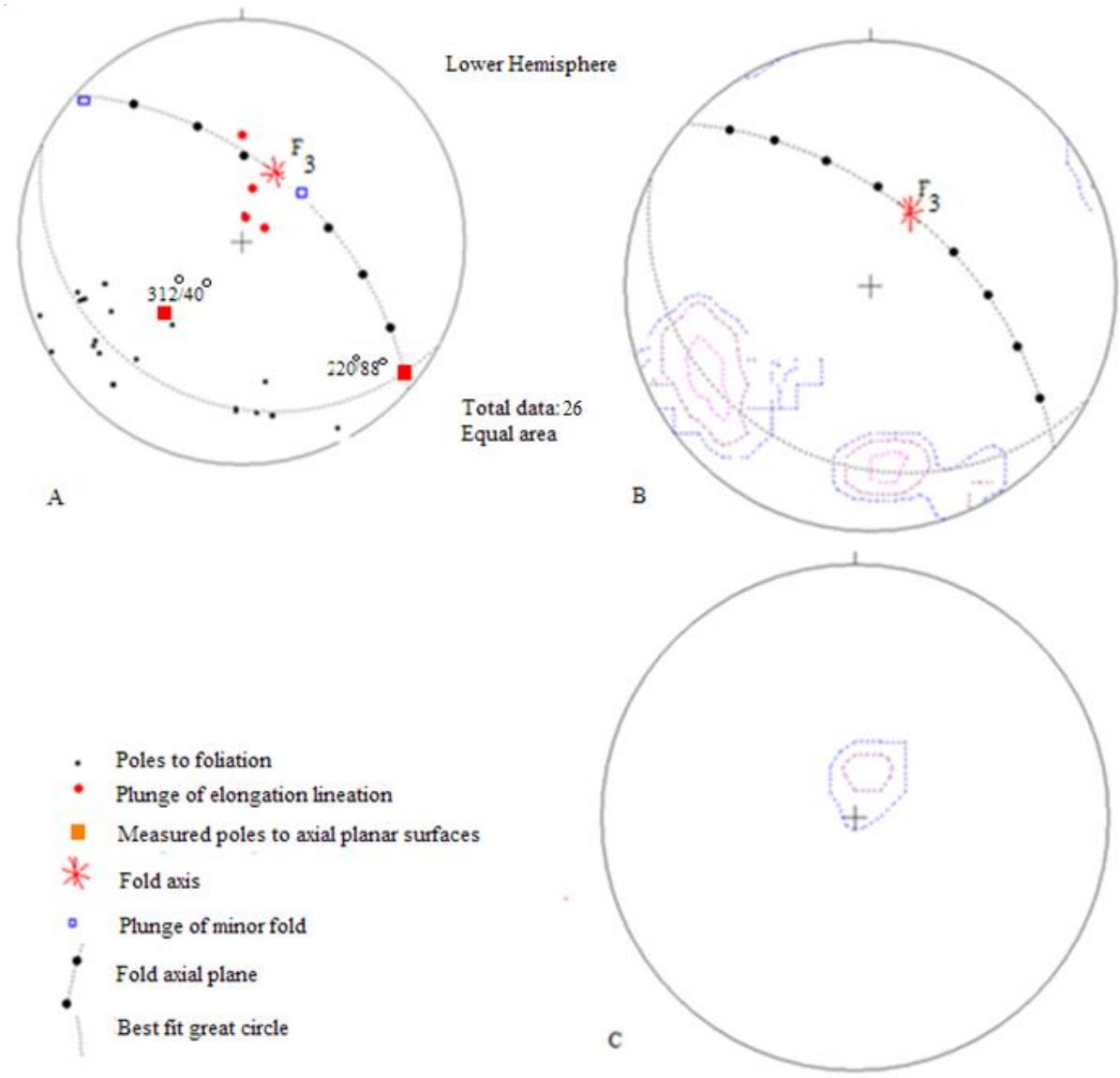

Figure 3:51 A: A. Equal area, lower hemisphere projections of poles to foliation (S_1), elongation lineation and plunge of minor folds from Domain 4. B. Contoured plot of poles to foliation in A. C): Contoured plot of elongation lineation data in A. The fold axis in A plunges sub-horizontally to the NW and plots in the NW quadrant close to the perimeter of the plot. Note the F_3 fold axis in Fig A plunges to the NNE, the same orientation as the plunge of minor fold in Figure 3.50.

3.4 MINOR SHEAR ZONES

Across Domains 2 and 3 and 4, shearing along centimetre scale ductile shear zones has dragged the pre-existing fabric and layering into small-scale folds trending NE-SW (Figs 3.52 to 3.56). The minor shear zones cut the regional foliation (S_1) at high angles and are often filled by syn-tectonic felsic veins. The minor shears zones show predominantly NNE-SSW trends (020°-040°) and have dextral displacement. These shear zones mostly lie on sub-horizontal smooth outcrop surfaces that make it difficult for changes in orientation to be measured, and are restricted to the granitoid gneisses i.e. have not been observed in the metasedimentary outcrops. They are orientated sub-parallel to the axial trace of the minor folds deforming the foliation (S_1). Shear strain (γ) in the order of 3 to 4 was calculated for the shear zones in all domains using the formula γ = d/w where (w) represent width of the shear zone and (d) represent amount of displacement as illustrated in Figures 3.53 A, 3.55 B and 3.56 A. It should be noted however that the shear strain was calculated from values measured directly off the photograph.

3.4.1 DOMAIN 2

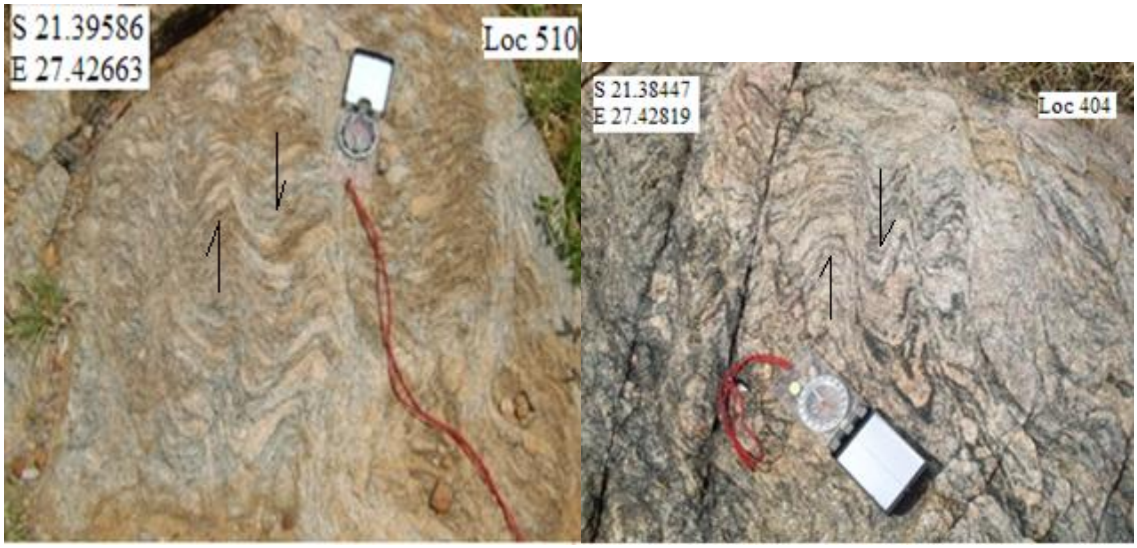

A Strike and dip of fold axial surface 180°/70°. S of Shashe Village

B. Strike and dip of fold axial surface; 220°/88°. W of Shashe Village

Figure 3.52: A-B: Plan views of drag folds (defined by felsic bands) developed in megacrystic granite gneiss (Domain 2) due to dextral shearing. The small-scale shear zones occur along the limbs of the folds. N.B. the minor folds have steeply dipping to almost sub-vertical fold axial surfaces that lie parallel to the shear zones. Black arrows indicate sense of movement.

3.4.2 DOMAIN 3

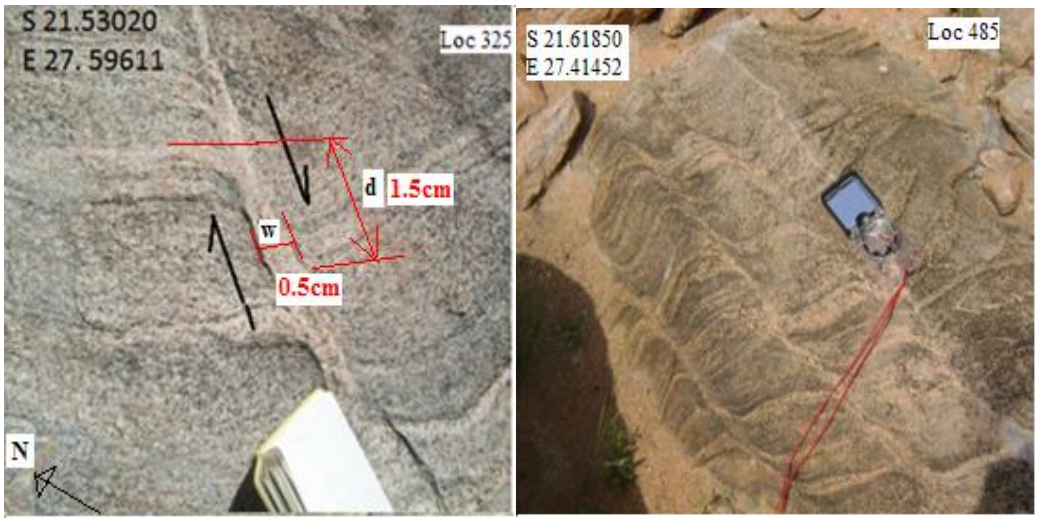

A.Trend of minor shear zone, 036°-216°. Megacrystic granite gneiss E of Gulushabe.

B. Strike and dip of minor shear zone, 225°/70°. Banded tonalitic gneiss inclusion in mecacrysticgranite gneiss. NE of Foley Village

Figure 3.53: Plan views of shear zones trending NE-SW deforming gneissic foliation (S_1) and undeformed felsic material along the trace of the shear zone. Calculated shear strain in A ~ 3. Note: the shear zone in B is restricted to the banded gneiss inclusion.

A.Trend of shear zone~065°. E of Gulushabe Settlement

B. Trend of minor shear zone~060°. S of Gulushabe settlement

Figure 3.54: A-B: Foliation (S_1) and foliation parallel felsic bands are dextrally rotated into a NE-SW trending ductile shear zone developed in megacrystic granite gneiss.

3.4.3 DOMAIN 4

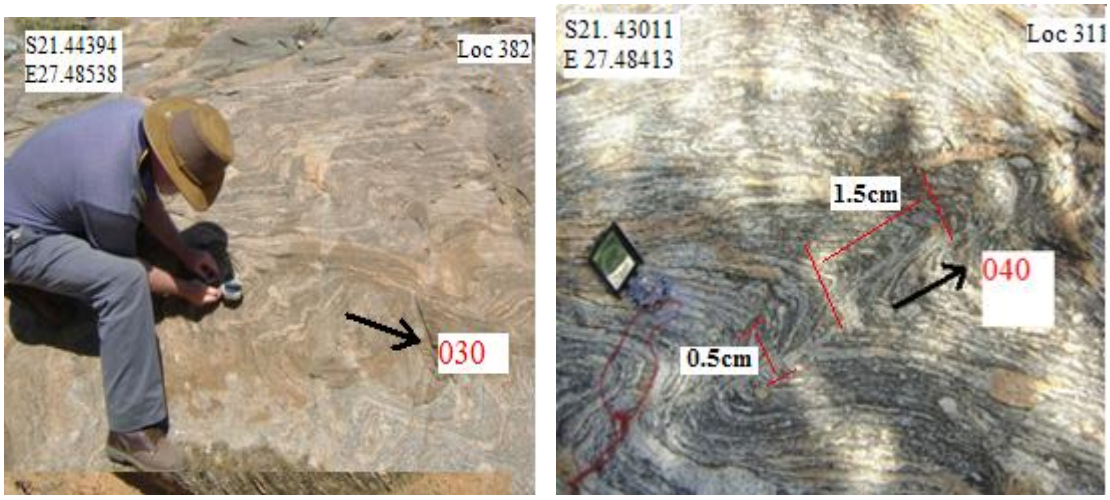

A: Foliation 327°/86° B:Foliation; 332°/56°

Figure 3.55: A-B: NNE-SSW trending ductile shear zone dextrally deforming both the gneissic foliation (S_1) and felsic bands in megacrystic tonalite gneiss. Associated small-scale fold in B plunges 60°/040 sub-parallel to the trend of the shear zone.

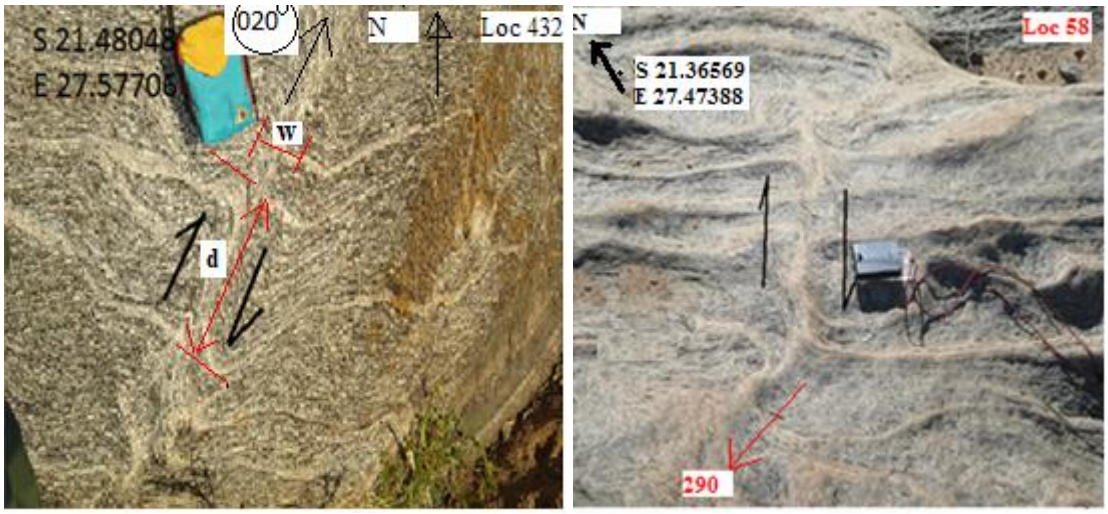

A. NE of Gulushabe structure B. NE of Shashe

Figure 3.56: Foliation (S_1) and foliation parallel felsic bands deformed along A. NNE-SSW trending ductile shear zone A in megacrystic granite gneiss. Rotation of veins into shear zone gives a clear dextral sense of movement.

3.5 DISCUSSION

The foliation (S_1) in the metasedimentary rocks of Domain 1 (the Foley synformal and the Gulushabe antiformal structures) is folded into NE to ENE trending folds with axial surfaces dipping to the NW (Table 3.1) and NNW (Fig 3.12 and 3.23). The development of these large scale folds is attributed to a NW or NNW orientated horizontal compression. There is a consistent geometry shown by these fold structures. The only difference between the fold structures is that, whereas the Foley structure has a steeply plunging NW (310º) to NNW (340º) elongation lineation defined by deformed quartz pebbles ((Figs. 3.3 to 3.6 and Fig 3.12), the prominent lineation associated with the Gulushabe structure is defined by deformed aggregates of quartz and feldspar (Figs. 3.16 to 3.19, 3.23), although locally an elongation lineation defined by the long axis of pebbles plunges NNW (Fig 3.15). Measured minor fold structures plunge NE to ENE in the Foley (Figs. 3.7 to 3.10) and ENE in the Gulushabe structure (Fig. 3.21 and 3.23). However, unlike these minor folds, fold axes given by the software for both the Foley and Gulushabe structures plunge NNE (Fig 3.12 and Fig 3.23). The NNE plunges of the fold axes are interpreted to reflect F_3 deformation. F_3 folds (e.g. Fig 3.11) and folds developed on the NW limb of the Gulushabe structure show a dominant NNE trend.

Table 3.1. Summary of the structural geology of Domains

Domain no.	Lithological unit	Primary structure	Foliation	Lineation	Minor folds
1	Metasedimentary rocks	bedding (S_0)	Cleavages; main cleavage(S_1) and crenulation cleavage (S_2)	L_2: elongation lineation in the pebble- quartzite bearing unit plunging NW to NNW L_3: Crenulation cleavage plunging NNE	NE to ENE trending folds with steeply NW to NNW dipping axial planes (F_2) Crenulations plunging NNE with axial surfaces that dip to the NW (F_3)
2	Granitoid gneiss (megacrystic granite gneiss with layers of banded tonalite gneiss).	-	S_1 foliation trending NNE to NE and defined by preferred orientation of mineral grains (quartz, feldspar, biotite)	Rare steeply NW plunging elongation lineation, elongation lineation plunging N to NNE and SW	Small-scale folds deform foliation, fold axis trend NNE, and fold axial surfaces dip to the WNW (F_2), top to ESE displacement is indicated.
3	Megacrystic granite gneiss	-	S_1 foliation trending ENE, defined by Preferred orientation of mineral grains (quartz, K-feldspar megacrysts and biotite)	ENE trending elongation lineation defined by K-feldspar megacrysts (L-tectonite)	Not found
4	Megacrystic tonalitic gneiss along Gulushabe shear zone	-	Alignment of K-feldspar, quartz and biotite. Banding	N-NNE plunging elongation lineation defined by deformed aggregates of quartz and feldspar	NW striking axial planes dipping to the NE, top to SW sense of displacement (F_1) NE plunging folds with NE-SW trending axial surfaces dipping NW (F_2)

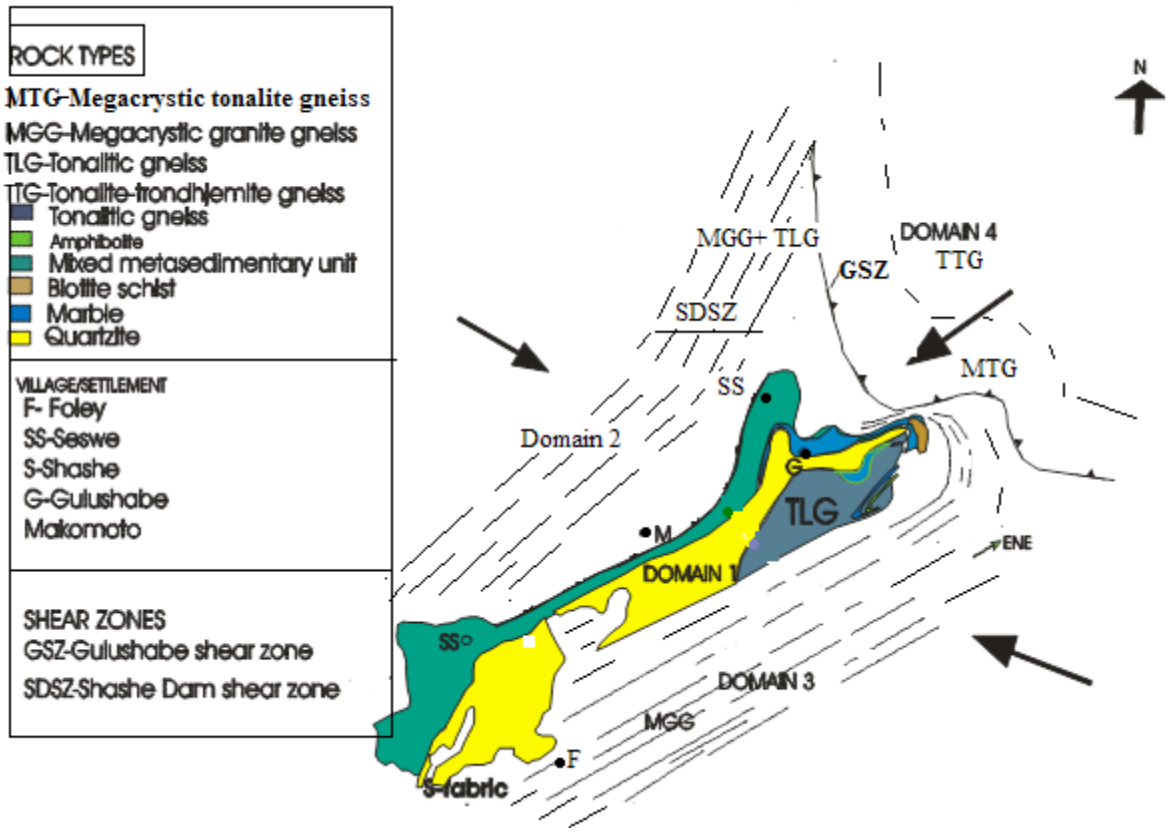

Figure 3.57: Structural sketch map showing distribution of shear zones in the SFT area. Big arrows indicate direction of maximum compression that produced the large scale fold structures.

The foliation (S_1) in Domain 3 dips NNW and trends ENE parallel to metasedimentary belt and it appears to be deformed around the NE end of the Gulushabe structure (Fig 3.43). The cause of this deformation is unknown but may reflect folding around the Gulushabe structure or deformation related to the Gulushabe shear zone. Figure 3.41 and 3.42 present evidence for a local sub-horizontal L tectonite in the vicinity of Foley settlement. Horizontal elongation lineation is normally related to strike-slip deformation but no kinematic indicators were found in Domain 3 to confirm the shear sense. This deformation fabric is parallel to large scale ENE-WSW trending ductile dextral strike-slip shear zones (Regional D4 structures) that define the northern boundary to the Central Zone of the Limpopo belt namely, the Magogaphate-Molabe-Lepokole shear system (Table 1.6, Paya, 1996). These SE dipping shear zones are thought to have been active at

the same time. The only difference is that whereas D4 structures in the Limpopo belt dip to the SE, the fabric in Domain 3 dips to the NNW.

The structural grain of Domain 4 is defined by foliation (S_1) trending E-W to NNW and dipping N to NE. Two generation of folds thought to have formed by different tectonic events have been recognized in Domain 4. The first generation of folds has NW–striking axial planes dipping to the NE (Table 3.1). The folds verge to the SW indicating top to SW sense of movement. The folds are related to thrust sense shearing along the foliation (S_1). The second generation folds (Set 2 of section 3.3.3.2) have axial planes striking NE to ENE and dipping steeply NW to WNW. Folds with a similar plunge direction have been identified in Domain 1 (50º/006º on Fig. 3.12) and Domain 2 (28º/017 ºon Figure 3.39). The axial planes of these folds are sub-parallel to foliation (S_1) in Domain 1 and 2. The map pattern and the stereographic plot in Figure 3.51A implies the Gulushabe shear zone and its N to NNE dipping foliation (S_1) is folded by structures trending NE-SW and plunging to the NE. Structural evidence (this study) indicates the thrust sense shearing characterises the SW vergent Gulushabe shear zone which forms the boundary between the SFT area and the SE margin of the Tati greenstone belt. The shear zone transects the northeastern part of the SFT region and has affected rocks exposed along the Shashe river bed to the N of Gulushabe area. The SW rotation of folds in this zone indicates a SW directed ductile shearing event. The width of the shear zone is variable ranging from about 1 to 3 kilometres. The N to NE dip of the Gulushabe shear zone is in conflict with previous interpretations (Paya, 1996, Ranganai *et al*., 1999 and McCourt *et al*., 2004) which model this structure as an extension of the NE verging Shashe shear zone. The current interpretation is supported by the structural data collected along the boundary during the present study. Further work is required to resolve the regional kinematics. In the northern part of the SFT area, the foliation in Domain 2 is seen to truncate that of Domain 4, implying that the deformation in Domain 4 is older than that in Domain 2.

Based on the data collected during this study the geometry of the deformation features recognized in various structural domains can be compared. These features are summarized in Table 3.2. All rocks in each of the structural domains have been deformed. The metasedimentary rocks in Domain 1 have evidence at outcrop and map

scale for two phases of folding (F_1, F_2) with associated foliation. These folds plunge NE to ENE. An associated elongation lineation best defined by the long axis of pebbles in deformed pebbly quartzite plunges WNW and NNW. In addition to these co-axial events the bedding and foliation data plotted on Figures 3.12 and 3.23 define a fold axis plunging to the NNE. Folds related to this F_3 event are recognized at map scale along the NW limb of the Gulushabe structure (Fig 3.14), at locality 12 on the dissertation map and Fig 3.11. The megacrystic granitoid rocks of Domain 2 and 3 are strongly foliated but minor folds of the foliation were only recognized in Domain 2. These folds plunge N to NNE and have axial surfaces that dip predominantly WNW. The granitoid gneisses of Domain 4 are characterized by a foliation that dips N and NE and has a well developed elongation lineation that plunges down dip. F_2 folds deforming this foliation verge to the SW and are related to thrust sense displacement along the Gulushabe shear zone. A second set of folds plunge N-NNE parallel to the dip of the foliation and have axial surfaces dipping NW. Based on general orientation and plunge, these folds in Domain 4 may be correlated with the F_2 folds of Domain 2 and the F_3 folds.

Table 3.1: Structural data related to orientation of folds and lineation in domains. Locality and Figure no. provided.

DOMAIN	Map scale orientation of structure	Measured plunge of minor folds, generation of fold, Figure no. and locality no.	Calculated plunge of main fold and generation of fold indicated	Measured strike and dip of axial surfaces, Figure no. and locality no.	Strike and dip of calculated axial surface	Plunge of lineation (angle and direction) and locality no. and type of lineation.
Domain 1 Foley structure	NE-NW	NE: 10°/050° (Set 2, Fig. 3.7, Locality, 33) NE:32°/055° (F_2, Fig. 3.8, Locality 27) ENE: 60°/70° (Set 2, Fig. 3.9, Locality 475) NE: 32°/55°: (Set 2, Fig. 3.10, Locality 27) NNE: 32°/010° (Set 3, Fig. 3.11, Locality, 12)	50°/006° (F_3)	230°/65° (Fig. 3.7, Locality, 33) 240°/62° (Fig. 3.8, Locality, 27) 250°/68° (Fig. 3.9, Locality, 475 235°/50° (F_2, Fig. 3.10, Locality, 27) 220°/60° (Fig. 3.11, Locality, 12)	244°/55° (Fig 3.12)	NNW: 80°/340° (Fig. 3.3, Locality 11), long axes of pebbles. NW: 60/310 (Fig.3.4, Locality 23), long axes of pebbles. NNW: 66°/340° Fig. 3.5, Locality 12), long axes of pebbles. NW: 62°/329° (Fig. 3.6, Locality 40), Long axis of pebbles.

Table 3.1 continued……..

DOMAIN	Map scale orientation of structure	Measured plunge of minor folds	Calculated plunge of main fold, and correlative	Measured strike and dip of axial surfaces	Calculated axial surface	Plunge of lineation (angle and direction)
Gulushabe structure	ENE-WSW	65°/068° (Set 2, Fig. 3.21, Locality 447) 60/248 (Set 2, Fig. 3.22, Locality 205)	49°/014° (F_3)	248°/88° (Fig. 3.21, Locality, 447) 248/60(Fig. 3.22, locality 205)	254°/53° (Fig 3.23)	66/335 (Fig.3.15, Locality, 188), long axes of pebbles. 75/060 (Fig. 3.16, Locality 446), streaks of deformed quartz and biotite"ribbing" 85/30 (Fig. 3.17, Locality 446), "ribbing" deformed quartz and biotite grains. 68/005 (Fig. 3.18, Locality 191), "ribbing", deformed quartz and biotite grains. 60/360 (Fig. 3.19, Locality, 204), deformed quartz and biotite grains or slickenlines.
Domain 2	NNE trending zone	10/005 (Set 2, Fig. 3.34, Locality 44) 00/020 (Set2, Fig. 3.36, Locality 9) 90/030 (F_2, Fig. 3.37, Locality 16)	28/017 (F_3)	210/56 (Fig. 3.38, Locality 16) 200º/70º (Fig 3.36, Locality 9) 210/60 (Fig 3.37 B, Locality 16	215/60 (Fig 3.39)	76/310 (Fig. 3.28,Locality 36) 90/300 (Fig. 3.29, Locality 446, elongation on dyke contact). 45/220 (Fig. 3.31, Locality 3), 28/360 (Fig. 3.32, Locality 369). 25/20 (Fig. 3.33,

						Locality 1), elongation lineations.
Domain 3	ENE-WSW trending zone		42/280 (unknown)	Not found	223°/47° (Fig 3.43)	30/260 (Fig 3.40, Locality 482 24°/070 (Fig. 3.42, Locality 405, L-tectonite).
Domain 4	E-W to WNW	03°/310° (Set 1, Fig. 3.49, Locality 413 60°/052° (Set 2, Fig 3.49, locality 411)	60°/027° (F_3)	312°/40°	312°/60° (Fig 3.52)	50°/360° (Fig 3.47, Locality 382), 80/005 (Fig 3/48, Locality 161)

CHAPTER 4: U-PB ZIRCON GEOCHRONOLOGY

4.1. INTRODUCTION

U-Pb zircon geochronology was carried out on selected granitoid rocks from the study area in order to produce a temporal framework into which the magmatic events of the SFT region can be placed as well as determining deformation events present. This was done in an attempt to better understand the evolution of the granitoid rocks in the study area. The zircon grains separated from 5 samples of the main units recognised in the field were analysed by Dr. Richard Armstrong at the Research School of Earth Sciences (RSES) at The Australian National University using the SHRIMP method (Sensitive High Mass Ion Microprobe). The zircon descriptions that follow are based on his report to the Geological Survey of Botswana. Standard analytical techniques as outlined in numerous publications incorporating SHRIMP data were followed. An outline of how the SHRIMP method works and analytical procedure are given in Appendix 1. A global positioning system was used to record the coordinates of the sample locations.

It is important to mention that the mineral zircon contains high U and Th, and low Pb at the time an igneous rock forms. Its U-Pb signatures and internal structure remain undisturbed even at the high temperatures required for partial melting (e.g. Rubatto and Herman, 2003). The age of the zircon is therefore the age of the protolith to the host rock (zircon inheritance). Owing to its large size and low charge radiogenic Pb is expelled from zircon during recrystallization due to metamorphism, alteration and metamictisation (loss of radiogenic Pb due to U and Th decay). As a result, zircons yield discordant ages that plot off the Concordia curve as colinear data points. A regression line through these data points intercepts the Concordia curve. Plots of the Concordia curve are used as reference. The upper intercept gives the age of primary crystallization. Cathodoluminescence (CL) imaging technique has been used to reveal the different internal zonation of zircons which is a requirement in distinguishing magmatically derived (igneous) zircons from non-magmatic (metamorphically grown) zircons. The widely accepted contention that magmatic zircons have Th/U ratios that are typically >

0.2 whereas non-magmatic zircons have Th/U ratios < 0.1 is followed in this study (e.g. Bowring and Williams, 1999).

4.1 RATIONALE FOR STUDY

The primary objective of the SHRIMP work was to establish the emplacement age of the protoliths to the tonalitic gneiss (MLM-SRP 3), megacrystic granite gneiss (MLM-SRP 1 and 5) and pink gneissic granite (MLM-SRP 2) thereby quantifying the relative age relationships recognised in the field. The tonalitic gneiss was dated to establish the crystallization age of the igneous protolith which following Bagai (2008) and Kampunzu *et al*. (2003) was produced during subduction along the southwest margin of the Zimbabwe craton. Zircon grains from the pink gneissic granite and the megacrystic granite gneiss were dated to constrain their emplacement ages. Mylonite from shear zones constrain the maximum age of deformation and displacement along these structures. In addition a sample of Tonota biotite gneiss (MLM-SRP 4) was processed to see if the zircon population provided any insight into whether the gneiss was derived from a sedimentary or magmatic protolith. The Tonota biotite gneiss is a fine grained leucogneiss with diffuse compositional layering and occurs associated with metasedimentary rocks around Tonota and Shashe Villages. The Tonota biotite gneiss is considered of sedimentary origin (e.g. Aldiss, 1991). The latter interpretation stems from its association with metasedimentary rocks and the local occurrence of sillimanite in the Tonota biotite gneisses. The age data obtained from these zircons were used to constrain the depositional or emplacement age of the protolith. The current chapter concludes by comparing U-Pb zircon ages from this study with published U-Pb zircon ages from the Tati greenstone belt, Matsitama belt and the Central Zone of the Limpopo belt. An evaluation of how age constraints on deformation features in the SFT area relates to those in the adjacent terranes is undertaken.

4.2 SAMPLE LOCALITIES

The lithology and sample locations of rocks selected for U-Pb zircon age determinations are listed in Table 4.1 and plotted on the dissertation map. The results of U-Pb zircons isotope analysis are presented in Tables 4.2 to 4.6. Cathodoluminescence (CL) images of zircon populations and the Concordia diagrams are shown in Figures 4.1 to 4.10.

Table 4.1: Sample No, location and lithologies sampled for SHRIMP work.

SAMPLE NO.	COORDINATES (longitude/latitude	AREA	LITHOLOGY
MLM-SRP 1	S 21.67581 E 27.36751	Foley East	Megacrystic granite gneiss
MLM-SRP 2	S 21.67581 E 27.36751	Foley East	Pink foliated granite gneiss
MLM-SRP 3	S 21.47403 E 27.53267	SW of Ditladi Village	Tonalitic gneiss
MLM-SRP 4	S 21.44802 E 27.44663	SE of Tonota Village	Tonota biotite gneiss
MLM-SRP 5	S 21.52411 E 27.44227	SW of Gulushabe Settlement	Megacrystic granite gneiss

4.3 RESULTS

4.3.1 MEGACRYSTIC GRANITE GNEISS (MLM-SRP1, S 21.67581 E 27.36751)

This sample yielded 20 zircon grains from which 25 analysis were made. Zircons from this unit have high U concentrations ranging from 85 to 2137ppm and high Th/U ratios ranging from 0.15 to 1.02 which suggest a magmatic origin. Zircons are dark brown with variable opacity and complexity. Some areas of metamictisation (radiation damage due to U and Th decay) and/or alteration obscures detail, but the general characteristic of this population is that they are zoned, magmatic grains with occasional cores - which may or may not be inherited. The last stage of zircon growth is a dark rim obvious on the CL images in Fig. 4.1 (spots 10.1 & 20.1). These rims have a high U content and a low Th/U ratio, suggesting that they are metamorphic in origin. Analyses 10.1 and 20.1 (Fig. 4.2) plot at the lower end of the discordia line (Fig. 4.2) and correspond to ages of 1183.3 ± 9.6 Ma and 1270 ± 12 Ma (Table 4.2) which together with the low Th/U ratio represent a metamorphic event related to Mesoproterozoic orogeny.

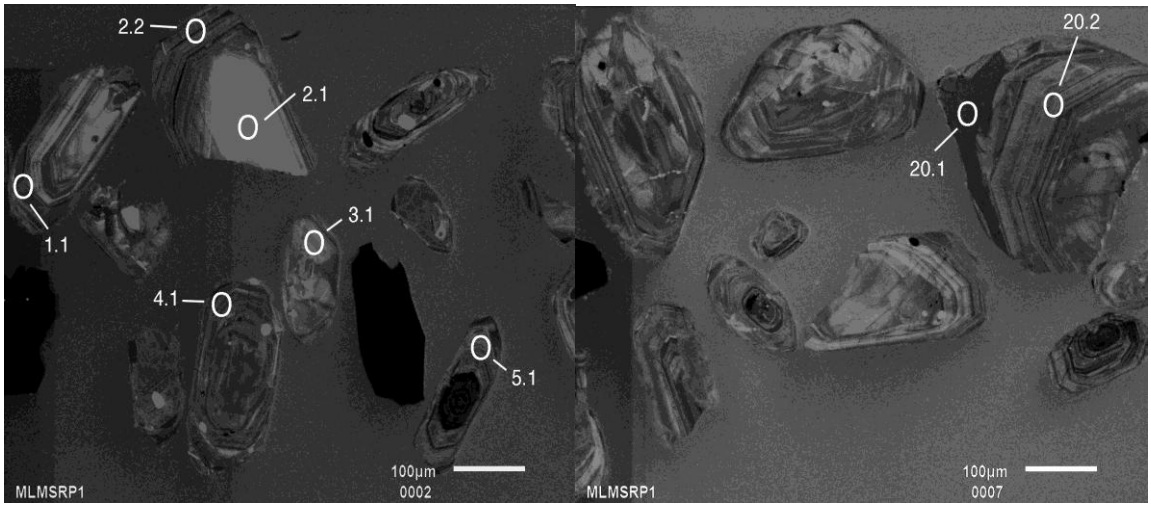

A B

Figure 4.1 A-F: CL-images of zircons extracted from the megacrystic granite gneiss unit. Note some grains with euhedral and oscillatory zoned centres. Numbers refer to the spots at which the analyses were taken

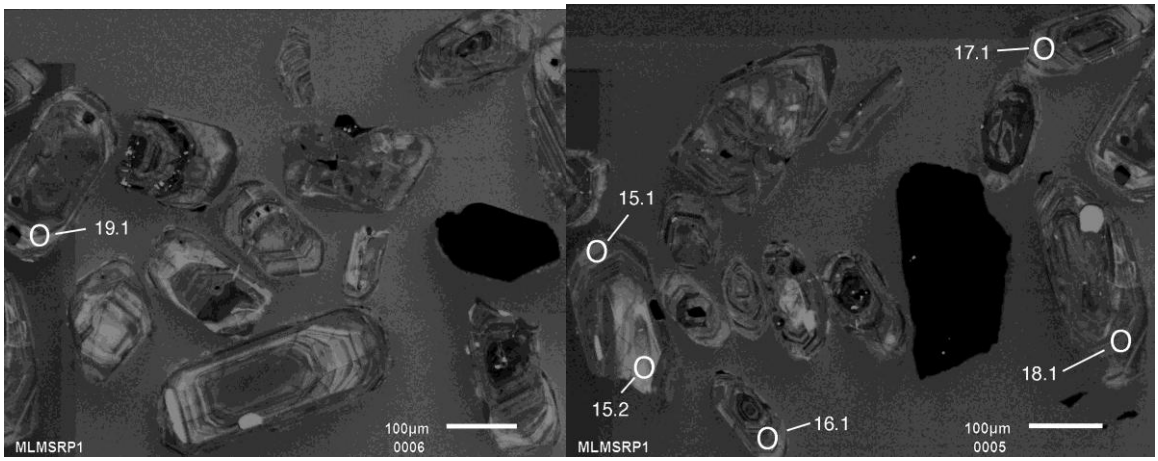

C D

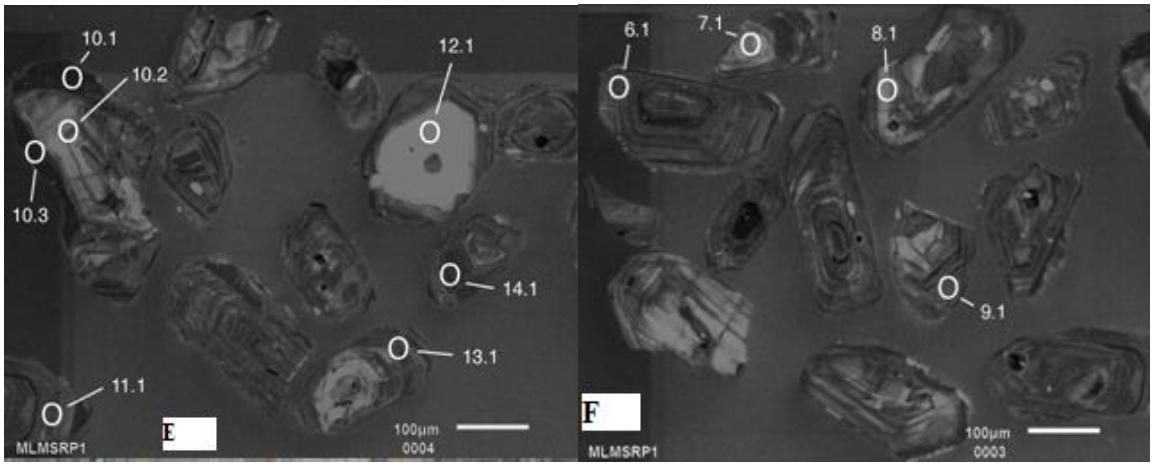

Figure 4.1 continued

The data are generally discordant and there is additionally slight scatter of the data about a discordia. If one interprets these data in terms of the petrographic details revealed by the CL imaging, then it is possible to differentiate a possible older generation of "cores" [analyses; 8.1, 10.2, 12.1, 15. 2] and a possible younger phase of zoned, magmatic zircon. This is shown in the Concordia plot (Fig. 4.2) with the light yellow error ellipses representing the older core components. It is difficult and unfortunately somewhat subjective in interpreting some of these structures as older cores, especially for those in grains #2.1, 7.1 and 19.1. These "cores" could also be magmatically zoned, low-U zircons that grew early in the same magma (i.e. coeval) as the more highly zoned overgrowths.

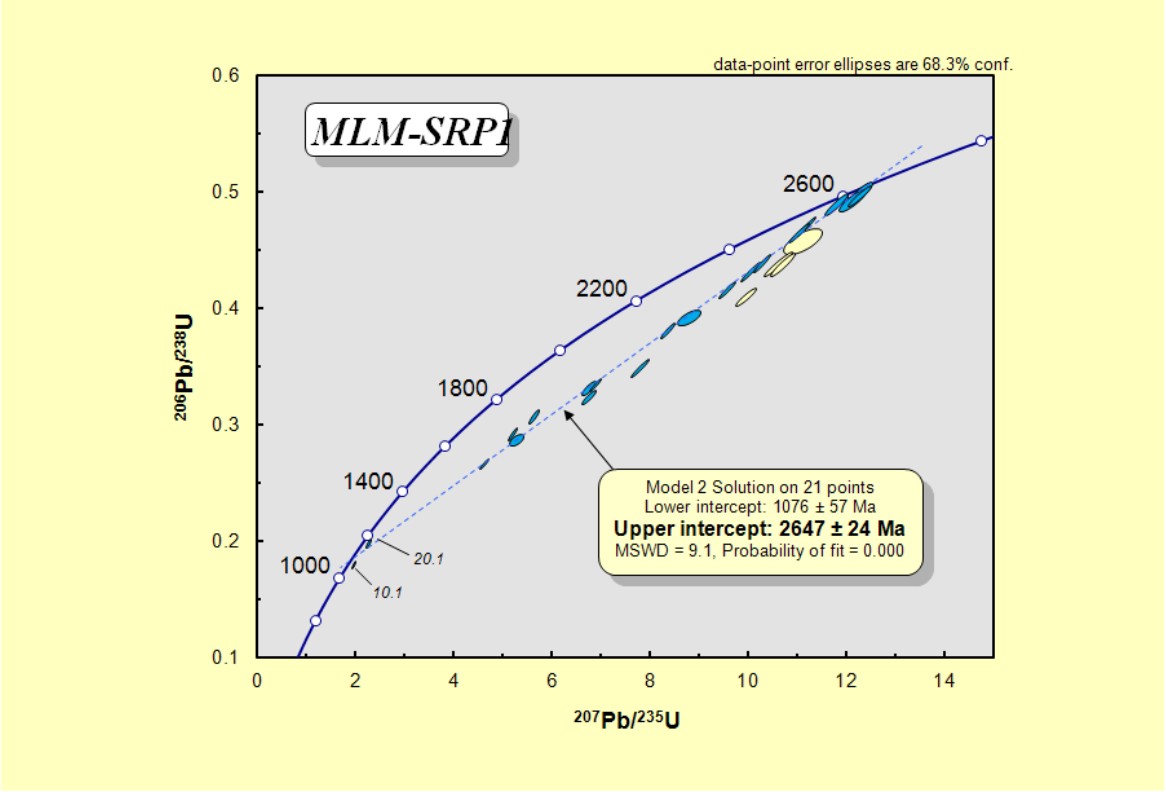

Figure 4.2: Wetherill plot of SHRIMP analyses for core and magmatic zircon for a megacrystic granite gneiss sample MLMSRP 1 from Foley East.

In calculating an age from these data all the cores interpreted to be inherited (listed above) are excluded from the regression, which yields an upper intercept age of 2647 ± 24 Ma (Fig. 4.2), interpreted to be the emplacement age of the protolith (porphyritic granite) to the megacrystic granite gneiss. The high MSWD of 9.1 reflects the significant scatter about the discordia. The 4 cores identified as possible inherited grains combine to give an upper intercept date of 2620 ± 39 Ma (MSWD = 0.81; probability = 0.45). This result is within error of that obtained for the zoned magmatic zircons from the general population, suggesting their interpretation as older cores may be incorrect.

Table 4.2: U-Th-Pb isotopic compositions and age calculations of zircons from megacrystic granite gneiss, sample MLM-SRP 1.

Grain. Spot	% $^{206}Pb_c$	ppm U	ppm Th	$^{232}Th/^{238}U$	ppm $^{206}Pb^*$	(1) $^{206}Pb/^{238}U$ Age		(1) $^{207}Pb/^{206}Pb$ Age		% Dis-cor-dant	(1) $^{207}Pb^*/^{206}Pb^*$	±%	(1) $^{207}Pb^*/^{235}U$	±%	(1) $^{206}Pb^*/^{238}U$	±%	err corr
1.1	0.12	565	267	0.49	226	2463	±24	2582.6	± 4.7	5	0.17256	0.28	11.07	1.2	0.4654	1.2	.971
2.1	0.09	93	83	0.92	39.8	2609	±30	2641	±11	1	0.1787	0.68	12.29	1.5	0.4988	1.4	.899
2.2	0.20	707	104	0.15	187	1724	±18	2147.1	± 9.3	20	0.1337	0.53	5.653	1.3	0.3067	1.2	.912
3.1	0.00	198	131	0.68	84.7	2604	±26	2645.4	± 6.5	2	0.17919	0.39	12.3	1.3	0.4978	1.2	.953
4.1	0.13	472	339	0.74	169	2243	±22	2531.9	± 5.1	11	0.1674	0.3	9.61	1.2	0.4162	1.2	.967
5.1	0.56	666	332	0.51	186	1804	±18	2369.5	± 8.7	24	0.15208	0.51	6.771	1.3	0.3229	1.1	.914
6.1	0.99	615	430	0.72	210	2135	±21	2485	±20	14	0.1628	1.2	8.81	1.7	0.3927	1.2	.698
7.1	0.00	153	104	0.71	64.3	2570	±27	2607.9	± 7.6	1	0.1752	0.45	11.83	1.4	0.4899	1.3	.942
8.1	0.07	196	166	0.87	69.2	2215	±24	2622.1	± 7.8	16	0.1767	0.47	9.99	1.4	0.41	1.3	.938
9.1	0.09	702	452	0.67	230	2082	±21	2449.9	± 6.4	15	0.15946	0.38	8.38	1.2	0.3811	1.2	.951
10.1	0.33	2137	33	0.02	328	1057	±11	1183.3	± 9.6	11	0.07945	0.48	1.952	1.2	0.1782	1.1	.918
10.2	0.13	133	83	0.65	50.1	2343	±29	2629.7	± 8.4	11	0.17751	0.5	10.73	1.5	0.4382	1.5	.945
10.3	0.18	542	77	0.15	136	1650	±17	2085.7	± 7.1	21	0.12909	0.4	5.191	1.3	0.2916	1.2	.947
11.1	0.07	497	293	0.61	184	2313	±24	2552	± 4.7	9	0.16943	0.28	10.08	1.2	0.4316	1.2	.974
12.1	2.72	85	74	0.89	34.5	2430	±32	2620	±28	7	0.1764	1.7	11.14	2.3	0.4577	1.6	.682
13.1	0.26	791	194	0.25	226	1845	±18	2327	±12	21	0.1484	0.72	6.779	1.3	0.3314	1.1	.846
14.1	0.26	837	654	0.81	207	1623	±17	2152	±27	25	0.134	1.5	5.29	1.9	0.2863	1.2	.606
15.1	0.05	634	351	0.57	239	2348	±23	2556.3	± 5	8	0.16986	0.3	10.29	1.2	0.4394	1.1	.967
15.2	0.07	173	170	1.02	65	2344	±33	2615.5	± 7.4	10	0.17599	0.45	10.64	1.7	0.4384	1.7	.966
16.1	0.30	460	367	0.82	138	1925	±26	2481.9	± 6.4	22	0.16251	0.38	7.8	1.6	0.348	1.5	.971
17.1	0.19	749	526	0.73	215	1857	±19	2346.8	± 5.1	21	0.15007	0.3	6.907	1.2	0.3338	1.2	.968
18.1	0.01	536	274	0.53	217	2486	±24	2585.6	± 4.1	4	0.17287	0.25	11.22	1.2	0.4707	1.1	.978
19.1	0.15	191	166	0.90	81	2587	±27	2638	±12	2	0.1784	0.73	12.15	1.5	0.4938	1.3	.866
20.1	0.50	1681	23	0.01	286	1158	±12	1270	±12	9	0.08302	0.61	2.253	1.3	0.1968	1.1	.879
20.2	0.21	877	377	0.44	201	1520	±15	2047.7	± 6	26	0.12634	0.34	4.631	1.2	0.2658	1.1	.958

Errors are 1-sigma; Pb_c and Pb^* indicate the common and radiogenic portions, respectively.
Error in Standard calibration was 0.28% (not included in above errors but required when comparing data from different mounts).
(1) Common Pb corrected using measured ^{204}Pb.

4.3.2 PINK GNEISSIC GRANITE (MLM-SRP2, S 21.67581 E 27.36751)

This sample was taken from a pink gneissic granite dyke that occurs spatially associated with megacrystic granite gneiss (MLM-SRP 1) in the Foley East area. A total of 24 analyses were carried out on the 21 zircon grains obtained from this sample. Concentrations of U and Th in these grains range from 105 to 916ppm and 57 to 550ppm respectively (Table 4.3). The Th/U ratio varies from 0.14 to 1.43, which is consistent with a magmatic origin for the zircons. The sample produced brown, subhedral to anhedral zircons with some slight rounding of grains (Fig. 4.3). A few grains show significant areas or zones of reworking (e.g. grain #6) with patchy recrystallized (bright-CL) zones and some darker embayments (e.g. spot 6.2, Figure 4.3E) that are discordant to the magmatic zoning. There are possible cores to complicate the dating (e.g. spot 10.1)

but these are discordant and thus are difficult to date. For the purposes of this study in which the priority was to establish the emplacement age of the pink gneissic granite, these possible core regions were ignored.

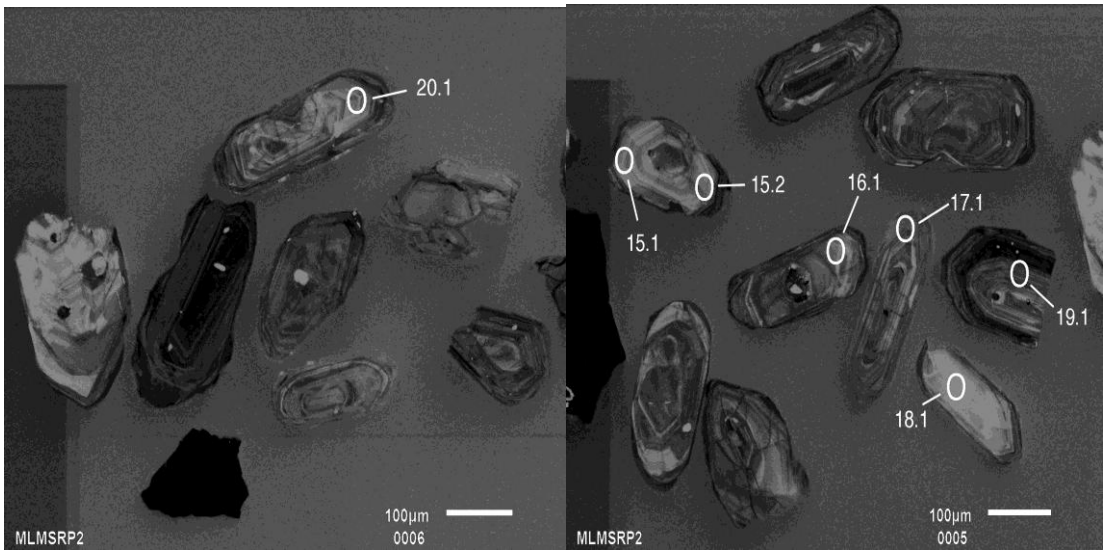

A B

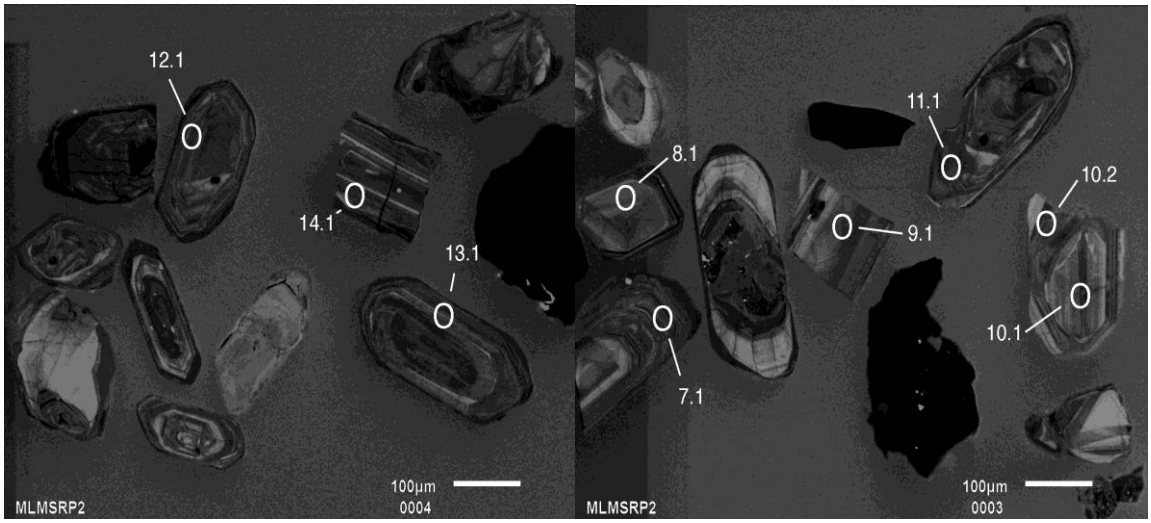

C D

Fig. 4.3 A-G: CL-images of some selected zircons from pink gneissic granite to illustrate their quality, and some analysed spots shown by white circles. Point labels are keyed to numbers in first column of Table 4.3. Note the euhedral texture and the magmatic zoning. Most of the analysed spots are on the rim of the grains.

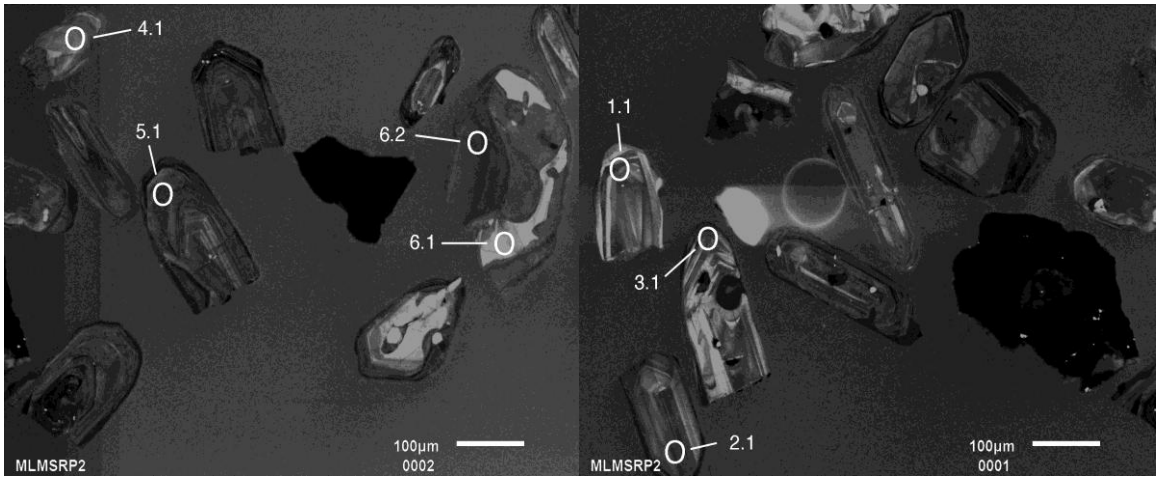

E F

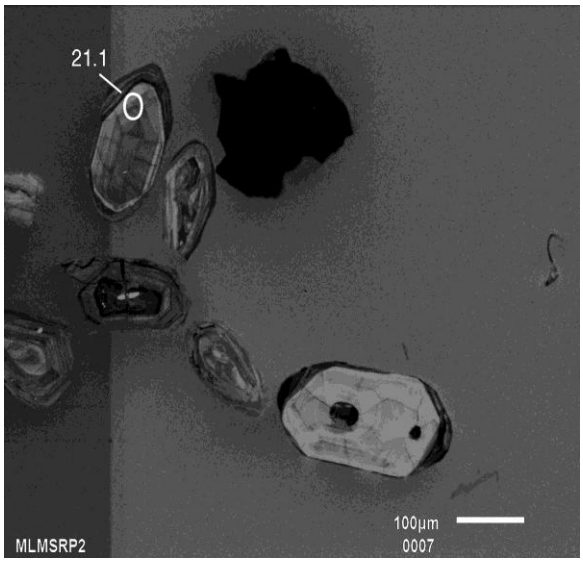

G

Figure 4.3 continued.

The results of the SHRIMP analyses show some serious disturbance of the U-Pb systematics, with discordance and scatter making it difficult to define a unique age. There is, however, a group of 10 concordant to subconcordant data (plotted in blue in Figure 4.4) that are used to calculate a weighted mean 207Pb/206Pb age of 2631.5 ± 4.4 Ma (MSWD = 0.87; probability-of-fit = 0.55), which is interpreted as the emplacement age

of the protolith to the pink gneissic granite. The two analyses from the reworked zircon in grain #6 were excluded from this group and calculation. Together these two analyses appear to be slightly younger than the general population and give a weighted mean 207Pb/206Pb age of 2614 ± 7.7 Ma. This result would suggest that the reworking (by whatever process) of this zircon occurred soon after crystallization of the main magma.

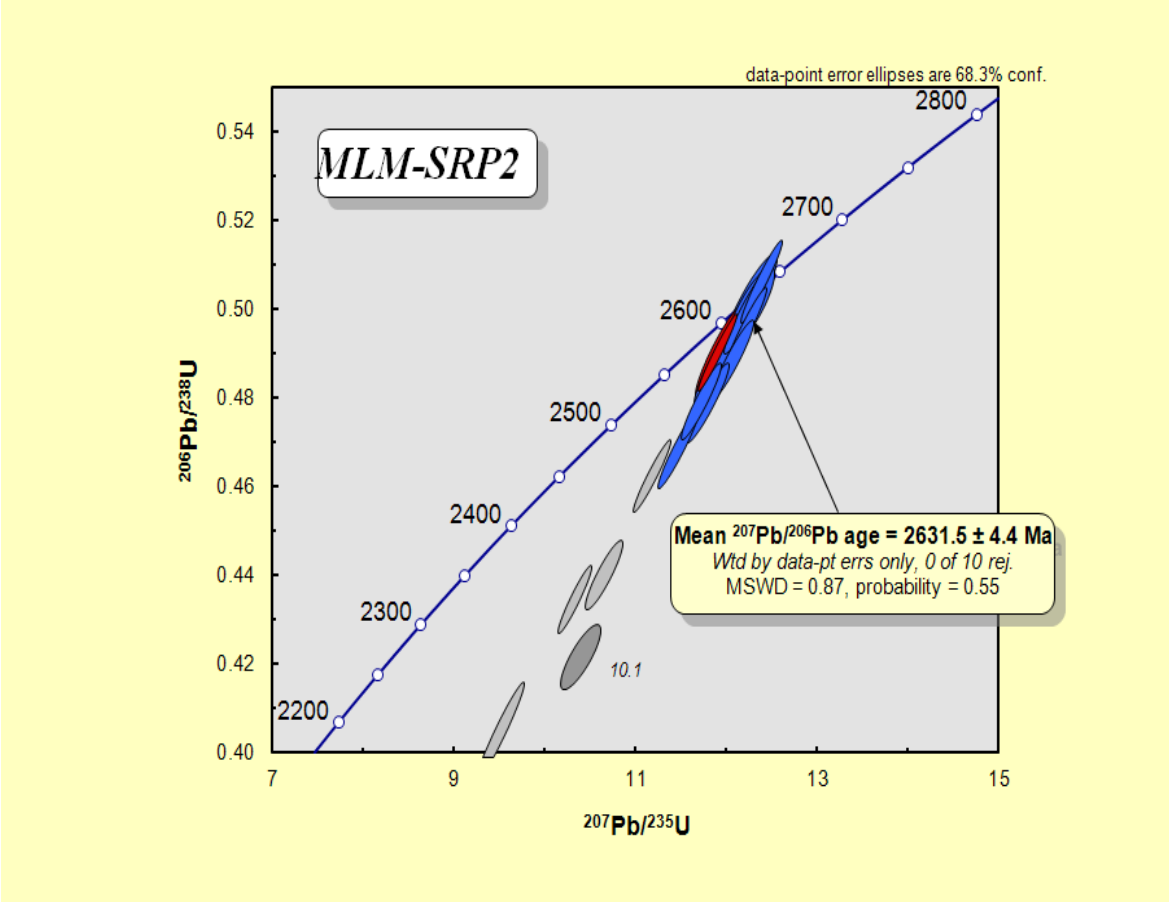

Figure 4.4: U-Pb Concordia plot of SHRIMP data for core and magmatic zircon for pink gneissic granite from Foley East.

Table 4.3: U-Th-Pb isotope data for zircons from the pink gneissic granite, Sample no. MLM-SRP 2

Grain. Spot	% $^{206}Pb_c$	ppm U	ppm Th	$^{232}Th/^{238}U$	ppm $^{206}Pb^*$	(1) $^{206}Pb/^{238}U$ Age		(1) $^{207}Pb/^{206}Pb$ Age		% Dis-cor-dant	(1) $^{207}Pb^*/^{206}Pb^*$	±%	(1) $^{207}Pb^*/^{235}U$	±%	(1) $^{206}Pb^*/^{238}U$	±%	err corr
1.1	0.02	260	84	0.33	111	2597	±25	2639.1	± 5.6	2	0.17851	0.34	12.21	1.2	0.4961	1.2	.962
2.1	0.04	229	277	1.25	92.2	2480	±25	2627.8	± 6.3	6	0.17731	0.38	11.47	1.3	0.4692	1.2	.956
3.1	0.12	273	188	0.71	112	2526	±25	2626.3	± 6.9	4	0.17714	0.41	11.72	1.3	0.4797	1.2	.944
4.1	0.08	188	92	0.51	80.9	2612	±26	2627.2	± 6.7	1	0.17724	0.41	12.21	1.3	0.4997	1.2	.950
5.1	0.08	479	83	0.18	150	2007	±28	2487.6	± 6.8	19	0.16306	0.4	8.21	1.7	0.3652	1.6	.970
6.1	0.09	105	94	0.92	44.5	2574	±29	2617	± 9	2	0.17616	0.54	11.92	1.5	0.4907	1.4	.929
6.2	0.02	426	57	0.14	180	2574	±24	2613.8	± 4.4	2	0.17582	0.26	11.9	1.2	0.4907	1.1	.975
7.1	0.81	858	550	0.66	178	1383	±14	2230	±21	38	0.1403	1.2	4.627	1.6	0.2393	1.1	.685
8.1	0.03	268	164	0.63	117	2641	±26	2628.3	± 5.4	0	0.17736	0.33	12.38	1.2	0.5064	1.2	.964
9.1	0.03	322	327	1.05	94	1885	±19	2618.1	± 6	28	0.17628	0.36	8.26	1.2	0.3397	1.2	.956
10.1	1.48	414	255	0.64	153	2272	±22	2638	±13	14	0.1784	0.79	10.39	1.4	0.4225	1.1	.823
11.1	0.15	916	221	0.25	230	1651	±16	2217.3	± 5.9	26	0.1392	0.34	5.601	1.2	0.2918	1.1	.955
11.2	0.86	374	78	0.21	143	2354	±23	2607.6	± 9	10	0.17516	0.54	10.64	1.3	0.4407	1.2	.905
12.1	0.40	479	341	0.74	180	2330	±22	2576.4	± 6.2	10	0.17192	0.37	10.32	1.2	0.4353	1.1	.951
13.1	0.22	403	82	0.21	141	2195	±34	2557	± 8	14	0.16993	0.48	9.51	1.9	0.4057	1.9	.968
14.1	0.11	323	123	0.39	129	2453	±24	2607.1	± 5.6	6	0.17511	0.34	11.18	1.2	0.4631	1.2	.961
15.1	0.02	185	190	1.06	79.6	2621	±31	2626	±11	0	0.1771	0.68	12.25	1.6	0.5017	1.4	.903
15.2	1.08	243	191	0.81	74.6	1952	±30	2603	±15	25	0.1747	0.9	8.52	2	0.3537	1.8	.890
16.1	0.03	229	106	0.48	98.4	2617	±26	2631	±13	1	0.1776	0.79	12.26	1.4	0.5007	1.2	.836
17.1	0.23	694	277	0.41	180	1700	±17	2391.2	± 6.5	29	0.15403	0.38	6.411	1.2	0.3018	1.1	.947
18.1	0.08	106	146	1.43	44.3	2564	±28	2622.4	± 9	2	0.17673	0.54	11.9	1.5	0.4885	1.3	.928
19.1	0.04	317	296	0.97	133	2566	±25	2642.8	± 7.2	3	0.17891	0.43	12.06	1.3	0.4889	1.2	.941
20.1	0.25	209	125	0.62	86.4	2525	±25	2637	± 7.3	4	0.17828	0.44	11.79	1.3	0.4795	1.2	.940
21.1	0.79	270	216	0.83	91.9	2134	±21	2557	±11	17	0.1699	0.65	9.19	1.3	0.3924	1.2	.876

Errors are 1-sigma; Pb_c and Pb^* indicate the common and radiogenic portions, respectively.

Error in Standard calibration was 0.42% (not included in above errors but required when comparing data from different mounts).

(1) Common Pb corrected using measured ^{204}Pb.

4.3.3 TONALITIC GNEISS (MLM-SRP3, S 21.47403 E 27.53267)

Sample MLM-SRP 3 collected from a locality SE of Tonota is homogeneous, medium grained grey foliated tonalitic gneiss. The tonalitic gneiss normally occur as bands within the predominant megacrystic granite gneiss unit but locally, xenoliths of the tonalitic gneiss occurs within the megacrystic granite gneiss (Fig. 2.18). Eighteen (18) analyses were obtained from the zircon population of 19 grains. The Th/U ratios vary from 0.24 to 0.5, with many grains having Th/U ratio >0.2 (Table 4.4), compatible with zircon population derived from a magmatic protolith. Uranium concentrations are between 135 to 657 ppm and Th concentrations rage between 32 and 248ppm. The zircons are light brown and generally somewhat elongate with slight rounding of grain tips. Well-developed oscillatory zoning indicates that these zircons crystallized from felsic magma (Fig. 4.5). Some dark brown grains are clearly altered/metamict and were avoided for dating purposes.

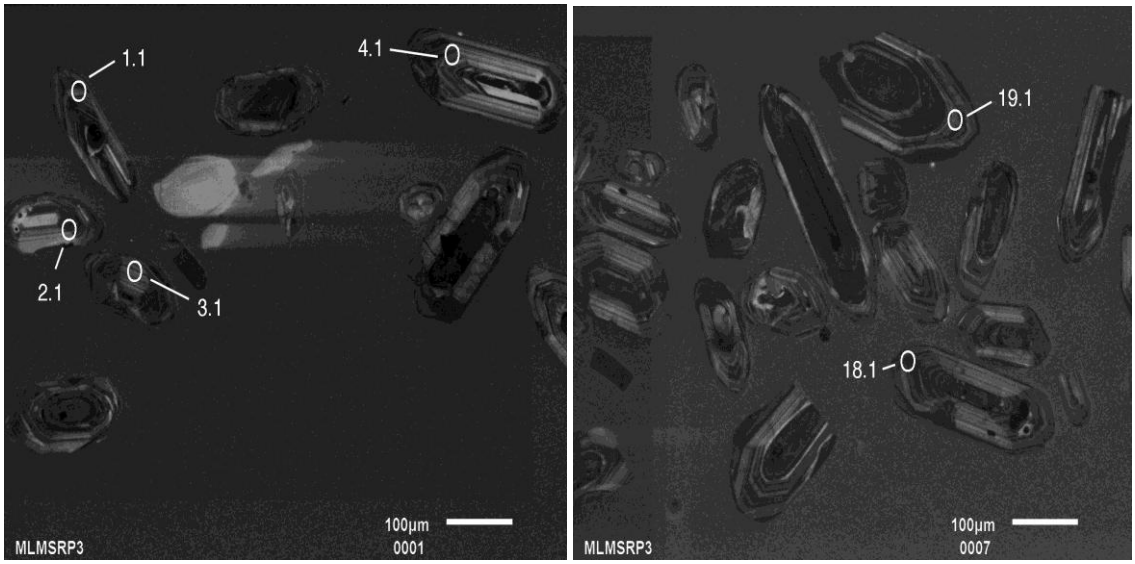

A B

Fig. 4.5: CL-images of zircons from tonalitic gneiss unit illustrating zircon quality, oscillatory zoning and the spots analysed.

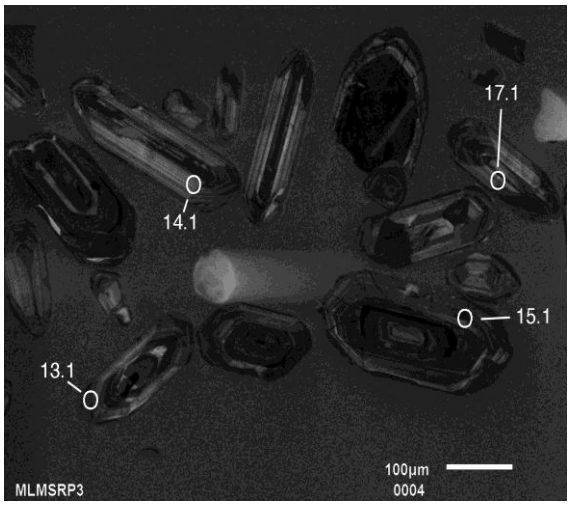

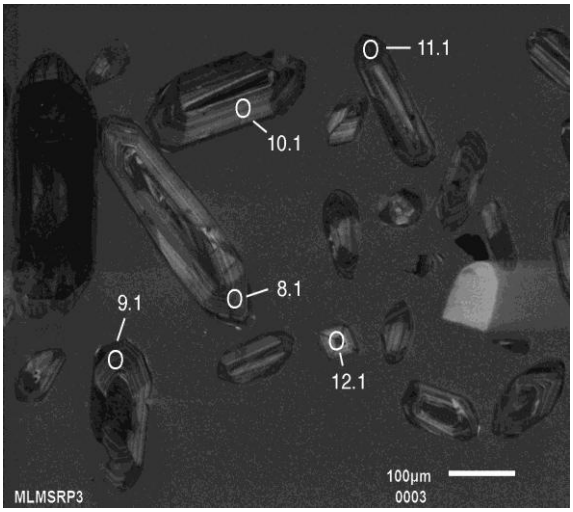

C D

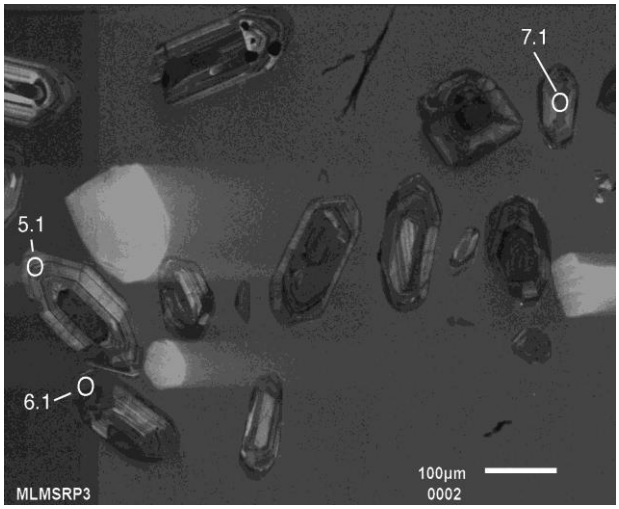

E

Figure 4.5 continued

The data as plotted on a conventional Wetherill Concordia plot are highly discordant, but show little scatter about a discordia, which gives upper and lower intercepts of 2698.9 ± 9.2 Ma and 633 ± 83 Ma respectively (Fig. 4.6). The MSWD of 2.6 indicates some excess scatter, but compared to other samples from this area the data are relatively simple, with no inheritance observed. The upper intercept age of 2698.9 ± 9.2 Ma is interpreted as the emplacement age of the precursor igneous rock to the tonalitic gneiss.

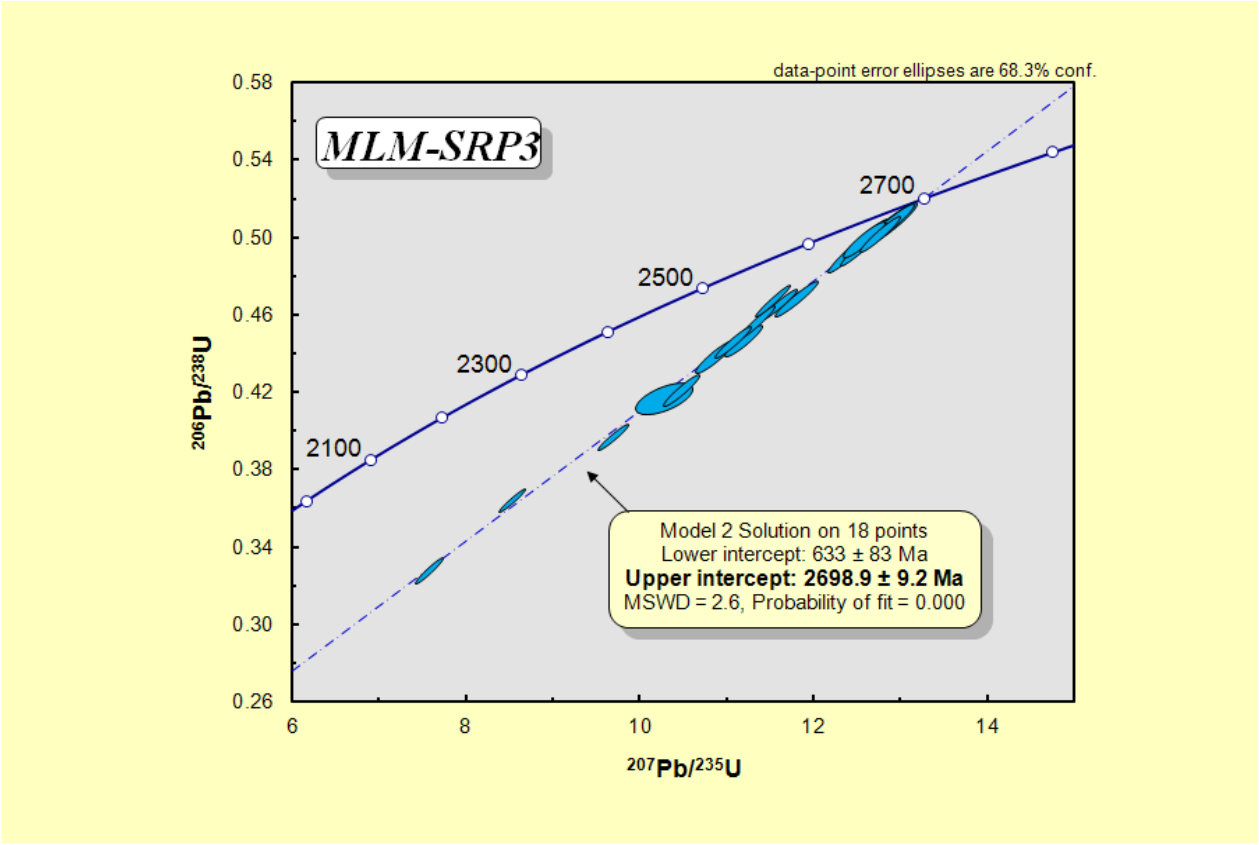

Figure 4.6: Wetherill plot of SHRIMP data for core and magmatic zircon for tonalitic gneiss sampled to the SE of Tonota.

Table 4.4 U-Pb isotope data for zircons extracted from a sample of tonalitic gneiss, MLM-SRP 3.

Grain. Spot	% $^{206}Pb_c$	ppm U	ppm Th	$^{232}Th/^{238}U$	ppm $^{206}Pb^*$	(1) $^{206}Pb/^{238}U$ Age		(1) $^{207}Pb/^{206}Pb$ Age		% Dis-cor-dant	(1) $^{207}Pb^*/^{206}Pb^*$	±%	(1) $^{207}Pb^*/^{235}U$	±%	(1) $^{206}Pb^*/^{238}U$	±%	err corr
1.1	0.01	275	95	0.36	120	2644	±33	2693.2	± 9	2	0.1844	0.55	12.89	1.6	0.5071	1.5	.940
2.1	0.04	147	34	0.24	62.6	2597	±38	2680.4	± 7.4	3	0.18302	0.45	12.52	1.8	0.496	1.8	.971
3.1	0.00	200	46	0.24	85.7	2611	±26	2679.8	± 8.2	3	0.18295	0.5	12.59	1.3	0.4993	1.2	.925
4.1	0.08	204	50	0.25	82.4	2478	±27	2677.5	± 6.4	7	0.1827	0.39	11.81	1.4	0.4686	1.3	.958
5.1	0.03	416	201	0.50	167	2473	±24	2642.6	± 4.5	6	0.17889	0.27	11.53	1.2	0.4676	1.1	.973
6.1	0.03	657	32	0.05	206	2003	±19	2553.8	± 5	22	0.16961	0.3	8.521	1.2	0.3644	1.1	.967
7.1	0.00	223	66	0.31	96.2	2624	±26	2693.6	± 5.9	3	0.18449	0.36	12.78	1.3	0.5024	1.2	.959
8.1	0.03	218	50	0.24	93	2601	±31	2687.9	± 6	3	0.18385	0.36	12.6	1.5	0.4969	1.4	.970
9.1	0.14	324	74	0.24	124	2380	±23	2652.5	± 5.8	10	0.17996	0.35	11.08	1.2	0.4466	1.2	.958
10.1	0.25	154	36	0.24	58.4	2346	±24	2649	± 8.6	11	0.17958	0.52	10.87	1.3	0.4389	1.2	.923
11.1	0.20	406	118	0.30	139	2157	±21	2621.5	± 5.6	18	0.17664	0.34	9.68	1.2	0.3974	1.1	.959
12.1	0.19	308	107	0.36	119	2383	±23	2666.3	± 7.7	11	0.18146	0.46	11.19	1.3	0.4473	1.2	.929
13.1	0.09	331	88	0.27	133	2465	±24	2659.1	± 5.4	7	0.18067	0.32	11.6	1.2	0.4658	1.2	.964
14.1	0.06	135	32	0.25	58.9	2641	±32	2693	± 7.6	2	0.18441	0.46	12.87	1.6	0.5063	1.5	.956
15.1	0.07	279	74	0.27	110	2424	±24	2656.6	± 5.7	9	0.18041	0.34	11.36	1.2	0.4566	1.2	.960
17.1	2.18	180	55	0.32	65.8	2247	±25	2639	±28	15	0.1785	1.7	10.26	2.1	0.417	1.3	.613
18.1	0.31	542	248	0.47	153	1830	±22	2525.8	± 6.5	28	0.1668	0.39	7.55	1.4	0.3282	1.4	.962
19.1	0.28	282	87	0.32	102	2267	±24	2655.3	± 6.9	15	0.18027	0.42	10.48	1.3	0.4215	1.2	.948

Errors are 1-sigma; Pb_c and Pb^* indicate the common and radiogenic portions, respectively.
Error in Standard calibration was 0.28% (not included in above errors but required when comparing data from different mounts).
(1) Common Pb corrected using measured ^{204}Pb.

4.3.4 TONOTA BIOTITE GNEISS (MLM-SRP4, S 21.44802 E 27.44663)

Sample MLM-SRP 4 is from the Tonota biotite gneiss which occurs interlayered with amphibolite around Tonota Village. The origin of the protolithic of this unit has been uncertain (Section 1.6). Previous work indicates a sedimentary origin based on their spatial association with metasedimentary rocks of the SFT belt. The contents of U and Th are variable with ranges of 115 to 784 and 11 to 284 ppm (Table 4.5). Th/U ratios of the zircon grains vary from 0.02 to 0.54 with many grains having Th/U ration> 0.11, suggesting a magmatic origin. Additional support for a magmatic origin is shown by oscillatory zoning in CL images. This sample produced a very poorly preserved crop of

zircons for dating. They are dark brown, opaque and have slightly rounded or resorbed tips and edges (Fig. 4.7). Clearly they are highly metamict, but some areas still preserve strong oscillatory, magmatic zoning, and may have cores of what appear to be inherited zircon. Some of these are also highly altered/metamict and the original zircon has completely broken down.

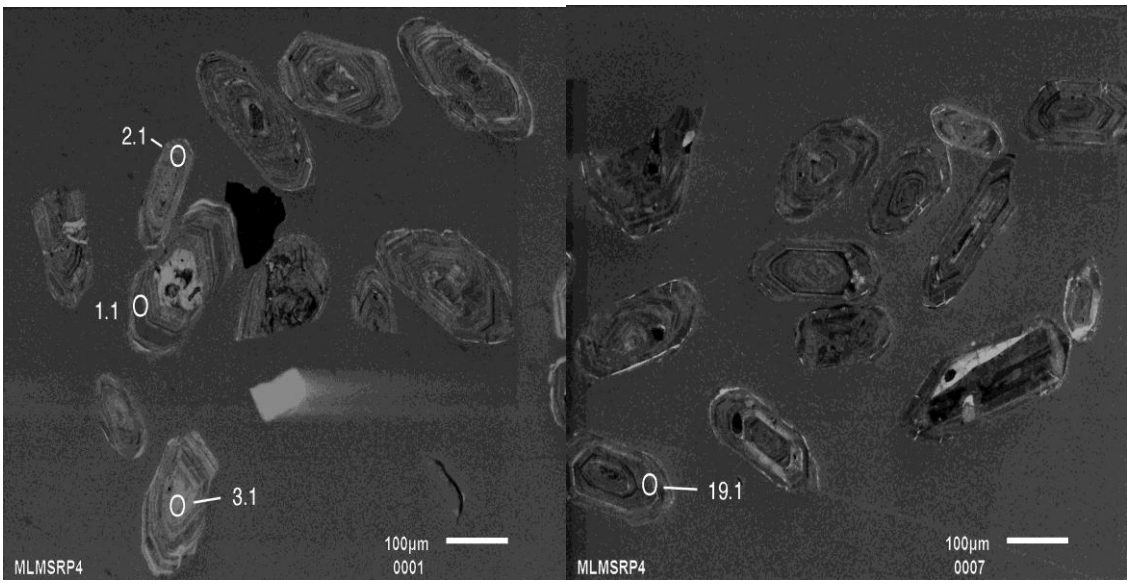

A B

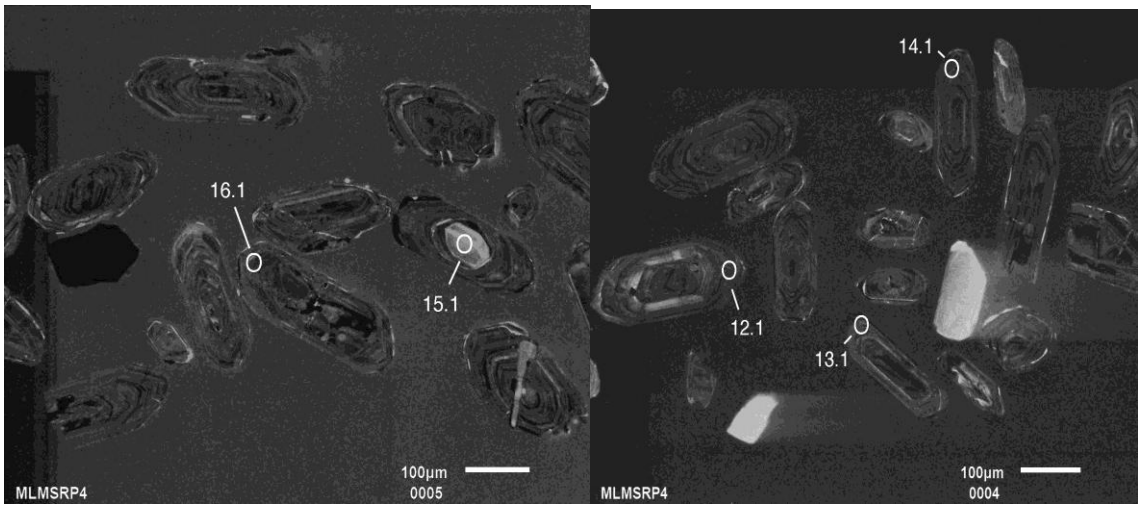

C D

Figure 4.7: Cathodoluminescence images of zircon from the Tonota biotite gneiss comprising oscillatory zoned cores.

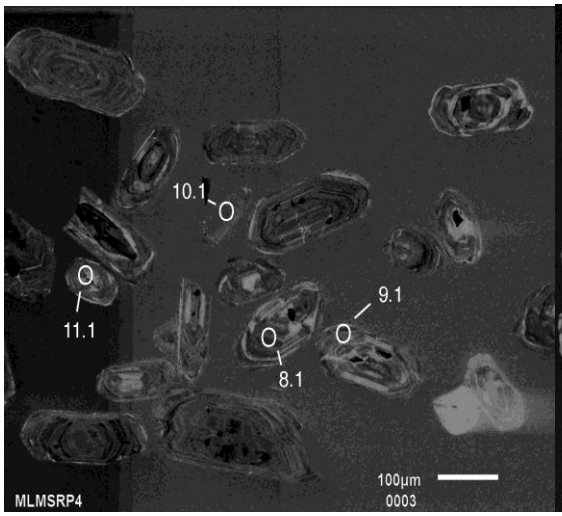

E

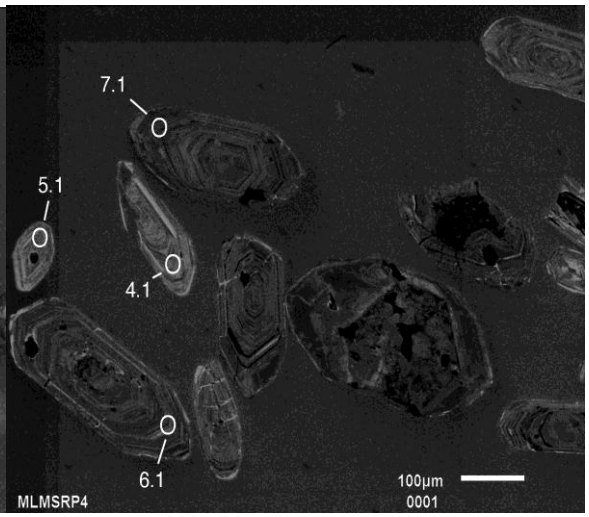

F

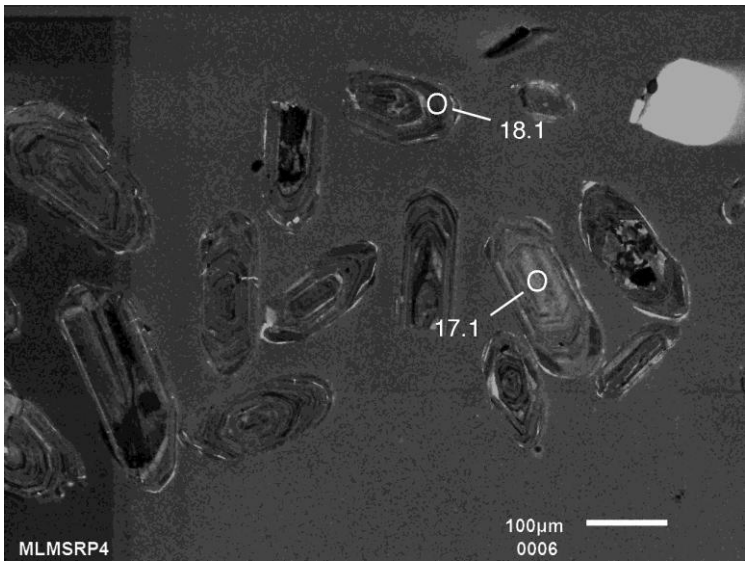

G

Fig. 4.7 continued

Finding areas to analyse that are in good enough condition and might give concordant results was difficult and all spots chosen produced highly discordant data. One low-U core (15.1) gives the least discordant (4%) result with a minimum $^{207}Pb/^{206}Pb$ age of 2978 ± 7.4 Ma. The remaining seventeen spots lie, with unsatisfactory scatter on a Pb-loss trend which an upper intercept age of 2724 ± 48 Ma (Fig. 4.8). The high MSWD = 9.5,

however, shows the effects of the excess scatter of the data. The lower intercept suggest Pb-loss associated with a Mesoproterozoic event.

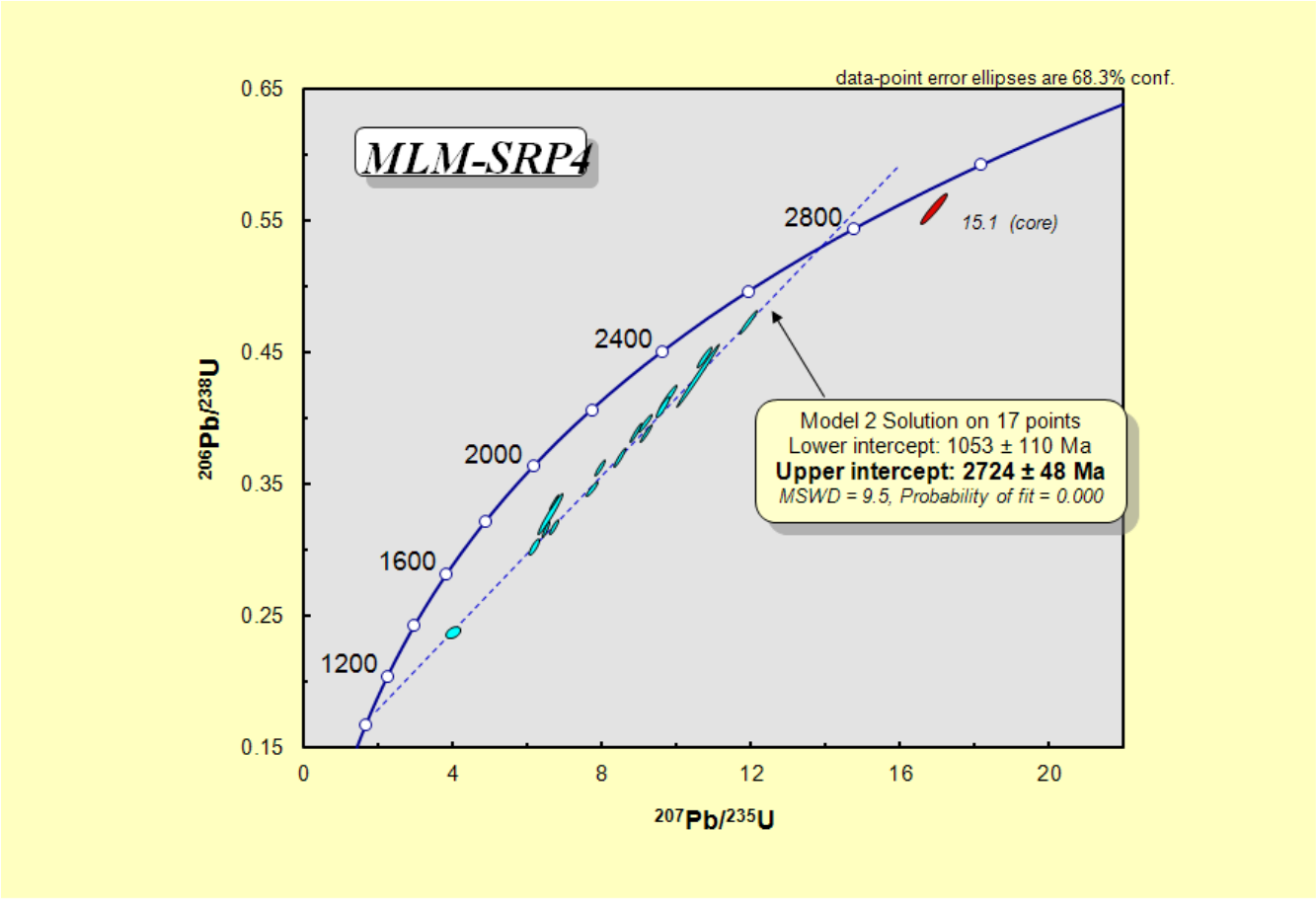

Figure 4.8: U-Pb Concordia (Wetherill) plot of SHRIMP data for core and magmatic zircon for sample MLMSRP 4 from the Tonota biotite gneiss

Table 4.5: U-Pb isotopic compositions and age calculations of zircons from sample MLM-SRP 4 from the Tonota biotite gneiss

Table 4: Summary of SHRIMP U-Pb zircon data for sample MLMSRP4

Grain.Spot	% $^{206}Pb_c$	ppm U	ppm Th	$^{232}Th/^{238}U$	ppm $^{206}Pb^*$	(1) $^{206}Pb/^{238}U$ Age		(1) $^{207}Pb/^{206}Pb$ Age		% Dis-cor-dant	(1) $^{207}Pb^*/^{206}Pb^*$	±%	(1) $^{207}Pb^*/^{235}U$	±%	(1) $^{206}Pb^*/^{238}U$	±%	err corr
1.1	0.07	446	33	0.08	182	2497	±24	2682.7	± 4.5	7	0.18327	0.27	11.96	1.2	0.4731	1.2	.973
2.1	0.41	677	353	0.54	185	1773	±17	2335.8	± 8.6	24	0.14911	0.5	6.507	1.2	0.3165	1.1	.913
5.1	0.40	482	204	0.44	144	1917	±19	2482.4	± 8	23	0.16256	0.48	7.764	1.2	0.3464	1.1	.922
4.1	0.30	685	265	0.40	214	1998	±19	2450.9	± 7.1	18	0.15955	0.42	7.993	1.2	0.3634	1.1	.937
6.1	0.26	407	150	0.38	130	2034	±20	2520.9	± 6.4	19	0.16631	0.38	8.51	1.2	0.3709	1.1	.950
7.1	0.32	465	51	0.11	179	2382	±23	2607.1	± 6.4	9	0.17511	0.38	10.79	1.2	0.447	1.1	.948
8.1	0.13	530	284	0.55	177	2119	±21	2575.4	± 5.4	18	0.17182	0.32	9.22	1.2	0.3891	1.2	.963
9.1	0.10	409	122	0.31	146	2242	±28	2568.6	± 7.1	13	0.17112	0.43	9.81	1.5	0.4159	1.5	.960
10.1	0.02	391	133	0.35	145	2317	±70	2632.8	± 6.1	12	0.17784	0.37	10.61	3.6	0.433	3.6	.995
11.1	0.34	315	129	0.42	111	2212	±22	2567.7	± 8.8	14	0.17103	0.53	9.65	1.3	0.4094	1.2	.911
12.1	0.26	532	125	0.24	179	2121	±21	2522.1	± 5.6	16	0.16643	0.33	8.94	1.2	0.3897	1.1	.960
13.1	0.02	623	46	0.08	180	1870	±19	2285.1	± 4.8	18	0.14477	0.28	6.719	1.2	0.3366	1.2	.972
14.1	0.22	594	220	0.38	155	1706	±19	2336	±14	27	0.1492	0.81	6.232	1.5	0.303	1.3	.843
15.1	0.08	115	103	0.93	55.4	2863	±31	2978.4	± 7.4	4	0.2197	0.46	16.94	1.4	0.5592	1.3	.947
16.1	0.53	677	11	0.02	186	1779	±18	2390.6	± 9.2	26	0.15398	0.54	6.749	1.3	0.3179	1.1	.902
17.1	0.54	784	175	0.23	222	1831	±52	2306	±13	21	0.1466	0.76	6.64	3.3	0.329	3.2	.973
18.1	0.36	528	85	0.17	181	2155	±21	2538.9	± 6.1	15	0.16811	0.36	9.2	1.2	0.3969	1.1	.953
19.1	0.86	697	273	0.40	144	1379	±16	2001	±49	31	0.1231	2.8	4.05	3.1	0.2385	1.3	.414

Errors are 1-sigma; Pb_c and Pb^* indicate the common and radiogenic portions, respectively.
Error in Standard calibration was 0.28% (not included in above errors but required when comparing data from different mounts).
(1) Common Pb corrected using measured ^{204}Pb.

4.3.5 MYLONITIC MEGACRYSTIC GRANITE GNEISS (MLM-SRP 5, S 21.52411 E 27.44227)

This was sampled from a megacrystic granite gneiss unit south of Tonota. The rock is petrographically similar to MLM-SRP 1 containing megacrysts of K-feldspar and quartz embedded in a medium grained matrix of biotite and quartz. The megacrysts are deformed, showing evidence for flattening perpendicular to foliation (S_1) surface and elongation parallel to the foliation (S_1). The rock is flanked to the E by metasedimentary rocks but field/age relationship between the two rock units remains unknown because the contact is not exposed. High U and Th concentrations of the order 72 to 1708 and 38 to 479 ppm and a Th/U ratio range of 0.22 to 1.45 provide evidence for a magmatic origin for the emplacement of the protolith of this rock (Table 4.6). The zircons from this sample have a range of colours from brown to light grey and also show a range of sizes

and shapes. Cathodoluminescence imaging shows some complex internal structures to the grains, including low-U central growth areas and some large embayed areas (e.g. grain #2). The zircon grains are subhedral to anhedral and have oscillatory magmatic zoning in varying degrees of intensity. Many grains show evidence of resorption (Fig. 4.9).

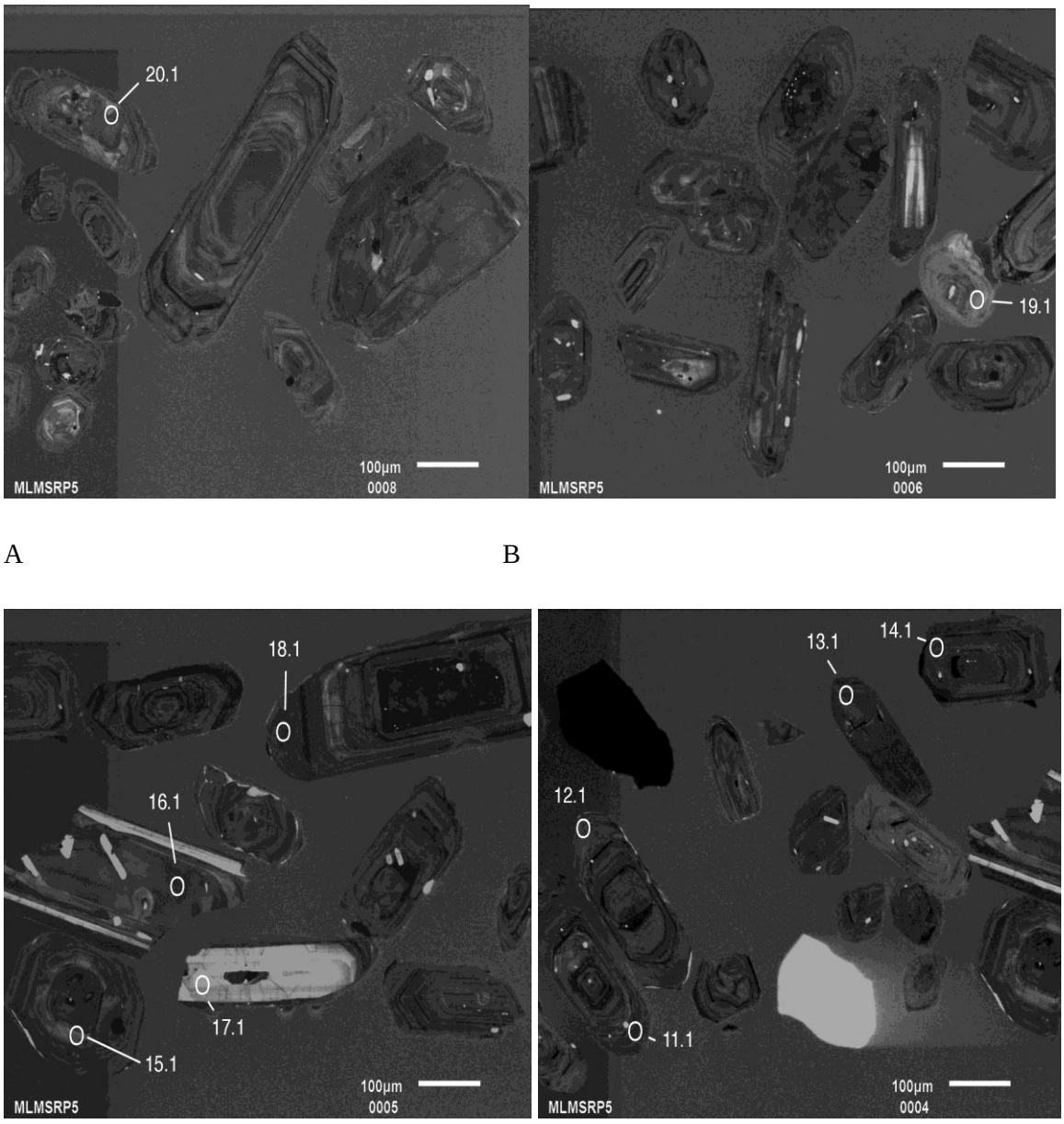

Figure 4.9: Cathodoluminescence images of zircons from megacrystic granite gneiss (sample MLM-SRP 5). The analysed points are in Table 4.6.

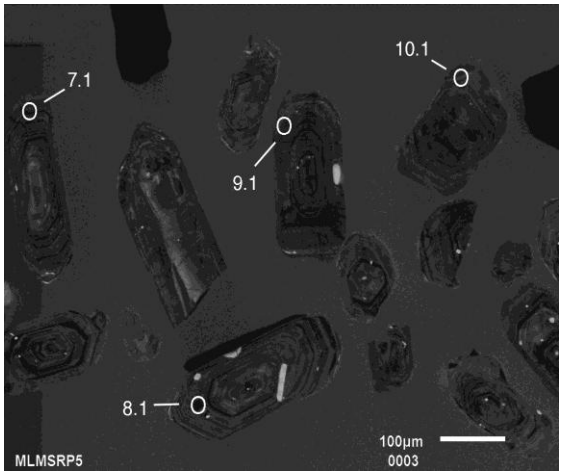

E

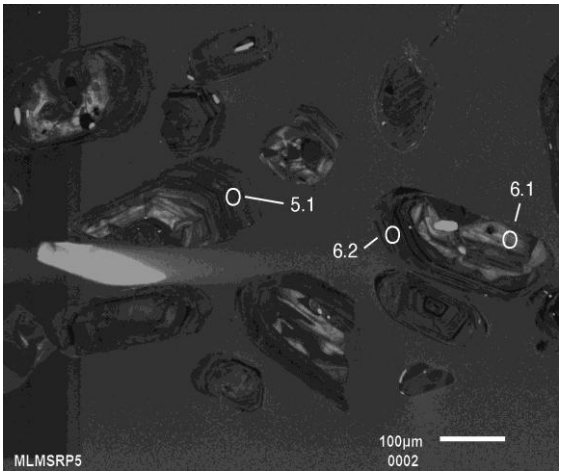

F

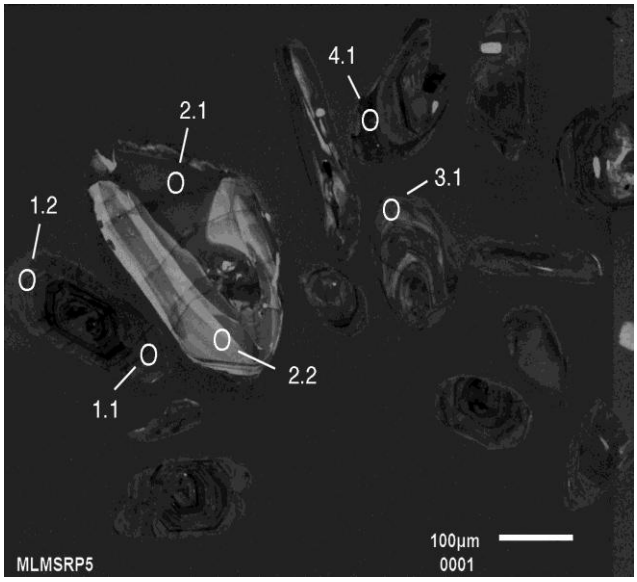

G

Fig. 4.9 continued

Most data are highly discordant but follow a discordia trend, albeit with some scatter. A number of analyses of relatively low-U areas are subconcordant. These are from centers of grains (which could be cores) and from embayments such as # 2.1. As with the other samples in this suite, it is difficult to unequivocally conclude that some of the central areas are not inherited cores. But in this case, the "cores" (which would be the oldest component) and the embayments (such as #2.1 which postdate the zoned, outer, magmatic growth) are indistinguishable in age. Regression of the data as shown in the Concordia plot (Fig. 4.10.) produces an upper intercept age of 2625 ± 14 Ma (MSWD = 3.4; probability = 0.000), which is interpreted as the age of the protolith and thus the maximum age of shearing. This age is within error of the age determined for MLM-SRP1 (2647 ± 24 Ma).

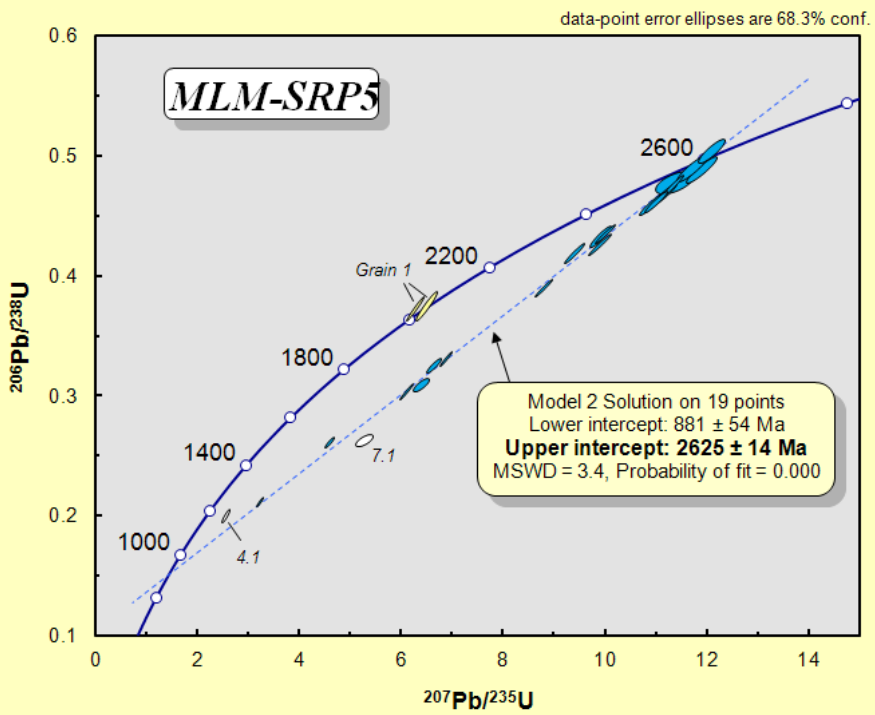

Figure 4.10: Wetherill plot of SHRIMP data for core and magmatic zircon for sample megacrystic granite gneiss, MLM-SRP 5 from Tonota south area.

The high MSWD and low probability-of-fit reflect the scatter about the single Pb-loss or discordia trend. The regression excluded a number of data points: both analyses from grain #1 and spots 4.1 and 7.1. Grain #1 appears to be a normal strongly zoned magmatic zircon, indistinguishable from the general population. It is, however very different in terms of its U-Pb character to the general population, with the two spots plotting on or near Concordia (yellow ellipses on Fig 4.10). The two analyses are significantly different in terms of the Pb-Pb ages and it is possible that this grain is recording severe Pb-loss at about 2 Ga. The two spots were located in identical, zoned tips at either end of the grain. The other data for spots 4.1 and 7.1 were excluded from the regression as they clearly fall significantly off the calculated discordia and have a different Pb-loss history and possible origins.

Table 4.6: U-Pb isotopic compositions and age data from zircons from a megacrystic granite gneiss-sample MLM-SRP 5.

Grain. Spot	% $^{206}Pb_c$	ppm U	ppm Th	$^{232}Th/^{238}U$	ppm $^{206}Pb^*$	(1) $^{206}Pb/^{238}U$ Age		(1) $^{207}Pb/^{206}Pb$ Age		% Dis-cor-dant	(1) $^{207}Pb^*/^{206}Pb^*$	±%	(1) $^{207}Pb^*/^{235}U$	±%	(1) $^{206}Pb^*/^{238}U$	±%	err corr
1.1	0.23	863	370	0.44	276	2034	±37	2058	±11	1	0.12705	0.62	6.5	2.2	0.3709	2.1	.959
1.2	0.17	939	487	0.54	298	2025	±31	2002.6	± 6.2	-1	0.12317	0.35	6.27	1.8	0.3691	1.8	.982
2.1	0.02	449	95	0.22	182	2492	±27	2598.7	± 4.5	4	0.17423	0.27	11.34	1.3	0.4719	1.3	.979
2.2	0.06	92	84	0.95	38.4	2560	±32	2602	±12	2	0.1746	0.71	11.74	1.7	0.4876	1.5	.906
3.1	0.18	293	184	0.65	115	2429	±27	2590.6	± 7.2	6	0.17338	0.43	10.94	1.4	0.4576	1.3	.952
4.1	0.86	1708	38	0.02	287	1143	±20	1518	±16	25	0.09449	0.83	2.528	2.1	0.194	1.9	.919
5.1	0.11	829	270	0.34	233	1823	±20	2378.6	± 4.5	23	0.1529	0.27	6.892	1.3	0.3269	1.3	.979
6.1	0.07	139	153	1.14	55.6	2462	±29	2601.5	± 7.9	5	0.17452	0.48	11.19	1.5	0.4651	1.4	.949
6.2	0.24	686	181	0.27	190	1793	±20	2352.8	± 9.7	24	0.15061	0.57	6.66	1.4	0.3207	1.3	.917
7.1	2.54	811	428	0.54	185	1480	±17	2323	±24	36	0.148	1.4	5.26	1.9	0.258	1.3	.687
8.1	0.20	998	343	0.35	221	1472	±17	2087.1	± 8.7	29	0.1292	0.5	4.571	1.4	0.2566	1.3	.933
9.1	0.00	532	135	0.26	196	2306	±25	2531.3	± 8.7	9	0.16735	0.52	9.92	1.4	0.43	1.3	.930
10.1	0.05	635	306	0.50	211	2106	±23	2511	± 4.2	16	0.16534	0.25	8.81	1.3	0.3864	1.3	.982
11.1	0.33	1332	799	0.62	237	1209	±14	1854.8	± 7.2	35	0.11341	0.4	3.225	1.3	0.2062	1.3	.955
12.1	0.05	613	172	0.29	227	2314	±25	2539.5	± 4.3	9	0.16817	0.26	10.01	1.3	0.4318	1.3	.981
13.1	0.09	517	144	0.29	184	2238	±25	2504.1	± 5.5	11	0.16467	0.33	9.42	1.4	0.415	1.3	.971
14.1	0.10	842	326	0.40	216	1687	±20	2329.4	± 4.5	28	0.14856	0.26	6.126	1.4	0.2991	1.4	.982
15.1	0.16	369	162	0.45	146	2437	±27	2597.2	± 6.3	6	0.17407	0.38	11.03	1.4	0.4594	1.3	.961
16.1	0.03	311	292	0.97	127	2506	±28	2597	±30	4	0.174	1.8	11.4	2.2	0.4751	1.3	.603
17.1	0.12	72	101	1.45	30.2	2554	±34	2634	±11	3	0.178	0.66	11.93	1.7	0.4862	1.6	.924
18.1	0.13	559	150	0.28	204	2276	±28	2554.4	± 4.6	11	0.16967	0.28	9.91	1.5	0.4234	1.5	.983
19.1	0.51	1298	479	0.38	341	1711	±19	2377	±16	28	0.1528	0.96	6.4	1.6	0.304	1.3	.800
20.1	0.57	338	92	0.28	147	2621	±29	2608	±12	0	0.1752	0.7	12.12	1.5	0.5018	1.3	.884

Errors are 1-sigma; Pb_c and Pb^* indicate the common and radiogenic portions, respectively.
Error in Standard calibration was 0.31% (not included in above errors but required when comparing data from different mounts).
(1) Common Pb corrected using measured ^{204}Pb.

4.4 DISCUSSION

Age constraints in NE Botswana are based on crystallization of granitoid rocks and detrital zircons in metasedimentary rocks (McCourt *et al*., 2004). The zircons from the samples analysed are characterized by severe Pb-loss in some instances and the common resorbed edges and tips would suggest some degree of metamorphic rounding at some stage. The lower intercept ages are imprecise due to the scatter commonly observed in the data, but if the lower intercept dates are reliable indicators of the timing of the Pb-loss, then there appears to be two Pb-loss events at about 1000 Ma and 600-700 Ma (with some considerable uncertainty). The younger of these two Pb-loss events may represent a response to the Neoproterozoic "Pan African" Damara Orogeny while the Mesoproterozoic ages of 1183.3 ± 9.6 Ma and 1270 ± 12 Ma obtained from zircons in sample MLM-SRP 1, could be linked to the "Kibaran event" as documented from the Kgwebe Hills in NW Botswana by Kampunzu *et al*. (1998), implying co-existence of Archaean, Neoproterozoic and Mesoproterozoic elements in granitoid gneiss in the SFT area. The study area is cut by the Okavango Dyke Swarm and although the great majority of the dykes in this swarm are Phanerozoic (Karoo) in age there are some dykes that are Proterozoic in age (Jourdan *et al*., 2004). The 600-700Ma lower intercepts on the Concordia plots may be related to this magmatism. Mesoproterozoic ages have not been reported in either the Francistown Complex (Bagai, 2002) or the Mosetse Complex (Majaule and Davis, 1998). The Pb loss event at 2 Ga recorded in sample MLM-SRP 5 (grain # 1 and spots 4.1 and 7) may be related to the Palaeoproterozoic Magondi orogeny or the 2 Ga (reactivation) events reported in the Limpopo belt. The minimum age of the Magondi orogeny is 1997.5 ±2.6 Ma (McCourt *et al*., 2001).

Deciphering the internal structures of these grains, even with the use of CL and other imaging has been difficult and sometime subjective. Although this is not an uncommon feature of felsic rocks, the small gap (if any) between the magmatic, zoned zircon and the possible cores suggest that if these cores were inherited, then the source of the inheritance was not much different to the age of the host rocks. This suggests that the zircon analysed and the rocks from which they were extracted formed in a short-lived environment, with no significant history before 2700 Ma. Certainly these rocks do not appear to have a

significant inherited input from a much older source. An active arc would be such an environment. This might have petrological and tectonic implications for the interpretation of this Archaean crustal block and its possible correlation with other cratonic crust in the broader region.

Based on the high Th/U ratios for zircons extracted from the Tonota biotite gneiss together with the limited age range of the grains analysed, the protolith to this gneiss is interpreted to have been an igneous rather than sedimentary as previously proposed (Aldiss, 1991). From the zircon grains analysed, the age of the protolith to the Tonota biotite gneiss is 2724 ± 48 Ma making it the oldest rock in the SFT area. Tonalitic gneiss (sample MLM-SRP 3) gave an upper intercept age 2698.9 ± 9.2 Ma. This is interpreted as the emplacement age of the protolith to the tonalitic gneiss and implies subduction of the Matsitama-Motloutse Complex beneath the SW margin of the Zimbabwe craton (reported by McCourt *et al.* (2004) was active at 2699 Ma to produce the tonalitic magma. Megacrystic granite gneiss from Foley East area yielded an upper intercept age of 2647 ± 24 Ma. Pink gneissic granite that crop out as dykes cutting the foliation (S_1) in the megacrystic granite gneiss (Figs 2.19 and 2.27) and the banded tonalitic gneiss (Fig. 2.28) has an age of 2631.5 ± 4.4 Ma. The emplacement age of the pink granite is within error of the megacrystic granite gneiss suggesting they could relate to the same magmatic event. However, the pink gneissic granite occurs as dykes discordant to the foliation (S_1) in the megacrystic granite gneiss indicating that the original porphyritic granite was metamorphosed and deformed (to produce the gneiss) prior to the emplacement of the pink granite. The crystallization ages of the granitoid gneisses ranges between 2724 ± 48 Ma and 2632 ± 4 Ma, spanning a period of about 93 million years. U-Pb zircon age of 2625 ± 16 Ma was obtained from mylonitic megacrystic granite gneiss sampled south of Tonota Village. This age (the age of the rock deformed in the shear zone) is interpreted to give the maximum age of shearing.

It is suggested that the metasedimentary belt in the SFT and Topisi area to the south, form part of the same supracrustal assemblage. This is based on their spatial distribution as well as their lithological similarity. Detrital zircon grains from a quartzite sampled in the Topisi area indicate the maximum age of deposition of these rocks was 2661± 8 Ma

(McCourt *et al*., 2004) and this age also helps constrain the timing of supracrustal deposition in the SFT area. The metasedimentary sequences within the Matsitama-Motloutse Complex were deposited between 2661 and 2647 Ma with the provenance being the Francistown Arc Complex (*also* Francistown Granite Greenstone Complex) and the regions behind it (McCourt *et al*., 2004). The metasedimentary rocks and the granitoid gneiss have the same deformation fabrics. These rocks are dominated by NE-SW orientated foliation (S_1) that dips steeply to the NW. The foliation (S_1) is cut by the pink gneissic granite (Fig. 2.27 and 2.28) thus deformation of the metasedimentary rocks and the granitoid gneiss occurred before intrusion of the protolith to the pink gneissic granite at 2631.5 ± 4.4 Ma. This age combined with the detrital zircon data from the Topisi area indicates that the deformation event responsible for the regional foliation (S_1) in the SFT area occurred between 2661 Ma and 2632 Ma, a duration of about 30 million years.

Bagai *et al.* (2002) constrained the age of TTG magmatism and volcanism in the Vumba granite-greenstone terrane to between 2696 ± 4 Ma and 2647 ± 4 Ma. This age range is similar to that of Majaule and Davis (1998) of 2710 ± 10 Ma to 2646 ± 3 on tonalitic gneisses from the Mosetse area. The granitoid magmatism associated with the Neoarchaean evolution of the SFT area is thus constrained between 2724 ± 48 Ma and 2632 ± 4 Ma i.e. the same age range (Fig. 4.11) with those obtained by previous work in the Mosetse (Majaule and Davis, 1998) and Phikwe (B.K. Paya, pers.com. 2010, unpublished research data) areas. Figure 4.11 shows that the age of the pink gneissic granite (2631.5 ± 4.4 Ma) is within error of the age of the megacrystic granite gneiss whereas the age of the tonalitic gneiss (2699 ± 9 Ma) is within error of the Tonota biotite gneiss (2724 ± 48 Ma) although the latter is poorly constrained. Coeval or slightly older ages in the range 2710 ± 19 to 2639.7 ± 7.9 Ma were obtained from igneous rocks from the Tati and Vumba greenstone belts (Bagai, 2002, Kampunzu *et al*., 2003, Bagai, 2008) of the Francistown Complex suggesting they could relate to the same magmatic event.

Bagai (2008) obtained a U-Pb zircon age of 2630 ± 4.7 Ma for both the leucosome component of the Shashe migmatitic gneiss and the protolith to the Shashe augen gneiss collected within the Shashe River bed i.e. along the tectonic boundary between the SFT

and the Tati granitoid greenstone belt. This places a maximum age on the deformation responsible for the augen gneiss and constrains collision/accretion along this boundary to around 2630 Ma (Bagai, 2008). The tectonic fabric in the megacrystic granite gneiss is cut by the pink gneissic granite which was emplaced at 2630 ± 5 Ma. Deformation and metamorphism in the SFT area is indistinguishable in age to the rocks dated by Bagai (2008).

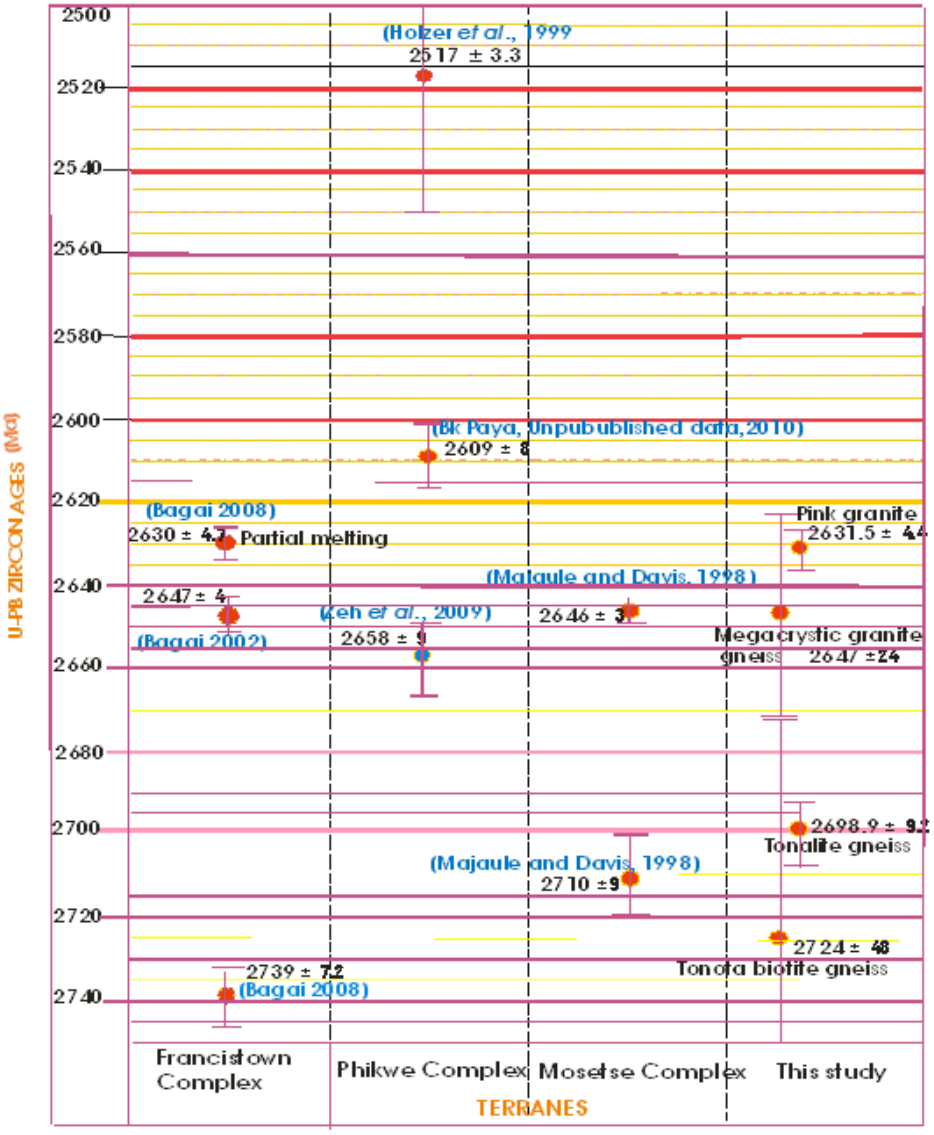

Figure 4.11: A comparison of age data obtained from terranes in NE Botswana. Note, only minimum and maximum emplacement ages from the different authors were selected. Holzer *et al.* (1999) data included. The oldest zircon grain from the Tonota biotite gneiss at 2978 ± 7Ma has not been plotted as it is interpreted as an inherited grain.

CHAPTER 5. STABLE ISOTOPE GEOCHEMISTRY

5.1 RATIONALE FOR STUDY

In this section new carbon and oxygen isotope data is presented for metacarbonate rocks from the SFT, Topisi, Monatshane and the Matsitama areas. At the end of this section the stable isotope signature of the samples from the SFT area are compared with those from Topisi, Monatshane and Matsitama areas in NE Botswana as well as those published for the Gumbu Group carbonates in the Musina area, eastern part of the Central Zone of the Limpopo belt in South Africa. The Gumbu Group carbonates have high $\delta^{13}C$ values taken to suggest that the carbonates are younger than previously believed (i.e. Palaeoproterozoic and not Archaean). Buick *et al*. (2003) obtained U-Pb dates on detrital zircon that were interpreted to indicate that the Gumbu Group is Palaeoproterozoic in age. These authors also demonstrated that the Gumbu Group metacarbonates have a similar $\delta^{13}C$ signature to that recorded in the Duitschland Formation carbonates of the Transvaal Supergroup and considered the high $\delta^{13}C$ to be diagnostic of Palaeoproterozoic and therefore may be used as a proxy for age. According to Master *et al*. (2010) the high $\delta^{13}C$ values record a sea water signature and therefore reflect the carbonate composition of open ocean at 2.2-2.1 Ga. The composition of carbonate sea water changed at 2.2-2.1 Ga, prior to plate reorganization at 2.1-2.0 Ga (Master *et al*., 2010). The reorganization affected ocean circulation and redox thus availing conditions suitable for burial of organic matter. Previous geochronological studies and work presented thus far in this dissertation show that the metasedimentary rocks of the SFT area are late Archaean in age. Therefore stable isotope analysis of metacarbonates and calc-silicates rocks in the SFT area and equivalent units in adjacent areas was undertaken to establish whether a high $\delta^{13}C$ is present in these rocks. If so, it would argue against the suggestion that such values are confined to the Palaeoproterozoic.

5.2 SAMPLE LOCALITIES

A total of 27 samples of metacarbonate rocks collected from 22 sites in the SFT, Monatshane, Topisi and Matsitama areas were chosen for carbon and oxygen isotope analyses (Tables 5.1, 5.2 and 5.3). Their locations are shown in Table 5.1 and Figure 5.1. Those in the SFT area are also shown on the dissertation map. At these localities the most common rock type is marble and both calcite and dolomite varieties are present (Tables 5.2 and 5.3). Samples were cut to remove weathered surfaces if necessary. They were sent to the Stable Isotope for Innovative Research (SIFIR) laboratory at the University of Manitoba, where they were analysed by Dr. Andrey Bekker. The descriptions in Appendix 2 are from his report.

Table 5.1: Sample number, location and GPS coordinates for samples analysed for carbon and oxygen isotope values.

Sample no.	Rock type	Location	GPS Coordinates
MLM 255	carbonate	Gulushabe area	S21.49258 E27.47347
MLM 261	carbonate	Sesweu hill, Topisi	S22.22253 E27.30575
MLM 271	carbonate	west of Moshaiwa Hill	S21.62394 E27.30789
MLM 276	carbonate	North of Tonota	S21.40406 E27.45147
MLM 277	carbonate	Shashe area	S21.38314 E27.43856
MLM 279	carbonate	Gulushabe area	S21.49597 E27.55317
MLM 286	carbonate	Matsitama area	S21.05653 E26.77092
MLM 289	carbonate	Seswe area	S21.60064 E27.30778
MLM 301	carbonate	Gulushabe area	S21.46786 E27.47969
MLM 308	carbonate	Gulushabe area	S21.47414 E27.48419
MLM 312	carbonate	E of Tonota along Shashe River	S21.43472 E27.48000
MLM 320	carbonate	Gulushabe area	S21.49547 E27.48461
MLM 337	carbonate	N of Tonota Village	S21.40075 E27.46794
MLM 354	carbonate	N of Gulushabe area	S21.44094 E27.47842
MLM 366	carbonate	E of Gulushabe area	S21.47647 E27.59139
MLM 386	carbonate	Gulushabe area	S21.46964 E27.50419
MLM 434	carbonate	Gulushabe area	S21.49492 E27.52169
MLM 436	carbonate	Gulushabe area	S21.49375 E27.53211
MLM 441	carbonate	Matsitama area	S21.07936 E27.92231
MLM 443	carbonate	Monatshane area	S21.79522 E27.77556
MLM 448	carbonate	Gulushabe	S21.53558 E27.46314
MLM 496	carbonate	Tonota area	S21.40669 E27.43767

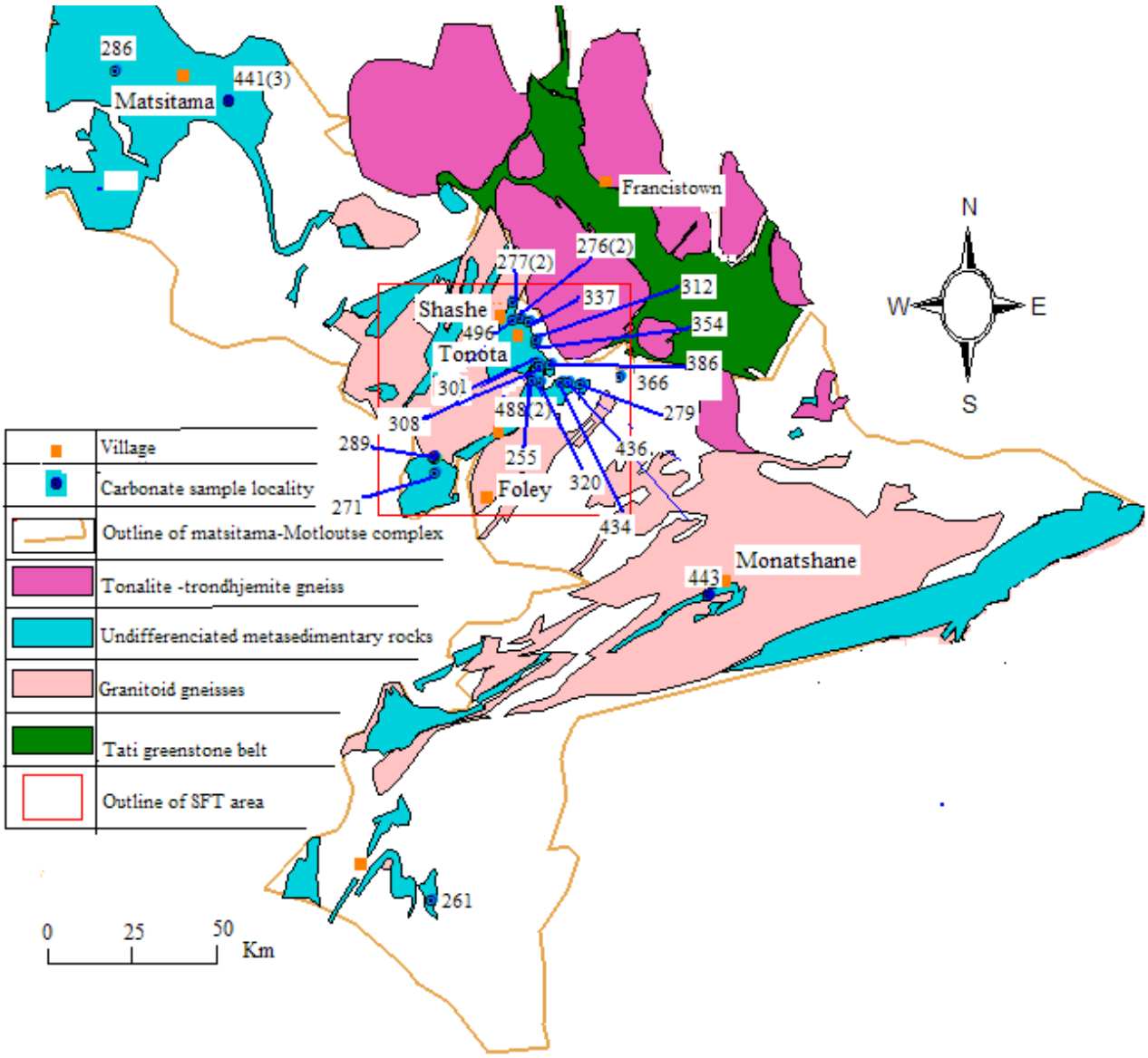

Fig. 5.1: Sample location map for metacarbonate rocks sampled and analysed for carbon and oxygen isotope analysis. NB. See also dissertation map for plot of sample locations that falls within the SFT area.

5.3 RESULTS

Table 5.2. $\delta^{13}C$ (Cc) and $\delta^{18}O$ (Cc) values obtained from 20 samples of metacarbonate rocks from 17 localities in the SFT area.

Lab ID	Client ID	Mineralogy	$\delta^{13}C$ (‰, VPDB)	$\delta^{18}O$ (‰, VPDB)	$\delta^{18}O$* (‰, VSMOW)
GB-10-0089	MLM 255	Non Ferroan calcite	-0.7	-14.0	16.5
GB-09-1021	MLM 271	Dolomite	13.2	-12.1	18.4
GB-09-1022	MLM 276	Dolomite	1.0	-14.1	16.4
GB-09-1023	MLM 276b	Dolomite	0.9	-14.2	16.3
GB-09-1026	MLM 277b1	Dolomite	6.3	-8.2	22.4
GB-09-1110	MLM 277b2	Dolomite	6.8	-8.6	22.1
GB-09-1032	MLM 279	Dolomite	8.0	-8.5	22.1
GB-09-1034	MLM 301	Dolomite	8.3	-8.0	22.7
GB-09-1107	MLM 308	Dolomite	7.9	-5.9	24.8
GB-10-0091	MLM 312	Non Ferroan dolomite	4.8	-8.6	22.0
GB-09-1113	MLM 320	Dolomite	10.6	-8.2	22.5
GB-09-1028	MLM 337	Dolomite	1.6	-11.9	18.7
GB-09-1116	MLM 354	Dolomite	2.3	-13.9	16.6
GB-10-0092	MLM 366	Non Ferroan calcite	7.5	-10.5	20.0
GB-09-1111	MLM 386	Dolomite	5.0	-15.3	15.1
GB-09-1106	MLM 434	Dolomite	7.1	-9.0	21.6
GB-09-1105	MLM 436	Dolomite	8.7	-7.8	22.9
GB-10-0099	MLM 448A	Dolomite	14.2	-9.3	21.4
GB-1-0102	MLM 448 B	Non ferroan dolomite	14	-8.3	22.3
GB-09-1112	MLM 496	Dolomite	7.8	-9.3	21.3

Table 5.3: shows $\delta^{13}C$ (Cc) and $\delta^{18}O$ (Cc) values obtained from 7 samples of metacarbonate obtained from 5 localities in the Topisi, Matsitama, Seswe and Monatshane areas.

Lab ID	Client ID	Mineralogy	$\delta^{13}C$ (‰, VPDB)	$\delta^{18}O$ (‰, VPDB)	$\delta^{18}O$* (‰, VSMOW)
GB-09-1020	MLM 261	Dolomite	9.9	-10.1	20.5
GB-10-0090	MLM 286	Non Ferroan calcite	7.0	-8.9	21.7
GB-09-1029	MLM 289	Dolomite	1.7	-12.0	18.6
GB-10-0096	MLM 441A	Ferroan calcite	5.9	-17.7	12.6
GB-10-0105	MLM 441B-dup	Ferroan calcite	5.9	-17.9	12.4
GB-10-0097	MLM 441 B	Ferroan calcite	6	-17.7	12.6
GB-10-0098	MLM 443	Dolomite	5.7	-10.3	20.3

5.4 DISCUSSION

The metacarbonates yielded $\delta^{13}C$ (Cc) and $\delta^{18}O$ (Cc) values in the range 0.9‰ to +14‰ (relative to PDB) and +12.6 to +24.8‰ (relative to SMOW), respectively. The dolomite minerals have some $\delta^{13}C$ (Cc) values slightly higher and some in the same range (overlapping) with those obtained from ferroan and non-ferroan calcite. The data for sample MLM 255 is anomalous (-0.7‰0) and it is not discussed further. from the Gulushabe areaThe $\delta^{13}C$ values of carbonates from the SFT area (Gulushabe structure), show no significant difference compared to those from Matsitama (MLM 286), Monatshane (MLM 443) and Topisi (MLM 261) areas suggesting that they may be part of the same package.

There is a previous contention that the sedimentary protoliths to supracrustal rocks in the Central Zone were deposited at 3.3 Ga (e.g. Barton 1983, Kröner *et al*., 1999) but SHRIMP U-Pb detrital ages obtained on detrital zircon grains from metapelite and metapsammite samples from the Gumbu Group are no older than 2.68 Ga and possibly as young as 2.2 Ga (Buick *et al*., 2003). Buick *et al*. (2003) also report high $\delta^{13}C$ and $\delta^{18}O$ stable isotope data from the Gumbu Group carbonates. A plot of $\delta^{13}C$ vs $\delta^{18}O$ of carbonates from the present study yielded a pattern comparable to that obtained for carbonate data from the Gumbu Group (Fig. 5.2 A and B). In Figure 5.2 A, 12 samples have $\delta^{13}C$ values less than or equal to 6 and are thus directly comparable with the samples from the Gumbu Group shown on Fig. 5.2 B. Eight of the 12 samples in Fig. 5.2

A with $\delta^{13}C$ values below 6 are from the SFT area but there are 13 samples from the SFT area with $\delta^{13}C$ values above 6 and there is no obvious geographical significance to the spread of these values across the sample set analysed.

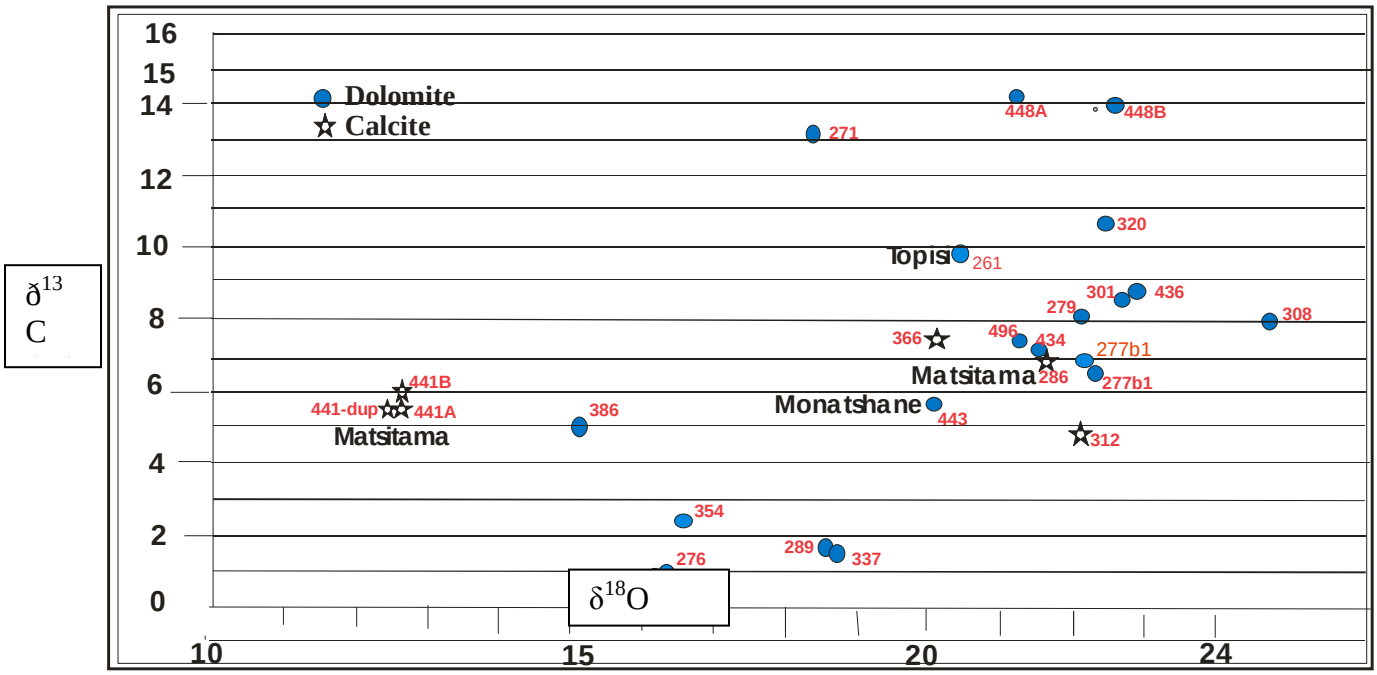

Figure 5.2 A: Plot of stable isotope data from SFT, Topisi, Matsitama and Monatshane areas showing variation between $\delta^{13}C$ and $\delta^{18}O$. NB: the unnamed data points are from the SFT area.

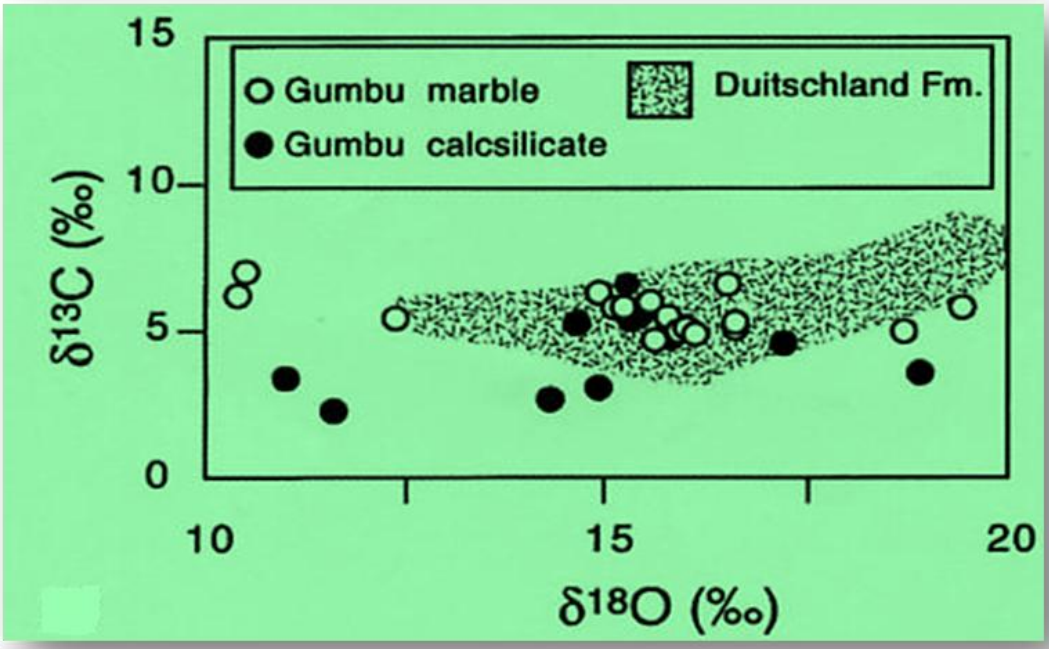

Fig. 5.2 B: Variation between $\delta^{13}C$ and $\delta^{18}O$; Gumbu area, Central Zone, South Africa (from Buick *et al.*, 2003). NB: the Duitschland Formation forms the upper most part of the Chuniespoort Group (Transvaal Supergroup) and is younger than 2480Ma (Eriksson *et al.*, 2006).

What is apparent however is that the majority of the samples analysed in the present study have higher $\delta^{13}C$ and $\delta^{18}O$ values (4.8‰ to +14‰ and +12.6 to +24.8‰) than those documented by Buick *et al*. (2003) from the Gumbu Group (+2.3‰ to +7‰ and +10 to +19.2‰) but the significance of this requires further research. The sampled localities in the Gumbu Group are underlain by metasedimentary rocks dominated by quartzite, marble and calc-silicate with minor metapelites and amphibolite suggesting the protoliths of these rocks are the same as those in the SFT, Matsitama and Monatshane areas.

The maximum age of deposition of 2661 ± 8 Ma reported by McCourt *et al*. (2004) for quartzite from Topisi area (Matsitama-Motloutse Complex) is within error of the maximum age of 2680 Ma reported by Buick *et al* (2003) for the deposition of metapsammite from the Gumbu Group. This suggests that the maximum age of

deposition of the metasedimentary rocks in the current study is coeval with the maximum age of deposition of the protoliths to the Gumbu Group.

The similarity between stable isotope and detrital zircon ages obtained from the Gumbu Group rocks and those from the SFT, Matsitama and Monatshane areas suggest that the metasedimentary belts may represent parts of the same sequence possibly related to the same geodynamic cycle. Buick *et al*. (2003) concluded that the supracrustal rocks in the Central Zone of the Limpopo belt are not exclusively Archaean in age but that a younger Palaeoproterozoic sequence is also present.

In the SFT area:

1. Late Archaean U-Pb zircon ages were obtained from granitoid gneisses from the SFT area.

2. The U-Pb zircon age determinations show that deformation and metamorphism of the SFT metasedimentary rocks and the granitoids occurred in the Late Archaean. Deformation in the metasedimentary sequence and the granitoids rocks predates 2631 Ma (pink gneissic granite) since S_1 foliation in the pink gneissic granite can be traced into the metasedimentary rocks.

3. Whereas the Gumbu Group metacarbonates may be Palaeoproterozoic in age, (Buick *et al*. 2003) those of the SFT area are Late Archaean in age.

4. Therefore high $\delta^{13}C$ signature is not confined to Palaeoproterozoic carbonate rocks but also occurs in Late Archaean carbonate rocks.

CHAPTER 6: DISCUSSION AND CONCLUSIONS

6.1 CORRELATION OF THE SFT AREA WITH ADJACENT TERRANES

Available geochronological data show that the Limpopo belt is a product of Neoarchaean orogenic event/orogeny and the Central Zone (CZ) was overprinted by a Palaeoproterozoic tectono-metamorphic event (McCourt and Armstrong 1998; Kramers *et al*., 2011)). There is no evidence for a ~2.0 Ga event in the Vumba granite-greenstone terrane (Bagai *et al*. 2002), the Francistown Complex (Bagai, 2008) or the Mosete Complex (Majaule and Davis, 1998). However, a zircon grain (analysis # 1 in Table 4.6) from sample MLM-SRP5 yielded an age of 2058 ± 11Ma, suggesting presence of a Palaeproterozoic component in the SFT area. Support for this is comes from Zeh *et al*. (2009), who found Palaeoproterozoic zircon overgrowth in a sample from Motloutse Complex (sample SP1; Table 1.7).

Lithologically, there is no significant difference between supracustal rocks from the Mosetse Complex (Matsitama belt), the Motloutse Complex and the Phikwe Complex. They are characterised by a carbonate-metapelite-quartzite association interlayered with granitoid gneisses. There is a general contention that the protoliths to the sedimentary rocks in the Central Zone of the Limpopo belt were deposited at ~3.3 Ga (e.g. Barton and Sergeev, 1997; Kroner *et al*., 1999). Supracrustal rocks in the Motloutse Complex (SFT) are younger (2661 Ga) than those in the Central Zone of the Limpopo belt and the Francistown Arc Complex (McCourt *et al*., 2004). McCourt *et al*. (2004) suggested that the source area for the metasedimentary rocks in the Matsitama and Motloutse areas was the Francistown Arc Complex.

The Zimbabwe craton is different to the other terranes in that the supracrustal rocks are dominated by greenstone belts lithologies, metavolcanics and minor metasedimentary rocks. Whereas rocks in the Zimbabwe craton are at greenschsist to amphibolite facies metamorphism, the Motloutse Complex was metamorphosed at upper amphibolite facies (Tables 1.3 and 6.1). Peak metamorphism in the Phikwe Complex occurred under granulite facies conditions but there has been widespread retrogression to upper

amphibolite facies. No evidence for retrogression has been reported in the Motloutse Complex. Despite differences in metamorphic grade, the structural style in the Motloutse Complex (e.g. SFT area), and Topisi area (Key *et al*., 1994), that include approximately NE-SW trending folds and main regional structure that strikes approximately NE also characterises the Phikwe Complex.

Table 6.1: Compilation of data for type of supracrustal assemblages, age of clastic sedimentation, age range of magmatism and grade of metamorphism in the SFT area relative to the Francistown, Phikwe and Mosetse Complexes.

	Francistown Complex	Phikwe Complex	Mosetse Complex	SFT area
Supracustal rocks	Greenstone belt rocks, mafic-ultramafic metavolcanics overlain by intermediate to felsic rocks	quartzite-carbonate-metapelite association	Matsitama metasedimentary group-quartzite-carbonate-metapelite association	Shashe metasedimentary group-quartzite-carbonate-metapelite association
Age of deposition	2733 ± 5 Ma to 2690 ± 4 Ma (McCourt *et al.*, 2004 using Bagai *et al*, 2002 data)	3300 Ma to 3150 Ma (Kröner *et al*., 1999) in South Africa)	2638 ±15Ma (McCourt *et al*. 2004-Matsitama belt)	< 2661± 8 Ma (McCourt *et al.,* 2004-Matsitama-Motloutse Complex)
Age of magmatism	2739 ± 7.2 to 2647 ± 4 Ma (Bagai 2008)	2658 ± 9 to 2517 ± 33 Ma (Zeh *et al*. (2009), Holzer *et al.* (1999), B.K Paya, pers. com, unpublished data, 2010) and McCourt and Armstrong (1998) data included in the range).	2710 ± 10 to 2646 ± 2.5 Ma (Majaule and Davis, 1998)	2724 ± 48 to 2631.5 ± 4.4 Ma (this study)
Metamorphic facies	Greeenschist-amphibolite Facies	Granulite facies retrogression at 2.0 Ga	greenschist and amphibolite facies	Medium-high grade (upper amphibolite facies)

The regional strike of planar fabrics in the SFT region is orientated NNE to ENE whereas those in the Francistown Complex and Matsitama belt are orientated NW-SE. The NNE trends in the SFT area do not conform to the NW trend of the Shashe belt (Crockett 1968 and Bennett 1970), the Limpopo Shashe Belt (Ranganai *et al*., 2002) or to the Matsitama-Motloutse Complex (McCourt *et al.* 2004).

Previous accounts of the structural history of the NE Botswana document 4 deformation events: D_1 is linked to the pre-granitoid folding that caused inversion of the Tati and Matsitama belts (Litherland, 1975); D_2 is the event responsible for the regional foliation; and D_3 and D_4 are events that deform the regional foliation and associated structures with D_4 being the ENE striking shear zones along the boundary between the Motloutse Complex and the Phikwe Complex i.e. the Magagophate, Molabe and Lepokole shear zones (Paya, 1996).

The deformation history described in the present account is similar to that described from Topisi, Phikwe and Francistown areas. However, no evidence was found in the SFT area for top to NE directed thrusting (first reported in NE Botswana by Litherland (1975) and also reported in the Topisi, Phikwe and Francistown areas (Key 1976; Key *et al.*, 1994). The compression which produced NNE-ENE trending folds ($F_1/F_2/F_3$) in the SFT area is comparable with deformations reported in neighbouring areas e.g. D2/D3 in Foley area (Table 1.2), D3 in the Motloutse Complex (Table 1.4), D3 in the Topisi area (Table 1.5) and D2 in the Bobonong area (Table 1.6).

The SFT and Topisi areas are characterised by ENE trending map scale folds defining Type 3 interference structures (this study; Key *et al.*, 1994) e.g. the Gulushabe structure in the SFT area and the Sesweu hill structure in Topisi area. The two areas have the same supracrustal assemblage dominated by quartzite and quartz-mica schist and minor amphibolite, marble and calc-silicates. The granitoids gneisses are very similar. The grey gneiss regarded as paragneiss by Key *et al*. (1994) may be an equivalent of the Tonota biotite gneiss in the SFT area while the unit described as porphyritic granite (locally augen gneiss) is represented by the wide spread megacrystic granite gneiss. However, ultramafic rocks and anorthosites reported in the Topisi area are absent in the SFT area. Compilation of data for type of supracrustal assemblages, age of clastic sedimentation

and age range of magmatism and grade of metamorphism in the SFT area relative to the Francistown, Phikwe and Mosetse Complexes is given in Table 6.1. A comparison of new age data for granitoid gneisses in the SFT region with publishe ages for granitoids and supracrustals rocks from the Topisi (McCourt *et al*., 2004) the Matsitama area-Mosetse area (Majaule and Davis, 1998) and the Francistown Complex (Bagai, 2008) suggest that the deposition of supracrustal rocks in these terranes is coeval or slightly younger than spatially associated granitic intrusions. Magmatism occurred between about 2.6 and 2.7 Ga in these terranes. The similarity of U-Pb zircon ages for Neoarchaean granitoid gneisses in the SFT area (Motloutse Complex), Zimbabwe craton and Limpopo belt suggest a close link in their evolution between 2.6 and 2.7 Ga.

Stereographic plots of poles to foliation and lineation data from the northern part of the Topisi Sheet (Figures 6.1A and B, Key *et al*., 1994) are analogous to those from the SFT area. Poles to the S_1 and S_2 foliation from the north eastern part of the Topisi sheet (Fig 6.1A) are very similar to those of $S_1$and S_2 from the SFT area (Figures 3.12A and 3.23A) and the pole to the best fit great circle for these data defines a fold axis plunging NNE as in the study area. The plot of the intersection lineation data from the Topisi area (Fig. 6.1B) and lineation data from the Gulushabe structure (Fig. 3.23A) is also to the NNE and thus coincident with the fold axis. This is strong evidence that the geometry of the youngest fold structures in the SFT and Topisi areas is very similar. It is obvious from the projections that fold axes plunge NNE (Fig 6.1A). The above mentioned similarities suggest similar geodynamic setting for the SFT and Topisi areas both of which fall within the Motloutse Complex.

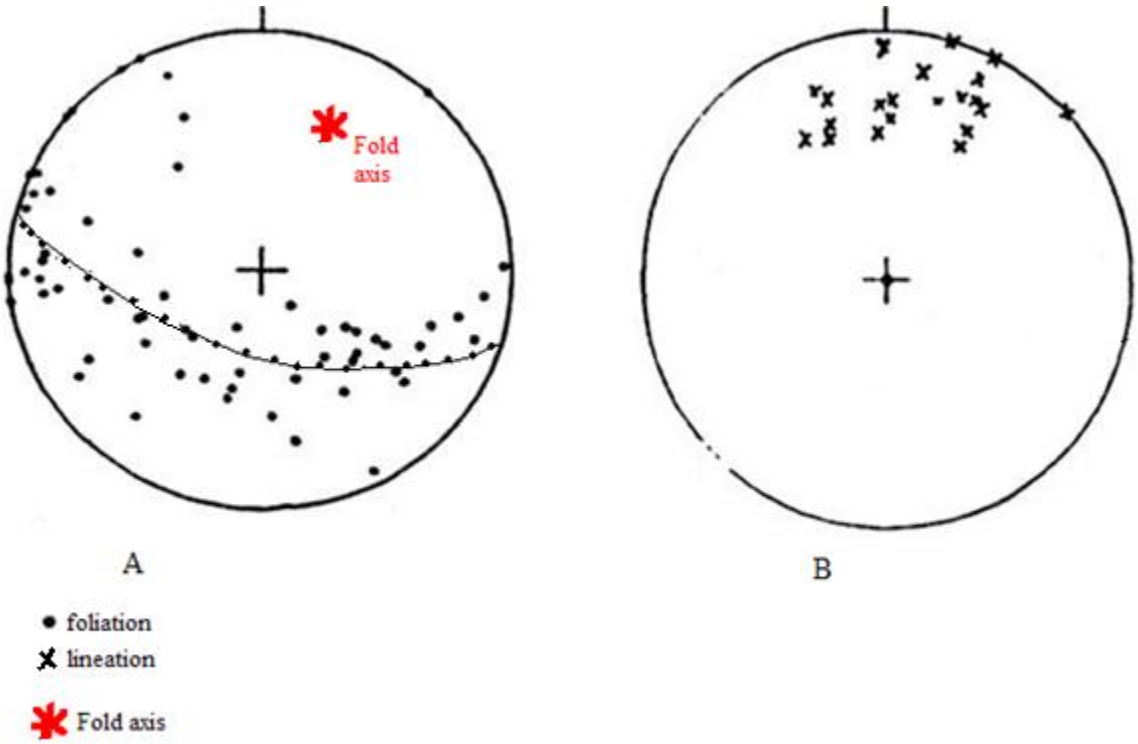

Figure 6.1: Equal area-Lower Hemisphere of poles to foliation from the NE part of the Topisi area (Sheet 2727 A2, Key *et al.*, 1994) and the related lineation data from quartzite and gneisses is shown in Figure 6.1B (from Key *et al.*, 1994). The pole to the best fit great circle (hand drawn) defines a fold axis plunging NNE.

The age data for the rocks of the SFT area, those adjacent parts of the Motloutse Complex as defined by Aldiss (1991) and in the SW part of the Zimbabwe craton (Bagai, 2008) suggest a close link in the evolution of these areas between 2.7 and 2.6 Ga. It is therefore probable that conclusions reached by Kampunzu *et al*. (2003) and Bagai (2008) for the granitoid rocks associated with the Tati and Vumba greenstone belts on the SW part of the Zimbabwe craton can be applied to the granitoid rocks of the SFT area. The tonalitic gneisses of the SFT area are therefore can interpreted as equivalent to the tonalitic component in the TTG gneiss of the Tati granitoid greenstone terrane thought to have been produced by partial melting in a flat subduction zone and the megacrystic granite gneiss may be part of the young K-rich granites produced by partial melting of the TTG material as reported by Kampunzu *et al.* (2003) and Bagai (2008).

6.2 REGIONAL ANALYSIS AND IMPLICATIONS

An analysis of a mosaic of published geological maps allows the recognition of a regional scale WNW/SSE trending system of thrust sense ductile shear zones that is traceable from the southeastern corner of the Mosetse sheet, onto the northeastern part of the Matsitama sheet across the Shashe sheet (and thus through the study area), into the SW corner of the Francistown Sheet and eventually onto the Magogaphate/ Bobonong Sheet (Fig. 6.2). Within this system the regional dip of the thrust sense shear zones (Mosupe shear zone, Mooke shear zone and Shashe shear zone) is to the SW (Table 3.1 and Fig. 6.2) but in the study area the Gulubashe shear zone deviates from this orientation and dips N to NE suggesting it has a geometry of a back-thrust in an overall NE verging system.

Aldiss (1989) reports that NE trending foliation in the Shashe area extends into the Tati Siding Granite exposed N of the SFT area, in the Francistown area (Fig. 6.2). The age of 2734 ± 39 Ma (Zeh *et al.,* 2009) obtained from the Tati Siding granite (referred to as Tati TTG in Table 1.7) provides a maximum age for the deformation along the Shashe Dam shear zone. To the west of the SFT area, biotite gneiss associated with metasedimentary rocks of the Matsitama belt is separated from the banded tonalitic gneiss of the Francistown Granite Greenstone Complex by a zone of deformation characterized by horizontal or gently plunging lineation (L-S tectonite fabrics; Aldiss, 1989). The lineation plunges SW and is inclined at angles of 45 degrees and often less than 10 degrees on the foliation. The same lineation also characterizes the contact between the southwestern outcrops of the Jankie gneisses (Fig. 6.2) with the Motloutse Complex migmatites. The lineation developed during regional deformation which imparted an LS-fabric on both units. The contrast in tectonic style suggests that the zone characterized by L>S-tectonite may be a major tectonic break, along which a subhorizontal motion is indicted by the attitude of the lineations. This zone is herein named the Jamataka shear zone (after Jamataka settlement, Fig. 6.2), and corresponds to the boundary of the Mosetse and Motloutse Complexes as defined by Aldiss (1991). See Table 6.1 for details. The orientation of the Jamakata shear zone is similar to the Shashe Dam shear zone but in contrast to the Jamakata shear zone there is no clear evidence for simple shear displacement along the Shashe Dam shear zone. This requires further investigation.

According to Crockett (1968) the N to NNE trending fabrics (e.g. the Shashe Dam shear zone) locally modify WNW striking structures associated with deformation of the Tati greenstone belt implying they are younger. This suggests the thrust sense shear zones along the southern margin of the Zimbabwe craton (Aldiss 1991, Kampunzu *et al*., 2003 and McCourt *et al*., 2004) are older than the N to NNE trending zones of foliation.

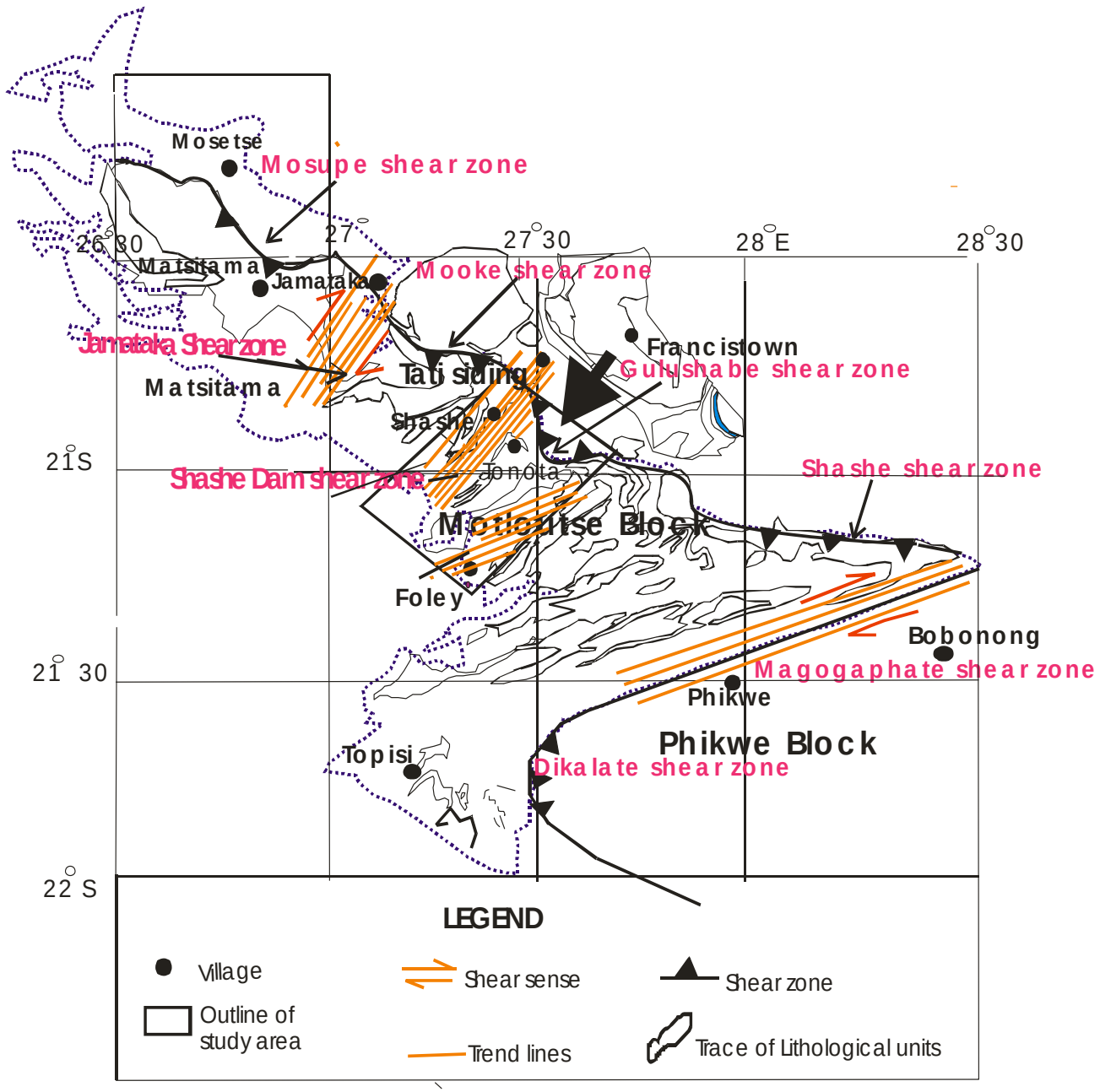

Figure 6.2: Sketch map showing the mosaic of Quarter Degree Geological Sheets covering the basement of NE Botswana and the position of the regional NW-SE trending thrust sense shear zone system across these sheets; the various sectors of the thrust system are identified by name. Barbs on the thrust sense shear zones indicate the hanging wall block in each case. Motloutse and Phikwe Blocks after Paya (1996). Mosupe shear zone after Majaule (1999), Mooke shear zone after Aldiss (1989), Shashe shear zone after Paya (1996).

Table 6.1 Shear zones in NE Botswana; their locations, nature, orientations of structural elements and interpretations

Name of Boundary	Map Sheet	Nature of boundary	Foliation	Lineation	Interpretation
Mosupe shear zone (Majaule, 1999)	Mosetse Sheet	NE directed thrust sense shear zone	Foliation trends NW-SE and dips 15-20° S	Plunges south, subparallel to dip	Boundary between the Matsitama belt and the Jankie gneisses
Mosupe shear Zone (Majaule, 1999)	Matsitama sheet	1.5 km wide NE directed thrust sense ductile shear zone	Foliation trends WNW-ESE and dips moderately SW.	Oblique, and orientated NNW-SSE	Defines the NE boundary of the Matsitama belt with the Jankie gneiss unit
Jamataka shear zone (Aldiss, 1991)	Shashe Sheet	NE-SW strike–slip shear zone	NNE trending and dips steeply NW	moderately plunging to subhorizontal lineation; L>S and L tectonites	Defines the boundary between the Mosetse and Motloutse Complexes (Aldiss, 1991); separates Mosupe shear zone from the Mooke shear zone
Mooke shear zone	Shashe sheet	NE directed thrust sense ductile shear zone	Foliation trends WNW and dips steeply (60°) South	Lineation plunges down dip (south).	Defines boundary between the SW margin of the Francistown Complex and the (western) Motloutse Complex.
Shashe Dam shear zone (present study)	Shashe sheet	Shear zone (based on intense foliation)	NNE-NE trending and dips WNW to NW	Lineation plunges N-NNE	Separates the Mooke and Gulushabe shear zones
Gulushabe shear zone (present study	Shashe sheet	SW directed thrust sense ductile shear zone	Foliation trends E-W to WNW and dips steeply N and NNE	Lineation plunges N to NE	Defines the boundary between the SW margin of the Francistown Complex and the (central) Motloutse Complex
Shashe shear zone (Paya, 1996)	Bobonong/Magogaphate sheet	NE directed ductile thrust sense shear zone	Foliation trends WNW and dips S-dipping	Lineation plunges SW	Boundary between the Magogaphate block against southern margin of proto-Zimbabwe craton

The Motloutse Complex which includes the SFT area is interpreted to be a crustal block now attached to the SW margin of the Zimbabwe craton by accretion tectonics (Aldiss 1991; McCourt *et al*., 2004). The complex formed in an area of folding, granitoid intrusion, ductile thrusting and strike-slip deformation located between the Matsitama belt to the NW, the Tati greenstone belt to the immediate N, the Phikwe Complex to the E and an unknown terrane to the SW, now hidden beneath the Karoo cover. The metasedimentary rocks from the unknown terrane were thrust northeastwards over the magmatic arcs developed at the margin of the Zimbabwe craton, resulting in crustal thickening and high heat flow that prompted migmatization, anatexis and ductile deformation (Aldiss (1991). The overthrust sedimentary rocks were infolded with the granitoid gneisses. Key *et al*. (1994) report NE directed thrusting (indicated by SW plunging lineation in quartzite) in quartzite from the Topisi area. The current study however found no evidence for NE thrusting in the SFT area. The SW dipping thrust sense shear zones reported by Aldiss (1991) from the Shashe area were not found. The geological evolution of the SFT area is thus difficult to accommodate in the accretion-linked models for the SW margin of the Zimbabwe craton as suggested by Aldiss (1991), Kampunzu *et al*. (2003), McCourt *et al*. (2004 and Bagai (2008). Based on the foliation, lineation and fold data collected during mapping, the age data on zircon grains from selected granitoids and the stable isotope data from the metacarbonate rocks, the conclusions from the present study are as follows:

- The study area is characterised by NNE to ENE striking foliation present in both the supracrustal rocks (the metasedimentary belt) and the granitoids.

- The metasedimentary rocks of Domain 1 are deformed into large map scale NE to ENE trending folds structures deforming bedding (So) and foliation (S_1).

- The foliation in the metasedimentary rocks is parallel to bedding and there has been flattening normal to the foliation plane and elongation within the foliation. The foliation and the shape of deformed pebbles in the pebbly-quartzite is a product of oblate strain (flattening) in response to NW or NNW horizontal compression

- The axis of F_1 and F_2 minor folds in the metasedimentary rocks plunge NE-ENE indicating coaxial folding.

- Deformation of the metasedimentary belt involved NW-SE or NNW-SSE compression producing S_1. This was succeeded by a coaxial deformation (F_2) possibly involving top to ESE thrusting.

- Poles to bedding (So) and foliation (S_1), local minor folds and map scale folds associated with the Gulushabe define NNE plunging F_3 folds.

- Foliation in the megacrystic granite gneiss is defined by preferred orientation of K-feldspar megacrysts. The shapes of the megacrysts are related to flattening.

- The foliation in Domain 4 is at a high angle to the foliation in Domains 1, 2 and 3, trending E-W to WNW in Domain 4 and NNE to ENE in Domains 1, 2 and 3.

- The granitoid rocks SW of the Shashe Dam are intensely foliated suggesting a ductile ductile shear zone although there is no strongly developed lineation or shear sense indicators.

- U-Pb zircon dating of the granitoid rocks indicate granitoid magmatism occurred during the late Archaean. The crystallization ages of the proliths to the granitoid rocks range between 2724 ± 48 Ma and 2631 ± 4. Ma, spanning a period of about 93 Ma. The protolith to the Tonota biotite gneiss was emplaced first (2724 ± 48 Ma), followed by emplacement of the protolith to the tonalitic gneiss (2698.9 ± 9.2 Ma), megacrystic granite gneiss (2647 ± 24 Ma) and pink gneissic granite (2631 ± 4.4 Ma). The latter occurs that as dykes cutting the foliation (S_1) in the megacrystic granite gneiss (Figs 2.26) and the banded tonalitic gneiss (Fig. 2.27).

- U-Pb zircon age of 2625 ± 16 Ma was obtained from mylonitic megacrystic granite gneiss in Domain 2, S of Tonota Village. This U-Pb zircon age is interpreted to give the maximum age of local ductile shearing S of Tonota.

- In the granitoids the foliation (S_1) in the tonalitic gneiss (2699 Ma) and the megacrystic gneiss (2647 Ma) predate intrusion of the pink gneissic granite (2631 Ma). Since the foliation in the granitoid gneiss is equated with S_2 in the metasedimentary sequence (i.e. the foliations are concordant), deformation fabrics in both the metasedimentary sequence and granitoid rocks must predate 2631 Ma.

- The last deformation event is marked by widespread development of minor shear zones in the granitoid gneiss (section 5.3.4). The NNE to NE trending shear zones (020°-040°) have been interpreted as a distal expression of the event responsible for the Magogaphate shear zone (Key 1976, Aldiss 1991, Paya, 1996).

- The minor shear zones were not found in the pink granite gneiss implying that they developed prior to emplacement of the original pink granite i.e. they are older than 2631 Ma. The development of these minor ductile shear zone is constrained between 2647 Ma and 2630 Ma.

- The carbonate rocks (dolomites, marble and calc-silicates) from the SFT region have high positive $\delta^{13}C$ values (4.8 to 14.2‰). Such elevated $\delta^{13}C$ values suggest a Palaeoproterozoic (2.4-2.1) age ([3]A. Bekker, pers. com, 2011) for the carbonate rocks but this is incompatible with field data that indicates the structures that deform the metasedimentary rocks are older than 2631 Ma and thus the carbonate rocks are late Archaean in age.

[3]Andrey Bekker, Dept. of Geological Sciences, University of Manitoba, Winnipeg, Canada.

APPENDIX 1: OUTLINE OF THE SHRIMP METHOD

The Sensitive High Resolution Ion Microprobe (SHRIMP) is a large-diameter, double-focusing secondary ion mass spectrometer (SIMS) sector instrument produced by Australian Scientific Instruments in Canberra, Australia. The SHRIMP microprobe focuses a primary beam of ions on a sample sputtering secondary ions which are focused, filtered and measured according to their energy and mass. The SHRIMP is primarily used for geological and geochemical applications. It can rapidly measure the isotopic and elemental abundances in minerals at a micrometre-scale and is therefore well-suited for the analysis of complex minerals, as often found in metamorphic terrains, some igneous rocks, and for relatively rapid analysis of statistical valid sets of detrital minerals from sedimentary rocks. The most common application of the instrument is in uranium-thorium-lead geochronology, although the SHRIMP can be used to measure other isotopic and elemental abundances. The SHRIMP determines the ages of crystals by measuring their lead and uranium contents. SHRIMP works by firing a beam of oxygen ions (electrically charged oxygen atoms) at just one spot on the crystal. They hit the crystal and knock off atoms of all the elements in the crystal, including atoms of uranium and lead. These atoms are sucked away by electrical forces and then separated into their different types by magnetic forces (a process called mass spectrometry). The atoms of lead and uranium are counted and the age of the zircon at the target spot is calculated. http://en.wikipedia.org/wiki/Sensitive_high-resolution_ion_microprobe

Uranium converts slowly and steadily to lead by natural radioactive decay. All rocks take up small amounts of lead and uranium when they form, but some special minerals in rocks, such as zircon, take up only uranium. Any lead found in zircon crystals must therefore come from uranium decay. Uranium converts to lead so fast, so the ratio of lead to uranium in zircon tells how old it is. The difficulty with dating rocks using zircon is that many rocks contain zircon crystals of many different ages. Zircon is so tough that when new rocks form from older rocks, zircon crystals from the older rocks survive. Even if a rock is melted, the old zircon crystals simply grow a new layer. Dating such mixed crystals by traditional methods, even one by one, gives meaningless average ages. SHRIMP is able to measure the ages of layers within single zircon crystals as small as 10

micrometers (one hundredth of a millimeter) wide. The growth history of the crystal, which sometimes spans more than a thousand million years, is revealed.

Australian National University website:

http://www.anu.edu.au/CSEM/machines/SHRIMP.htm-27 June 2013.

SHRIMP ANALYTICAL PROCEDURE

N.B: The following analytical procedure is an extract from a report from Dr. Richard Armstrong, Research School of Earth Sciences (RSES), Australian National University.

Firstly zircon samples were crushed into powder and then either passed over a Wilfley Table to concentrate heavy minerals or hand selected. The zircons were analysed using SHRIMP II (Sensitive High Resolution Ion Microprobe). Each analysis consisted of five scans through the mass range. The zircons were mounted in epoxy resin together with the zircon standard AS3 and RSES standard SL13. The grains were sectioned approximately in half and polished. The spot diameter was about 15-3 microns, and the primary beam intensity was about 2 nA. The data have been reduced as described by Williams and Claesson (1987, and references therein), using the SQUID Excel Macro of Ludwig (2000). Reflected and transmitted light photomicrographs and Cathodoluminescence CL) SEM images were prepared for all zircons to aid in the selection of target areas and to decipher the internal structure of zircons. The zircons were then analysed for U-Th-Pb. The Pb/U ratios have been normalized relative to a value of 0.1859 (equivalent to an age of 1099 Ma) for AS3. Pb/Pb stepwise leaching experiments (PbSL) were applied. Mineral separates were obtained by standard techniques using jaw crusher and sieve analysis. The 150 to 250-ml sieve fractions were then purified by handpicking followed by repeated rinsing in deionized water; 200 mg of these materials were transferred to 7-ml Savillex1 screw-cap beakers for step-leaching. Successive 120°C acid leach steps (seven in total) involving various mixtures of HBr, HNO3, and HF were performed on each separate, to extract Pb selectively from the phases. The Ahrens-Wetherill Concordia plot (Wetherill 1956) has been prepared using Isoplot/EX (Ludwig 2003). Dates were calculated by use of radiometric ratios ^{207} Pb/ ^{206}Pb ratios and corrections for common Pb were undertaken by use of the measured ^{204}Pb and the appropriate common Pb composition. Ages for

zircon rims were calculated from their radiogenic $^{206}Pb/^{238}U$ ratios and correction for common Pb were made using the measured Pb/Pb and U/Pb as described in Williams and Claesson (1987). Uncertainties given for individual analyses (ratios and ages) and the error bars in the plotted ages are reported at 95% confidence limits

APPENDIX 2: CARBON AND OXYGEN STABLE ISOTOPE ANALYTICAL PROCEDURE

Carbon has two stable isotopes, ^{12}C and ^{13}C, and one radioactive isotope, ^{14}C. Carbon isotope ratios are measured against Vienna Pee Dee Belemnite (VPDB). They have been used to track ocean circulation, among other things. Oxygen has three stable isotopes, ^{16}O, ^{17}O, and ^{18}O. Oxygen ratios are measured relative to Vienna Standard Mean Ocean Water (VSMOW) or Vienna Pee Dee Belemnite (VPDB). Variations in oxygen isotope ratios are used to track water movement, paleoclimate and atmospheric gases such as ozone and carbon dioxide. Typically, the VPDB oxygen reference is used for paleoclimate, while VSMOW is used for most other applications. Oxygen isotopes appear in anomalous ratios in atmospheric ozone, resulting from mass-independent fractionation. Isotope ratios in fossilized foraminifera have been used to deduce the temperature of ancient seas (http://en.wikipedia.org/wiki/Isotope_geochemistry, 27 June 2013)

N.B: The following analytical procedure is an extract from a report from Dr. Andrey Bekker, who did the isotope analysis at the University of Manitoba

In the analyses calibration was performed by analyzing two internal calcite standards (CHI and USC-1) for data in Table 5.2 and three international and internal calcite standards (NBS18, NBS19 and CHI) for data in Table 5.3. During the analysis, calibration was done at the beginning, middle and end of each run. Calibration lines were calculated by least squares linear regression using the known and measured isotope values of the calibration standards. To check the quality of analysis, calibrated international or internal standards were analysed together with unknown samples. For dolomites minerals in Table 5.2, four calibrated internal calcite and dolomite standards (LiPO#3, $\delta^{13}C$ = +1.02‰ VPDB and $\delta^{18}O$ = -7.98‰ VPDB; Exp50, $\delta^{13}C$ = -3.80 ± 0.10‰ and $\delta^{18}O$ = -10.50 ± 0.10‰; MD, $\delta^{13}C$ = +1.00 ± 0.10‰ and $\delta^{18}O$ = -8.70 ± 0.10‰; Tytyri, $\delta^{13}C$ = +0.78‰ and $\delta^{18}O$ = -7.07‰) were analysed together with the unknown samples. Replicate analyses of internal standards yielded the results of $\delta^{13}C$ = +0.97 ± 0.08‰ and $\delta^{18}O$ = -8.01 ± 0.10‰ (n = 45) for LiPO#3, $\delta^{13}C$ = -3.93 ± 0.10‰

and $\delta^{18}O$ = -10.68 ± 0.11‰ (n = 48) for Exp50, $\delta^{13}C$ = +0.90 ± 0.07‰ and $\delta^{18}O$ = -8.47 ± 0.11‰ (n = 36) for MD, and $\delta^{13}C$ = +0.73 ± 0.10‰ and $\delta^{18}O$ = -5.92 ± 0.12‰ (n = 41) for Tytyri. For the dolomite and calcite minerals in Table 5.3, quality check was performed analyzing 2 calibrated internal calcite and dolomite standards (Exp50, $\delta^{13}C$ = -3.80 ± 0.10‰ VPDB and $\delta^{18}O$ = -10.50 ± 0.10‰ VPDB; Tytyri, $\delta^{13}C$ = +0.78 ± 0.01‰ and $\delta^{18}O$ = -7.07 ± 0.04‰) together with unknown samples. Replicate analyses of internal standards yielded the results of $\delta^{13}C$ = -3.90 ± 0.10‰ and $\delta^{18}O$ = -10.74 ± 0.14‰ (n = 66) for Exp50, and $\delta^{13}C$ = +0.73 ± 0.09‰ and $\delta^{18}O$ = -5.96 ± 0.14‰ (n = 70) for Tytyri.

ACKNOWLEDGEMENTS

I would like to express my special appreciation and thanks to my supervisor Professor Stephen McCourt for finding time for supervision and editorial work, you have been a tremendous mentor for me. I thank you for encouraging my research and for allowing me to grow as a research scientist. Without your supervision and constant help, this dissertation would not have been possible. Thanks are also due to anonymous examiner for the constructive and brilliant comments and suggestions. I would especially like to thank Dr. A. Bekker (Department of Geological Sciences, University of Manitoba, Canada) for the stable isotope analysis on carbonate samples. I am also grateful to the following; Dr. Richard Armstrong (RSES, The Australian National University, Canberra) for the SHRIMP work (zircon separation, CL imaging, dating of samples, data reduction and interpretation), Dr. Hoffman for the field visit, Peter Arone (GS field assistant), Alfred Pule (GS field assistant). I greatly acknowledge the Director of Geological Survey, Mr. Ngwisanyi and all the supporting staff of Geological Survey who provided assistance when I collected data for my research work. Special thanks to my family. Words cannot express how grateful I am to my Mother; your prayer for me was what sustained me thus far. I also thank my friends and everyone who incited me to strive towards my goal, the list is endless. Many thanks go to the local people in the STF area who were at all times showing willingness to assist. At the end, I would like to thank Kaone and Itumeleng Senatla who were always my support in the moments when there was no one to answer my queries. What kept me going was my unwillingness to give in. I have learnt to forge ahead and never to give up even during the tough and testing times. Most of all, I have learnt to be specific with directions. I will never again loose my bearings.

REFERENCES

Aldiss, D.T. (1983). The geology of the Semolale area. *Bulletin Geological Survey Botswana*, **25**, 64pp.

Aldiss, D.T. (1989). The geology of the Shashe area. *Bulletin Geological Survey Botswana*, **35**, 132pp.

Aldiss, D.T. (1991). The Motloutse complex and the Zimbabwe craton/Limpopo belt transition in Botswana. *Precambrian Research*, **50**, 89-109.

Bagai, Z. (2000). *Geochemical and geochronological investigations of the Vumba granite-greenstone terrane of northeast Botswana*. Unpublished MSc Thesis, University of Durham, England, 174pp.

Bagai, Z., Armstrong, R.A. and Kampunzu, A.B. (2002). U-Pb single zircon geochronology of granitoids in the Vumba granite-greenstone terrane (NE Botswana): Implication for the evolution of the Archaean Zimbabwe craton. *Precambrian Research*, **118**, 149-168.

Bagai, Z. (2008). *Geodynamic evolution and petrogenesis of the Neoarchaean Francistown granite-greenstone complex in NE Botswana, SW margin of the Zimbabwe craton.* Unpublished PhD thesis, University of Cape Town. Chapters 1-12.

Barton, J.M., and Key, R.M. (1981): The tectonic development of the Limpopo Mobile Belt and the evolution of the Archaean cratons of Southern Africa: in Kröner, A. (Ed), Elsevier, *Precambrian Plate Tectonics*, 185-212.

Barton, J.M. and Key, R.M. (1983). Rb-Sr ages and geological setting of certain rock units from the Central Zone of the Limpopo Mobile Belt, near Zanzibar, eastern Botswana: in van Biljon, W.J. and Legg, J.H (Eds). The Limpopo Belt. Special Publication, *Geological Society of South Africa,* **8**, 19-27.

Barton, J.R (1983). Our understanding of the Limpopo Belt-a summary with proposals for future research in: Van Biljon, W. J. and Legg, J. H. (Eds), The Limpopo Belt. Special Publication, *Geological Society of South Africa*, **8**, 191-203.

Barton, J.M., Jr. and Sergeev, S. (1997). High precision, U-Pb analyses of single grains of zircon from quartzite in the Beit Bridge Group yield a discordia. *South African Journal of Geology,* **100**, 37-42.

Bennett, J.D. (1968 a). A provisional description of the Mosetse-Matsitama area. Unpublished report, *Geological Survey of Botswana*, **JDB/21/68**, 42pp.

Bennett, J. D. (1968 b). The geology of the Mosetse-Matsitama area; an introduction (QDS 2926D and 2126B). Unpublished report, *Geological survey of Botswana*, **1**, 48pp.

Bennett, J.D. (1970). Craton-Mobile Belt relations with particular reference to the Mosetse-Matsitama area, northeastern Botswana. *Geological Magazine,* **107**, 113-123.

Bennett, J.D. (1971). The tectono-metamorphic complex of eastern Botswana (Geological map at scale of 1:50 000), *Geological Survey of Botswana*.

Blenkinsop, T.G., Mkweli, S., Rollinson, H.R., Fedo C.M., Paya, B.K., Kamber, B.S., Kramers, J.D. and Berger, M. (1995). The North Limpopo Thrust Zone (NLTZ): the northern boundary of the Limpopo belt in Zimbabwe and Botswana. *Extended Abstracts, Geological Society of South Africa, Centennial Geocongress,* **95**, 174-177.

Bowring, S.A. and Williams, I.S. (1999). Priscoan (4.00-4.03 Ga) orthogneisses from northwestern Canada. *Contribution to mineralogy and petrology, **134***, 3-16.

Buick, I. S., Williams, I.S. Gibson, R.L., Cartright, I, and Miller, J. A. (2003). Carbon and U-Pb evidence for a Palaeoproterozoic component in the Central Zone of the Limpopo belt, South Africa. *Journal of Geological Society of London,* **160**, 601-612.

Cahen, L., Snelling, N.J., Delhal, J. and Vail, J.R. (1984). *The geochronology and evolution of Africa.* Clarendon Press, Oxford. 512pp.

Carney, J.N., Aldiss, D.T. and Lock, N.P. (1994). The Geology of Botswana. *Bulletin Geological Survey of Botswana,* **37**, 113pp.

Chavagnac, V., Kramers, J.D., Naegler, T.F. and Holzer, L. (2001). The behavior of Nd and Pb isotopes during 2.0 Ga migmatization in paragneisses of the Central Zone of the Limpopo belt (South Africa and Botswana). *Precambrian Research,* **112**, 51-86.

Coward, M.P. and James, P.R. (1974). The deformation patterns of Archaean greenstone belts in Rhodesia and Botswana. *Precambrian Research,* **1**, 235-258.

Coward, M. P., James, P. R. and Wright, L. (1976). Northern Margin of the Limpopo Belt, Southern Africa. *Geological Society of America, Bulletin,* **87**, 601-611.

Cox, K.G., Johnson, R.L., Monkman, L.J., Vail J.R., and Wood, D.N. (1965). The Geology of the Nuanetsi Igneous Province. *Phil. Trans. R. Soc. Lond*., **A.257**, 71-218.

Crockett, R.N. (1968). Geological map of the Shashe area (QDS 2127A), with brief description. *Geological Survey of Botswana.*

Eriksson, P.G., Altermann, W. and Hartzer, F.J. (2006). The Transvaal Supergroup and its precursors. *In* Johnson, M.R., Anhaeusser, C.R. and Thomas, R.J. (Eds). *The Geology of South Africa*. *Geological Society of South Africa*, Council for Geoscience. Pretoria: 237-260.

Gerrard, I. (1963). The geology of the Foley area. *Records Geological Survey of Bechuanaland*, **1959/60**, 35-48.

Hickman, M.H. (1978): Isotopic evidence for crustal reworking in the Rhodesian Archaean craton, Southern Africa. *Geology*, **6**, 214-216.

Hickman, M.H. and Wakefield, J. (1975). Tectonic implications of new geochronological data from the Limpopo belt at Phikwe, Botswana, southern Africa. *Geological society of America Bulletin*, **86**, 1468-1472.

Holzer, L. Barton, J.M., Paya, B. K. and Kramers J.D. (1999). Tectonothermal history of the western part of the Limpopo belt: tectonic models and new perspectives. *Journal of African Earth Sciences,* **28**, 383-402.

Jelsma, H.A. and Dirks, P.H. (2002). Neoarchaean tectonic evolution of the Zimbabwe craton. In The Early Earth: Physical, chemical and biological development, **199** (Eds). C.M.R. Fowler, C.J. Ebinger, and C.J. Hawkesworth, Special Publications, *Geological Society London*, 183-211.

Jourdan, F., Féraud, G., Bertrand, H., Kampunzu, A.B., Watkeys, M.K., Le Gall, B. and Tshoso, G. (2004). New age constraints on the Karoo large igneous province: Triple junction and brevity questioned: *Geochimica et Cosmochimica Acta*, **68**. Elsevier, Armsterdam, p. A575.

Kamber, B.S., Kramers, J.D. Napier, R., Cliff, R.A. and Rollinson, H.R. (1995). The Triangle Shear zone, Zimbabwe, revisited; new data document an important event at 2.0 Ga in the Limpopo Belt. *Precambrian Reasearch, **70***, 191-213.

Kampunzu, A.B., Tombale, A.R., Zhai, M., Bagai, Z., Majaule, T.M. and Modisi, M. (2003). Major and trace element geochemistry of plutonic rocks from Francistown, NE Botswana: Evidence for Neoarchaean continental active margin in the Zimbabwe craton. *Lithos*, **71**, 431-460.

Kampunzu, A.B., Akanyang P., Mapeo, R.B.M., Modie B.N. and Wendorff, M.P. (1998). Geochemistry and Tectonic significance of the Mesoproterozoic Kgwebe Metavolcanic Rocks in NE Botswana: Implications for Evolution of the Kibaran Namaqua-Natal Belt. *Geological Survey of Botswana, 50th Anniversary International Conference. Abstract Volume*, p45.

Key, R.M. (1976). The geology of the area around Francistown and Phikwe, north-east and Central districts, Botswana. *District Memoir Geological Survey of Botswana*, **2**, 121pp.

Key, R.M., Litherland, M. and Hepworth, J.V. (1976). The evolution of Archaean crust of northeast Botswana. *Precambrian Research*, **3**, 275-413.

Key, R.M and Hutton, S.M. (1976). The tectonic generation of the Limpopo Mobile Belt, and a definition of its western extremity. *Precamrian Research, **3***, 79-90.

Key, R.M., Mapeo, R.B.M. Van Zyl, H.E.M., Hargreaves, R.L., and Holmes, H. (1994). The geology of the Topisi area. *Bulletin Geological Survey Botswana*, **38**, 84pp.

Kramers, J.D., McCourt, S., Roering, C., Smit, A., Dirk, D. and van Reenen, D.D., Eds (2011). Tectonic models proposed for the Limpopo Complex: Mutual compatibilities and constraints. *Geological Society of America Memoir*, **207**, 311-324.

Kröner, A., Jaeckel, P., Brandl, G., Nemchin, A.A. and Pidgeon, R.T. (1999). Single zircon ages for granitoid gneisses in the Central Zone of the Limpopo Belt, Southern Africa and geodynamic significance. *Precambrian Research*, **93**, 299-337.

Lintern, B.C. (1982). *The stratigraphy and structure of the Matsitama Schist Belt, Northeast Botswana.* Unpublished PhD Thesis, University of Leeds, 234pp.

Litherland, M. (1975). The geology of the area around Maitengwe, Sebina and Tshesebe, Northeast and Central Districts, Botswana. *District Memoir Geological Survey of Botswana*, **2**, 133pp.

Ludwig, K.R. (2003). User's Manual for Isoplot/Ex, Version 3.0, A geochronological toolkit for Microsoft Excel. Berkeley Geochronology Center, 2455 Ridge Road, Berkeley, CA 94709, USA *Berkeley Geochronology Center Special Publication No.* **4**, 70pp.

Ludwig, K. R. (2000). SQUID 1.00, A User's Manual; Ridge Road, Berkeley, CA 94709, USA. *Berke-ley Geochronology Center Special Publication*. *No.**2***, 2455pp

Majaule, T. (1993). *The geochemistry and evolution of the Matsitama Supracrustal Belt; University of Portsmouth,* Unpublished PhD Thesis, 215pp.

Majaule, T. (1999). Geological map of the Matsitama area with brief descriptions (QDS 2126B). *Geological Survey of Botswana.*

Majaule, T. and Davis D.W. (1998). U-Pb zircon dating and geochemistry of granitoids in the Mosetse area, NE Botswana, and tectonic implications. *Geological Survey of Botswana, 50th Anniversary International Conference. Abstract volume,* 46-48.

Majaule, T., Hall, P. and Hughes, D. (1997). Geochemistry of mafic and ultramafic igneous rocks of the Matsitama supracrustal belt, northeastern Botswana-Provenance implications. *South African Journal of Geology,* **100**, 169-179**.**

Mason, R. (1973 a). The Limpopo Mobile Belt, Southern Africa. *Philosophical Transactions of the Royal Society of London*, **A273**, 463-485.

Mason, R. (1973 b). The geology of the southern Tati area (Sheet 2127B). Unpublished report, *Geological Survey of Botswana*, **RM/34/68**. 60pp, with geological map.

Master, S., Bekker, A., Hofmann, A (2010). A review of the stratigraphy and geological setting of the Palaeoproterozoic Magondi Supergroup, Zimbabwe – Type locality for the Lomagundi carbon isotope excursion, *Precambrian Research,* **182**, 254–273.

McCourt, S., Kampunzu A.B., Bagai, Z. and Armstrong, R.A. (2004). The crustal architecture of Archaean terranes in Northeastern Botswana. *South African Journal of Geology*, **107**, 147-158.

McCourt, S. and Armstrong, R.A. (1998). SHRIMP U-Pb geochronology of granites from the Central Zone, Limpopo Belt. Southern Africa: implications for the age of the Limpopo orogeny. *South African Journal of Geology*, **101**, 329-338.

McCourt, S. and Vearncombe, J. R. (1987). Shear zones bounding the Central Zone of the Limpopo mobile belt, southern Africa. *Journal of Structural Geology*, **9**, 127-137.

McCourt, S., Hilliard, P., Armstrong, R.A. and Munyanyiwa, H. (2001). SHRIMP U-Pb zircon geochronology of the Hurungwe granite northwest Zimbabwe: Age constraints on the timing of the Magondi orogeny and implications for the correlation between the Kheis and Magondi Belts. *South African Journal of geology*, **104** (1), 39-46.

Millonig, L. Zeh, A., Gerdes, A., Klemd, R., Barton, M. (2010). Decompression heating of the Mahalapye Complex (Limpopo belt, Botswana): A response to Palaeoproterozoic magmatic underplating, *Journal of Petrology,* **51**, 703-729.

Paya, B.K. (1996). The Geology of the Bobonong area, *Bulletin Geological Survey of Botswana,* **40**, 111pp.

Paya, B.K., Key, R., Majaule, T. (1997). Shear zones of NE Botswana: Their tectonic significance in the evolution of the Zimbabwe craton and the Limpopo belt. In: Dirks, P.H.G.M., Jelsma, A.A. (Eds.), *Abstracts, Intraplate Magmatism and Tectonics of Southern Africa.* Harare, 38-40.

Ramsay, J.G. (1962). Interference patterns produced by the superposition of folds of similar types. *Journal of Geology*, **70**, 466-481.

Ramsay, J.G. (1967). *Folding and Fracturing of Rocks*. McGraw-Hill, New York. p. 518-555.

Ramsay, J.G. and Huber M.I. (1987). *The techniques of Modern Structural Geology*, ***2.*** *Folds and Fractures*. Academic press, London, 475-504.

Ranganai, R.T., Kampunzu, A.B., Atekwana, E.A., Paya, B.K., King, J.G., Koosimile, D.I. and Stettler, E.H. (2002). Gravity evidence for a larger Limpopo Belt in Southern Africa and geodynamic implications. *Geophysical Journal International,* **149**, F9-F14.

Robertson, I.D.M. and du Toit, M.C. (1981). The Limpopo Belt. In: Hunter D. R (Ed), *Precambrian of Southern Hemisphere.* Elsevier. Armsterdam, 641-670.

Rollinson, H.R., Blenkinsop, T. (1995). The magmatic, metamorphic and tectonic evolution of the Northern Marginal Zone of the Limpopo Belt in Zimbabwe. *Journal Geological Society London*, **152**, 65–75.

Rubatto, D. and Herman, J. (2003). Zircon formation during fluid circulation in eclogites (Monsovo, Western Alps): implications for zircon and Hf budget in subduction zones. *Geochimica et Cosmochia Acta,* **67** (12), 2173-2187.

Schaller, M., Steiner, O., Studer. I., Holzer, L., Herwegh, M. and Kramers, J.D. (1999). Exhumation of the Limpopo Central Zone granulites and dextral continent-scale transcurrent movement at 2.0 Ga along the Palala Shear Zone, Northern Province, South Africa. *Precambrian Research,* **96**, 263-288.

Simpson, C. (1983). Displacement and strain patterns from natural occurring shear zones terminations. *Journal of Structural Geology,* **5**, 597-506.

Simpson, C. and de Paor, D.G. (1993). Strain and kinematic analysis in general shear zones. *Journal of Structural Geology,* **15**, 1-20.

Smith, R.A. and Phofuitsile, P. (1985). The Geology of the Foley area. *Bulletin Geological Survey of Botswana*, **31**, 107pp.

Twiss, R.J. and Moore, E.M. (1992). *Structural Geology. Kinematic Models of folding*. Freeman and Company, United States of America, 238-261.

van Reenen, D. and Dodson, M.H. (1972). Metamorphic chronology of the Limpopo belt, southern Africa. *Bulletin Geological Society of America*, **83**, 2005-18.

van Reenen, D. D., Kramers, J. D., McCourt, S. and Perchuk, L. L., Eds (2011). Origin and evolution of Precambrian high grade gneiss terranes with special emphasis on the Limpopo Complex of Southern Africa. *Geological Society of America Memoir, **207***, 324pp

Watkeys, M.K. (1983). Brief explanatory notes of the provisional geological map of the Limpopo Mobile Belt and the environs. In: The Limpopo Belt, 5-8. Van Biljon, W.J. and Legg, J.H. (Eds). *Special Publication Geological Society of South Africa,* **8**, 203pp.

White, S.H., Baurows, S.E., Carreras, J., Shaw, N.D. and Humphreys, F.J. (1980). On mylonites in ductile shear zones. *Journal of Geology, **2***, 175-188.

Williams, I. S. and Claesson, S. (1987). Isotopic evidence for the Precambrian provenance and Caledonian metamorphism of high grade paragneisses from the Seve Nappes, Scandinavian Caledonides. II. Ion microprobe zircon U-Th-Pb. *Contrib. Mineral. Petrol*, **97**, 205–217.

Wetherill, G.W. (1956). Discordant Uranium-Lead Ages, I. *Trans Am Geophys Union,* **37** (3), 20-32.

Zeh, A., Gerdes, A., Klemd, R. and Barton, J. M., Jr (2007). Archaean to Proterozoic crustal evolution in the Central Zone of the Limpopo belt (South Africa/Botswana): Constraints from combined U-Pb and Hf isotope analyses of zircon. *Journal of Petrology*, **48**, 1605-1639.

Zeh, A., Gerdes, A. and Barton, J.M., Jr (2009). Archaean accretion and evolution of the Kalahari craton-the zircon age and Hf isotope record of granitic rocks from Barberton/Swaziland to the Francistown Arc. *Journal of Petrology,* **50**, 933-966.

Zhai M., Kampunzu, A. B., Modisi, M. P. and Bagai, Z. (2006). Sr and Nd isotope systematics of the Francistown plutonic rocks, Botswana: Implications for Neoarchaen crustal evolution of the Zimbabwe craton. *International Journal of Earth Sciences,* **95** (Geologische Rundschau), 355-369.